**DYNAMICS AND RHEOLOGY OF JANUS DROPS**

By

Misael Díaz Maldonado

A dissertation submitted in partial fulfillment of the requirements for the degree of

DOCTOR OF PHILOSOPHY

in

CHEMICAL ENGINEERING

UNIVERSITY OF PUERTO RICO
MAYAGÜEZ CAMPUS

2015

Approved by:

| | |
|---|---|
| Aldo Acevedo, Ph.D<br>Member, Graduate Committee | Date |
| Moses N. Bogere, Ph.D.<br>Member, Graduate Committee | Date |
| Jorge L. Almodovar-Montañez, Ph.D.<br>Member, Graduate Committee | Date |
| Ubaldo M. Córdova-Figueroa, Ph.D.<br>President, Graduate Committee | Date |
| Ricky Valentín, Ph.D.<br>Representative of Graduate Studies | Date |
| Aldo Acevedo Rullán, Ph.D.<br>Chairperson of the Department | Date |

## ABSTRACT

This dissertation sheds some light on the dynamics and rheological properties of compound multiphase drops in the creeping motion limit of the fluid phases from a fundamental standpoint. A compound multiphase drop can exhibit a fully engulfing configuration, as in the case of a drop encapsulating a smaller one, or a partly engulfed configuration, in which a pair of drops in contact resemble a snowman. A particular of the latter type that is under active research is the Janus drop due to its anisotropic properties. The term Janus, which takes after the god of two faces of Roman mythology, highlights that the drop consists of two parts of equal geometry but of different properties (anisotropic). It is found that the dynamics of such Janus drop in an external flow is similar to that of a spheroid of revolution. Interestingly, the effective viscosity of Janus drops that corresponds to the minimum dissipation energy has an analogous form to the expression derived by Taylor (1932) Proc. R. Soc. A 138, 41–48 for a single-phase drop in a steady shear flow.

## RESUMEN

Esta disertación arroja algo de luz sobre la dinámica y las propiedades mecánicas de gotas multifásicas compuestas en el límite de movimiento rastrero desde un punto de vista fundamental. Una gota multifásica compuesta puede exhibir una configuración totalmente envolvente, como en el caso de una gota que encapsula otra más pequeña, o una configuración envolvente parcial, en la cual un par de gotas en contacto asemejan a un muñeco de nieve. Un particular de este último grupo que está bajo investigación activa es la gota Janus debido a sus propiedades anisotrópicas. El término Janus, que proviene del dios de dos caras de la mitología romana, resalta que la gota se compone de dos partes de geometría identica, pero de diferentes propiedades (anisotrópica). Se ha encontrado que la dinámica de tales gotas Janus en un flujo externo es similar a la de un esferoide de revolución. Interesantemente, la viscosidad efectiva de las gotas Janus que corresponde a un mínimo de energía disipativa tiene una forma análoga a la expresión derivada por Taylor (1932) Proc. R. Soc. A 138, 41–48 para una gota de una sola fase en un flujo cortante estacionario.

This dissertation contains portions that were published by the author in the Journal of Fluid Mechanics of Cambridge University Press and Physics of Fluids of the American Institute of Physics. The article published in the Journal of Fluid Mechanics has been reprinted with permission of Cambridge University Press to be contained as part of this dissertation. Proper acknowledgement of the published work is made in the corresponding chapters of the dissertation. The author submitted part of the work present in this dissertation to be considered for publication in the International Journal of Multiphase Flow of Elsevier Inc. prior to the delivery of the accepted version of this dissertation to graduate school.

In the loving memory of my dear grandfather Johnny Rivera Resto.

ACKNOWLEDGMENTS

To the Lord Jesus Christ who has given me the strength, toughness and conviction to complete this degree.

To my family (Misael Díaz Placeres, Ada N. Maldonado Maldonado, Yamilette Díaz Maldonado, John M. Díaz Maldonado, Juan Díaz, Jovita Placeres, Jesús Torrado, Noemí Placeres, Abigail Maldonado, Iris Maldonado, Noemí Maldonado, Johnny Rivera Resto, Jesusa Resto, John Rivera, Ricky Rivera, and others) for their support, guidance and patience throughout my long academic career.

To my beloved sweetheart Martha Ligia Rozo Medina for her charming company and support regardless of the difficulties. She was always there next to me when all my strength and motivation dwindled. Just the gaze of her precious eyes telling me that she believed in me was all that I needed in those moments to continue the fight with the spirit to succeed. There is happiness in the world, one just have to train the eye to recognize it when it happens. Thanks honey for granting me the opportunity to experience this little but profound secret.

I am specially thankful to my dear friend and colleague Glenn C. Vidal Urquiza for the never ending and interesting conversations about our research projects. Seeing him work to no end with just his shear will made me want to work harder too. I have to admit that even though we were not fond of each other at first, we became great friends ... almost like family. I wish him the best of success in all aspects of life.

To my dear friend Sergey Shklyaev for his enlightening discussions, humorous comments and for the opportunity of participating as an invited researcher at the Institute of Continuous Media Mechanics in Perm, Russia. Sergey is accountable for

much of my advancement as a young researcher, which I hope to continue improving steadily over the years to come. It is a huge loss that he parted already from this world; I can only say that I am still shocked by the news. He was a great man, colleague and an unforgettable friend.

To Ronal de la Cruz for his instructive conversations and suggestions.

Special thanks to Javier Huertas. He is another meaningful person that has helped me countless times since the early years of my graduate studies. Our friendship started thanks to the course of transport phenomena... which we do not talk about it much anymore.

To Gerardo Lopez and Karina Gelis for sparing their precious time to help me conform this LaTeX template into grad school specifications.

I am very grateful to Fran Franke for taking her precious time in revising the correctness of the written language used in part of this dissertation.

I wish to thank all my friends, which I have not mentioned here but they know how important they have been in my life, that have supported me in one way or another. I would not have been able to realize all of this without them.

And last but not least, to my mentor Ubaldo M. Córdova-Figueroa for his patience, guidance and support. He took me in as his pupil when nobody else would to shape me into a serious researcher. I must say that he (unknowingly) has been God's instrument to break me down and make me anew.

TABLE OF CONTENTS

page

ABSTRACT ENGLISH . . . . . ii

ABSTRACT SPANISH . . . . . iii

ACKNOWLEDGMENTS . . . . . vi

LIST OF TABLES . . . . . xi

LIST OF FIGURES . . . . . xii

1 Introduction . . . . . 1

2 Low Reynolds number flows . . . . . 6

2.1 Introduction . . . . . 6
2.2 Axisymmetric flows . . . . . 16
2.2.1 Stokes flow past a solid sphere . . . . . 17
2.2.2 Stokes flow past a solid sphere subject to a superficial 'slip' velocity . . . . . 26
2.2.3 Stokes flow about a fluid drop or bubble . . . . . 32
2.2.4 Axisymmetric elongational flow about a fluid sphere . . . . 44
2.3 3D flows . . . . . 50
2.3.1 Hydrodynamic resistance tensor of a solid sphere in Stokes flow . . . . . 51
2.3.2 Singularity solutions of Stokes flow for a translating solid sphere . . . . . 64
2.3.3 Hydrodynamic resistance tensor of a fluid drop in Stokes flow 66
2.3.4 Stresslet of a solid sphere in a general straining flow . . . . 74
2.3.5 The stresslet produced by a fluid drop in a general straining flow . . . . . 87
2.3.6 The interior and exterior flows of a fluid drop in a shearing flow . . . . . 91
2.4 Effective viscosity of a dilute dispersion of drops in linear flows . . 104

3 Dynamics of a Janus drop in a uniform flow . . . . . 111

3.1 Abstract . . . . . 111
3.2 Introduction . . . . . 112
3.3 Problem formulation . . . . . 115
3.3.1 Shape of equilibrium drop . . . . . 115

3.3.2 Stokes flow . . . 118
3.4 Axisymmetric flow . . . 121
3.4.1 Vector potential formulation . . . 121
3.4.2 The limiting case $\eta_1 = \eta_2$ . . . 123
3.4.3 Different internal viscosities . . . 125
3.5 External flow, parallel to the internal interface ($\beta = \pi/2$) . . . 127
3.5.1 Small viscosity difference . . . 128
3.5.2 Finite viscosity difference . . . 131
3.6 Dynamics of the Janus drop . . . 131
3.6.1 The force for the arbitrary $\beta$ (fixed drop) . . . 131
3.6.2 Stable regime for a freely rotating drop . . . 133
3.6.3 Deformation of the internal interface . . . 134
3.7 Concluding remarks . . . 137

4 The anisotropic response of a Janus drop to a shearing fluid . . . 141

4.1 Abstract . . . 141
4.2 Introduction . . . 142
4.3 Problem statement . . . 146
4.4 Governing equations . . . 148
4.5 Solution . . . 150
4.5.1 Shear flow with a velocity gradient parallel to the internal interface . . . 152
4.5.2 Plane hyperbolic flow with a velocity gradient normal to the internal interface . . . 153
4.5.3 Shear flows with a velocity gradient normal to the internal interface . . . 156
4.5.4 Cross-streaming velocity of a Janus drop in a uniform flow 158
4.6 Grand resistance matrix of a Janus drop . . . 159
4.7 Conclusions . . . 177

5 Dynamics and rheology of Janus drops in a steady shear flow . . . 180

5.1 Abstract . . . 180
5.2 Introduction . . . 180
5.3 Model description . . . 184
5.4 Dynamics of a 'freely' suspended Janus drop in a linear shear flow 194
5.5 Cross-streaming velocity of a Janus drop in a shear flow . . . 199
5.6 Constitutive equation of a dilute Janus emulsion in a steady shear flow . . . 202
5.7 Conclusions . . . 211

6 Conclusions and Future Directions . . . 215

APPENDICES . . . 226

A . . . . . 227

A.1 Spherical cap subject to a uniform pressure field . . . . . 227
A.2 Stokes flow past a solid sphere - transformation of the boundary value problem . . . . . 229

B . . . . . 232

B.1 Representation of three-dimensional velocity fields for $\beta = \pi/2$ . . 232
B.2 Simplification of the velocity fields for $\beta = \pi/2$ at small $[\eta]/\eta$ . . . 235

LIST OF TABLES

Table page

4–1 Variation of the non-zero scalar resistance functions with the mean viscosity of the Janus drop (note that $Z^M = X^M$). . . . . 177

LIST OF FIGURES

Figure page

2–1 Plane Couette flow of a Newtonian fluid. The velocity field of this type of flow is linear: $u_x = \dot{\gamma}\, y$, where $\dot{\gamma} = U/H$ is the rate of strain. The viscous stress tensor $\tau_{xy}$ is equal to the applied force per unit area: $\tau_{xy} = F_x/A$, where the area $A$ is simply the width times the length of the plate. . . . . 9

2–2 Decomposition of the undisturbed flow into its elementary constituents: ($a$) straining flow $\dot{\gamma}/2\,(y\,\boldsymbol{e}_x + x\,\boldsymbol{e}_y)$ with axis of strain (or elongation) at a diagonal arrangement relative to the $x$–$y$ axes, ($b$) rotational flow $\dot{\gamma}/2\,(y\,\boldsymbol{e}_x - x\,\boldsymbol{e}_y)$ with axis of revolution pointing into the page, and ($c$) a uniform flow (or streaming flow) $U^\infty\,\boldsymbol{e}_x$. Note that the velocity components of the straining and rotational flows that are normal to the direction of the undisturbed flow cancel each other out identically. . . . . 11

2–3 Solid sphere of radius $a$ immersed in a streaming fluid of viscosity $\eta$. . 17

2–4 The streamlines about the solid sphere. . . . . 22

2–5 Axisymmetric streaming flow $\boldsymbol{u}_\infty$ of a viscous fluid (of viscosity $\eta$) about a solid sphere of radius $a$ subject to a 'slip' velocity $\boldsymbol{v}^s$ at its surface. . . . . 26

2–6 Streamlines about a solid sphere with a 'slip' length $\lambda/a = 5$. . . . . 31

2–7 Axisymmetric uniform flow $\boldsymbol{u}_\infty$ of a viscous ambient fluid '0' about a fluid sphere '1' of radius $a$. The dynamic viscosity and density of each fluid phase is represented by $\eta_j$ and $\rho_j$, respectively, where $j = 0, 1$. The vector $\boldsymbol{g}$ denotes the gravitational field. . . . . 34

2–8 The flows in and about a fluid sphere with a viscosity ratio $\lambda = 1/2$. . 40

2–9 Streamlines of a uniaxial elongational flow. The flow acts in the direction pointed by the arrows. . . . . 46

2–10 Streamlines in and about the fluid sphere in an elongational flow. . . 50

2–11 A neutrally buoyant fluid sphere of radius $a$ suspended in a viscous fluid that undergoes a uniform shear flow. The index ($j$) denotes the fluid phase of dynamic viscosity $\tilde{\eta}_j$. . . . . 92

2–12 Constituents of the uniform shear flow $\boldsymbol{u}^\infty = \dot\gamma y\, \boldsymbol{e}_x$: ($a$) Straining flow with its axis of strain (elongation) arranged at a diagonal with the $x$–$y$ axes $1/2\,\dot\gamma\,(y\boldsymbol{e}_x + x\boldsymbol{e}_y)$. ($b$) The solid-body rotation $1/2\,\dot\gamma\,(y\boldsymbol{e}_x - x\boldsymbol{e}_y)$ of the fluid with axis of rotation into the page from the perspective of the observer (clockwise rotation). . . . . 93

2–13 The velocity field of a fluid drop subject to a linear shear flow. The shown field corresponds to the velocity field at the $x$–$y$ plane. . . . 104

3–1 Model sketches: (a) Equilibrium Janus-like drop with contact angles $\alpha_{1,2}$; the dashed line is the symmetry axis. The radius $a_0$ and angle $\theta_0$ for the internal interface are introduced in the similar manner as $a_{1,2}$ and $\theta_{1,2}$, respectively; (b) A Janus drop in an external flow $-U\boldsymbol{l}$. The angle $\beta$ indicates the drop orientation with respect to the flow: $\beta = 0$ corresponds to the internal interface normal to the external flow (axisymmetric problem, Section 3.4), whereas $\beta = \pi/2$ corresponds to the internal interface parallel to the external flow (Section 3.5). . . . . 116

3–2 Variation of the contact angle $\alpha_1$ (the solid line, left axis) and the curvature of the internal interface $a_0^{-1}$ (the dotted line, right axis) with the difference of the surface tensions $[\gamma]$ for $\gamma = 100$. The dashed lines correspond to the asymptotic formulas, Equation (3.3). Vertical dashed-dotted lines indicate the values of $[\gamma]$ for which the drop shapes are shown. . . . . 117

3–3 The force $F_z/(2\pi)$ (in units $\tilde\eta_0 aU$) imposed on the Janus drop. Panel (a): Variation of $F_z/(2\pi)$ with $\eta$ for $\eta_1 = \eta_2 = \eta$. The solid line represents numerical results; the dashed line shows the Hadamard–Rybczynski formula, Equation (3.13). Panel (b): Variation of $F_z/(2\pi)$ with $[\eta]/(2\eta) = (\eta_2-\eta_1)/(\eta_1+\eta_2)$ for various mean viscosities of the drop $\eta = (\eta_1 + \eta_2)/2$; results of DNS (ANSYS Fluent) are shown by the dots. . . . . 124

3–4 The isolines of the velocity potential $\psi$ for axisymmetric flow, $\eta_2 = 1.5$, $\eta_1 = 0.5$ (a) and $\eta_2 = 0.7$, $\eta_1 = 0.3$ (b). The step between the isolines is 0.05 for the external flow and 0.005 inside the drop. . . . 126

3–5 Variation of the rescaled torque $T_y\eta/(8\pi[\eta])$ (in units $\tilde\eta_0 a^2 U$) acting on the Janus drop for small $[\eta]/(2\eta) = (\eta_2 - \eta_1)/(\eta_1 + \eta_2)$ with the mean viscosity of internal fluids $\eta = (\eta_1 + \eta_2)/2$. . . . . 129

3–6 Variation of the torque $T_y/(8\pi)$ (in units $\tilde\eta_0 a^2 U$) (a) and the force $F_x/(2\pi)$ (in units $\tilde\eta_0 aU$) (b) imposed on the Janus drop with $[\eta]/(2\eta) = (\eta_2 - \eta_1)/(\eta_1 + \eta_2)$ for different mean viscosities $\eta$ of the drop. Results of DNS (ANSYS Fluent) are shown as dots. . . . . 130

3–7 Force acting on a fixed Janus drop for $\eta = (\eta_1 + \eta_2)/2 = 1$. (a) Variation of the angle $\delta$ between the external flow and force on the drop with $\cos\beta$ for different $[\eta]/(2\eta)$, see Equation (3.20); (b) Variation of the maximum angle $\delta_c$ in radian (the solid line, right axis) and the value of $\beta_c$ for which $\delta$ reaches its maximum (the dashed line, left axis) with the weighted viscosity difference $[\eta]/(2\eta)$, see Equation (3.21). . . . . 132

3–8 Deformation of the internal interface by the flow. (a): Profiles $\zeta(r)$ at $\eta = (\eta_1 + \eta_2)/2 = 1$ and $[\eta] = \eta_2 - \eta_1 = 0,\ 1.6,\ 2$ (dotted, solid, and dashed lines, respectively). (b): Variation of maximum and minimum value of $\zeta$ with $[\eta]/(2\eta)$ for different $\eta$. . . . . 136

4–1 A 'perfect' Janus drop subject to a unidirectional shear flow. The vector $\boldsymbol{d}$ is parallel to the axis of symmetry of the Janus drop and points towards the less viscous fluid. . . . . 143

4–2 Transformation of $\boldsymbol{v}^{xz}$ into $\boldsymbol{v}_{\parallel}$ and $\boldsymbol{v}_{\perp}$. $(a)$ Alignment of the straining axis (dot-dashed line) of $\boldsymbol{v}^{xz}$ at a $-45°$ angle from its horizontal arrangement, plus a rotational field yields $\boldsymbol{v}_{\parallel}$. $(b)$ Alignment of the straining axis at a $45°$ angle from its horizontal position, plus a rotational field results in $\boldsymbol{v}_{\perp}$. . . . . 148

4–3 Variation of the force $F_z$ (in units of $a^2\tilde{\eta}_0 G$) with the viscosity contrast at constant values of $\eta$ when the Janus drop is subject to $\boldsymbol{v}^{xz}$ $(a)$. The force $F_x$ (in units of $a^2\tilde{\eta}_0 G$) on the Janus drop under the action of $\boldsymbol{v}_{\parallel}$ with increasing viscosity contrast at constant values of $\eta$ $(b)$. . 154

4–4 The couple $T_y$ (in units of $a^3\tilde{\eta}_0 G$) on a Janus drop with $\eta_1 = \eta_2$. . . . 157

4–5 The velocity fields of a Janus drop subject to $\boldsymbol{v}_{\parallel}$ $(a)$ and $\boldsymbol{v}_{\perp}$ $(b)$. . . . 158

4–6 Variation of the couple $T_y$ (in units of $a^3\tilde{\eta}_0 G$) with the viscosity contrast at constant values of the mean viscosity for $\boldsymbol{v}_{\parallel}$ $(a)$ and $\boldsymbol{v}_{\perp}$ $(b)$. . . . . 158

4–7 Dependence of the resistance functions with the mean drop viscosity $\eta$ for the case of equal internal viscosities. The resistance function $Z^M$ has been omitted because it is identical to $X^M$. . . . . 163

4–8 Variation of the hydrodynamic center of reaction $\boldsymbol{x}^{cr} = x^{cr}\boldsymbol{d}$ with the viscosity contrast $\Delta\eta/2\eta$ at constant values of the mean drop viscosity $\eta$. . . . . 168

4–9 Dependence of the resistance to rotation transversal to the axis of symmetry of the Janus drop with the viscosity contrast $\Delta\eta/2\eta$ at constant values of the drop mean viscosity $\eta$. . . . . 173

4–10 The dependence of the shear-torque resistance with the viscosity contrast and the mean drop viscosity $\eta$. . . . . 174

4–11 Variation of the stresslet resistance functions with the viscosity contrast $\Delta\eta/2\eta$ for selected values of the mean drop viscosity $\eta$. The resistance function $X^M$ is related to (axisymmetric) elongational flows, and $Y^M$ is associated to straining flow with principal axes at a diagonal with the axis of symmetry $\boldsymbol{d}$ of the Janus drop. . . . . 176

5–1 Unidirectional shear flow $\tilde{u}_1^\infty$ ($\tilde{u}_2^\infty = \tilde{u}_3^\infty = 0$) past a 'perfect' Janus drop of radius $a$. The fluids that constitute the Janus drop are confined to equally sized hemispheres. The symbol $(j)$ denotes the corresponding fluid phase of dynamic viscosity $\tilde{\eta}_j$ ($j = 0, 1, 2$). The unit vector $\boldsymbol{d}$ denotes the direction of the axis of symmetry of the Janus drop, and it is defined with respect to a set of right-handed Cartesian axes fixed in space $(x_1, x_2, x_3)$. The components of this vector are related to the azimuthal $\vartheta$ and polar $\phi$ angles of a spherical coordinate system in the traditional manner. . . . . 185

5–2 (Colors online) Influence of the shear to mean velocity ratio $Ga/U^\infty$ on the preferential orientation of a Janus drop of $(a)$ constant mean viscosity $\eta = 1$ with selected values of $\Delta\eta/2\eta$, and $(b)$ constant $\Delta\eta/2\eta = 0.4$ with selected values of $\eta$. . . . . 192

5–3 (Colors online) The effect of increasing viscosity contrast $\Delta\eta/2\eta$ at fixed values of the mean drop viscosity $\eta$ on $(a)$ the shear to mean velocity $Ga/U^\infty$ and $(b)$ the net hydrodynamic force $F_1$ (in units of $\tilde{\eta}_0 a U^\infty$). . . . . 193

5–4 (Colors online) $(a)$ Dependence of period orbits with the mean drop viscosity of a Janus drop with equal internal viscosities $\eta_1 = \eta_2$. $(b)$ The effect of the viscosity contrast $\Delta\eta/2\eta$ on the periodic orbits for a constant mean drop viscosity $\eta = 1$. . . . . 197

5–5 (Colors online) Apparent eccentricity factor as a function of the viscosity contrast $\Delta\eta/2\eta$ for constant values of the mean drop viscosity $\eta$. . . . . 198

5–6 (Colors online) $(a)$ The solid-line (red) depicts the dynamics of orientation and the dashed-line (blue) shows the non-dimensional ratio of the cross-streaming velocity with the external force. $(b)$ Cross-streaming velocity as a function of the arrangement of the axis of revolution of the Janus drop for constant values of $\eta$. . . . . 201

5–7 (Colors online) Variation of the stresslet functions $c_n$ ($n = 0, 1, 2$) with the mean drop viscosity $\eta$ for a Janus drop with equal internal viscosities. . . . . 206

5–8 (Colors online) Variation of the stresslet functions with the viscosity contrast $\Delta\eta/2\eta$ for selected values of the mean drop viscosity. . . . 207

5–9 (Colors online) The dependence of the stresslet associated to drop rotation with the viscosity contrast and mean drop viscosity. . . . . 208

5–10 The reduced zero-shear viscosity $\eta_r$ of a dilute Janus emulsion as a function of the drop mean viscosity and orientation. The minimum values of $\eta_r$ (at $\cos^2 2\phi = 0$) correspond to Taylor's result for single-phase drops. The axis of symmetry of the dispersed Janus drops $\boldsymbol{d}$ lie in the plane of shear. . . . . 209

A–1 Spherical cap subject to a uniform pressure field. The surfaces $S_0$ and $S_1$ denote the planar and curved surfaces of the spherical cap, respectively. . . . . 228

# CHAPTER 1
# INTRODUCTION

It may be somewhat surprising that several products (e.g. ointments, creams, inks, cements, gels) and foods (e.g. mayonaise, ice cream) that we consume everyday are complex fluids [1]. The simplest type of complex fluid, yet one of the most frequent ones, consists of a dispersion of one phase into another, where the dispersed phase can be a solid or a fluid. If the dispersed phase is a solid one, the complex fluid is referred to as a colloidal dispersion. Only when the dispersed phase is a fluid one it is denoted as an emulsion. The reader may imagine the emulsion to be comprised by a collection of drops dispersed in a continuous fluid phase. Emulsions are not limited to dispersions of drops of a single fluid phase. A more general type of emulsion of engineering interest is the compound multiphase drop due to its high selectivity to mass transport, which make them attractive for the micro-encapsulation of cells [2], drug-delivery and food processing applications [3], purification of water resources [4], micro-reactors [5], single-cell analysis [6] and direct-contact heat and mass exchangers [7].

Despite the various uses of multiphase compound drops little is known from both experimental and theoretical standpoints about how these drops affect the rheological properties of the host fluid. In general one is concerned with changes in the resistance of the complex fluid to flow—its viscosity. Compound multiphase drops are more complicated to study because of the different morphologies that they can adopt in comparison to traditional emulsions (spherical drops). Compound multiphase drops can exhibit a fully engulfing configuration (a small drop encapsulated

by another one) or a partial engulfing geometry [8]. The first to study the rheology of compound drops with full engulfment are Davis & Brenner [9] and Stone & Leal [10]. It appears that the corresponding analysis for compound drops with partial engulfment have not been carried out previously; possibly due to the more complex shape of the compound drop. In this dissertation the rheological study is conducted on a simpler, yet representative member of this group—the Janus drop. The term Janus, which takes after the god of two faces of Roman mythology, highlights that the drop consists of two parts of equal geometry but of distinct fluid properties (i.e. density and viscosity). It will be shown that the sole presence of the internal interface that bounds the fluids that comprise the Janus drop impart it with anisotropic hydrodynamics, which is a feature entirely absent in encapsulated drops. This finding is one of the major contributions of this dissertation. The analysis of the hydrodynamics and rheology of Janus drops is performed in the limit of low-Reynolds-number flows (total absence of inertia effects) due to the small length scales of Janus drops in practice. A brief outline of the chapters of this dissertation is provided below.

Chapter 2 provides a brief introduction to low-Reynolds-number flows (fluid motion in the total absence of inertia effects) and presents fundamental problems that naturally arise in the subsequent chapters. The reader unfamiliar to the field of fluid mechanics is strongly encouraged to carefully consider the problems addressed in this introductory chapter. The problem of Stokes flow about a solid sphere is solved to introduce the reader to the solution of fluid flow problems of axisymmetric nature. It is demonstrated that a fluid drop that translates in quiescent fluid does not deform in the absence of inertia effects. Lamb's solution is introduced to solve the 3D flows that arise in a linear shear flow. The chapter concludes with the calculation of the effective viscosity of an emulsion, as an example of the calculation of the viscosity of a dilute dispersion, which is carried later in this dissertation for

a dispersion of Janus drops.

The hydrodynamic properties of a Janus drop under static and fluid flow conditions are investigated in Chapter 3. The contents of this chapter were recently published in the journal of Physics of Fluids: S. Shklyaev, A. O. Ivantsov, M. Díaz-Maldonado and U. M. Córdova-Figueroa, "Dynamics of a Janus drop in an external flow", *Phys. Fluids*, v. **25**, 082105 (2013). The link to the mentioned article is the following: http://dx.doi.org/10.1063/1.4817541. (Any of the authors can include, reuse or modify the published article for a dissertation without formal permission from the American Institute of Physics AIP; evidence of this statement can be found in this link http://publishing.aip.org/authors/copyright-reuse.) Under static conditions, the existence of a compound multiphase drop close to a Janus one is discussed in terms of weak distortions to the ideal situation of a Janus drop that consists of two hemispheres of equal radii. At conditions in which the fluid phases are subject to motion, the hydrodynamic behavior of the Janus drop in a streaming flow is explored. Interestingly, the magnitude of drag force on the Janus drop is found to vary with the direction of the streaming flow. This is the first indication that elucidates the hydrodynamic anisotropic properties of the Janus drop. It is found that the Janus drop displays hydrodynamic properties of a solid of revolution despite being comprised by fluid phases because of the no-penetrability property of the internal interface. The chapter concludes with the analysis of the dynamics of a Janus drop falling in a viscous fluid by the action of gravity, where it is found that the drop exhibits a steady orientation as it falls that depends on the density and viscosity of the pair of fluids that comprise the Janus drop. This behavior has several important implications that are examined in the last chapter of this dissertation.

In Chapter 4 the hydrodynamic properties of a Janus drop are studied in a linear shear flow. This chapter is principally based on an article published in the

Journal of Fluid Mechanics: M. Díaz-Maldonado and U. M. Córdova-Figueroa, "On the anistropic response of a Janus drop to a viscous shearing fluid", *J. Fluid Mech.*, v. **770**, R2 (2015). The contents of this article have been reprinted with permission from Cambridge University Press; an electronic link to the online version of the published article can be found here: http://dx.doi.org/10.1017/jfm.2015.148. This chapter is an extension to the paper published in the Journal of Fluid Mechanics this year. Linear shear flows can arise in the gap of fluid between a pair of parallel plates that slide in opposite directions, and it is frequently encountered in various industrial and technological applications. The problem is analyzed as a function of the direction of the imposed flow and the velocity-gradient of the undisturbed flow in a systematic manner. Once again, the hydrodynamic properties of the Janus drop are found to be analogous to those of a solid of revolution; however, now there is a dependence of the arrangement of the velocity-gradient of the undisturbed flow. In the particular situation of a velocity-gradient parallel to the internal interface of the Janus drop is found to behave as a single-phase drop. Thus, showing that the behavior of a Janus drop is sensitive to its orientation in the linear shear flow (anisotropic response to the flow). In order to fully characterize the hydrodynamic properties of the Janus drop the grand resistance matrix for this system is generated, which is of utter relevance to the analyses carried out in the next chapter.

In Chapter 5 the condition in which a Janus drop can exhibit a preferential orientation in a linear shear flow is studied; this has potential applications in the determination of the velocity to velocity-gradient ratio of a general ambient flow (sensor type of application). The dynamics of a Janus drop in a linear shear flow under 'freely' suspended conditions is also considered, where it is found that the orientation of the Janus drop is periodic in time, and falls between that of a solid-sphere and a disk under analogous conditions. The analysis of the cross-flow migration of a Janus drop in a linear shear flow is carried out as well. From the results of this

phenomenon it is inferred that a dispersion of multiphase drops in a Poiseuille flow (pressure-driven flow) can exhibit a non-uniform spatial distribution, which is a first indication that a dispersion of Janus drops can display inhomogeneous rheological properties. The chapter concludes with the calculation of the effective viscosity of a dilute dispersion of Janus drops in a linear shear flow. Interestingly, the analysis reveals that the effective viscosity is analogous to that derived by Taylor [11] for a dispersion of single-phase drops but with a viscosity equivalent to the average viscosity of the pair of fluids that comprise the Janus drop. In contrast to the rheology of double emulsions [10], non-Newtonian behavior is found (difference in the normal stresses) for a Janus drop on account of its anisotropic hydrodynamic properties. This work has been submitted for publication to the International Journal of Multiphase Flow.

This dissertation concludes with general remarks and future directions of research in Chapter 6.

# CHAPTER 2
# LOW REYNOLDS NUMBER FLOWS

## 2.1 Introduction

It is common knowledge that the average skydiver reaches a terminal velocity of about 56 $m/s$ in nearly 12 $s$ when the net drag force exerted by air evens out exactly the weight of the diver [12]. If the skydiver where to fall in an atmosphere a billion times more viscous than Earth's atmosphere (with a suitable breathing equipment) and all other conditions kept the same, the terminal velocity of free-fall would be around 2 $cm/s$, and the diver would immediately reach his terminal velocity because inertia is rapidly dissipated by the highly viscous atmosphere. This simple example illustrates that the motion of an object in a fluid depends intrinsically on both the rate and mechanism of momentum transfer. In the former case, for the first couple of seconds of free-fall the predominant transport mechanism of momentum is inertia, which is a convective type of momentum transport; it is not until the skydiver has reached sufficient speed that there is an interplay between inertia and viscous transport of momentum, which is a diffusive kind of momentum transfer and represents the molecular level of resistance of the fluid to flow [13]. In the latter case, the rate of viscous transport occurs so rapidly in comparison to convective transport that the body reaches its terminal velocity in no appreciable time, which is just the reflection of the absence of inertia effects ubiquitous in everyday experience.

The present dissertation focuses on the motions of particles in a fluid in the complete absence of inertia effects of both the particle and fluid. (The term 'particles' used here extends to both solid and fluid objects.) To the general audience it may

seem at first that this work is of limited applicability because of the derived notion from a world influenced by inertia, which for us to perceive in flesh would need to be exposed to extraneous worlds. Nonetheless, it is the world microorganisms have endured and adapted to since the beginning of life [14], and it is also the environment colloidal particles (about 1 $\mu m$ in size) are subjected to. Without being aware, we interact with colloidal dispersions everyday since these range from paints, cleaning products, makeup, inks, ointments, cements, pharmaceuticals, foods, and biological fluids such as blood [1]. Thus, it should not be surprising that the development of the products that we use today and the creation of novel ones relies much on the fundamental understanding of low Reynolds number flows. The success of a product may ultimately depend on how well its flow-ability properties match the targeted specifications for the intended application to guarantee customer satisfaction, and in other cases of deeper significance, to save countless of lives.

The Reynolds number $Re$ is a non-dimensional group that compares the characteristic scales of viscous to convective transport of momentum in a fluid:

$$Re \equiv \frac{\text{characteristic time over which viscous transport occurs}}{\text{characteristic time over which convective transport occurs}} = \frac{L^2/\nu}{L/U}, \quad (2.1)$$

where $L$ is the length scale of the particle (e.g. radius of a sphere), $\nu$ is the kinematic viscosity of the surrounding fluid, and $U$ is the representative magnitude of the fluid velocity. The limit of low Reynolds number flow arises when the characteristic time of viscous to convective transport of momentum is negligible: $L^2/\nu \ll L/U$ for the Reynolds number to be vanishingly small. To those familiar with heat transfer phenomena, can take advantage of the inherent analogy of the Péclet number, a dimensionless group that weights the importance of conductive (a diffusive mechanism) to convective heat transport, with the Reynolds number. Note that for colloidal particles the Reynolds number is intrinsically low because of the smallness of the particles; it is not necessary to suspend colloidal particles in a highly viscous

fluid for inertia effects to be negligible. The example of the skydiver above required a fluid with unrealistic viscous properties because the size of a person is considerably large for diffusive transport of momentum to overcome inertia effects.

The equations that govern the motion of a fluid at low Reynolds numbers are (vector and tensor quantities are presented as boldsymbols from this point onward):

$$\boldsymbol{\nabla} p = \eta \nabla^2 \boldsymbol{u}, \quad \boldsymbol{\nabla} \cdot \boldsymbol{u} = 0, \tag{2.2}$$

where $\boldsymbol{\nabla}$ and $\nabla^2 = \boldsymbol{\nabla} \cdot \boldsymbol{\nabla}$ are the gradient and Laplacian operators, respectively, the centered dot denotes the scalar product of vectors, $p$ is the pressure field, $\eta$ is the dynamic viscosity of the fluid, and $\boldsymbol{u}$ is the velocity vector field. Together, the creeping flow and continuity equations are often referred to as the Stokes equations. An interesting consequence of the continuity equation ($\boldsymbol{\nabla} \cdot \boldsymbol{u} = 0$) is that the pressure field satisfies the Laplace equation $\nabla^2 p = 0$ and the velocity vector field satisfies the biharmonic equation $\nabla^4 \boldsymbol{u} = \boldsymbol{0}$ [13]. (It is quite straightforward to derive these relations by application of the divergence and Laplacian operators to the creeping flow equation.) The advantage of this property is that the velocity and pressure fields can be obtained independently under certain conditions, as it will be shown later in this chapter.

It is beyond the purpose of this introductory chapter to present the derivation of the Stokes equations; the interested reader is referred to well-known textbooks on transport phenomena and fluid mechanics [13, 15–20]. Nevertheless, it is worth mentioning that the Stokes equations arise from momentum and mass balances over a differential volume in the fluid under the assumptions of incompressible flows (constant density) and Newtonian stress tensor. Several kinds of fluids, such as water and gases flowing below the speed of sound, exhibit Newtonian properties: a rate of strain independent viscosity, and a linear dependence of the viscous stress tensor $\boldsymbol{\tau} = 2\,\eta\,\boldsymbol{E}$ with the rate-of-strain tensor $\boldsymbol{E} = \left(\boldsymbol{\nabla u} + (\boldsymbol{\nabla u})^t\right)/2$, where $t$ denotes

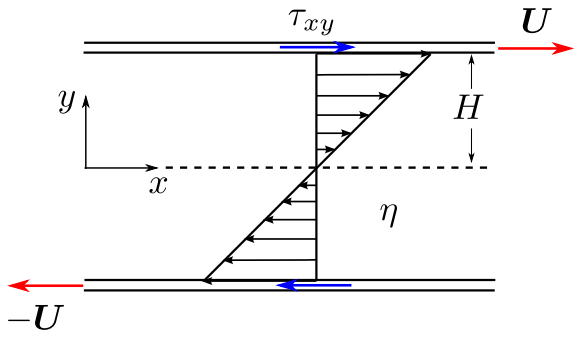


Figure 2–1: Plane Couette flow of a Newtonian fluid. The velocity field of this type of flow is linear: $u_x = \dot{\gamma}\, y$, where $\dot{\gamma} = U/H$ is the rate of strain. The viscous stress tensor $\tau_{xy}$ is equal to the applied force per unit area: $\tau_{xy} = F_x/A$, where the area $A$ is simply the width times the length of the plate.

the transpose operator. This simply means that a Newtonian fluid confined between two parallel plates sliding in opposite directions at a constant velocity $\boldsymbol{U}$ (a plane Couette device) exhibit a linear velocity profile [13]. A sketch diagram is provided in figure 2–1 for further clarification. Regardless of the applied sliding speed the ratio of the applied stress (force per unit area) $\tau_{xy}$ to the rate of strain $\dot{\gamma}$ remains constant for a Newtonian fluid: $\tau_{xy}/\dot{\gamma} = \eta$, and this constant corresponds to the dynamic viscosity $\eta$ of the fluid. In physical terms this signifies that a Newtonian fluid dissipates mechanical energy proportionally to the applied rate of strain $\dot{\gamma}$. In addition, Newtonian fluids are isotropic (direction-independent behavior) such that if the viscosity where to be measured in several types of apparatuses the fluid will invariably exhibit the same viscosity. It is interesting to note that the mechanical properties of colloidal dispersions can, under certain circumstances, exhibit deviations from Newtonian behavior even if the host fluid is Newtonian [1, 21]. The problems addressed in this dissertation categorize as one of such examples.

It is instructive to consider an overall view of the problem of a small particle suspended in a plane Couette flow (also commonly referred to as a shear flow) shown above to gain some insights of the properties of low Reynolds number flows. Additionally, the material presented here provides a global picture of the fundamental arguments and methodologies used in this dissertation for the convenience of the

general audience. If the particle is small enough such that $L/H \ll 1$, here $L$ denotes the characteristic length of the particle, one can safely neglect the effect of walls of the apparatus; from the perspective of the particle, it is suspended in an infinite unbounded fluid. In general, the particle may be placed at an arbitrary position in the fluid such that the velocity field that the particle is subjected to at long distances ($r \to \infty$) is equal to the undisturbed velocity evaluated at the location of the particle:

$$\boldsymbol{u}^{\infty} = \dot{\gamma}(y + h)\, \boldsymbol{e}_x, \tag{2.3}$$

where the term 'undisturbed' means without the presence of the particle, $h$ defines the vertical position of the particle in the fluid with respect to the set of Cartesian axes shown in figure 2–1, and $\boldsymbol{e}_x$ is the unit vector that points in the positive direction of the $x$–axis. (The particle position along the $x$–axis is irrelevant because the flow is fully developed: $\nabla_x u_x^{\infty} = 0$.) Note that if the particle has been placed in the plane of zero velocity ($h = 0$), one would recover the original expression for the velocity field ($u_x^{\infty} = \dot{\gamma}\, y$). On account of the linearity of the undisturbed velocity field, one may rewrite it in the following equivalent form:

$$\boldsymbol{u}^{\infty} = \frac{1}{2}\dot{\gamma}\,(y\,\boldsymbol{e}_x + x\,\boldsymbol{e}_y) + \frac{1}{2}\dot{\gamma}\,(y\,\boldsymbol{e}_x - x\,\boldsymbol{e}_y) + U^{\infty}\,\boldsymbol{e}_x, \tag{2.4}$$

where $U^{\infty} = \dot{\gamma}h$ is a uniform velocity field, as in the original expression above. Note that the undisturbed flow has been broken down into its elemental components: straining, rotational and uniform flows, respectively. Figure 2–2 depicts a sketch that shows that the undisturbed flow local to the particle consists of these elementary flows. As one may suspect, this result is a direct consequence of the linearity property of the Stokes equations. In the scientific literature, extensive use of the linearity property of Stokes flow is made to simplify the analysis of complicated flows [17, 19, 22–30]. The linearity property is also useful for constructing the full velocity field about a particle in an ambient flow: the disturbance caused by the presence

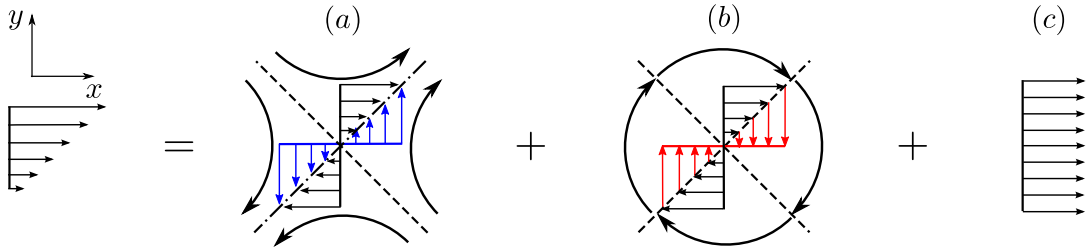


Figure 2–2: Decomposition of the undisturbed flow into its elementary constituents: ($a$) straining flow $\dot{\gamma}/2\,(y\,\boldsymbol{e}_x + x\,\boldsymbol{e}_y)$ with axis of strain (or elongation) at a diagonal arrangement relative to the $x$–$y$ axes, ($b$) rotational flow $\dot{\gamma}/2\,(y\,\boldsymbol{e}_x - x\,\boldsymbol{e}_y)$ with axis of revolution pointing into the page, and ($c$) a uniform flow (or streaming flow) $U^\infty\,\boldsymbol{e}_x$. Note that the velocity components of the straining and rotational flows that are normal to the direction of the undisturbed flow cancel each other out identically.

of the particle plus the unperturbed velocity field far away via Lamb's generalized solution [31], as shown later in this introductory chapter when dealing with 3D flow fields. Knowledge of the velocity field everywhere in the fluid it generally is a necessary step towards the determination of the hydrodynamic force $\boldsymbol{F}$, torque $\boldsymbol{T}$ and stresslet $\boldsymbol{S}$ on the particle.

Knowledge of the force, torque and stresslet on the particle is of relevance to develop dynamical equations of particle motion in a colloidal suspension, which in turn, are useful for the determination of the effective viscosity of the suspension in a linear shear flow. A colloidal dispersion can be treated, under certain conditions, as an homogeneous fluid with effective mechanical properties; being the viscosity the principal mechanical property of interest. As mentioned earlier, the viscosity of a fluid is intrinsically associated with the rate of viscous dissipation. The presence of particles moving in a colloidal dispersion (as a consequence of the imposed flow) tend to increase the bulk rate of viscous dissipation, such that the effective viscosity of the dispersion is greater than that of the host fluid. Therefore, to determine the effective properties of a colloidal dispersion in a linear flow it is a fundamental step to consider the force, torque and stresslet on the particle by each of the elemental flows shown in figure 2–2—pure hydrodynamic problems. (These calculations are simplified under the assumption that the particle remains stationary regardless of

the applied flow.) This serves the purpose of characterizing the effect the imposed flow has over the motion of the particle. Completion of the overall force and torque balances on the particle naturally yields the dynamical equations of motion, as in any classic problem of physics; the introductory problem of free-fall of the skydiver categorizes as one of such problems. And the stresslet represents the additional contribution to the bulk stress from the individual particles in the dispersion.

In principle the force is the manifestation of the overall rate of momentum transferred from the fluid to the particle, and it is obtained by direct calculation of the fluid stresses over the surface of the particle:

$$\boldsymbol{F} = \oint_{S_p} \boldsymbol{n} \cdot \boldsymbol{\sigma} \, \mathrm{d}S_p, \tag{2.5}$$

where $\boldsymbol{n}$ is the unit normal vector at any point on the particle surface, $\boldsymbol{\sigma}$ is the fluid stress (force per unit area), and $S_p$ is the surface area of the particle. The net torque on the particle is given by the first moment of the surface tractions:

$$\boldsymbol{T} = \oint_{S_p} \boldsymbol{x} \times (\boldsymbol{n} \cdot \boldsymbol{\sigma}) \, \mathrm{d}S_p, \tag{2.6}$$

where $\boldsymbol{x}$ is the position vector relative to the origin of the particle, which for a particle of arbitrary shape it may be calculated from any reference point. The stresslet is a quantity the general audience may be less familiar with; it encompasses the shape information of the particle, the distribution of the stresses at the particle surface, and the long-ranged nature of the disturbance field caused by the particle [13, 31]. Nevertheless, it is a quantity of fundamental importance to the determination of the bulk mechanical properties (or rheological properties) of colloidal dispersions. The stresslet is a second-rank tensor that unfolds from the second moment of the surface tractions:

$$\boldsymbol{S} = \oint_{S_p} \boldsymbol{x} \, (\boldsymbol{n} \cdot \boldsymbol{\sigma}) \, \mathrm{d}S_p. \tag{2.7}$$

These are the principal quantities of interest to study the dynamics and rheological properties of colloidal dispersions. In principle, this dissertation is devoted to the calculation of these quantities to gain insights on the behavior of a colloidal dispersion that consists of anisotropic particles. The subsequent chapters discuss this topic in greater detail, and therefore, it is only mentioned here.

A useful method to analyze the response of particles to low Reynolds number flows is the grand resistance matrix [31], because it summarizes the force, torque and stresslet on a particle undergoing solid-body motions in a general linear flow in an organized scheme:

$$\begin{pmatrix} \boldsymbol{F} \\ \boldsymbol{T} \\ \boldsymbol{S} \end{pmatrix} = \eta \begin{pmatrix} \boldsymbol{A} & \tilde{\boldsymbol{B}} & \tilde{\boldsymbol{G}} \\ \boldsymbol{B} & \boldsymbol{C} & \tilde{\boldsymbol{H}} \\ \boldsymbol{G} & \boldsymbol{H} & \boldsymbol{M} \end{pmatrix} \begin{pmatrix} \boldsymbol{U}^{\infty} - \boldsymbol{u} \\ \boldsymbol{\Omega}^{\infty} - \boldsymbol{\omega} \\ \boldsymbol{E}^{\infty} \end{pmatrix}, \tag{2.8}$$

where $(\boldsymbol{u} - \boldsymbol{U}^{\infty})$ and $(\boldsymbol{\omega} - \boldsymbol{\Omega}^{\infty})$ are the particle solid-body motions of translation and rotation, respectively, in a quiescent fluid, and $\boldsymbol{E}^{\infty}$ is the rate-of-strain tensor of the undisturbed flow. The grand resistance matrix consists of tensor quantities that solely depend on the shape of the particle. The tilde on top a tensor here denotes its transpose. The structure of the grand resistance matrix dictates that the resultant force on the particle is the sum of the forces that arise from the solid-body motions and the rate-of-strain of the undisturbed flow:

$$\boldsymbol{F} = \eta\, \boldsymbol{A} \cdot (\boldsymbol{U}^{\infty} - \boldsymbol{u}) + \eta\, \tilde{\boldsymbol{B}} \cdot (\boldsymbol{\Omega}^{\infty} - \boldsymbol{\omega}) + \eta\, \tilde{\boldsymbol{G}} : \boldsymbol{E}^{\infty}, \tag{2.9}$$

where the double-dot denotes the product of tensors [18], $\boldsymbol{A}$ is a second-rank tensor (with units of length $L$) commonly referred to as the translation tensor, $\boldsymbol{B}$ is the coupling tensor (a second-rank tensor with units of $L^2$), and $\boldsymbol{G}$ is the 'shear-force' tensor (a third-rank tensor with units of $L^2$). It is worth mentioning that solids of revolution (e.g. spheroidal particles) are characterized by zero coupling and 'shear-force' tensors on account of the fore and aft symmetry of the particle. As one may

suspect, the translation tensor is anisotropic for a spheroid; for example, a prolate spheroid experiences less frictional resistances from the fluid when it translates along its major axis (symmetry axis) in comparison to its minor axis. (The converse is true for an oblate spheroid.) And a solid sphere displays an isotropic translation tensor in agreement with the evident symmetry arguments; this is formally shown later in this chapter.

Similarly, the torque on the particle is given by:

$$\boldsymbol{T} = \eta\, \boldsymbol{B} \cdot (\boldsymbol{U}^{\infty} - \boldsymbol{u}) + \eta\, \boldsymbol{C} \cdot (\boldsymbol{\Omega}^{\infty} - \boldsymbol{\omega}) + \eta\, \tilde{\boldsymbol{H}} : \boldsymbol{E}^{\infty}, \tag{2.10}$$

where $\boldsymbol{C}$ is the rotation tensor (second-rank with units of $L^3$), and $\boldsymbol{H}$ is the 'shear-torque' tensor (third-rank tensor with units of $L^3$). And, finally, the expression for the stresslet on the particle is:

$$\boldsymbol{S} = \eta\, \boldsymbol{G} \cdot (\boldsymbol{U}^{\infty} - \boldsymbol{u}) + \eta\, \boldsymbol{H} \cdot (\boldsymbol{\Omega}^{\infty} - \boldsymbol{\omega}) + \eta\, \boldsymbol{M} : \boldsymbol{E}^{\infty}, \tag{2.11}$$

where $\boldsymbol{M}$ is a fourth-rank tensor with units of $L^3$.

The dynamical equations of particle motion in a general ambient flow under freely suspended conditions are obtained by requiring the overall force and torque to be zero ($\boldsymbol{F} = \boldsymbol{T} = \boldsymbol{0}$). Note that under freely suspended conditions there are no forces other than hydrodynamic ones; exceptionally, buoyant forces do not enter because it is implicit that the density of the particle and the fluid are equal to each other in these conditions. The force and torque–free condition of the particle is just a consequence of the absence of inertia in low Reynolds number flows. In general, a system of coupled differential equations that describe the position and orientation of the particle result from the force and torque–free conditions. This conveys the necessary information to know the positions and orientations of the particles in a colloidal dispersion. For particles of non-spherical shape the stresslet depends

intrinsically on the particle orientation relative to the undisturbed flow; hence the necessity of establishing dynamical equations for the particles in the dispersion.

So far, the linearity properties of low Reynolds number flows has been exposed by introducing the classic problem of a particle subject to a linear shear flow. It has been shown that a linear shear flow consists of a straining, rotating and uniform flow components, and that each component has individual contributions to the net force, torque and stresslet on the particle via the grand resistance matrix. Under freely suspended conditions there are no other forces and torques other than hydrodynamic ones, and since there are no inertia effects at low Reynolds number the resultant force and torque on the particle are zero. (This does not mean that the elemental contributions of the flow to the force and torque are zero; just the overall quantities.) And the importance of obtaining dynamical equations for the position and orientation is due to the fact that the stresslet depends on the orientation of the particle with respect to the undisturbed flow. As it will be shown in the subsequent chapters, this leads to non-Newtonian mechanical properties of colloidal dispersions that consists of anisotropic particles. This completes the overall and brief picture of the field to the general audience.

The rest of this chapter is devoted to the presentation of the fundamental problems considered in this dissertation. There are instances when the more general problems addressed in the subsequent chapters reduce to classic fluid mechanics problems, and therefore, it is appropriate to present them here in detail for the reader to gain an insightful view of the physics before exploring the more involved problems that await. In addition, the technical details of the solution to these fundamental problems are thoroughly shown to those interested in learning useful methods for solving fluid mechanics problems. Note that incorporation of these technical details into the corresponding chapters could disrupt their original narrative, and therefore, it is preferable to do so here. This chapter is organized as follows: in Section 2.2

there are various examples concerned on the solution of axisymmetric flow problems via the stream function—such as the classic problem of Stokes flow past a solid sphere. Section 2.3 is entirely devoted to the solution of 3D flow problems, which is of fundamental relevance to the understanding of the problems treated in the subsequent chapters. The chapter concludes with the calculation of the effective viscosity of a dilute dispersion of drops in a linear shear flow given in Section 2.4.

## 2.2 Axisymmetric flows

Axisymmetric flow problems are those that can be described fully by means of two velocity components. Problems that fall into this category are either planar or spherically symmetric. Of particular relevance to this dissertation, only the latter are discussed since fluid flow is analyzed about bodies of spherical shape (e.g. droplets). Fluid flow is spherically symmetric everywhere in the fluid if the flow only has radial and azimuthal components (i.e. $v_r, v_\vartheta$ with no dependence on the polar angle $\phi$) [13]. Note that spherically symmetric flows still have a 3D representation with respect to a system of Cartesian coordinates; therefore, only one can categorize a flow as spherically axisymmetric when expressed with respect to a system of spherical coordinates.

An outline of the problems addressed here is provided as follows. In Section 2.2.1 the classic problem of Stokes flow past a solid sphere is solved. The effect of relaxing the no-slip condition at the surface of the solid sphere is considered in Section 2.2.2. The flow inside and about a fluid droplet in Stokes flow is realized in Section 2.2.3, where it is demonstrated that there is no tendency of the fluid droplet to deform from its spherical shape in the absence of inertia effects. In 2.2.4 the subject of axisymmetric flows closes with the problem of elongational flow about a fluid droplet; distortions to the shape of the droplet are not considered here since it lies outside the scope of this dissertation.

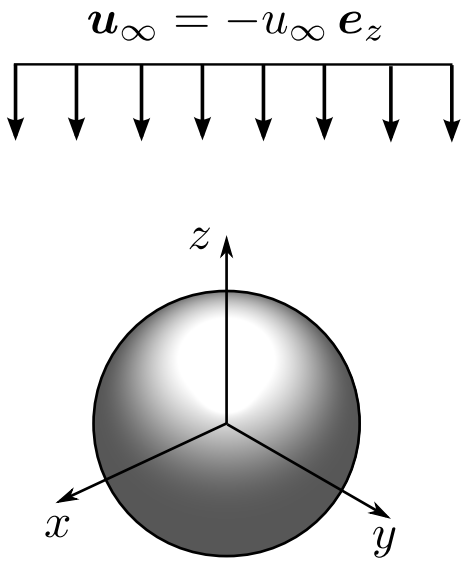


Figure 2–3: Solid sphere of radius $a$ immersed in a streaming fluid of viscosity $\eta$.

### 2.2.1 Stokes flow past a solid sphere

The problem of Stokes flow past a stationary solid-sphere is a classic fluid mechanics problem, and it is natural that it is considered first since it is used as a basis to solve other related problems, such as, the problem of Stokes flow past a fluid drop. The objective of this section is to show how to use the stream function to determine the flow (pressure and velocity fields) about a solid sphere subject to a uniform flow. Solution to the problem is finalized with the calculation of Stokes' law for the drag force on the solid sphere.

Figure 2–3 illustrates a sketch model of a solid sphere of radius $a$ immersed in a viscous fluid undergoing an axisymmetric streaming flow $\boldsymbol{u}_\infty = -u_\infty\, \boldsymbol{e}_z$ far away (Stokes flow problem). The index '0' denotes the ambient fluid. It is not really necessary to define an index for problems concerning a single fluid phase; however, it is reasonable to introduce it prior to dealing with multiphase flow problems. In mutiphase flow problems the convention to denote each fluid phase — with corresponding pressure and velocity fields — with a superscript will be taken; since there is only one fluid phase in this problem, it is omitted for clarity of the presentation. The objective is to find the fluid velocity $\boldsymbol{u}$ and pressure $p$ about the sphere. In

unbounded problems the direction of gravity is irrelevant, and therefore, the analysis can be carried out with respect to the dynamic pressure (the hydrostatic component of the pressure balances identically the gravitational forces) [13]. It is assumed that the solid sphere is subject to an incompressible flow and that the fluid is of Newtonian character (the viscosity of the fluid is independent of the shear rate). Under the mentioned conditions, the equations that govern fluid motion in the zero Reynolds number limit (absence of inertia) are expressed with respect to a system of spherical coordinates $(r, \vartheta, \phi)$:

$$\boldsymbol{\nabla} p = \eta \nabla^2 \boldsymbol{u}, \quad \boldsymbol{\nabla} \cdot \boldsymbol{u} = 0, \tag{2.12a}$$

$$u_r = 0, \; u_\vartheta = 0, \quad \text{at} \quad r = a, \tag{2.12b}$$

$$\boldsymbol{u} = -u_\infty \boldsymbol{e}_z, \quad \text{as} \quad r \to \infty, \tag{2.12c}$$

where $\eta$ is the viscosity of the ambient fluid. The surface of the sphere is impenetrable such that there cannot be fluid flow through it ($u_r = 0$). In addition, the fluid does not 'slip' about the surface of the sphere $u_\vartheta = 0$ (fluids tend to match the velocity of the solid tangent to its surface). The no-slip condition has been verified to hold in a substantial number of experiments, and therefore, it is regarded as a plausible assumption in most practical settings [13, 32]. Nevertheless, the presence of microscopic imperfections or defects at the surface of a solid may cause the nearby fluid to undergo an apparent slip-velocity [33]. However, for the time being we restrict our attention to scenarios where the no-slip condition remains valid. In section 2.2.2 the problem of Stokes flow past a solid sphere with a slip surface is considered.

It is straightforward to see that there is a uniform pressure far away from the solid sphere by applying the creeping flow equation to the far field flow: $\boldsymbol{\nabla} p_\infty = \eta \nabla^2 \boldsymbol{u}_\infty = \boldsymbol{0}$ (because $\boldsymbol{u}_\infty$ is a constant vector field). Clearly, $p_\infty$ must be a constant for $\boldsymbol{\nabla} p_\infty = \boldsymbol{0}$, and moreover, $p_\infty$ may be safely set to zero in unbounded problems

like this one because it does not alter the flow nor the drag force on the solid sphere. The latter statement holds even for bodies of arbitrary shape; it is well known that a uniform pressure field imposes a zero net force about completely submerged bodies [13]. For example, the spherical cap (which lacks fore and aft symmetry) experiences a zero net force in a uniform pressure field; the reader may refer to Appendix A.1, where it is shown that the force on the curved surface cancels identically the force on its planar counterpart.

It is worthwhile to notice that the flow about the solid sphere is axisymmetric; that is, $u_\phi = 0$ and $u_r$ and $u_\vartheta$ are independent $\phi$ everywhere. This can be deduced by taking into account that the flow far away is solely described by two velocity components ($\boldsymbol{u}_\infty = -u_\infty \boldsymbol{e}_z = -u_\infty \cos\vartheta\, \boldsymbol{e}_r + u_\infty \sin\vartheta\, \boldsymbol{e}_\vartheta$) and that the body is spherically symmetric. Under those conditions, there is no reason to have any dependence of $u_r$ and $u_\vartheta$ on the polar angle (since $\boldsymbol{u}_\infty$ is independent of $\phi$) nor a flow in the $\phi$-direction ($v_\phi = 0$). The latter is the case since the solid sphere is not subject to rotational motions (fixed). Hence, the necessary conditions for an axisymmetric flow are met.

The velocity components are related to the stream function $\psi(r, \vartheta)$ via the expressions:

$$u_r = \frac{1}{r^2 \sin\vartheta} \frac{\partial \psi}{\partial \vartheta}, \quad u_\vartheta = -\frac{1}{r \sin\vartheta} \frac{\partial \psi}{\partial r}. \tag{2.13}$$

Rewriting the governing equations and corresponding boundary conditions with respect to the stream function yields a simpler boundary value problem:

$$E^4 \psi(r, \vartheta) = 0, \tag{2.14a}$$

$$\psi = 0, \ \frac{\partial \psi}{\partial r} = 0, \quad \text{at} \quad r = a, \tag{2.14b}$$

$$\psi = -\frac{1}{2} u_\infty r^2 \sin^2\vartheta, \quad \text{as} \quad r \to \infty. \tag{2.14c}$$

Note that the above boundary conditions were obtained by transforming the velocity components with respect to the stream function. The reader interested in the steps taken to carry out the transformation is referred to Appendix A.2.

The advantage of the stream function formulation is that the fluid flow problem is now solved without directly dealing with the pressure field. Moreover, the mathematical problem is reduced to the determination of a scalar function $\psi(r, \vartheta)$. In the untransformed problem one has to solve two components of the creeping flow equation, the equation of continuity and the Laplace equation for the pressure field simultaneously; this is a daunting task even for this apparently simple problem.

The usual approach chosen by many authors is to determine a solution to the Stokes flow problem past a sphere by proposing the form of the stream function to be $\psi(r, \vartheta) = f(r) \sin^2 \vartheta$, and obtain an equidimensional equation of fourth order for $f(r)$ by application of $E^4\psi = 0$. Then, the boundary conditions given in Equation (2.14) are redefined for the scalar function $f(r)$ and used to obtain a closed-form solution for the stream function. The reader interested in following the classic procedure is referred to [13]. Instead, the solution strategy presented here is to make use of the generalized solution of the stream function for axisymmetric problems.

For axisymmetric flows, the generalized solution of the stream function is well known [20]:

$$\psi(r, \vartheta) = \sum_{n=2}^{\infty} \left[ A_n r^{n+2} + B_n r^n + C_n r^{3-n} + D_n r^{1-n} \right] \mathscr{I}_n(\vartheta), \tag{2.15}$$

where $\mathscr{I}_n(\vartheta)$ is the *nth* order Gegenbauer function of degree $-1/2$. For convenience the first few Gegenbauer functions are shown below:

$$\mathscr{I}_0(\vartheta) = 1, \quad \mathscr{I}_1(\vartheta) = -\cos\vartheta, \tag{2.16}$$

$$\mathscr{I}_2(\vartheta) = \frac{1}{2}\sin^2\vartheta, \quad \mathscr{I}_3(\vartheta) = \frac{1}{2}\sin^2\vartheta\cos\vartheta. \tag{2.17}$$

(For linear flows, such as this one, higher orders of the Gegenbauer functions are not needed.) The reader may find that the general solution provided by Deen [13] initiates at order $n = 1$ and that some of the expressions of the Gegenbauer functions differ from those presented here. Nonetheless, for the purposes of solving linear axisymmetric flows both solutions are equivalent. Solutions in the range $0 \leq n \leq 1$, generally, have no physical relevance, as discussed by Happel & Brenner [20].

It is instructive to consider the far field condition first in unbounded problems because it usually incurs in considerable simplifications of the generalized solution. From the far field condition (2.14c) it is deduced that only the second order of the Gegenbauer function $\mathscr{I}_2(\vartheta) = -\sin^2\vartheta/2$ is needed to describe the flow about the sphere. (The minus sign introduced in $\mathscr{I}_2(\vartheta)$ is incorporated as a matter of convenience; it does not affect the final solution nor the direction of the flow.) Consider that all other coefficients associated with higher orders of the Gegenbauer function are unnecessary ($A_n = B_n = C_n = D_n = 0$ for $n > 2$). Moreover, for the stream function to scale as $r^2$ at distances far from the sphere ($r \to \infty$) the leading coefficient $A_2$ cannot be retained because it grows more rapidly than the far field. Performing the mentioned simplifications on the generalized solution (2.15) yield the stream function that describes the flow past the sphere:

$$\psi(r,\vartheta) = -\frac{1}{2}\left[B_2\, r^2 + C_2\, r + D_2\, r^{-1}\right]\sin^2\vartheta. \tag{2.18}$$

Note that now the number of unknown coefficients $(B_2, C_2, D_2)$ in the generalized solution match identically the number of boundary conditions presented in Equation (2.14) — a fully determined system of independent equations is obtained.

From the far field condition it is easy to see that $B_2 = u_\infty$ by noting that $r^{-1}$ decays to zero and that the $C_2$ term only grows linearly with position in the far field limit ($r \gg a$). Therefore the leading order of the stream function in the far field limit is $\psi = -B_2\, r^2 \sin^2\vartheta/2$, and to match $\psi_\infty = -u_\infty\, r^2 \sin^2\vartheta/2$ the coefficient

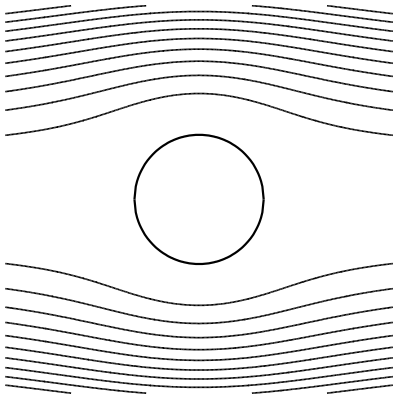

Figure 2–4: The streamlines about the solid sphere.

$B_2 = u_\infty$. Application of the no-penetration and no-slip conditions at the surface of the sphere results in the following system of linear equations for the coefficients $C_2, D_2$:

$$-a^2\, u_\infty - \frac{1}{2} a\, C_2 + \frac{1}{2} a^{-1}\, D_2 = 0, \tag{2.19}$$

$$-\frac{1}{2} a^2\, u_\infty - \frac{1}{2} a\, C_2 - \frac{1}{2} a^{-1}\, D_2 = 0, \tag{2.20}$$

where the values of the coefficients that satisfy the set of linear equations are:

$$C_2 = -\frac{3}{2} a\, u_\infty, \quad D_2 = \frac{1}{2} a^3\, u_\infty. \tag{2.21}$$

With the obtained values the stream function that describes the flow about the solid sphere reads:

$$\psi(r, \vartheta) = -\frac{1}{2}\left[u_\infty\, r^2 - \frac{3}{2} a\, u_\infty\, r + \frac{1}{2} a^3\, u_\infty\, r^{-1}\right] \sin^2 \vartheta, \tag{2.22}$$

where it is easy to see that the stream function satisfies the boundary value problem (2.14). An illustration of the streamlines of the disturbance flow caused by the solid sphere is shown in figure 2–4.

After some elementary steps the velocity components are obtained by substitution of the stream function into Equation (2.13):

$$u_r(r,\vartheta) = u_\infty \left[-1 + \frac{3}{2}\left(\frac{a}{r}\right) - \frac{1}{2}\left(\frac{a}{r}\right)^3\right] \cos\vartheta, \tag{2.23a}$$

$$u_\vartheta(r,\vartheta) = u_\infty \left[1 - \frac{3}{4}\left(\frac{a}{r}\right) - \frac{1}{4}\left(\frac{a}{r}\right)^3\right] \sin\vartheta. \tag{2.23b}$$

It is readily seen that the velocity components satisfy the no-penetration and no-slip tangent at the surface of the sphere ($r = a$), and that the undisturbed streaming velocity $u^\infty_{r,\vartheta}$ is recovered at distances far from the sphere ($r \gg a$).

The drawback of the stream function formulation is that determination of the pressure field $p(r,\vartheta)$ is a rather cumbersome task. Nonetheless, it can be found by introducing the velocity components into either the radial or azimuthal component of the creeping flow equation. It is convenient to choose the azimuthal component of the creeping flow equation in order to determine that the integration constant that arises for the pressure is zero:

$$p(r,\vartheta) = \frac{3}{2}\frac{\eta\, u_\infty}{a}\left(\frac{a}{r}\right)^2 \cos\vartheta + \mathscr{C}(r), \tag{2.24}$$

where the integration constant is formally a scalar function of position $\mathscr{C}(r)$ because integration takes over the azimuthal dimension. The important observation is that $\mathscr{C}(r)$ cannot be a function of position because the pressure is uniform far away from the solid sphere: $\mathscr{C}(r) = p_\infty$. The reader may verify that introduction of the velocity field on the radial component of the creeping flow equation yields the same expression for the pressure, as above, but with an integration constant that depends on the azimuthal angle. Since the solution for the pressure field is unique and the integration constant cannot be both a function of position and the azimuthal angle, it is inferred that $\mathscr{C}$ can only take a constant value. Moreover, the integration constant may be set to zero because the magnitude of the far field pressure is irrelevant for the purposes of determining the flow and drag force on the solid sphere. Thus, the

pressure field about the solid sphere reads:

$$p(r,\vartheta) = \frac{3}{2}\frac{\eta\, u_\infty}{a}\left(\frac{a}{r}\right)^2 \cos\vartheta. \tag{2.25}$$

From the form of the pressure field it is interpreted that the fluid encounters a pressure build-up at the upstream face of the sphere and a region of low pressure at the downstream face (in both regions the pressure 'retards' fluid motion).

It is of interest to calculate the net drag force imparted by the fluid on the solid sphere. For example, in the problem of sedimentation of a solid sphere, the gravitational force is balanced by the drag force to obtain the velocity of sphere. The drag force is determined by integration of the fluid stresses that act normal to the surface of the sphere:

$$\boldsymbol{F} = \oint_{S_p} \boldsymbol{n}\cdot\boldsymbol{\sigma}\,\mathrm{d}S_p, \tag{2.26}$$

where $\boldsymbol{F}$ is the force, $S_p$ is the surface of the sphere, $\boldsymbol{\sigma} = -p\,\boldsymbol{\delta} + \boldsymbol{\tau}$ is the total stress that consists of an isotropic contribution from the pressure and another from the viscous properties of the fluid, which is known as the deviatoric (or viscous) stress $\boldsymbol{\tau}$. For a Newtonian fluid the viscous stress tensor is given by:

$$\boldsymbol{\tau} = \; 2\,\eta\,\boldsymbol{\Gamma} = \eta\Big(\boldsymbol{\nabla u} + (\boldsymbol{\nabla u})^t\Big), \tag{2.27}$$

where $\boldsymbol{\Gamma}$ is the rate-of-strain tensor, and here $t$ denotes the transpose operator.

Owing to the spherical symmetry of the body, there can be no drag force transversal to the direction of the undisturbed flow (i.e. $F_x = F_y = 0$) and therefore, one only needs to calculate the $z$-component of the force:

$$F_z = \boldsymbol{e}_z \cdot \left[\oint \left(-p\,\boldsymbol{e}_r + \tau_{r\vartheta}\,\boldsymbol{e}_\vartheta\right)\,\mathrm{d}S\right], \tag{2.28}$$

where $\tau_{r\vartheta}$ is the shear stress. Note that $\tau_{rr}$ has been omitted above because it is well known that this component of the viscous stress vanishes at solid surfaces [13] (which is a direct consequence of the no-slip and impenetrability conditions). The

shear stress at the surface of the solid sphere ($r = a$) is calculated via [13]:

$$\tau_{r\vartheta} = \eta \left[ r \frac{\partial}{\partial r} \left( \frac{u_\vartheta}{r} \right) + \frac{1}{r} \left( \frac{\partial u_r}{\partial \vartheta} \right) \right], \tag{2.29}$$

where $\partial_\vartheta u_r = 0$ at $r = a$ because of the impenetrability condition $u_r(r = a, \vartheta) = 0$. (Hence, no variations all over the surface of the sphere.) Therefore, the viscous shear stress at contact reads:

$$\tau_{r\vartheta}(r = a, \vartheta) = \eta \, r \partial_r (u_\vartheta / r) = \frac{3}{2} \frac{\eta \, u_\infty}{a} \sin \vartheta. \tag{2.30}$$

Now that the non-vanishing components of the total stress (the pressure and the viscous shear stress) have been found at the surface of the sphere, calculation of the drag force proceeds by introducing $\boldsymbol{e}_z$ (constant vector) into the surface integral and performing the following elementary calculations:

$$\begin{aligned} F_z &= - \oint \Big( p \, \cos \vartheta + \tau_{r\vartheta} \, \sin \vartheta \Big) \, \mathrm{d}S, \\ &= - \int_0^{2\pi} \int_0^{\pi} \Big( p \, \cos \vartheta + \tau_{r\vartheta} \, \sin \vartheta \Big) a^2 \sin \vartheta \, \mathrm{d}\vartheta \mathrm{d}\phi, \\ &= - \, 2\pi a^2 \int_0^{\pi} \Big( p \, \cos \vartheta + \tau_{r\vartheta} \, \sin \vartheta \Big) \sin \vartheta \, \mathrm{d}\vartheta, \\ &= - \, 3\pi \, a \eta \, u_\infty \int_0^{\pi} \Big( \cos^2 \vartheta + \sin^2 \vartheta \Big) \sin \vartheta \, \mathrm{d}\vartheta, \\ &= - \, 3\pi \, a \eta \, u_\infty \int_0^{\pi} \sin \vartheta \, \mathrm{d}\vartheta, \\ &= - \, 6\pi \, a \eta \, u_\infty, \end{aligned} \tag{2.31}$$

where the well-known Stokes' law is obtained for the drag force on a solid sphere subject to a streaming flow in the zero Reynolds limit. Note that the scalar products $\boldsymbol{e}_z \cdot \boldsymbol{e}_r = \cos \vartheta$ and $\boldsymbol{e}_z \cdot \boldsymbol{e}_\vartheta = - \sin \vartheta$ have been carried out to obtain Stokes' law.

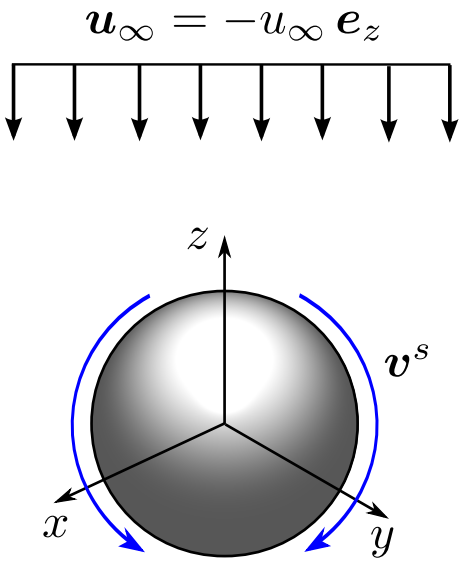


Figure 2–5: Axisymmetric streaming flow $\boldsymbol{u}_\infty$ of a viscous fluid (of viscosity $\eta$) about a solid sphere of radius $a$ subject to a 'slip' velocity $\boldsymbol{v}^s$ at its surface.

### 2.2.2 Stokes flow past a solid sphere subject to a superficial 'slip' velocity

The objective of this section is to determine the pressure field $p$, the velocity field $\boldsymbol{u}$, and drag force $\boldsymbol{F}$ on a solid sphere with a 'slip' surface under the action of an axisymmetric streaming flow $\boldsymbol{u}_\infty = -u_\infty\,\boldsymbol{e}_z$. A schematic representation of the system of interest is provided in figure 2–5 Currently, there is substantial experimental evidence that shows the no-slip condition to break down when the length scale of the particle (or channel in bounded flows) $a$ scales with the 'slipping' length $\lambda$, or in terms of dimensionless groups, when the Knudsen number is finite ($\mathrm{Kn} = \lambda/a \geq 1$) [34]. For gases, the 'slipping' length corresponds to the mean free path of the molecules between collisions. Unfortunately, no unified molecular interpretation of the 'slipping' length exists for liquids; because, the corresponding mean free path is several orders of magnitude smaller than the 'slipping' length found in experiments. Nevertheless, the 'slip' velocity for liquids can be still described by an effective Knudsen number identical to that for gases. The reader interested in reviewing the experimental studies that demonstrate the occurrence of a 'slip' velocity is referred to the selected number of publications [35–39].

The most used phenomenological expression to describe the 'slip' velocity at surfaces is that of Navier [40], where the 'slip' velocity is a function of the 'slip' length and the local shearing-rate at the surface of the solid:

$$\boldsymbol{v}^s = 2\lambda \left(\boldsymbol{\delta} - \boldsymbol{nn}\right) \cdot \boldsymbol{\Gamma} \cdot \boldsymbol{n}, \tag{2.32}$$

where $\boldsymbol{v}^s$ is the 'slip' velocity at the surface of the solid (it is implied that the solid is at rest), and $\Gamma_{jk} = \left(\nabla_j u_k + \nabla_k u_j\right)/2$ is the rate-of-strain tensor. (The dot products indicate that only the shearing component of the rate-of-strain tensor normal to the surface of the solid is accountable for the observed 'slip' velocity.) Note that in the limit of $\lambda \ll 1$ the no-slip condition is restored, and in the opposite extreme ($\lambda \gg 1$) the solid is characterized by a 'perfect slip' surface of negligible resistance to the flow — analogous to an air–liquid interface. It will be shown in section 2.2.3 that the drag force on a sphere with a 'perfect slip' surface ($\lambda \gg 1$) subject to a uniform flow is identical to the drag force on a spherical bubble (or equivalently, a drop of low viscosity compared to the ambient one).

A number of theoretical studies have examined fluid flow about solid surfaces subject to the Navier 'slip' condition. Basset [41] was the first to obtain a solution to the problem of Stokes flow about a 'slip' sphere. Lauga & Squires [34] studied the Brownian motion of a probe particle near a 'slip' wall. Willmott [42] analyzed the Stokes flow about a solid sphere with an inhomogeneous 'slip' at its surface. The motion of a 'slip' sphere about a solid wall was investigated by Luo & Pozrikidis [43]. Swan & Khair derived Faxén-type expressions to characterize the hydrodynamics of "slip–stick" spheres (only a fraction of the sphere 'slips'). Subsequently, Ramachandran & Khair [44] studied the dynamics and effective viscosity of a dilute suspension of "slip–stick" spheres in linear flows.

Here, it is proceed by following an analogous scheme to that of Stokes flow past a solid sphere with the no-slip condition (section 2.2.1). First, a constitutive-type expression for the 'slip' velocity in terms of the shear stress is derived for this particular problem. Then, the governing equations of fluid motion are modified to account for the Navier 'slip' at the surface of the sphere. Followed by introduction of the stream function to obtain expressions for the velocity and pressure fields. Calculations finalize with determination of the drag force imparted by the fluid on the 'slip' sphere. For the sake of being concise, many of the expressions given in section 2.2.1 are alluded.

It is advantageous to define the rate-of-strain tensor $\boldsymbol{\Gamma}$ with respect to the viscous stress tensor $\boldsymbol{\tau}$ via Equation (2.27), such that the Navier 'slip' velocity now reads:

$$\boldsymbol{v}^s = \frac{\lambda}{\eta}\,(\boldsymbol{\delta} - \boldsymbol{nn}) \cdot \boldsymbol{\tau} \cdot \boldsymbol{n}. \tag{2.33}$$

Performing the scalar products on the viscous stress tensor reveals that the 'slip' velocity depends only on the shear component of the stress at the surface of the sphere:

$$\boldsymbol{v}^s = \frac{\lambda}{\eta}\tau_{r\vartheta}\,\boldsymbol{e}_\vartheta \quad \text{at} \quad r = a. \tag{2.34}$$

Note that the above expression for the 'slip' velocity indicates that it is tangent to the surface of the sphere along the $\vartheta$-axis (the axisymmetric character of the flow implies no flows along the $\phi$-axis). Moreover, it is easy to see that $v_r^s = 0$, as it should, because of the orthogonality of the unit vectors ($\boldsymbol{e}_r \cdot \boldsymbol{e}_\vartheta = 0$). The 'slip' velocity is further simplified by introducing the definition of the shear stress given in Equation (2.29) into the above expression:

$$v^s = u_\vartheta = \lambda\, r \frac{\partial}{\partial r}\left(\frac{u_\vartheta}{r}\right) \quad \text{at} \quad r = a, \tag{2.35}$$

where it has been noted that $\partial_\vartheta v_r = 0$ because of the no-penetration condition at the surface of the 'slip' sphere ($r = a$).

The boundary value problem that describes the flow about the 'slip' sphere is analogous to that of a solid sphere with the exception that now there is velocity tangent to the surface of the sphere:

$$\boldsymbol{\nabla} p = \eta \nabla^2 \boldsymbol{u}, \quad \boldsymbol{\nabla} \cdot \boldsymbol{u} = 0, \tag{2.36a}$$

$$u_r = 0, \; u_\vartheta = \lambda\, r \frac{\partial}{\partial r}\left(\frac{u_\vartheta}{r}\right), \quad \text{at} \quad r = a, \tag{2.36b}$$

$$\boldsymbol{u} = -u_\infty \boldsymbol{e}_z, \quad \text{as} \quad r \to \infty. \tag{2.36c}$$

As in the problem of Stokes flow past a sphere, the problem is axisymmetric. The existence of a 'slip' velocity at the surface of the sphere does not affect the axisymmetric character of the external flow. (Nonetheless, an inhomogeneous distribution of the 'slip' condition at the surface of the sphere would certainly break the symmetry of the flow.) Therefore, the stream function is introduced to solve the fluid flow problem:

$$E^4 \psi(r, \vartheta) = \; 0, \tag{2.37a}$$

$$\psi = \; 0, \; \frac{1}{r^2}\frac{\partial \psi}{\partial r} = \lambda \frac{\partial}{\partial r}\left[\frac{1}{r^2}\frac{\partial \psi}{\partial r}\right], \quad \text{at} \quad r = a, \tag{2.37b}$$

$$\psi = -\frac{1}{2} u_\infty\, r^2 \sin^2 \vartheta, \quad \text{as} \quad r \to \infty. \tag{2.37c}$$

Once again, the far field condition indicates that the second order Gegenbauer functions are needed to describe the flow everywhere, such that the general form of the stream function reads:

$$\psi(r, \vartheta) = -\frac{1}{2}\left[B_2\, r^2 + C_2\, r + D_2\, r^{-1}\right] \sin^2 \vartheta. \tag{2.38}$$

To satisfy the far field condition, it is evident that $B_2 = u_\infty$, which leaves $C_2$ and $D_2$ to be determined by the set of algebraic equations that arise from the 'slip' and

no-penetration conditions:

$$a^{-1}u_\infty + a^{-2}C_2 + a^{-4}D_2 = 0, \tag{2.39a}$$

$$2a^{-1}u_\infty(1+\lambda/a) + a^{-2}C_2(1+2\lambda/a) - a^{-4}D_2(1+4\lambda/a) = 0. \tag{2.39b}$$

Note that the algebraic expression that arises from the no-penetration condition (2.39a) has been scaled by a factor of $a^{-3}$ to match the units of its counterpart (2.39b), and that $\lambda/a$ is a non-dimensional quantity. The set of algebraic equations for the unknown constants is linearly independent. Simultaneous solution of the above set yields the following values for the coefficients:

$$C_2 = -\frac{3}{2}a\,\frac{1+2\lambda/a}{1+3\lambda/a}\,u_\infty, \quad D_2 = \frac{1}{2}a^3\,\frac{1}{1+3\lambda/a}\,u_\infty. \tag{2.40}$$

As one may expect, it verifies that in the limit of $\lambda/a \to 0$ the values of the coefficients approach asymptotically those of the solid sphere with a no-slip surface (2.21).

The stream function for the solid sphere subject to a 'slip' velocity at its surface reads:

$$\psi(r,\vartheta) = -\frac{1}{2}u_\infty\left[r^2 - \frac{3}{2}\,a\left(\frac{1+2\lambda/a}{1+3\lambda/a}\right)r + \frac{1}{2}\,a^3\left(\frac{1}{1+3\lambda/a}\right)r^{-1}\right]\sin^2\vartheta. \tag{2.41}$$

Figure 2–6 illustrates that the disturbanced flow caused by the presence of the 'slip' sphere is qualitatively similar to that of a solid sphere. Of course, this is the expected result even for $\lambda/a \gg 1$; marked differences in the streamlines would be observed in the $\lambda/a \gg 1$ limit if the $r$ term vanished instead of $r^{-1}$. Then, the flow about the 'slip' sphere would be irrotational (or potential) in nature.

The corresponding velocity components are found to be equal to:

$$u_r = -u_\infty\left[1 - \frac{3}{2}\,\frac{1+2\lambda/a}{1+3\lambda/a}\left(\frac{a}{r}\right) + \frac{1}{2}\,\frac{1}{1+3\lambda/a}\left(\frac{a}{r}\right)^3\right]\cos\vartheta, \tag{2.42a}$$

$$u_\vartheta = u_\infty\left[1 - \frac{3}{4}\,\frac{1+2\lambda/a}{1+3\lambda/a}\left(\frac{a}{r}\right) - \frac{1}{4}\,\frac{1}{1+3\lambda/a}\left(\frac{a}{r}\right)^3\right]\sin\vartheta. \tag{2.42b}$$

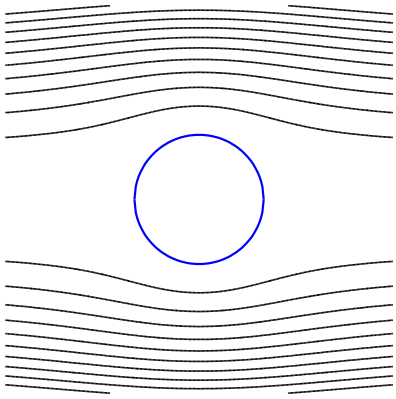

Figure 2–6: Streamlines about a solid sphere with a 'slip' length $\lambda/a = 5$.

Determination of the pressure field follows analogous arguments to those used for the solid sphere with a no-slip surface:

$$p = \frac{3}{2}\frac{\eta u_\infty}{a}\left(\frac{a}{r}\right)^2 \frac{1+2\lambda/a}{1+3\lambda/a}\cos\vartheta. \tag{2.43}$$

Instead of carrying out the tedious task of integrating the normal stresses at the surface of the sphere to calculate the drag force, the well known expression for the drag force on a body subject to an axisymmetric flow is used [13, 31]:

$$F_z = 4\pi\eta C_2 = -6\pi a\eta u_\infty \left(\frac{1+2\lambda/a}{1+3\lambda/a}\right). \tag{2.44}$$

As expected, in the limit $\lambda/a \ll 1$ the drag force approaches that of a no-slip sphere. In the opposite extreme of $\lambda/a \gg 1$ the surface of the sphere behaves as a 'free' streaming surface with a drag force equal to that of a spherical bubble (Section 2.2.3):

$$F_z = -4\pi a\eta u_\infty. \tag{2.45}$$

Analogous to the solid sphere, the only non-vanishing component of the drag force is the $z$-component ($F_x = F_y = 0$), which is clear from evident symmetry arguments. There are no means for the fluid to impose a net force lateral to the direction of the streaming velocity; an analysis of the lateral forces on the hemispherical domain of the sphere ($z > 0$) would reveal that the force on its counterpart is of equal

magnitude but opposite in direction. In Section 2.3.1 it is demonstrated that the drag force always acts in the direction of the undisturbed flow; this is because the solid sphere offers an isotropic resistance to the streaming flow.

### 2.2.3 Stokes flow about a fluid drop or bubble

The objective of this section is to determine the flows inside and outside a spherical drop (or bubble) subject to Stokes flow (zero inertia effects). The analysis presented here will be useful to the understanding of the dynamics of multiphase systems considered in this dissertation. From this point onward the expression 'fluid sphere' will be used to refer to both the drop and the bubble in a general sense; wherever needed, the distinction between the two will be made.

An understanding of the motions of drops and bubbles is of broad relevance to diverse areas of engineering and multi-disciplinary research. For example, heat and mass transfer phenomena in multiphase systems (e.g. direct-contact exchangers) [7] and liquid–liquid extraction processes [45] depend, intrinsically, on the motions of the bubbles or drops in contact with the bulk phase. Heterogeneous systems comprised of a continuous fluid phase and a dispersed phase of another fluid (emulsions) have been found to exhibit shear-dependent viscosity and viscoelasticity owing to the individual motions and shape distortions of the dispersed phase [46, 47]. Also, the stability of emulsions is affected to some extent by the motions of the dispersed phase [48]. The phenomenological understanding of the influence of walls (or channels) over the motion of drops has been of importance to model the flow of complex fluids (e.g. flow in blood vessels) [49]. Lastly, the use of *Marangoni*-driven flows (from gradients in interfacial tension) has been explored for the processing of materials in space shuttles [50].

The problem of Stokes flow past a fluid sphere is a classic fluid mechanics problem present in many texts [13, 16, 20, 31]. The original treatment of the subject is by Hadamard [51] and Rybczynski [52], who independently analyzed the motion

of a fluid sphere in a quiescent fluid at zero Reynolds number (absence of inertia effects). It is important to point out that fluid flow problems concerning drops (or bubbles) are free-surface problems that require the simultaneous solution of the internal and outer flows along with the shape of the fluid–fluid interface. The criteria for the determination of the shape of the fluid–fluid interface is that the jump in the normal stresses must be zero there. Generally, no analytical progress can be made to determine simultaneously the shape, and the internal and outer flows; except in the limit of small deviations from the equilibrium shape. In those cases, the distorted shape can be determined via a perturbation technique [53–56]. The opposite extreme of substantial shape-distortions can also be treated analytically via slender-body theory [57]. For intermediate deformations, one has to resort to numerical calculations such as the boundary integral method [58].

Experimental observations have shown that fluid drops (or bubbles) adopt a spherical shape in the absence of fluid motion to minimize their surface energy [11, 13, 59], and that a streaming flow has no tendency to distort the spherical shape in the absence of inertia effects [53]. It turns out that the streaming flow produces no jumps in the normal stresses across the fluid–fluid interface that would otherwise deflect the interface until a balance is reached. Therefore, the analysis presented here that considers the flows in and about a drop (or bubble) is analogous to that of a solid sphere in the sense that the shape is 'known'. In contrast to the problem of Stokes flow past a solid sphere, the gravitational force is included in the governing equations for reasons that will become apparent later. The analysis concludes by showing that the jump in the normal stresses at the fluid–fluid interface is identically zero for completeness.

Figure 2–7 depicts a diagram of a drop (or bubble) of density $\rho_1$ suspended in a viscous fluid of density $\rho_0$ undergoing an axisymmetric streaming flow far away. The

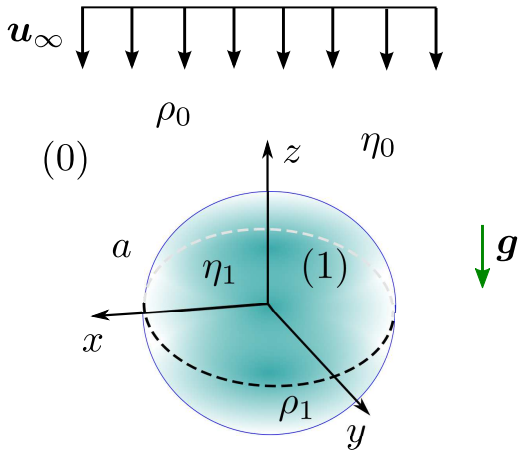


Figure 2–7: Axisymmetric uniform flow $\boldsymbol{u}_\infty$ of a viscous ambient fluid '0' about a fluid sphere '1' of radius $a$. The dynamic viscosity and density of each fluid phase is represented by $\eta_j$ and $\rho_j$, respectively, where $j = 0, 1$. The vector $\boldsymbol{g}$ denotes the gravitational field.

indexes '0' and '1' denote the ambient and internal fluids, respectively. Conventionally, it is assumed that gravity acts in the opposite sense of the $z$-axis ($\boldsymbol{g} = -g\,\boldsymbol{e}_z$) and that the fluid sphere is suspended in a denser ambient fluid ($\rho_1 < \rho_0$) such that the sphere experiences a lift from the net buoyant force. The uniform flow far away is just the manifestation of taking a reference frame moving with the fluid sphere: $\boldsymbol{u}_\infty = -u_\infty \boldsymbol{e}_z$. It is assumed that the fluids are immiscible (no mixing of the fluid phases) and Newtonian (the viscous properties remain constant regardless of the local velocity gradients). The dynamic viscosity and density of the *jth* fluid phase are denoted, respectively, by $\eta_j$ and $\rho_j$; $j = 0, 1$. The assumption of incompressible flow is assumed to hold on each fluid phase (Considering that the characteristic velocity $u_\infty$ would have to be comparable with the velocity of sound for compressibility to occur, it is highly unlikely that it would be an important factor in the creeping motion limit.) Moreover, it is assumed that the fluid–fluid interface is free of surfactant agents; the presence of surfactants in experiments have been shown to result in discrepancies with the theory because of a reduction in the interfacial velocity [60, 61].

It is instructive to start the analysis under hydrostatic conditions $\left(\boldsymbol{u}^{(j)} = \mathbf{0}\right)$. Since in this particular problem fluid motion arises from buoyancy effects, hydrostatic conditions can only occur in the absence of gravity $\boldsymbol{g} = \mathbf{0}$; moreover, this also implies that each fluid phase is characterized by a uniform pressure: $p^{(1)} = \hat{p}$, $p^{(0)} = p_\infty$. A balance of the normal stresses at the fluid–fluid interface dictates that:

$$\sigma_{nn}^{(1)} - \sigma_{nn}^{(0)} + p_\gamma = 0, \tag{2.46}$$

where $p_\gamma = -2\mathscr{H}\gamma$ is the capillary pressure, $\mathscr{H} = -a^{-1}$ is the mean curvature for a sphere, and $\gamma$ is the interfacial tension of the fluid–fluid interface. Replacement of the stress with that of a Newtonian fluid gives:

$$\left(-p^{(1)} + \tau_{nn}^{(1)}\right) - \left(-p^{(0)} + \tau_{nn}^{(0)}\right) + \frac{2\gamma}{a} = 0. \tag{2.47}$$

Since the viscous part of the stress tensor is identically zero under hydrostatic conditions $\left(\tau_{nn}^{(j)} = 0\right)$, the above expression simplifies to a balance of the internal and outer pressure with the capillary pressure:

$$\hat{p} - p_\infty = \frac{2\gamma}{a}. \tag{2.48}$$

This expression is commonly known in the literature as the Young-Laplace equation [13]; and it shows that a drop (or bubble) undertakes a spherical shape in the absence of external flows.

Under conditions of fluid motion, the underlying physics of the fluid–fluid interface require the velocity and stresses tangent to the interface to be continuous from the outer to the inner fluid. The deflection of the interface from its equilibrium shape under hydrostatic conditions is determined by the jump in the normal stresses at each point along the interface. It will be demonstrated that for a fluid sphere under Stokes flow the jump in normal stresses is zero $\left(\sigma_{nn}^{(1)} - \sigma_{nn}^{(0)} = 0\right)$ in the absence of inertia; that is, the flow does not distort the spherical shape of the

drop (or bubble). The immiscibility of the fluids dictates that no flow can penetrate through the fluid–fluid interface. From these physical arguments, it is evident that fluid motion must be analyzed in both the internal and ambient fluids. In the limit of zero inertia, the flow of each fluid phase is governed by the Stokes equations (shown with respect to spherical coordinates $(r, \vartheta, \phi)$ for convenience):

$$\boldsymbol{\nabla} p^{(j)} = \eta_j \nabla^2 \boldsymbol{u}^{(j)} + \rho_j \, \boldsymbol{g}, \quad \boldsymbol{\nabla} \cdot \boldsymbol{u}^{(j)} = 0, \tag{2.49a}$$

$$u_r^{(j)} = 0, \ [u_\vartheta] = 0, \ [\sigma_{r\,\vartheta}] = 0, \quad \text{at} \quad r = a, \tag{2.49b}$$

$$\boldsymbol{u}^{(0)} = -u_\infty \boldsymbol{e}_z, \quad \text{as} \quad r \to \infty, \tag{2.49c}$$

where $p^{(j)}$ and $\boldsymbol{u}^{(j)}$ are the pressure and velocity fields, respectively, of the *jth* fluid phase. The brackets denote a jump of the enclosed property from the outer to the inner fluid (e.g. $u_\vartheta^{(1)} - u_\vartheta^{(0)} = 0$). Therefore, the velocity and stress tangent to the fluid–fluid interface ($u_\vartheta$ and $\sigma_{r\,\vartheta}$) are required to be continuous from one fluid phase to the other. Again, $u_r = 0$ defines the no-penetration condition for the fluid–fluid interface in accordance with the immiscibility of the phases. Far away, the velocity of the ambient fluid reduces to the undisturbed velocity.

Note that the boundary value problem for the bubble is much simpler than for the fluid drop. One may obtain an expression for the drag force by analyzing the outer flows alone. Owing to the smallness of the viscosity of a gaseous phase in comparison to that of a liquid one, the shear stress imparted on the liquid by the bubble is negligible ($\sigma_{r\,\vartheta}^{(1)} \ll \sigma_{r\,\vartheta}^{(0)}$). Thus, the boundary conditions that describe the outer flows simplify to $u_r = 0$ and $\sigma_{r\,\vartheta}^{(0)} = 0$ at the surface of the bubble ($r = a$). Nonetheless, the solution for the bubble can also be obtained from the results of the fluid sphere in the limit of $\eta_1 \ll \eta_0$, which is the strategy followed here. It is important to note that having a negligible shear stress on the liquid side of the fluid–fluid interface is different from having a zero shear stress; this is the case because the bubble still experiences a shear stress from the liquid side of the interface.

From the experience gained by dealing with the previous problems, it is expected that the flows inside and outside the fluid sphere are of axisymmetric character. Therefore, the solution to the fluid flow problem can be formulated via the stream function.

Nevertheless, the condition of the zero jump in the shear stress at the surface of the fluid sphere deserves some attention prior to expressing the boundary value problem with respect to the stream function. Substitution of the definition for the shear stress of a Newtonian fluid in the zero jump condition for the shear stress results in the following expressions:

$$\sigma_{r\vartheta}^{(1)} - \sigma_{r\vartheta}^{(0)} = 0, \tag{2.50}$$

$$\eta_1 \frac{\partial}{\partial r}\left(\frac{u_\vartheta^{(1)}}{r}\right) - \eta_0 \frac{\partial}{\partial r}\left(\frac{u_\vartheta^{(0)}}{r}\right) = 0, \tag{2.51}$$

where it has been noted that $\partial_\vartheta v_r = 0$ at $r = a$ because of the no-penetration condition, as in the problem of Stokes flow past a solid sphere. It is convenient to introduce the viscosity ratio $\lambda = \eta_1/\eta_0$, and rewrite the velocity gradients with respect to the stream function to obtain the sought condition:

$$\lambda \frac{\partial}{\partial r}\left(\frac{1}{r^2}\frac{\partial}{\partial r}\psi^{(1)}\right) - \frac{\partial}{\partial r}\left(\frac{1}{r^2}\frac{\partial}{\partial r}\psi^{(0)}\right) = 0. \tag{2.52}$$

Redefining the boundary value problem with respect to the stream function yields the following expressions:

$$E^4\psi^{(j)} = 0, \tag{2.53}$$

$$\psi^{(j)} = 0, \quad \left[\frac{\partial \psi}{\partial r}\right] = 0, \quad \lambda \frac{\partial}{\partial r}\left(\frac{1}{r^2}\frac{\partial}{\partial r}\psi^{(1)}\right) - \frac{\partial}{\partial r}\left(\frac{1}{r^2}\frac{\partial}{\partial r}\psi^{(0)}\right) = 0, \text{ at } r = a, \tag{2.54}$$

$$\psi^{(0)} = -\frac{1}{2}u_\infty r^2 \sin^2\vartheta, \quad \text{as} \quad r \to \infty, \tag{2.55}$$

where, again, the brackets denote a jump across the fluid–fluid interface. Note that to simplify the governing equations for the stream function, the analysis of the flow is performed with respect to the dynamic pressure such that gravity does not appear.

As in the previous axisymmetric problems, Sections 2.2.1 and 2.2.2, it is expected that the the flows inside and outside the fluid sphere are described by a stream function of the form:

$$\psi^{(1)} = -\frac{1}{2}\left[A_1\, r^4 + B_1\, r^2 + C_1\, r + D_1\, r^{-1}\right] \sin^2\vartheta, \tag{2.56}$$

$$\psi^{(0)} = -\frac{1}{2}\left[A_0\, r^4 + B_0\, r^2 + C_0\, r + D_0\, r^{-1}\right] \sin^2\vartheta, \tag{2.57}$$

where the subscript of the unknown coefficients denote the corresponding fluid phase. It follows from basic reasoning and prior experience that the chosen form of the stream function is appropriate to describe the outer flows; because, these must reduce to the undisturbed flow far away, as in the former problems. However, it is not so clear, at first, that the chosen form holds as well for the internal flows. The deduction follows by noting that continuity of the tangent velocity at the fluid–fluid interface dictates (implicitly) that the internal flows should have the same angular variation over the surface of the fluid sphere; on the contrary, it would be impossible to match the inner flows with the outer ones.

As in the previous problems it is evident that $A_0 = 0$ for the stream function to have the appropriate scaling with position far from the fluid sphere. In addition, recall that $C_1$ and $D_1$ have been found to be associated with decaying flows ($r^{-n}$), which are clearly prohibited inside the fluid sphere for the internal flows to be finite, specially near $r = 0$. Thus, the stream functions simplify to:

$$\psi^{(1)} = -\frac{1}{2}\left[A_1\, r^4 + B_1\, r^2\right] \sin^2\vartheta, \tag{2.58}$$

$$\psi^{(0)} = -\frac{1}{2}\left[B_0\, r^2 + C_0\, r + D_0\, r^{-1}\right] \sin^2\vartheta. \tag{2.59}$$

Application of the far field condition to the outer flows sets $B_0 = u_\infty$, which reduces the problem to the determination of 4 unknowns with a set of 4 boundary conditions (a set of linearly independent equations).

The following equations arise from the no-penetration condition:

$$a^4 A_1 + a^2 B_1 = 0, \tag{2.60}$$

$$a^2 u_\infty + a C_0 + a^{-1} D_0 = 0. \tag{2.61}$$

The zero jump in the tangent velocity and shear stress at the surface of the fluid sphere gives the last pair of equations:

$$\left(4a^3 A_1 + 2a B_1\right) - \left(2a u_\infty + C_0 - a^{-2} D_0\right) = 0, \tag{2.62}$$

$$\lambda\left(4a^3 A_1 - 2a B_1\right) - \left(-2a u_\infty - 2C_0 + 4a^{-2} D_0\right) = 0. \tag{2.63}$$

The latter expression has been multiplied by a factor of $a^3$ to match the units of the former one. Simultaneous solution of the set of equations yields the following values for the coefficients:

$$C_0 = a u_\infty \frac{2+3\lambda}{2+2\lambda}, \quad D_0 = a^3 u_\infty \frac{1}{2+2\lambda}, \tag{2.64}$$

$$A_1 = a^{-2} u_\infty \frac{1}{2+2\lambda}, \quad B_1 = -u_\infty \frac{1}{2+2\lambda}. \tag{2.65}$$

Note that the coefficients that correspond to the ambient fluid reduce to those of a solid sphere (2.21) in the limit the viscosity of the fluid sphere is large compared to the ambient fluid ($\lambda \gg 1$). The coefficients of the inner fluid decay asymptotically to zero with increasing values of $\lambda$ until the inner phase exhibits solid-like behavior (no inner flows).

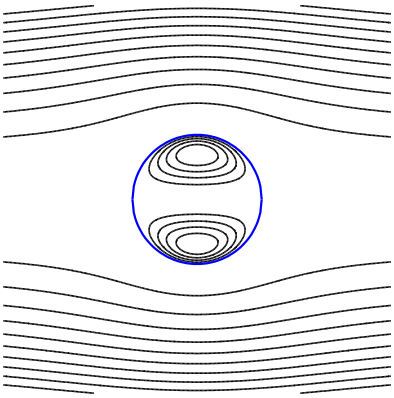

Figure 2–8: The flows in and about a fluid sphere with a viscosity ratio $\lambda = 1/2$.

The stream functions that solve the boundary value problem for the inner and outer fluids are found to be:

$$\psi^{(1)}(r,\vartheta) = -\frac{1}{2}\left[a^{-2}u_\infty \frac{1}{2+2\lambda}\, r^4 - u_\infty \frac{1}{2+2\lambda}\, r^2\right]\sin^2\vartheta, \tag{2.66}$$

$$\psi^{(0)}(r,\vartheta) = -\frac{1}{2}\left[u_\infty r^2 - a u_\infty \frac{2+3\lambda}{2+2\lambda}\, r + a^3 u_\infty \frac{\lambda}{2+2\lambda}\, r^{-1}\right]\sin^2\vartheta. \tag{2.67}$$

An illustration of the streamlines for the flows inside and outside the fluid sphere are provided in figure 2–8. As one may imagine, the inner flows exhibit a toroidal-type structure, and the outer flows are qualitatively similar to those of a solid sphere.

The velocity components of the inner fluid read:

$$u_r^{(1)} = u_\infty \frac{1}{2+2\lambda}\left[1 - \left(\frac{r}{a}\right)^2\right]\cos\vartheta, \tag{2.68a}$$

$$u_\vartheta^{(1)} = -u_\infty \frac{1}{2+2\lambda}\left[1 - 2\left(\frac{r}{a}\right)^2\right]\sin\vartheta. \tag{2.68b}$$

And those of the outer fluid read:

$$u_r^{(0)} = -u_\infty \left[1 - \frac{2+3\lambda}{2+2\lambda}\left(\frac{a}{r}\right) + \frac{\lambda}{2+2\lambda}\left(\frac{a}{r}\right)^3\right]\cos\vartheta, \tag{2.69a}$$

$$u_\vartheta^{(0)} = u_\infty \left[1 - \frac{2+3\lambda}{4+4\lambda}\left(\frac{a}{r}\right) - \frac{\lambda}{4+4\lambda}\left(\frac{a}{r}\right)^3\right]\sin\vartheta. \tag{2.69b}$$

The reader may check that the velocity fields satisfy the no-penetration condition $\left(u_r^{(j)} = 0\right)$ and the zero jump condition for the velocity ($[u_\vartheta] = 0$) at the fluid–fluid interface ($r = a$); and that the outer flow reduces to the undisturbed flow at large distances compared to the size of the fluid sphere ($r/a \to \infty$). It is interesting to note that the outer flows about a spherical bubble ($\lambda \ll 1$) are identical to those of a solid sphere with a 'perfect slip' surface (2.42); thus, it unfolds from this finding that the surface of 'perfect slip' sphere acts as a freely streaming surface. In the opposite exterme ($\lambda \gg 1$) the velocity of the outer fluid reduces to that about a solid sphere (2.23), and the internal one vanishes to zero.

The inner and outer pressure fields are obtained by substitution of the corresponding velocity components into the azimuthal component of the Stokes equation:

$$p^{(1)} = -\frac{\eta_0 u_\infty}{a}\frac{5\lambda}{1+\lambda}\left(\frac{r}{a}\right)\cos\vartheta - \rho_1 g r\cos\vartheta + \hat{p}, \tag{2.70}$$

$$p^{(0)} = \frac{\eta_0 u_\infty}{a}\left(\frac{a}{r}\right)^2\frac{2+3\lambda}{2+2\lambda}\cos\vartheta - \rho_0 g r\cos\vartheta + p_\infty. \tag{2.71}$$

Note that the corresponding pressure fields under hydrostatic conditions have been superimposed to recover the equilibrium condition (2.48) in the absence of fluid motion. Additionaly, it is important to notice that the dynamic part of the pressure has been defined with respect to the viscosity of the ambient fluid, which will be useful when the jump in the normal stresses at the fluid–fluid interface is evaluated.

For the purposes of calculating the net hydrodynamic force and showing that there is a zero jump in the normal stresses at the interface, it is necessary to determine the viscous stress tensor of the internal and outer fluids. The viscous stress tensor of the inner fluid is presented in terms of the non-vanishing components:

$$\tau_{r\,r}^{(1)} = -\frac{\eta_0 u_\infty}{a}\frac{4\lambda}{2+2\lambda}\left(\frac{r}{a}\right)\cos\vartheta, \tag{2.72}$$

$$\tau_{r\,\vartheta}^{(1)} = \frac{\eta_0 u_\infty}{a}\frac{\lambda}{2+2\lambda}\left[\left(\frac{a}{r}\right) + 2\left(\frac{r}{a}\right)\right]\sin\vartheta. \tag{2.73}$$

And those of the outer fluid are given by:

$$\tau_{r\,r}^{(0)} = -\frac{\eta_0 u_\infty}{a}\left[\frac{4+6\lambda}{2+2\lambda}\left(\frac{a}{r}\right)^2 - \frac{6\lambda}{2+2\lambda}\left(\frac{a}{r}\right)^4\right]\cos\vartheta, \tag{2.74}$$

$$\tau_{r\,\vartheta}^{(0)} = \frac{\eta_0 u_\infty}{a}\left[-\left(\frac{a}{r}\right) + \frac{2+3\lambda}{2+2\lambda}\left(\frac{a}{r}\right)^2 + \frac{2\lambda}{2+2\lambda}\left(\frac{a}{r}\right)^4\right]\sin\vartheta. \tag{2.75}$$

Note that the appearance of $r^{-1}$ in the shear component of the stress in the internal fluid is just a manifestation of using spherical coordinates to express the stress tensor; the reader can easily verify that the stresses at the center of the fluid sphere vanish identically via: $\oint \boldsymbol{n}\cdot\boldsymbol{\sigma}^{(1)}\,\mathrm{d}S = \mathbf{0}$ as $r \to 0$.

Evaluation of the components of the viscous stress tensor at the surface of the drop (or bubble) yields the sought expressions for each fluid phase:

$$\tau_{r\,r}^{(1)} = -\frac{\eta_0 u_\infty}{a}\frac{4\lambda}{2+2\lambda}\cos\vartheta, \quad \tau_{r\,\vartheta}^{(1)} = \frac{\eta_0 u_\infty}{a}\frac{3\lambda}{2+2\lambda}\sin\vartheta, \tag{2.76}$$

$$\tau_{r\,r}^{(0)} = -\frac{\eta_0 u_\infty}{a}\frac{4}{2+2\lambda}\cos\vartheta, \quad \tau_{r\,\vartheta}^{(0)} = \frac{\eta_0 u_\infty}{a}\frac{3\lambda}{2+2\lambda}\sin\vartheta. \tag{2.77}$$

It is evident, from the above equations, that the condition of zero jump in the shear stresses at the fluid–fluid interface has been satisfied appropriately. Note that in the extreme situation of a drop with a viscosity much greater than the viscosity of the ambient fluid ($\lambda \gg 1$), the normal and shear components of the stress reduce to that of a solid sphere. Thus, the solution to the problem of Stokes flow past a solid sphere is recovered in this extreme case. Although the viscous stresses of the internal fluid remain finite when $\lambda \gg 1$ (because of the $[\sigma_{r\,\vartheta}] = 0$ condition), the internal velocity decays to zero $\left(\boldsymbol{u}^{(1)} = \mathbf{0}\right)$ and $\eta_1 \to \infty$, which is akin of a solid body.

The net hydrodynamic force is given by the integral of the fluid stresses at the outer surface of the fluid sphere:

$$\boldsymbol{F} = \oint \left(\boldsymbol{n}\cdot\boldsymbol{\sigma}^{(0)}\right)\,\mathrm{d}S. \tag{2.78}$$

On account of the axisymmetric character of the flow and the spherical shape of the drop (or bubble), $F_z$ is the only meaningful component of the force (i.e. $F_x = F_y = 0$):

$$F_z = \oint \left[ \left( -p^{(0)} + \tau_{rr}^{(0)} \right) \cos\vartheta + \tau_{r\vartheta}^{(0)} \sin\vartheta \right] \mathrm{d}S. \tag{2.79}$$

After some elementary steps (analogous to those shown for the solid sphere in Section 2.2.1) the net hydrodynamic force on the fluid sphere is found to be:

$$F_z = -2\pi a \eta_0 u_\infty \left( \frac{2+3\lambda}{1+\lambda} \right) + \frac{4}{3}\pi a^3 \rho_0 g, \tag{2.80}$$

where the latter term corresponds to the bouyant force on the fluid sphere. Consequently, the drag force on the fluid sphere is given by:

$$F_z = -2\pi a \eta_0 u_\infty \left( \frac{2+3\lambda}{1+\lambda} \right), \tag{2.81}$$

where for a bubble ($\lambda \ll 1$) it simplifies to $F_z = -4\pi a \eta_0 u_\infty$, in agreement with the previous remark that the drag force on a 'perfect slip' sphere reduces to that of a spherical bubble.

The overall force balance is completed by inclusion of the gravitational force for a zero net force on the fluid sphere (there are no other forces acting on the fluid sphere other than the viscous, buoyant and gravitational forces):

$$\Sigma_j F_j = -2\pi a \eta_0 u_\infty \left( \frac{2+3\lambda}{1+\lambda} \right) + \frac{4}{3}\pi a^3 \left( \rho_0 - \rho_1 \right) g = 0. \tag{2.82}$$

Arrangement of the overall force balance for the terminal velocity of the fluid sphere results in the well known Hadamard-Rybczynski equation [13]:

$$u_\infty = \frac{2a^2 \left( \rho_0 - \rho_1 \right) g}{3\eta_0} \left( \frac{1+\lambda}{2+3\lambda} \right). \tag{2.83}$$

As one may expect, the velocity of sedimentation of a solid sphere is obtained in the limit of $\lambda \gg 1$.

Now that the velocity and stress fields are known inside and outside the fluid sphere, it is instructive to check if there is a jump in the normal stresses at the fluid–fluid interface ($r = a$):

$$\sigma_{nn}^{(1)} - \sigma_{nn}^{(0)} + p_\gamma = 0, \tag{2.84}$$

$$\left(-p^{(1)} + \tau_{rr}^{(1)}\right) - \left(-p^{(0)} + \tau_{rr}^{(0)}\right) + p_\gamma = 0. \tag{2.85}$$

After some algebraic manipulations the above expression can be written as:

$$\left[\frac{3}{2}\frac{\eta_0 u_\infty}{a}\left(\frac{2+3\lambda}{1+\lambda}\right) - (\rho_0 - \rho_1)\, ag\right]\cos\vartheta + (p_\infty - \hat{p} + p_\gamma) = 0, \tag{2.86}$$

where the bracketed and parenthetical terms correspond to the dynamic and hydrostatic parts of the normal stresses, respectively. It is readily seen that the parenthetical term is equivalent to the Young-Laplace equation (2.48), and hence, vanishes to zero. Notably, the bracketed term becomes identical to the overall force balance on the fluid sphere (2.82) via multiplication of a factor of $-4\pi a^2/3$. As a consequence of the zero net force on the fluid sphere, the bracketed term vanishes as well. Thus, it ensues from this analysis that there is no jump in the normal stresses at the fluid–fluid interface for a fluid drop subject to Stokes flow.

### 2.2.4 Axisymmetric elongational flow about a fluid sphere

Elongational flows arise by the action of velocity gradients in the principal direction of the imposed flow. A simple way to understand the behavior of elongational flows is to imagine a slender mass of fluid being streched (or compressed) by the action of a velocity gradient down the length of the mass of fluid. Elongational flows are known to occur in four-roller mills, turbulent flows, blood vessels, cross-slots, contractions, and bifurcations [62–64]. Elongational flows have found applications in polymer science by providing new pathways towards the synthesis of polymers with chemical properties that respond to mechanical stimuli [65]. For many mammals,

the compression mechanics of joints (e.g. knees) is greatly influenced by the elongational flows that occur within them [66]. An important aspect elongational flows to the rheology of suspensions is that emulsions (a dispersion of drops in another fluid) can exhibit non-Newtonian and visco-elastic behavior despite that the constituent fluids are Newtonian [47]. The elongational flow gives rise to an unbalance in the stresses normal to the surface of the drops that induce them to undertake a spheroidal shape.

The purpose of the this section is to analyze the flows in and about a fluid sphere of radius $a$ centered in an axisymmetric elongational flow $\boldsymbol{u}_\infty = \boldsymbol{E}^\infty \cdot \boldsymbol{x}$, where $\boldsymbol{x}$ is the position vector, $\boldsymbol{E}^\infty = -\dot{\gamma}\left(\boldsymbol{e}_x\boldsymbol{e}_x + \boldsymbol{e}_y\boldsymbol{e}_y - 2\boldsymbol{e}_z\boldsymbol{e}_z\right)$ is the rate-of-strain tensor of the undisturbed flow and the constant $\dot{\gamma}$ is the shearing rate. (The analysis of the flow of a fluid sphere in a general straining flow is considered in Section 2.3.5.) The undisturbed rate-of-strain tensor for an axisymmetric elongational flow can be alternatively represented as a diagonal matrix of zero trace:

$$\boldsymbol{E}^\infty = -\dot{\gamma}\begin{pmatrix} 1 & \cdot & \cdot \\ \cdot & 1 & \cdot \\ \cdot & \cdot & -2 \end{pmatrix}, \tag{2.87}$$

where the dots represents zero values in those elements of the tensor. Carrying out the dot product results in an expression for the far field velocity $\boldsymbol{u}_\infty$ expressed with respect to Cartesian coordinates:

$$\boldsymbol{u}_\infty = -\dot{\gamma}\left(x\boldsymbol{e}_x + y\boldsymbol{e}_y - 2z\boldsymbol{e}_z\right). \tag{2.88}$$

A pictorial representation of an axisymmetric elongational flow is provided in figure 2–9, in which the shown arrows indicate the direction of the flow for $\dot{\gamma} > 0$; this type of flow is known as a uniaxial elongational flow. It is readily seen from the figure that the fluid approaches from far away along the $x$–$y$ plane and exits in the direction parallel to the $z$–axis (the reader is to understand that the flow

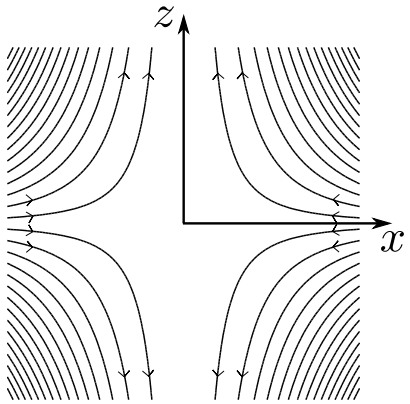


Figure 2–9: Streamlines of a uniaxial elongational flow. The flow acts in the direction pointed by the arrows.

has rotational symmety about the $z$–axis). For $\dot{\gamma} < 0$ a biaxial elongational flow is obtained with the flow in the opposite sense. From here on the analysis of the flow inside and outside the fluid sphere is carried out.

The boundary value problem that describes the motion of the fluid phases that comprise the fluid sphere '1' and the ambient fluid '0' are defined with respect to the stream function $\psi(r, \vartheta)$ (a detailed derivation of the governing equations for a fluid sphere with respect to the stream function can be found in Section 2.2.3):

$$E^4\psi^{(j)} = 0, \tag{2.89}$$

$$\psi^{(j)} = 0, \quad \left[\frac{\partial\psi}{\partial r}\right] = 0, \quad \lambda\frac{\partial}{\partial r}\left(\frac{1}{r^2}\frac{\partial}{\partial r}\psi^{(1)}\right) - \frac{\partial}{\partial r}\left(\frac{1}{r^2}\frac{\partial}{\partial r}\psi^{(0)}\right) = 0, \text{ at } r = a, \tag{2.90}$$

$$\psi^{(0)} = \psi_\infty, \quad \text{as} \quad r \to \infty, \tag{2.91}$$

where $j = 0, 1$, $\lambda = \eta_1/\eta_0$ is the viscosity ratio of the inner to the outer fluid phase, and $\psi_\infty$ denotes the stream function of the undisturbed flow. Note that the conditions of no-penetration and no-slip tangent at the surface of the fluid sphere are taken to describe the inner and outer flows.

The stream function of the far field is derived by transforming the undisturbed flow $\boldsymbol{u}_\infty$ with respect to spherical coordinates:

$$\boldsymbol{u}_\infty = r\,\dot{\gamma}\left(3\cos^2\vartheta - 1\right)\boldsymbol{e}_r - 3\,r\,\dot{\gamma}\sin\vartheta\cos\vartheta\,\boldsymbol{e}_\vartheta, \tag{2.92}$$

where $\boldsymbol{e}_r$ and $\boldsymbol{e}_\vartheta$ are unit vectors that point in the radial and azimuthal directions, respectively. The finding that the direction of the unperturbed flow is solely defined by these two vectors and that there is no dependence in the polar angle $\phi$ confirms that the flow is of axisymmetric character. By means of Equation (2.13), the stream function far away is found to be given by:

$$\psi_\infty = r^3\dot{\gamma}\sin^2\vartheta\cos\vartheta. \tag{2.93}$$

Note that the form of the far field flow suggests that the Gegenbauer function of order $n = 3$, $\mathscr{I}_3(\vartheta) = \sin^2\vartheta\cos\vartheta/2$, describes the flow inside and outside the fluid sphere. Therefore, the stream function form of the inner and outer flows, respectively, is deduced from the generalized solution (2.15):

$$\psi^{(1)}(r,\vartheta) = \left[A_1 r^5 + B_1 r^3\right]\mathscr{I}_3(\vartheta), \tag{2.94}$$

$$\psi^{(0)}(r,\vartheta) = \left[B_0 r^3 + C_0 + D_0 r^{-2}\right]\mathscr{I}_3(\vartheta), \tag{2.95}$$

where radially decaying terms have been omitted in the expression for $\psi^{(1)}$, and $A_0$ is clearly zero because $\psi^{(0)}$ cannot grow faster than the undisturbed flow $\psi_\infty$ in the radial dimension.

It is easy to see that the far field condition requires that $B_0 = 2\dot{\gamma}$ for the stream function of the ambient $\psi^{(0)}$ to match the flow as $r \to \infty$.

Application of the remaining boundary conditions to each fluid phase yields the following system of algebraic equations for the unknown constants:

$$a^5 A_1 + a^3 B_1 = 0, \tag{2.96}$$

$$2a^3\dot{\gamma} + C_0 + a^{-2} D_0 = 0, \tag{2.97}$$

$$5a^4 A_1 + 3a^2 B_1 - 6a^2\dot{\gamma} + 2a^{-3} D_0 = 0, \tag{2.98}$$

$$a\lambda A_1 - a^{-6} D_0 = 0. \tag{2.99}$$

After some algebraic manipulations, it is found that:

$$A_1 = \frac{3}{1+\lambda} a^{-2}\dot{\gamma}, \quad B_1 = -\frac{3}{1+\lambda}\dot{\gamma}, \tag{2.100}$$

$$B_0 = 2\,\dot{\gamma}, \quad C_0 = -\frac{2+5\lambda}{1+\lambda} a^3\dot{\gamma}, \quad D_0 = \frac{3\lambda}{1+\lambda} a^5\dot{\gamma}. \tag{2.101}$$

Thus, the stream functions for the corresponding inner and outer fluids are given by:

$$\psi^{(1)}(r,\vartheta) = \frac{3}{2+2\lambda} a^3\dot{\gamma}\left[\left(\frac{r}{a}\right)^5 - \left(\frac{r}{a}\right)^3\right]\sin^2\vartheta\cos\vartheta, \tag{2.102}$$

$$\psi^{(0)}(r,\vartheta) = a^3\dot{\gamma}\left[\left(\frac{r}{a}\right)^3 - \left(\frac{2+5\lambda}{2+2\lambda}\right) + \frac{3\lambda}{2+2\lambda}\left(\frac{a}{r}\right)^2\right]\sin^2\vartheta\cos\vartheta. \tag{2.103}$$

Note that in the limit of a highly viscous drop ($\lambda \gg 1$) the stream function of the ambient fluid reduces to that of a solid sphere in an elongational flow; the reader may compare the resulting expression with that provided by Deen [13].

The velocity components of the flows inside and outside the drop are recovered by means of Equation (2.13):

$$u_\vartheta^{(1)} = -\frac{3}{2\,(1+\lambda)} a\,\dot{\gamma}\left[5\left(\frac{r}{a}\right)^3 - 3\left(\frac{r}{a}\right)\right]\sin\vartheta\cos\vartheta, \tag{2.104a}$$

$$u_r^{(1)} = \frac{3}{2\,(1+\lambda)} a\,\dot{\gamma}\left[\left(\frac{r}{a}\right)^3 - \left(\frac{r}{a}\right)\right]\left(3\cos^2\vartheta - 1\right), \tag{2.104b}$$

$$u_\vartheta^{(0)} = -3\,a\,\dot{\gamma}\left[\left(\frac{r}{a}\right) - \frac{\lambda}{1+\lambda}\left(\frac{a}{r}\right)^4\right]\sin\vartheta\cos\vartheta, \tag{2.104c}$$

$$u_r^{(0)} = a\,\dot{\gamma}\left[\left(\frac{r}{a}\right) - \frac{2+5\lambda}{2\,(1+\lambda)}\left(\frac{a}{r}\right)^2 + \frac{3\lambda}{2\,(1+\lambda)}\left(\frac{a}{r}\right)^4\right]\left(3\cos^2\vartheta - 1\right), \tag{2.104d}$$

where it is evident that the rigid body limit is reached when the viscosity of the drop is large compared to the ambient viscosity ($\lambda \gg 1$); that is, $\boldsymbol{u}^{(1)} \to \mathbf{0}$ and $\boldsymbol{u}^{(0)}$ reduces to that of solid sphere in an elongational flow [13]. An interesting feature of the inner flows is that there is no flow through the $x$–$y$ plane at $z = 0$. The expressions for the pressure fields of the fluid phases are obtained by introducing the velocity components into the creeping motion equation followed by integration of the pressure gradient:

$$p^{(1)} = \eta_1\,\dot{\gamma}\left(\frac{21}{2\,(1+\lambda)}\right)\left(\frac{r}{a}\right)^2\left(3\cos^2\vartheta - 1\right), \tag{2.105a}$$

$$p^{(0)} = -\eta_0\,\dot{\gamma}\left(\frac{2+5\lambda}{1+\lambda}\right)\left(\frac{a}{r}\right)^3\left(3\cos^2\vartheta - 1\right). \tag{2.105b}$$

Note that the pressure far from the fluid sphere $p_\infty$ is an arbitrary constant that has been set to zero for simplicity.

Figure 2–10 illustrates the streamlines of the flows that occur inside and outside the fluid sphere. It is interesting to see that the inner flows are characterized by two counter-rotating toroidal-like vortices, and that the undisturbed flow is recovered quite rapidly in comparison with the streamlines for a fluid sphere in a uniform flow (figure 2–8). The principal reason for this finding is that the disturbance to the

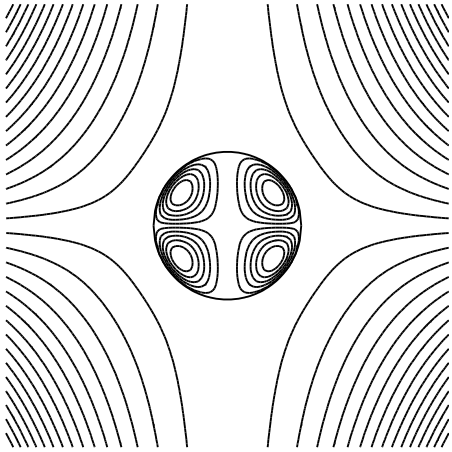

Figure 2–10: Streamlines in and about the fluid sphere in an elongational flow.

imposed flow caused by a fluid sphere in a streaming flow decays as $1/r$, whereas, in a straining flow it decays as $1/r^2$.

From the symmetry of the imposed flow, it is clear that there is a zero net force on the fluid sphere ($\boldsymbol{F} = \boldsymbol{0}$). One can easily imagine that the force imposed by the flow on any hemispherical section of the fluid sphere is cancelled by its counterpart at $r = a$. (Note that the orientation of the hemispherical domain with the flow is irrelevant.) By analogous symmetry arguments, the net torque on the fluid sphere is identically zero ($\boldsymbol{T} = \boldsymbol{0}$). In Section 2.3.5 stronger arguments are given to elucidate that the fluid drop is both force and torque–free in a general straining flow.

## 2.3 3D flows

This section concerns methods of solution to full 3D problems. The 'velocity' dyad and 'pressure' vector are introduced in Section 2.3.1 to derive closed-form expressions for the force, torque and stresslet on bodies of spherical shape subject to low Reynolds number flows. The disturbance field caused by the presence of the solid sphere and its relation with the Oseen tensor is presented in Section 2.3.2. In Section 2.3.3, the analogous calculation of the force, torque and stresslet is carried out for a fluid drop in a uniform flow. The stresslet of a solid sphere and fluid drop in a generalized straining flow is calculated in Sections 2.3.4 and 2.3.5, respectively.

The classic problem of finding the circulation and exterior flows of a fluid drop under the action of a uniform shear flow is solved with Lamb's solution in Section 2.3.6. The series of problems culminates with the calculation of the effective viscosity of a dilute dispersion of drops in a linear shear flow of a Newtonian fluid in Section 2.4.

### 2.3.1 Hydrodynamic resistance tensor of a solid sphere in Stokes flow

The principal objective is to show that a solid sphere has an isotropic resistance tensor to a uniform flow. The resistance tensor $\boldsymbol{A}$ (which has units of length) depends only on the shape of the body and relates the drag force $\boldsymbol{F}$ to the viscosity of the ambient fluid $\eta$ and the undisturbed velocity $\boldsymbol{u}_\infty$ via the linear relationship: $\boldsymbol{F} = \eta \boldsymbol{A} \cdot \boldsymbol{u}_\infty$. In principle the properties of the creeping flow equations furnishes the linear relationship that exist between these quantities and it can be equally applied to bodies of arbitrary shape [20]. Additionally, it is shown that the solid sphere is torque–free, followed by the calculation of the stresslet, which is a measure of the long-range effect of a body to the stress in a fluid. The latter has important implications on the effective viscosity of a dispersion of spheres in a fluid subject to a uniform shear flow, such that the bulk viscous properties of the dispersion exceed that of the host fluid [67]. To this end it necessary to revisit the problem of Stokes flow but in an arbitrary direction relative to the set of axes centered on the body. (That is, the uniform flow does not act along any of the axes affixed to the particle.) The solution is formulated by introduction of the 'pressure' vector $\boldsymbol{P}(\boldsymbol{x})$ and the 'velocity' dyad $\boldsymbol{V}(\boldsymbol{x})$. The symbol $\boldsymbol{x}$ denotes the position vector of magnitude $r$ and direction given by the radial unit vector $\boldsymbol{e}_r$ of a spherical coordinate system centered on the solid sphere. The 'pressure' vector is related to the fluid pressure via $p = \eta \boldsymbol{P}(\boldsymbol{x}) \cdot \boldsymbol{u}_\infty$, and similarly, the relation of the 'velocity' dyad with the fluid velocity is $\boldsymbol{u} = \boldsymbol{V}(\boldsymbol{x}) \cdot \boldsymbol{u}_\infty$; note that $\boldsymbol{P}(\boldsymbol{x})$ has units of $a^{-1}$ and $\boldsymbol{V}(\boldsymbol{x})$ is a non-dimensional second-rank tensor.

Introducing the above definitions for the pressure and the fluid velocity into the Stokes equations yields the boundary value problem for the 'pressure' vector and 'velocity' dyad:

$$\big[\boldsymbol{\nabla}\boldsymbol{P}(\boldsymbol{x}) - \nabla^2\boldsymbol{V}(\boldsymbol{x})\big]\cdot\boldsymbol{u}_\infty = \boldsymbol{0}, \tag{2.106a}$$

$$[\boldsymbol{\nabla}\cdot\boldsymbol{V}(\boldsymbol{x})]\cdot\boldsymbol{u}_\infty = 0, \tag{2.106b}$$

$$[\boldsymbol{V}(\boldsymbol{x})]\cdot\boldsymbol{u}_\infty = \boldsymbol{0} \quad \text{at } r = a, \tag{2.106c}$$

$$[\boldsymbol{V}(\boldsymbol{x}) - \boldsymbol{\delta}]\cdot\boldsymbol{u}_\infty = \boldsymbol{0} \quad \text{as } r \to \infty, \tag{2.106d}$$

where $\boldsymbol{\delta}$ is the identity tensor. Note that the velocity $\boldsymbol{u}_\infty$ is an arbitrary vector, and hence, only the bracketed terms are required to be identically zero. Thus, the boundary value problem now reads:

$$\boldsymbol{\nabla}\boldsymbol{P}(\boldsymbol{x}) = \nabla^2\boldsymbol{V}(\boldsymbol{x}), \quad \boldsymbol{\nabla}\cdot\boldsymbol{V}(\boldsymbol{x}) = 0, \tag{2.107a}$$

$$\boldsymbol{V}(\boldsymbol{x}) = \boldsymbol{0} \quad \text{at } r = a, \tag{2.107b}$$

$$\boldsymbol{V}(\boldsymbol{x}) = \boldsymbol{\delta} \quad \text{as } r \to \infty. \tag{2.107c}$$

The boundary conditions define that the flow normal to the surface of the solid sphere vanishes because the fluid cannot penetrate the surface of the solid, and far from the sphere the velocity reduces to the undisturbed velocity. To arrive at the above expressions it has been noted that $\boldsymbol{u}_\infty$ is a constant, arbitrary vector that can be extracted out from the differential operators. It is important to mention that this formulation is not restricted to a solid body of spherical shape. Brenner [68–73] extensively used this formulation to develop a theory for the hydrodynamic resistance of arbitrarily shaped bodies subject to fluid flow in the creeping motion limit. For instance, the formulation has been central to studies concerned with the dynamical and rheological behavior of colloidal suspensions [74].

It is key to point out at this early stage of the solution formulation that the creeping flow equation can be interpreted as a partial differential equation of second order with the pressure gradient acting as an inhomogeneous term. This is a consequence of the pressure satisfying the equation of Laplace $\nabla^2 p = 0$, which is a well-known feature of low Reynolds number flows [13]. Therefore, one may take advantage of the linearity property to break down the 'velocity' dyad $\boldsymbol{V}(\boldsymbol{x})$ into homogeneous and particular terms: $\boldsymbol{V}(\boldsymbol{x}) = \boldsymbol{V}^h(\boldsymbol{x}) + \boldsymbol{V}^p(\boldsymbol{x})$. Therefore, the creeping flow equation now consists of two parts:

$$\nabla^2 \boldsymbol{V}^h(\boldsymbol{x}) = \boldsymbol{0} \tag{2.108}$$

$$\nabla^2 \boldsymbol{V}^p(\boldsymbol{x}) = \boldsymbol{\nabla} \boldsymbol{P}(\boldsymbol{x}). \tag{2.109}$$

Later, it will be shown that the particular solution $\boldsymbol{V}^p(\boldsymbol{x})$ is exclusively associated with the fluid pressure, as it should, and that the continuity equation cannot be satisfied by the homogeneous solution $\boldsymbol{V}^h(\boldsymbol{x})$ alone.

The solution to the problem of Stokes flow past a solid sphere follows by deduction of the appropriate form of $\boldsymbol{P}(\boldsymbol{x})$. Since the formulation is independent of the direction of motion, the obtained solution to the axisymmetric problem provided in section 2.2.2 can be used to guess the right form of the general problem. By noting that for axisymmetric flow $p \sim r^{-2} \cos\vartheta$, and that $\cos\vartheta = \boldsymbol{x} \cdot \boldsymbol{u}_\infty$ because $\boldsymbol{u}_\infty = \boldsymbol{e}_z$, the pressure may be written as $p = \eta \boldsymbol{P}(\boldsymbol{x}) \cdot \boldsymbol{u}_\infty = [f(r)\, \boldsymbol{x}] \cdot \boldsymbol{u}_\infty$, where $f(r)$ is a scalar function. The bracketed expression corresponds to the 'pressure' vector $\boldsymbol{P}(\boldsymbol{x}) = f(r)\, \boldsymbol{x}$.

It is instructive to calculate the gradient of the pressure $\boldsymbol{\nabla} \boldsymbol{P}(\boldsymbol{x})$ in order to guess the structure of the 'velocity' dyad. Index notation is adopted from here on

to operate over the field variables:

$$\begin{aligned}\boldsymbol{\nabla P}(\boldsymbol{x}) =& \frac{\partial}{\partial x_i} P_j, \\ =& \frac{\partial}{\partial x_i} \left( f(r)\, x_j \right), \\ =& f(r)\, \delta_{ij} + \frac{1}{r} f'(r)\, x_i x_j, \\ =& f(r)\, \boldsymbol{\delta} + \frac{1}{r} f'(r)\, \boldsymbol{x}\boldsymbol{x},\end{aligned} \tag{2.110}$$

where the replacement of $\partial x_j / \partial x_i$ with the identity tensor $\delta_{ij}$ has taken place. The chain rule has been used to differentiate $f(r)$:

$$\frac{\partial}{\partial x_i} f(r) = \left( \frac{\partial r}{\partial x_i} \right) \frac{\partial}{\partial r} f(r), \tag{2.111}$$

and it has been noted that $\partial r / \partial x_i = x_i / r$ (this relation is obtained by differentiating $\boldsymbol{x} \cdot \boldsymbol{x} = x_i^2 = r^2$, which is simply the equation for a sphere of radius $r$).

Since it is simpler to deal with the homogeneous part of the 'velocity' dyad first, it is assumed that it has the same form as the pressure gradient:

$$\boldsymbol{V}^h(\boldsymbol{x}) = h(r)\, \boldsymbol{\delta} + g(r)\, \boldsymbol{x}\boldsymbol{x}, \tag{2.112}$$

where $h(r)$ and $g(r)$ are scalar functions that must satisfy the homogenous part of the creeping flow equation; that is, $\nabla^2 \boldsymbol{V}^h(\boldsymbol{x}) = \boldsymbol{0}$. By recalling that $\nabla^2 = \boldsymbol{\nabla} \cdot \boldsymbol{\nabla}$, the gradient of the 'velocity' dyad is calculated first to then determine its Laplacian, as shown below:

$$\begin{aligned}\boldsymbol{\nabla V}^h(\boldsymbol{x}) &= \frac{\partial}{\partial x_i} V^h_{jk} \\ &= \frac{\partial}{\partial x_i} \Big( h(r)\, \delta_{jk} \Big) + \frac{\partial}{\partial x_i} \Big( g(r)\, x_j x_k \Big), \\ &= \frac{1}{r} h'(r)\, x_i\, \delta_{jk} + g(r) \Big( \delta_{ij} x_k + x_j \delta_{ik} \Big) + \frac{1}{r} g'(r)\, x_i x_j x_k.\end{aligned} \tag{2.113}$$

The Laplacian of $\boldsymbol{V}^h(\boldsymbol{x})$ unfolds from elementary operations (steps not shown for the sake of being concise):

$$=\frac{\partial}{\partial x_i}\left[\frac{\partial}{\partial x_i}h(r)\,\delta_{j\,k}\right]+\frac{\partial}{\partial x_i}\left[g(r)\left(\delta_{i\,j}\,x_k+x_j\delta_{i\,k}\right)\right]+\frac{\partial}{\partial x_i}\left[\frac{1}{r}g'(r)\,x_ix_jx_k\right], \quad (2.114)$$

where the first bracketed term simply becomes $\nabla^2 h(r)\delta_{j\,k}$, the Laplacian operator in spherical coordinates is used here for convenience, the second bracketed term yields $2\,g(r)\,\delta_{j\,k}+2\,g'(r)/r\,x_jx_k$, and the third one gives $\left(g''(r)+4\,g'(r)/r\right)x_jx_k$. The following properties have been used in order to arrive at the final expressions: $x_i^2=r^2$, $\delta_{i\,i}=3$, $x_k\delta_{k\,j}=x_j$, and $\delta_{i\,j}\delta_{i\,k}=\delta_{j\,k}$. Therefore, the expression for the Laplacian of $\boldsymbol{V}^h(\boldsymbol{x})$ now reads:

$$\nabla^2\boldsymbol{V}^h(\boldsymbol{x})=\left(\nabla^2 h(r)+2\,g(r)\right)\boldsymbol{\delta}+\left(g''(r)+\frac{6}{r}g'(r)\right)\boldsymbol{x}\boldsymbol{x}=\boldsymbol{0}. \quad (2.115)$$

The finding that the governing equations are expressed solely with respect to the scalar functions is an indication that the assumed form for $\boldsymbol{P}(\boldsymbol{x})$ and $\boldsymbol{V}(\boldsymbol{x})$ is correct. In order for $\nabla^2\boldsymbol{V}^h(\boldsymbol{x})=\boldsymbol{0}$, the scalar functions $h(r)$ and $g(r)$ must satisfy:

$$g''(r)+\frac{6}{r}g'(r)=0, \quad (2.116)$$

$$h''(r)+\frac{2}{r}h'(r)+2g(r)=0, \quad (2.117)$$

where the resulting ordinary differential equations are equidimensional equations with general solution $r^n$ and $r^{-n}$. Given that the undisturbed flow must be recovered at large distances from the solid sphere, the scalar functions must consist of the decaying terms. On account of the linearity of the above set of differential equations, it is useful to determine first the homogeneous solutions by substitution of $g(r)=h(r)=r^{-n}$ to obtain the corresponding algebraic expressions:

$$n(n-5)\,r^{-n-2}=0, \quad (2.118)$$

$$n(n-1)\,r^{-n-2}=0, \quad (2.119)$$

where it is straightforward to see that $g(r) = Br^{-5}$ and that $h(r) = Cr^{-1} + D$, where the latter constant is retained to satisfy the far field velocity. Substitution of the newly acquired expression for $g(r)$ into the complete differential equation for $h(r)$ yields the following algebraic equation by assuming that the particular solution is also equidimensional $h^p(r) = E\, r^{-n}$:

$$n(n-1)\, E\, r^{-n-2} = -2B\, r^{-5}, \tag{2.120}$$

where a particular solution exists if $n = 3$ and $E = -B/3$, such that now the complete expression of $h(r) = -B/3\, r^{-3} + Cr^{-1} + D$.

An attempt to satisfy the continuity equation with the homogeneous part of the 'velocity' dyad (i.e. $\boldsymbol{\nabla}\cdot\boldsymbol{V}^h(\boldsymbol{x}) = \mathbf{0}$) is made in order to demonstrate that it is impossible to achieve that in this particular problem. Application of the divergence operator to the homogeneous part of the 'velocity' dyad results in an ordinary differential equation that cannot be solved by non-trivial solutions of the scalar functions $h(r)$ and $g(r)$:

$$\boldsymbol{\nabla}\cdot\boldsymbol{V}^h(\boldsymbol{x}) = \frac{\partial}{\partial x_i}\Big(h(r)\,\delta_{jk}\Big)\delta_{ij} + \frac{\partial}{\partial x_i}\Big(g(r)\,x_j x_k\Big)\delta_{ij}, \tag{2.121}$$

$$= \left(\frac{1}{r}h'(r) + rg'(r) + 4g(r)\right)\boldsymbol{x}. \tag{2.122}$$

Once more, $\boldsymbol{x}$ is an arbitrary vector such that the ordinary differential equation must be identically zero for the 'velocity' dyad to satisfy the continuity equation. Substitution of the corresponding scalar functions reveal that Equation (2.122) cannot be satisfied for non-zero values of the constant $C$. Note that $C = 0$ corresponds to the trivial solution $\boldsymbol{u} = \mathbf{0}$ everywhere, and that is a contradiction since motion of the solid sphere in a quiescent fluid creates a disturbance that decays as $r^{-1}$. This is an indication that the 'velocity' dyad requires an inhomogeneous component; the connection of this term with the 'pressure' vector will become evident later on.

The homogeneous contribution of the 'velocity' dyad $\boldsymbol{V}^h(\boldsymbol{x})$ suggests that its inhomogeneous counterpart must be of the form $\boldsymbol{V}^p(\boldsymbol{x}) = p(r)\,\boldsymbol{x}\boldsymbol{x}$ because $\nabla^2\boldsymbol{V}^p(\boldsymbol{x}) = 2p(r)\,\boldsymbol{\delta} + (p''(r) + 6p'(r)/r)\,\boldsymbol{x}\boldsymbol{x}$ has the same structure as $\boldsymbol{\nabla}\boldsymbol{P} = f(r)\,\boldsymbol{\delta} + f'(r)/r\,\boldsymbol{x}\boldsymbol{x}$. On the contrary, the Laplacian of a scalar function times the identity tensor as for $h(r)\,\boldsymbol{\delta}$ results in $\nabla^2 h(r)\,\boldsymbol{\delta}$, which lacks the $\boldsymbol{x}\boldsymbol{x}$ dependence of $\boldsymbol{\nabla}\boldsymbol{P}$. And consequently, there is only one suitable choice for the inhomogeneous term of the 'velocity' dyad.

Operating the divergence operator to the full 'velocity' dyad results in the following characteristic equation for $p(r)$:

$$\boldsymbol{\nabla}\cdot\left(\boldsymbol{V}^h(\boldsymbol{x}) + \boldsymbol{V}^p(\boldsymbol{x})\right) = \left(rp'(r) + 4p(r) - Cr^{-3}\right)\boldsymbol{x} = \boldsymbol{0}, \tag{2.123}$$

where the terms of $h(r)$ and $g(r)$ that cancel each other out have been omitted for clarity. As one may expect, the divergence of the full 'velocity' dyad results in a non-homogeneous equidimensional equation with particular solution $p(r) = Cr^{-3}$. With the obtained particular solution the full 'velocity' dyad now reads:

$$\boldsymbol{V}(\boldsymbol{x}) = \left(-\frac{1}{3}Br^{-3} + Cr^{-1} + D\right)\boldsymbol{\delta} + \left(Br^{-5} + Cr^{-3}\right)\boldsymbol{x}\boldsymbol{x}. \tag{2.124}$$

One may be inclined to apply the boundary conditions given by Equations (2.107b) and (2.107c) in order to determine the unknown constants $B$, $C$ and $D$; nevertheless, it is a good practice to check for consistency of the scalar functions of the 'velocity' dyad with that of the 'pressure' vector. Note that the 'velocity' dyad has been fully determined by solely guessing the right form of the 'pressure' vector $\boldsymbol{P}(\boldsymbol{x}) = f(r)\,\boldsymbol{x}$ without a formal expression for the scalar function $f(r)$. Of course, it is a trivial matter to deduce the expression of $f(r)$ from the solution to the axisymmetric problem; however, there is little gain in doing so for the purposes of delineating a rigorous method of solution that may be applied to other problems where the form of $f(r)$ is not known in advanced.

The characteristic equation for $f(r)$ unfolds from application of $\nabla^2 \boldsymbol{P}(\boldsymbol{x}) = \boldsymbol{0}$ (obtained by elementary operations):

$$\nabla^2 \boldsymbol{P}(\boldsymbol{x}) = \left( f''(r) + \frac{4}{r} f'(r) \right) \boldsymbol{x} = \boldsymbol{0}, \tag{2.125}$$

which is another form of an equidimensional differential equation with solution $f(r) = Ar^{-3}$. The gradient of the 'pressure' vector now reads:

$$\boldsymbol{\nabla P}(\boldsymbol{x}) = Ar^{-3}\, \boldsymbol{\delta} - 3Ar^{-5}\, \boldsymbol{xx}. \tag{2.126}$$

Substitution of the 'pressure' gradient and the Laplacian of the 'velocity' dyad into the creeping flow equation defined in (2.107a) reveals that the scalar functions $p(r)$ and $f(r)$ are related by a factor of two; that is, $C = A/2$. But more importantly, it is found that the components of $\nabla^2 \boldsymbol{V}(\boldsymbol{x})$ and $\boldsymbol{\nabla P}(\boldsymbol{x})$ are consistent. Partly, this is because $\nabla^2 \boldsymbol{P}(\boldsymbol{x})$ is a consequence of satisfying $\boldsymbol{\nabla} \cdot \boldsymbol{V}(\boldsymbol{x}) = \boldsymbol{0}$. This property could have been used earlier but, it has been postponed until now for the sake of providing a thorough analysis.

Application of the pertaining boundary conditions allows for the determination of the constants:

$$A = -\frac{3}{2}a, \quad B = \frac{3}{4}a^3, \tag{2.127}$$

$$C = -\frac{3}{4}a, \quad D = 1, \tag{2.128}$$

such that now the scalar functions read:

$$h(r) = 1 - \frac{3}{4}\, a\, r^{-1} - \frac{1}{4}\, a^3\, r^{-3}, \tag{2.129}$$

$$g(r) = \frac{3}{4}\, a^3\, r^{-5}, \quad p(r) = -\frac{3}{4}\, a\, r^{-3}. \tag{2.130}$$

For the purposes of testing the correctness of the 'velocity' dyad and 'pressure' vector, it is convenient to express them with respect to the unit normal vector

($\boldsymbol{e}_r = \hat{\boldsymbol{x}} = r^{-1}\boldsymbol{x}$):

$$\boldsymbol{P}(\hat{\boldsymbol{x}}) = -\frac{3}{2}\, a^{-1} \left(\frac{a}{r}\right)^2 \hat{\boldsymbol{x}}, \tag{2.131a}$$

$$\boldsymbol{V}(\hat{\boldsymbol{x}}) = \left[1 - \frac{3}{4}\left(\frac{a}{r}\right) - \frac{1}{4}\left(\frac{a}{r}\right)^3\right] \boldsymbol{\delta} + \left[-\frac{3}{4}\left(\frac{a}{r}\right) + \frac{3}{4}\left(\frac{a}{r}\right)^3\right] \hat{\boldsymbol{x}}\hat{\boldsymbol{x}}. \tag{2.131b}$$

The reader can effortlessly verify that the velocity and pressure fields for an axisymmetric streaming flow past a solid sphere, Equations (2.23) and (2.25), are recovered via $\boldsymbol{u} = \boldsymbol{V} \cdot \boldsymbol{u}_\infty$ and $p = \eta \boldsymbol{P} \cdot \boldsymbol{u}_\infty$, where $\boldsymbol{u}_\infty = -u_\infty \boldsymbol{e}_z$.

The Stokes law for the drag force on the solid sphere can be obtained from calculation of the net fluid stresses at its surface:

$$\boldsymbol{F} = \oint_{S_p} \boldsymbol{n} \cdot \boldsymbol{\sigma}\, \mathrm{d}S_p. \tag{2.132}$$

To obtain an expression for the force with respect to the 'pressure' vector and 'velocity' dyad, it is useful to express the stress tensor in the following form:

$$\boldsymbol{\sigma} = -\boldsymbol{\delta}\, p + \eta \left[\boldsymbol{\nabla}\boldsymbol{u} + (\boldsymbol{\nabla}\boldsymbol{u})^t\right], \tag{2.133}$$

where, again, $t$ denotes the transpose operator. Introduction of the definitions of the 'pressure' vector ($p = \eta \boldsymbol{P}(\boldsymbol{x}) \cdot \boldsymbol{u}_\infty$) and 'velocity' dyad ($\boldsymbol{u} = \boldsymbol{V}(\boldsymbol{x}) \cdot \boldsymbol{u}_\infty$) into Equation (2.133) yields the following expression for the stress tensor:

$$\boldsymbol{\sigma} = \eta \Big[ -\boldsymbol{\delta}\boldsymbol{P}(\boldsymbol{x}) + \boldsymbol{\nabla}\boldsymbol{V}(\boldsymbol{x}) + (\boldsymbol{\nabla}\boldsymbol{V}(\boldsymbol{x}))^t \Big] \cdot \boldsymbol{u}_\infty, \tag{2.134}$$

where the above bracketed expression corresponds to the 'stress' triad:

$$\boldsymbol{\Pi}(\boldsymbol{x}) = -\boldsymbol{\delta}\boldsymbol{P}(\boldsymbol{x}) + \boldsymbol{\nabla}\boldsymbol{V}(\boldsymbol{x}) + (\boldsymbol{\nabla}\boldsymbol{V}(\boldsymbol{x}))^t. \tag{2.135}$$

In analogy with the stress tensor $\boldsymbol{\sigma}$, the 'stress' triad $\boldsymbol{\Pi}$ is also a symmetric tensor [20].

For a solid sphere subject to Stokes flow, the 'stress' triad $\boldsymbol{\Pi}(\boldsymbol{x})$ reads:

$$\Pi_{i\,j\,k} = -\,f(r)\,\delta_{i\,j}\,x_k + \frac{h'(r)}{r}\Big(x_i\,\delta_{j\,k} + x_j\,\delta_{i\,k}\Big) + \frac{G'(r)}{r}\Big(x_i\,x_j\,x_k + x_j\,x_i\,x_k\Big) + \\ G(r)\left[\Big(\delta_{i\,j}\,x_k + \delta_{j\,i}\,x_k\Big) + \Big(x_i\,\delta_{j\,k} + x_j\,\delta_{i\,k}\Big)\right], \tag{2.136}$$

where, we have defined $G(r) = g(r) + p(r)$ for clarity of the presentation. Note that Equation (2.136) is a general expression that applies to other problems that involve bodies of spherical shape (such as, drops and bubbles) under the influence of a uniform flow. For the purposes of calculating the drag force, it is convenient to rewrite first the 'stress' triad with respect to the unit position vector $\boldsymbol{\Pi}(\hat{\boldsymbol{x}})$ via the replacement $\boldsymbol{x} = r\,\hat{\boldsymbol{x}}$:

$$\Pi_{i\,j\,k} = -\,r f(r)\,\delta_{i\,j}\,\hat{x}_k + h'(r)\Big(\hat{x}_i\,\delta_{j\,k} + \hat{x}_j\,\delta_{i\,k}\Big) + G'(r)\Big(\hat{x}_i\,\hat{x}_j\,\hat{x}_k + \hat{x}_j\,\hat{x}_i\,\hat{x}_k\Big) + \\ rG(r)\left[\Big(\delta_{i\,j}\,\hat{x}_k + \delta_{j\,i}\,\hat{x}_k\Big) + \Big(\hat{x}_i\,\delta_{j\,k} + \hat{x}_j\,\delta_{i\,k}\Big)\right]. \tag{2.137}$$

Then, to obtain the stresses normal to the surface of the solid sphere, the dot product is carried out $\hat{\boldsymbol{x}}\cdot\boldsymbol{\Pi}(\hat{\boldsymbol{x}})$ (note that the unit vector $\hat{\boldsymbol{x}}$ is normal to the surface of the sphere):

$$\hat{x}_i\,\Pi_{i\,j\,k} = \Big[h'(r) + rG(r)\Big]\delta_{j\,k} + \Big[-\,rf(r) + h'(r) + 2r^2G'(r) + 3rG(r)\Big]\,\hat{x}_j\,\hat{x}_k. \tag{2.138}$$

Evaluation of $\hat{\boldsymbol{x}}\cdot\boldsymbol{\Pi}(\hat{\boldsymbol{x}})$ at the surface of the sphere ($r = a$) reveals that

$$\hat{\boldsymbol{x}}\cdot\boldsymbol{\Pi}(\hat{\boldsymbol{x}}) = \frac{3}{2}\,a^{-1}\,\boldsymbol{\delta}. \tag{2.139}$$

By noting that $\eta\left(\hat{\boldsymbol{x}}\cdot\boldsymbol{\Pi}(\hat{\boldsymbol{x}})\right)\cdot\boldsymbol{u}_\infty$ is equivalent to $\boldsymbol{n}\cdot\boldsymbol{\sigma}$, it is replaced into the expression for the drag force on the solid sphere to obtain:

$$\boldsymbol{F} = \eta\left[\oint_{S_p}\hat{\boldsymbol{x}}\cdot\boldsymbol{\Pi}(\hat{\boldsymbol{x}})\;\mathrm{d}S_p\right]\cdot\boldsymbol{u}_\infty, \tag{2.140}$$

where the bracketed expression is known as the resistance tensor of the solid sphere to an external uniform flow (a 2nd rank tensor proportional to $a$):

$$\boldsymbol{A} = \oint_{S_p} \hat{\boldsymbol{x}} \cdot \boldsymbol{\Pi}(\hat{\boldsymbol{x}}) \, \mathrm{d}S_p. \tag{2.141}$$

After carrying out the surface integral, the classic expression for the hydrodynamic resistance of a solid sphere to a streaming flow is obtained:

$$\boldsymbol{A} = 6\pi a \, \boldsymbol{\delta}, \tag{2.142}$$

where the appearance of the identity tensor indicates that the resistance of the solid sphere is isotropic (independent of the direction of the imposed flow). It is important to mention that $\boldsymbol{A}$ depends only on the shape of the body; it is independent of the properties of the surrounding fluid and strength of the external flow (provided that $Re \ll 1$). (For an arbitrarily shaped body $\boldsymbol{A}$ scales with the characteristic length of the body $L$; the reader is referred to [20, 31]).

Stokes' law for the drag force on the solid sphere simplifies to the dot product of the resistance tensor $\boldsymbol{A}$ with the velocity of the undisturbed flow $\boldsymbol{u}_\infty$:

$$\boldsymbol{F} = 6\pi a\eta \, \boldsymbol{\delta} \cdot \boldsymbol{u}_\infty = 6\pi a\eta \boldsymbol{u}_\infty, \tag{2.143}$$

where it is evident that the generalized expression above is consistent with Equation (2.31). Owing to the isotropic character of the hydrodynamic resistance of the solid sphere to the external flow, the force is found to act in the direction of the undisturbed velocity; that is, there are no forces lateral to the flow acting on the body. This is a consequence of the spherical symmetry of the particle, for other axisymmetric bodies (for example, spheroids) there can be a force lateral to the direction of the streaming flow that depends on the relative orientation of the body with the flow [20]. Such bodies exhibit a migration lateral to the streamlines of the

undisturbed flow. For example, those bodies move sideways to a vertical gravitational field while undergoing sedimentation.

It is straightforward to see that the torque imparted by the streaming fluid on the solid sphere is identically zero (evident from purely geometrical deductions) by calculating the first moment of the normal stresses at the surface of the sphere:

$$\boldsymbol{T} = \oint_{S_p} \boldsymbol{x} \times (\boldsymbol{n} \cdot \boldsymbol{\sigma}) \ \mathrm{d}S_p, \tag{2.144}$$

where, once more, the normal stresses can be expressed in terms of the 'stress' triad to obtain:

$$\boldsymbol{T} = \eta \left[ \oint_{S_p} \boldsymbol{x} \times (\hat{\boldsymbol{x}} \cdot \boldsymbol{\Pi}(\hat{\boldsymbol{x}})) \ \mathrm{d}S_p \right] \cdot \boldsymbol{u}_\infty, \tag{2.145}$$

where the bracketed term is the coupling tensor (of rank 2):

$$\boldsymbol{B} = \oint_{S_p} \boldsymbol{x} \times (\hat{\boldsymbol{x}} \cdot \boldsymbol{\Pi}(\hat{\boldsymbol{x}})) \ \mathrm{d}S_p, \tag{2.146}$$

where for the solid sphere it vanishes identically:

$$\boldsymbol{B} = 6\pi a^2 \, \boldsymbol{x} \times \boldsymbol{\delta} = \boldsymbol{0}, \tag{2.147}$$

because of the identity $\boldsymbol{x} \times \boldsymbol{\delta} = x_i \delta_{jl} \epsilon_{ijk} = 0$, which is clearly zero becuase of the combined symmetry of the identity tensor and the anti-symmetry of the permutation symbol $\epsilon_{ijk} = -\epsilon_{jik}$. Therefore, it is found that a uniform flow imposes a zero torque on the solid sphere:

$$\boldsymbol{T} = 6\pi a^2 \eta \, \boldsymbol{B} \cdot \boldsymbol{u}_\infty = \boldsymbol{0}. \tag{2.148}$$

It is important to point out that the coupling tensor is, in general, not zero specially for bodies with broken fore and aft symmetry. Note also that the coupling tensor can vary from point to point on the body; unlike the resistance tensor $\boldsymbol{A}$, which remains invariant regardless of the reference point used for calculation. Fortunately, the coupling tensor at an arbitrary point in the body can be determined from knowledge of the translation tensor and the coupling tensor at a some other

location of reference, in an analogous manner to how the solid body motion at one point is related to that at any other point. This analysis lies outside the scope of this dissertation; nonetheless, the interested reader is referred to the classic book by Happel & Brenner [20].

Another quantity of interest to the field of microhydrodynamics is the stresslet (also known as the hydrodynamic dipole), which is determined by the second moment of the normal stresses [13, 31]:

$$\boldsymbol{S} = \oint_{S_p} (\boldsymbol{n} \cdot \boldsymbol{\sigma})\, \boldsymbol{x}\, \mathrm{d}S_p, \tag{2.149}$$

where, once more, we can express the normal stresses with respect to the 'stress' triad to find that the stresslet is identically zero for a solid sphere subject to a uniform flow:

$$\boldsymbol{S} = \frac{3}{2} a^{-1} \eta\, \boldsymbol{u}_\infty \cdot \left[ \oint_{S_p} \boldsymbol{\delta}\, \boldsymbol{x}\, \mathrm{d}S_p \right], \tag{2.150}$$

$$= \frac{3}{2} a^{-1} \eta\, \boldsymbol{u}_\infty \left[ \oint_{S_p} \boldsymbol{x}\, \mathrm{d}S_p \right] = \boldsymbol{0}, \tag{2.151}$$

because of the identity $\oint_{S_p} \boldsymbol{x}\, \mathrm{d}S_p = \boldsymbol{0}$ (see the appendix given by Deen [13]). The stresslet for symmetric solid bodies (such as spheroidal particles) is usually associated with the straining motion of the ambient fluid. The shape of the body must at least lack fore and aft symmetry to generate a stresslet in a uniform flow; classic examples are the spherical cap [75] and the aggregate of spheres of different radii [76]. In Section 2.3.4 a closed-form expression for the stresslet of a solid sphere in a general straining flow is derived.

It is well known that the viscous properties of a colloidal dispersion (a solid or liquid phase dispersed in a continous phase, such as a collection of small particles dispersed in a liquid phase) is influenced by the presence of the dispersed phase [21, 31]. That is, the viscous properties exhibited the dispersion are greater than those

of the host fluid, which gives rise to the concept of an effective viscosity. For a dilute dispersion of non-interacting particles the effective viscosity is readily determined by an average of the stresslets over all the particles that comprise the colloidal dispersion [13].

From the above result, the effective viscosity of a dilute dispersion of solid spheres exclusively subject to translation (or streaming flows) is zero. That is, the viscous properties of the dispersion are solely determined by the viscosity of the suspending fluid.

### 2.3.2 Singularity solutions of Stokes flow for a translating solid sphere

The velocity disturbances caused by the motion of a body can, in general, be described by a distribution of singular solutions to the Stokes flow equations [13, 31]. In this section, we use the results from the problem of Stokes flow past a solid sphere (Section 2.3.1) to determine the singular solutions that describe the disturbances caused by a solid sphere that translates.

The problem of a solid sphere that translates with a constant velocity $\boldsymbol{U}$ in a viscous, quiescent fluid at zero Reynolds number is considered here. In this limit, the problem of translation of the solid sphere in a fluid at rest is analogous to the problem of Stokes flow past a stationary sphere (just an interchange of the reference of motion). Now, the fluid is at rest far from the solid sphere, and the fluid in contact with the solid sphere moves with the velocity of the particle because of the no-slip and no-penetration conditions.

Thus, the governing equations read:

$$\left[\boldsymbol{\nabla P}(\boldsymbol{x}) - \nabla^2 \boldsymbol{V}(\boldsymbol{x})\right] \cdot \boldsymbol{U} = \boldsymbol{0}, \tag{2.152a}$$

$$\left[\boldsymbol{\nabla} \cdot \boldsymbol{V}(\boldsymbol{x})\right] \cdot \boldsymbol{U} = 0, \tag{2.152b}$$

$$\left[\boldsymbol{V}(\boldsymbol{x}) - \boldsymbol{\delta}\right] \cdot \boldsymbol{U} = \boldsymbol{0} \quad \text{at } r = a, \tag{2.152c}$$

$$\left[\boldsymbol{V}(\boldsymbol{x})\right] \cdot \boldsymbol{U} = \boldsymbol{0} \quad \text{as } r \to \infty. \tag{2.152d}$$

By following an analogous procedure to that shown in section 2.3.1, one finds the following expressions for the 'pressure' vector and 'velocity' dyad (the reader may refer to Happel & Brenner [20]):

$$\boldsymbol{P}(\boldsymbol{x}) = \frac{3}{2}\, a\, r^{-3}\, \boldsymbol{x}, \tag{2.153a}$$

$$\boldsymbol{V}(\boldsymbol{x}) = \frac{3}{4}\, a\Big(r^{-1}\, \boldsymbol{\delta} + r^{-3}\, \boldsymbol{x}\boldsymbol{x}\Big) + \frac{1}{4}\, a^3\Big(r^{-3}\, \boldsymbol{\delta} - 3r^{-5}\, \boldsymbol{x}\boldsymbol{x}\Big). \tag{2.153b}$$

The first parenthetical expression of the 'velocity' dyad is known as the Oseen tensor [31]:

$$\boldsymbol{J}(\boldsymbol{x}) = r^{-1}\, \boldsymbol{\delta} + r^{-3}\, \boldsymbol{x}\boldsymbol{x}, \tag{2.154}$$

which characterizes the disturbance field caused by a point-force (a sphere of zero volume); Deen [13] presents a simple approach to obtain the point-force solution from the disturbance velocity caused by a solid sphere of zero volume. It is interesting to note that the second parenthetical expression of the velocity dyad is proportional to the Laplacian of $\boldsymbol{J}(\boldsymbol{x})$, where it reads:

$$\nabla^2 \boldsymbol{J}(\boldsymbol{x}) = 2\, r^{-3}\, \boldsymbol{\delta} - 6\, r^{-5}\, \boldsymbol{x}\boldsymbol{x}, \tag{2.155}$$

such that $\boldsymbol{V}(\boldsymbol{x})$ may be written with respect to the Oseen tensor:

$$\boldsymbol{V}(\boldsymbol{x}) = \frac{3}{4}\, a\Big(\boldsymbol{J}(\boldsymbol{x}) + \frac{a^2}{6}\nabla^2 \boldsymbol{J}(\boldsymbol{x})\Big). \tag{2.156}$$

Note also that $a^2/6\, \nabla^2 \boldsymbol{J}(\boldsymbol{x})$ is a degenerate quadrupole, and like the point-force, it is a singular solution to the Stokes flow equations. The fundamental observation is that the disturbance flow-field caused by the translation of a solid sphere can be represented by the superposition of a point-force and a degenerate quadrupole. An useful application of the singular solutions to the Stokes flow equations is that these can be superimposed to characterize the disturbance field caused by bodies of other geometries (e.g. ellipsoidal particles). The interested reader is referred to the book of Kim and Karrila [31]. Additionally, the reader is referred to contribution of

Chwang & Wu [26], they introduced singular solutions to characterize the circulation flows of drops and bubbles in linear fields.

The disturbance velocity field $\boldsymbol{u}(\boldsymbol{x})$ caused by the motion of the sphere can be expressed as well with respect to the Oseen tensor by the relation $\boldsymbol{u}(\boldsymbol{x}) = \boldsymbol{U} \cdot \boldsymbol{V}(\boldsymbol{x})$ (note that $\boldsymbol{V}(\boldsymbol{x})$ is a symmetric tensor in this particular problem such that the scalar product yields the same result regardless of the side it is applied on):

$$\boldsymbol{u}(\boldsymbol{x}) = 6\pi a\eta \boldsymbol{U} \cdot \left[ \left( 1 + \frac{a^2}{6} \nabla^2 \right) \frac{\boldsymbol{J}(\boldsymbol{x})}{8\pi\eta} \right], \tag{2.157}$$

where the quantity $\boldsymbol{J}(\boldsymbol{x})/8\pi\,\eta$ is also known as the Oseen-Burgers tensor [13]. An important aspect of this result is that the force on the solid sphere ($\boldsymbol{F} = -6\pi a\eta \boldsymbol{U}$) is obtained without direct calculation via integration of the fluid stresses at the surface of the sphere. Note that the disturbance field caused by a stationary sphere in a uniform flow are also described by the above singularities due to the reversibility property of Stokes flow (just the sense the force acts is reversed).

### 2.3.3 Hydrodynamic resistance tensor of a fluid drop in Stokes flow

The main objective of this section is to derive a closed-form expression for the hydrodynamic resistance tensor of a fluid drop of radius $a$ to a uniform flow. The resistance tensor $\boldsymbol{A}$ (which has units of length) relates the undisturbed velocity $\boldsymbol{u}_\infty$ and the viscosity of the ambient fluid $\eta_0$ to the hydrodynamic force $\boldsymbol{F}$ on the drop via the linear relationship $\boldsymbol{F} = \eta_0 \boldsymbol{A} \cdot \boldsymbol{u}_\infty$. For the sake of completeness, it is shown that a fluid drop subject to Stokes flow is torque–free with a zero stresslet in a uniform flow. In order to achieve this it is necessary to find a solution to the Stokes flow problem in an arbitrary direction relative to the set of axes centered on the fluid drop. Thus, the analysis presented here is a generalization to the problem of Stokes flow (axisymmetric flow) about a fluid drop given in Section 2.2.3. For the sake of brevity, the notations and assumptions used in the axisymmetric counterpart of this problem are preserved; the exception, of course, being the axisymmetric character

of the flow everywhere. To that end, the 'pressure' vector and 'velocity' dyad are introduced for each fluid phase ($j = 0, 1$), which are related to the pressure and velocity fields in the usual manner:

$$p^{(j)}(\boldsymbol{x}) = \eta_j \boldsymbol{P}^{(j)}(\boldsymbol{x}) \cdot \boldsymbol{u}_\infty, \tag{2.158}$$

$$\boldsymbol{u}^{(j)}(\boldsymbol{x}) = \boldsymbol{V}^{(j)}(\boldsymbol{x}) \cdot \boldsymbol{u}_\infty. \tag{2.159}$$

As in the problem of a solid sphere in a 3D streaming flow, the governing equations are written with respect to the 'pressure' vector and 'velocity' dyad:

$$\boldsymbol{\nabla} \boldsymbol{P}^{(j)}(\boldsymbol{x}) = \nabla^2 \boldsymbol{V}^{(j)}(\boldsymbol{x}), \quad \boldsymbol{\nabla} \cdot \boldsymbol{V}^{(j)}(\boldsymbol{x}) = \boldsymbol{0}, \tag{2.160}$$

$$\boldsymbol{x} \cdot \boldsymbol{V}^{(j)}(\boldsymbol{x}) = \boldsymbol{0}, \ [\boldsymbol{V}(\boldsymbol{x})] = \boldsymbol{0}, \ \lambda\, \boldsymbol{x} \cdot \boldsymbol{\Pi}^{(1)}(\boldsymbol{x}) - \boldsymbol{x} \cdot \boldsymbol{\Pi}^{(0)}(\boldsymbol{x}) = \boldsymbol{0}, \quad \text{at } r = a, \tag{2.161}$$

$$\boldsymbol{V}(\boldsymbol{x}) = \boldsymbol{\delta}, \quad \text{as} \quad r \to \infty, \tag{2.162}$$

where the viscosity ratio of the internal to the ambient fluid is denoted by $\lambda = \eta_1/\eta_0$ (as in the axisymmetric problem), $\boldsymbol{\Pi}^{(j)}(\boldsymbol{x})$ is the 'stress' triad of the *jth* fluid phase, and, again, the brackets denotes a jump in the specified field from the outer to the inner fluid. The above set of boundary conditions specify the flow normal to the surface of the fluid sphere to vanish, and a zero jump in the velocity and stresses tangent to the surface of the sphere. The 'velocity' dyad reduces to the identity tensor far from the sphere (which is analogous to the recovery of the undisturbed flow far from the fluid drop).

A key aspect from the axisymmetric problem can be exploited here to further simplify the 'velocity' dyad for the ambient fluid. Since the flow about the fluid sphere is found to reduce to that of a solid sphere when $\lambda \gg 1$, one can propose that $\boldsymbol{V}^{(0)}(\boldsymbol{x})$ consists of the 'velocity' dyad of a solid sphere $\boldsymbol{V}_s(\boldsymbol{x})$ plus a correction $\tilde{\boldsymbol{V}}(\boldsymbol{x})$:

$$\boldsymbol{V}^{(0)}(\boldsymbol{x}) = \boldsymbol{V}_s(\boldsymbol{x}) + \tilde{\boldsymbol{V}}(\boldsymbol{x}). \tag{2.163}$$

The advantage of doing so is that $\boldsymbol{V}_s(\boldsymbol{x})$ automatically satisfies the far field condition. For the formulation to work, it is evident that the correction must vanish $\left(\tilde{\boldsymbol{V}}(\boldsymbol{x}) = \boldsymbol{0}\right)$ in the limit $\lambda \gg 1$. The reader may verify that such a construction is possible for the axisymmetric problem.

As in the 3D flow problem for the solid sphere, the linearity of Stokes equations allows the decomposition of the 'velocity' dyads into homogenuous and particular terms, such that the solution to the creeping flow equation simplifies to:

$$\nabla^2 \boldsymbol{V}_h^{(j)}(\boldsymbol{x}) = \boldsymbol{0}, \tag{2.164}$$

$$\nabla^2 \boldsymbol{V}_p^{(j)}(\boldsymbol{x}) = \boldsymbol{\nabla} \boldsymbol{P}^{(j)}. \tag{2.165}$$

Note that it follows from above that $\tilde{\boldsymbol{V}}(\boldsymbol{x})$ can also be decomposed into homogeneous and particular parts:

$$\nabla^2 \tilde{\boldsymbol{V}}_h(\boldsymbol{x}) = \boldsymbol{0}, \tag{2.166}$$

$$\nabla^2 \tilde{\boldsymbol{V}}_p(\boldsymbol{x}) = \boldsymbol{\nabla} \tilde{\boldsymbol{P}}. \tag{2.167}$$

In similarity with the 3D problem for a solid sphere, the following forms are assumed for the 'pressure' vectors and 'velocity' dyads (the reader may verify from the axisymmetric problem for the fluid sphere that the proposed forms work):

$$\boldsymbol{P}^{(j)} = f_j(r)\, \boldsymbol{x}, \tag{2.168}$$

$$\boldsymbol{V}_h^{(j)} = h_j(r)\, \boldsymbol{\delta} + g_j(r)\, \boldsymbol{x}\boldsymbol{x}, \quad \boldsymbol{V}_p^{(j)} = \frac{1}{2} f_j(r)\, \boldsymbol{x}\boldsymbol{x}. \tag{2.169}$$

Note that the analysis performed on the solid sphere showed that the particular term of the 'velocity' dyad is intrinsically related to $f_s(r)$. This becomes clear from the observation that the homogeneous functions alone ($h_s(r)$ and $g_s(r)$) could not satisfy $\boldsymbol{\nabla} \cdot \boldsymbol{V}_s(\boldsymbol{x}) = \boldsymbol{0}$ without the inclusion of the particular function $p_s(r)$, which turned out to be equal to $f_s(r)/2$. The closure point here is that $f_s(r)$ satisfies the Laplace equation for the 'pressure' vector ($\nabla^2 \boldsymbol{P}_s(\boldsymbol{x}) = \boldsymbol{0}$) and that this equation is

a direct consequence of requiring $\boldsymbol{\nabla} \cdot \boldsymbol{V}_s(\boldsymbol{x}) = \boldsymbol{0}$. Thus, it is only natural that $f_s(r)$ appears in the particular component of the 'velocity' dyad $\boldsymbol{V}_p(\boldsymbol{x})$. Note that this finding is a consequence of the Stokes equations, and therefore, it holds equally for the internal and outer flows of the fluid drop.

The scalar functions of the outer flows are further broken down to:

$$f_0(r) = f_s(r) + \tilde{f}(r), \tag{2.170}$$

$$h_0(r) = h_s(r) + \tilde{h}(r), \quad g_0(r) = g_s(r) + \tilde{g}(r), \tag{2.171}$$

where,

$$h_s(r) = \left[1 - \frac{3}{4}\left(\frac{a}{r}\right) - \frac{1}{4}\left(\frac{a}{r}\right)^3\right], \tag{2.172}$$

$$f_s(r) = -\frac{3}{2}a^{-1}r^{-3}, \quad g_s(r) = \frac{3}{4}a^3 r^{-5}. \tag{2.173}$$

In similarity with the problem of a solid sphere, the scalar functions satisfy the following system of ordinary differential equations (where the set arises from requiring $\nabla^2 \boldsymbol{P}^{(j)}(\boldsymbol{x}) = \boldsymbol{0}$ and $\nabla^2 \boldsymbol{V}_h^{(j)}(\boldsymbol{x}) = \boldsymbol{0}$):

$$f_j''(r) + \frac{4}{r} f_j'(r) = 0, \tag{2.174}$$

$$g_j''(r) + \frac{6}{r} g_j'(r) = 0, \quad h_j''(r) + \frac{2}{r} h_j'(r) + 2g_j(r) = 0. \tag{2.175}$$

It is easy to see that the above equations are equidimensional with solutions of the form of $r^n$ and $r^{-n}$ for internal and decaying flows, respectively. The scalar functions that describe the internal flows are found to be:

$$h_1(r) = -\frac{1}{3}B_1 r^2 + C_1, \tag{2.176}$$

$$f_1(r) = A_1, \quad g_1(r) = B_1, \tag{2.177}$$

and those of the ambient flow:

$$\tilde{h}(r) = -\frac{1}{3}\tilde{B}r^{-3} + \tilde{C}r^{-1}, \tag{2.178}$$

$$\tilde{f}(r) = \tilde{A}r^{-1}, \quad \tilde{g}(r) = \tilde{B}r^{-5}. \tag{2.179}$$

From application of the continuity equation it is found that:

$$A_1 = -\frac{5}{3}B_1, \quad \tilde{A} = 2\tilde{C}. \tag{2.180}$$

Thus, the 'velocity' dyads can now be expressed with respect to a set of 4 coefficients that must be determined from 4 independent boundary conditions (the problem is reduced to the determination of a group of constants in analogy with the stream function formulation):

$$\boldsymbol{V}^{(1)}(\boldsymbol{x}) = \left[-\frac{1}{3}B_1 r^2 + C_1\right]\boldsymbol{\delta} + \frac{1}{6}B_1\boldsymbol{x}\boldsymbol{x}, \tag{2.181}$$

$$\boldsymbol{V}^{(0)}(\boldsymbol{x}) = \boldsymbol{V}_s(\boldsymbol{x}) + \left[-\frac{1}{3}\tilde{B}r^{-3} + \tilde{C}r^{-1}\right]\boldsymbol{\delta} + \left[\tilde{B}r^{-5} + \tilde{C}r^{-3}\right]\boldsymbol{x}\boldsymbol{x}. \tag{2.182}$$

Note that $\boldsymbol{V}_s(\boldsymbol{x})$ vanishes identically at the surface of the sphere and reduces to the far field at large distances from the sphere. It will be shown later that it is only needed when considering the jump in shear stresses at the surface of the sphere.

Application of the no-penetration condition $\left(\boldsymbol{x}\cdot\boldsymbol{V}^{(j)}(\boldsymbol{x}) = \boldsymbol{0}\right)$ yields the first pair of equations:

$$-\frac{1}{6}a^2 B_1 + C_1 = 0, \tag{2.183}$$

$$\frac{2}{3}a^{-3}\tilde{B} + 2a^{-1}\tilde{C} = 0. \tag{2.184}$$

Requiring a zero jump in the velocity and stresses tangent to the surface of the fluid sphere result in the last pair of equations:

$$\left(-\frac{1}{3}a^2 B_1 + C_1\right) - \left(-\frac{1}{3}a^{-3}\tilde{B} + a^{-1}\tilde{C}\right) = 0, \tag{2.185}$$

$$\lambda\left(-\frac{1}{2}aB_1\right) - \left(\frac{3}{2}a^{-1} + 2a^{-4}\tilde{B}\right) = 0, \tag{2.186}$$

where Equation (2.138) has been used to calculate the shear stresses at the surface of the fluid sphere; note that the referenced function $G(r)$ in (2.138) corresponds to the expression that accompanies the $\boldsymbol{xx}$ term in the 'velocity' dyad. It is also important to realize that the expressions that accompany $\boldsymbol{\delta}$ in the 'velocity' and 'stress' tensors act tangent to the surface of the sphere (which is easy to see by considering that the dot product of any tangent vector $\boldsymbol{t}$ to the surface of the sphere satisfies $\boldsymbol{t}\cdot\boldsymbol{x} = 0$).

Solution of the above system of equations results in the sought expressions for the coefficients of the inner and outer flows:

$$A_1 = \frac{5}{1+\lambda}\,a^{-2}, \quad B_1 = -\frac{3}{1+\lambda}\,a^{-2}, \quad C_1 = -\frac{1}{2\,(1+\lambda)}, \tag{2.187}$$

$$\tilde{A} = \frac{1}{2\,(1+\lambda)}\,a, \quad \tilde{B} = -\frac{3}{4\,(1+\lambda)}\,a^3, \quad \tilde{C} = \frac{1}{4\,(1+\lambda)}\,a. \tag{2.188}$$

Therefore, the corresponding scalar functions of the internal fluid become:

$$h_1(r) = -\frac{1}{2\,(1+\lambda)}\left[1 - 2\left(\frac{r}{a}\right)^2\right], \tag{2.189a}$$

$$f_1(r) = \frac{5}{1+\lambda}\,a^{-2}, \quad g_1(r) = -\frac{3}{1+\lambda}\,a^{-2}, \tag{2.189b}$$

ambient fluid are:

$$\tilde{h}(r) = \frac{1}{4\,(1+\lambda)}\left[\left(\frac{a}{r}\right) + \left(\frac{a}{r}\right)^3\right], \tag{2.190a}$$

$$\tilde{f}(r) = \frac{1}{2\,(1+\lambda)}\,a\,r^{-3}, \quad \tilde{g}(r) = -\frac{3}{4\,(1+\lambda)}\,a^3\,r^{-5}, \tag{2.190b}$$

Therefore, the 'velocity' dyad of the internal and ambient can now be expressed as:

$$\boldsymbol{V}^{(1)}(\boldsymbol{x}) = -\frac{1}{2\,(1+\lambda)}\left[1-2\left(\frac{r}{a}\right)^2\right]\boldsymbol{\delta} - \frac{1}{2\,(1+\lambda)}\left(\frac{r}{a}\right)^2 \boldsymbol{x}\boldsymbol{x}, \tag{2.191}$$

$$\begin{aligned}\boldsymbol{V}^{(0)}(\boldsymbol{x}) = &\left[1-\frac{2+3\lambda}{4\,(1+\lambda)}\left(\frac{a}{r}\right)-\frac{\lambda}{4\,(1+\lambda)}\left(\frac{a}{r}\right)^3\right]\boldsymbol{\delta} \\ &+\left(\frac{3\lambda}{4\,(1+\lambda)}a\,r^{-3}-\frac{2+3\lambda}{4\,(1+\lambda)}a^3\,r^{-5}\right)\boldsymbol{x}\boldsymbol{x},\end{aligned} \tag{2.192}$$

where it is easy to see that $\boldsymbol{V}^{(0)}(\boldsymbol{x}) = \boldsymbol{V}_s(\boldsymbol{x})$ as $\lambda \to \infty$ in accordance to the aforementioned expectations. Note that the 'velocity' dyad of the internal fluid $\boldsymbol{V}^{(1)}(\hat{\boldsymbol{x}})$ vanishes to zero as $\lambda \to \infty$, which indicates that the internal phase behaves as a solid phase in this limit. The reader can easily verify that the velocity fields for a fluid sphere subject to an axisymmetric uniform flow, given in Equations (2.68) and (2.69), are recovered via $\boldsymbol{u}^{(j)} = \boldsymbol{V}^{(j)} \cdot \boldsymbol{u}_\infty$, where the undisturbed flow is given by $\boldsymbol{u}_\infty = -u_\infty \boldsymbol{e}_z$. As in the problem of the solid sphere, the 'velocity' dyads are independent of the direction of the undisturbed flow $\boldsymbol{u}_\infty$, and therefore, the corresponding velocity fields are always recovered regardless of the arrangement of the flow with respect to the reference frame on the body. This is one of the benefits of solving fluid flow problems with this formulation.

The 'pressure' vectors that develop inside and outside the fluid sphere are:

$$\boldsymbol{P}^{(1)}(\hat{\boldsymbol{x}}) = \; 5a^{-1}\frac{1}{1+\lambda}\left(\frac{r}{a}\right)\hat{\boldsymbol{x}}, \tag{2.193}$$

$$\boldsymbol{P}^{(0)}(\hat{\boldsymbol{x}}) = -\frac{3}{2}a^{-1}\left(\frac{a}{r}\right)^2\hat{\boldsymbol{x}} + \frac{1}{2}a^{-1}\frac{1}{1+\lambda}\left(\frac{a}{r}\right)^2\hat{\boldsymbol{x}}, \tag{2.194}$$

where, the latter term of $P^{(0)}(\hat{\boldsymbol{x}})$ corresponds to $\tilde{\boldsymbol{P}}(\hat{\boldsymbol{x}})$. The 'pressure' vector of the outer fluid can be rewritten in the more familiar manner:

$$\boldsymbol{P}^{(0)}(\hat{\boldsymbol{x}}) = -a^{-1}\left(\frac{2+3\lambda}{2+2\lambda}\right)\left(\frac{a}{r}\right)^2\hat{\boldsymbol{x}}. \tag{2.195}$$

It is straightforward to notice that the above expression for the 'pressure' vector is consistent with the pressure field given in Equation (2.71) for an axisymmetric streaming flow via $p^{(0)} = \eta_0 \boldsymbol{P} \cdot \boldsymbol{u}_\infty$. (Note that setting the gravitational field and the pressure far away in (2.71) to zero yields identical expressions.) Analogous arguments hold for $\boldsymbol{P}^{(1)}(\hat{\boldsymbol{x}})$ as well.

By following a procedure analogous to that of a solid sphere (Section 2.3.1) for the determination of the drag force $\boldsymbol{F}$ on the fluid sphere, one finds that $\boldsymbol{F}$ is always parallel to the flow:

$$\boldsymbol{F} = 2\pi a \eta_0 \left( \frac{2 + 3\lambda}{2 + 2\lambda} \right) \boldsymbol{u}_\infty. \tag{2.196}$$

Note that in the extremes of $\lambda \ll 1$ (negligible internal viscosity) and $\lambda \gg 1$ (rigid-body limit), the drag force reduces to that on a bubble and a solid sphere, respectively, in agreement with the findings of Section 2.2.3. From the above expression for the force, it follows that the hydrodynamic resistance of the fluid drop to a uniform flow is isotropic:

$$\boldsymbol{A} = 2\pi a \left( \frac{2 + 3\lambda}{2 + 2\lambda} \right) \boldsymbol{\delta}, \tag{2.197}$$

where the presence of the identity tensor $\boldsymbol{\delta}$ confirms that the fluid drop offers an isotropic resistance to a uniform flow. By following a procedure analogous to that done in Section 2.3.1 for the calculation of the torque on a solid sphere in Stokes flow, it can be found that the drop is also torque–free ($\boldsymbol{T} = \boldsymbol{0}$), which agrees well with one's intuition since there are no means for a uniform flow to impose a net torque on a spherical body with an isotropic resistance to the flow. (An example of a spherical body with an anisotropic resistance to a uniform flow is the 'slip–stick' sphere [77].) By following analogous arguments to those used for the solid sphere it can be found that the stresslet of the fluid drop to the uniform flow is identically zero, where again, is a consequence of the isotropic resistance of the body to the external flow.

On regard to the continuity of the normal stresses $\sigma_{nn}$ at the fluid–fluid interface ($r = a$), it is expected that there is no jump from one fluid phase to the other; the interested reader may add the gravitational term to the 'pressure' vector to obtain a result analogous to that found in the axisymmetric problem (Section 2.2.3). The normal stresses associated with fluid motion are evenly matched by those exerted by gravity at every point along the fluid–fluid interface for a zero jump in the normal stresses.

The disturbance to the flow ($\boldsymbol{u}_D(\boldsymbol{x}) = \boldsymbol{u}(\boldsymbol{x}) - \boldsymbol{u}_\infty$) caused by the presence of the fluid sphere can be readily derived from the 'velocity' dyad of the ambient fluid. By noting that the Oseen tensor $\boldsymbol{J}(\boldsymbol{x})$ appears in the 'velocity' dyad of the ambient flow, an expression for the disturbance is obtained after some algebraic manipulations:

$$\boldsymbol{V}_D(\boldsymbol{x}) = \boldsymbol{V}^{(0)}(\boldsymbol{x}) - \boldsymbol{\delta} = -\frac{3}{4}a\left(\frac{2+3\lambda}{3+3\lambda} + a^2\frac{\lambda}{6+6\lambda}\nabla^2\right)\boldsymbol{J}(\boldsymbol{x}), \tag{2.198}$$

where, in analogy with the problem of Stokes flow past a solid sphere, the disturbaced caused by the fluid sphere is described by a point-force and a degenerate quadrupole. Note that in the limit of a highly viscous drop ($\lambda \gg 1$) the singularities for a solid sphere are recovered.

### 2.3.4 Stresslet of a solid sphere in a general straining flow

In this section a closed-form expression for the stresslet of a solid sphere in a general straining flow is derived. The stresslet captures the distribution of the stresses at the surface of the body and the long-range disturbance effects in the fluid [13]. The stresslet is a quantity of primary importance for the fundamental understanding of the bulk viscous properties of colloidal suspensions under the influence of a uniform shear flow (which ubiquitous type of flow found in both nature and industrial applications). To this end, a solution to the Stokes equations is sought when the solid sphere is subject to a general straining flow $\boldsymbol{u}_\infty = \boldsymbol{E}^\infty \cdot \boldsymbol{x}$, where $\boldsymbol{E}^\infty$ is the rate-of-strain tensor of the undisturbed flow. The analysis that

follows only relies on the symmetry of the rate-of-strain tensor ($E^{\infty}_{kl} = E^{\infty}_{lk}$) and the zero trace constraint $E^{\infty}_{kk} = 0$ [13, 31] to derive an expression for the stresslet. (The traceless rate-of-strain tensor is a direct consequence of satisfying continuity of mass.) The problem considered in Section 2.2.4 corresponds to the particular case of an axisymmetric elongational flow, in which the stream function was conveniently used to analyze the flow. In this section one has to resort to the determination of the 'velocity' dyad and the 'pressure' vector to derive an exact expression for the stresslet on the solid sphere. For the sake of completeness, it is shown that the solid sphere is both force and torque–free in a general straining flow.

The boundary value problem of concern is presented with respect to the pressure $p(\boldsymbol{x})$ and velocity $\boldsymbol{u}(\boldsymbol{x})$ fields about the solid sphere:

$$\boldsymbol{\nabla} p(\boldsymbol{x}) = \eta \nabla^2 \boldsymbol{u}(\boldsymbol{x}), \quad \boldsymbol{\nabla} \cdot \boldsymbol{u}(\boldsymbol{x}) = 0, \tag{2.199}$$

$$\boldsymbol{n} \cdot \boldsymbol{u}(\boldsymbol{x}) = 0, \ \boldsymbol{t} \cdot \boldsymbol{u}(\boldsymbol{x}) = 0, \quad \text{at} \quad r = a, \tag{2.200}$$

$$\boldsymbol{u}(\boldsymbol{x}) = \boldsymbol{E}^{\infty} \cdot \boldsymbol{x}, \quad \text{as} \quad r \to \infty, \tag{2.201}$$

where $\boldsymbol{n}$ and $\boldsymbol{t}$ are the unit normal and tangent vectors to the surface of the sphere, respectively. Basically, there is no flow through the solid sphere, and no relative motion between the fluid and the solid at its surface. (The usual no-penetration and no-slip conditions at the surface of the solid.) The velocity field $\boldsymbol{u}(\boldsymbol{x})$ must reduce to the undisturbed velocity ($\boldsymbol{u}_{\infty} = \boldsymbol{E}^{\infty} \cdot \boldsymbol{x}$) at distances far from the sphere.

It is worth mentioning that for this particular problem it is far more convenient to deal directly with the pressure and velocity fields rather than with the 'pressure' vector and 'velocity' dyad. This is understood by recalling that for the problem of Stokes flow past a solid sphere (Section 2.3.1) $\boldsymbol{u}_{\infty}$ is a constant vector that can be easily extracted from the gradient and Laplacian operators such that analogous governing equations can be obtained for the 'pressure' vector and 'velocity' dyad. In this problem, however, the undisturbed velocity is not a constant vector with a

zero gradient, but a vector field characterized by a uniform gradient, which arises from the imposed rate of strain ($\boldsymbol{\nabla u}_\infty = \boldsymbol{E}^\infty$). Hence, unlike the Stokes problem, the governing equations for the 'pressure' vector and 'velocity' dyad would be complicated with the appearance of terms containing $\boldsymbol{\nabla u}_\infty$; defeating the purpose of introducing them in the first place.

Despite the inherent complications of a flow with a non-zero velocity gradient, the form of the pressure and velocity fields is not expected to differ from that of Stokes flow (the assumed forms are principally based on the geometry of the body):

$$p(\boldsymbol{x}) = \eta \left[ f(r)\, \boldsymbol{x} \right] \cdot \boldsymbol{E}^\infty \cdot \boldsymbol{x}, \tag{2.202}$$

$$\boldsymbol{u}(\boldsymbol{x}) = \Big[ h(r)\, \boldsymbol{\delta} + G(r)\, \boldsymbol{xx} \Big] \cdot \boldsymbol{E}^\infty \cdot \boldsymbol{x}, \tag{2.203}$$

where $f(r)$, $G(r)$ and $h(r)$ are scalar functions that are determined from application of the governing equations and boundary conditions to the pressure and velocity fields. It is noteworthy that the above bracketed expressions correspond to the 'pressure' vector $\boldsymbol{P}(\boldsymbol{x})$ and 'velocity' dyad $\boldsymbol{V}(\boldsymbol{x})$, respectively.

As in the problem of Stokes flow, the pressure field is treated as an inhomogeneous term in the Stokes equations by separating the velocity field $\boldsymbol{u}(\boldsymbol{x})$ into homogeneous $\boldsymbol{u}^h(\boldsymbol{x})$ and particular components $\boldsymbol{u}^p(\boldsymbol{x})$, such that solution to the creeping motion equation is achieved in two steps:

$$\nabla^2 \boldsymbol{u}^h(\boldsymbol{x}) = \boldsymbol{0}, \tag{2.204}$$

$$\eta \nabla^2 \boldsymbol{u}^p(\boldsymbol{x}) = \boldsymbol{\nabla} p(\boldsymbol{x}), \tag{2.205}$$

where,

$$\boldsymbol{u}^h(\boldsymbol{x}) = \Big[ h(r)\, \boldsymbol{\delta} + g(r)\, \boldsymbol{xx} \Big] \cdot \boldsymbol{E}^\infty \cdot \boldsymbol{x}, \tag{2.206}$$

$$\boldsymbol{u}^p(\boldsymbol{x}) = \left[ \mathscr{P}(r)\, \boldsymbol{xx} \right] \cdot \boldsymbol{E}^\infty \cdot \boldsymbol{x}, \tag{2.207}$$

which implies that $G(r) = g(r) + \mathscr{P}(r)$ in Equation (2.203). It will become apparent that the scalar function $\mathscr{P}(r)$ is directly related to the pressure field $p(\boldsymbol{x})$ later on.

The solution methodology to determine $p(\boldsymbol{x})$ and $\boldsymbol{u}(\boldsymbol{x})$ is concisely summarized here. First, an ordinary differential equation for $f(r)$ is obtained by requiring the pressure field to satisfy $\nabla^2 p(\boldsymbol{x}) = 0$ everywhere in the fluid. This is followed by the solution of $\nabla^2 \boldsymbol{u}^h(\boldsymbol{x}) = \boldsymbol{0}$ that leads to a pair of ordinary differential equations for $h(r)$ and $g(r)$. Then, $p(r)$ is determined by solution of $\eta \nabla^2 \boldsymbol{u}^p(\boldsymbol{x}) = \boldsymbol{\nabla} p(\boldsymbol{x})$. The equation of continuity $\boldsymbol{\nabla} \cdot \boldsymbol{u}(\boldsymbol{x}) = 0$ is applied to verify the solutions, and only then, the pertaining boundary conditions are imposed. The analysis of the flow concludes by showing that $p(\boldsymbol{x})$ and $\boldsymbol{u}(\boldsymbol{x})$ reduces to those obtained by the stream function for an axisymmetric elongational flow (consider Equations (2.105) and (2.104) in the limit of $\lambda \to \infty$). An important aspect of the solution is that it applies to any kind of straining motion with the structure of the flow contained in the rate-of-strain tensor.

Throughout the analysis that follows tensors are dealt with via index notation for convenience. Operating the gradient to the pressure field results in the following expression:

$$\frac{\partial p}{\partial x_j} = \eta \left[ 2 f(r)\, \delta_{j\,k} + \frac{1}{r} f'(r)\, x_j x_k \right] E^{\infty}_{kl}\, x_l, \tag{2.208}$$

where the replacement of $x_k\, E^{\infty}_{kl}\, \delta_{lj} = \delta_{jk}\, E_{kl}\, x_l$ has been carried out on account of the symmetry of the rate-of-strain tensor ($E^{\infty}_{kl} = E^{\infty}_{lk}$). It is interesting to see that the brackted expression is analogous to the 'pressure' gradient found for the Stokes flow problem past a solid sphere (2.110). The Laplace equation for the pressure field ($\nabla^2 p(\boldsymbol{x}) = 0$) is obtained by application of the divergence operator to the above equation and requiring it to vanish everywhere in the fluid:

$$\nabla^2 p = \eta \left[ f''(r) + \frac{6}{r} f'(r) \right] x_k\, E^{\infty}_{kl}\, x_l = 0, \tag{2.209}$$

where it is important to mention that the property $\delta_{jk}\, E^{\infty}_{kl}\, \delta_{lj} = E^{\infty}_{jj} = 0$ has been used to arrive to the above equation (in addition to other elementary identities that were introduced in Section 2.3.1). By noting that the term outside the brackets is just an arbitrary scalar quantity, the Laplace equation yields an ordinary differential equation for the function $f(r)$. The ordinary differential equation is identified to be of equidimensional character with general solutions $r^n$ and $r^{-n}$. The only meaningful solution to the problem at hand is the decaying one since the pressure field vanishes at distances far from the solid sphere (which is a consequence of imposing a linear flow: $\boldsymbol{\nabla} p_{\infty} = \nabla^2 \boldsymbol{u}_{\infty} = \boldsymbol{0}$.) Carrying out the substitution $f(r) = r^{-n}$ yields a simple algebraic equation for $n$:

$$n(n-5)\, r^{-n-2} = 0, \tag{2.210}$$

where, again, $r^{-n-2}$ is just an arbitrary constant, such that the algebraic equation is satisfied identically for $n = 5$ (the $n = 0$ solution is not needed in view of the mentioned arguments). Therefore, it is found that $f(r) = A\, r^{-5}$, where $A$ is a constant to be determined later from the boundary conditions. Unfortunately, it cannot be found at this point because the pressure is not known at any other location — such as the surface of the solid sphere — except far from the sphere. For the time being, that concludes the analysis for the pressure field.

In order to find an expression for $\nabla^2 \boldsymbol{u}^h(\boldsymbol{x}) = \boldsymbol{0}$, it is necessary to calculate first the velocity gradient $\boldsymbol{\nabla} u^h(\boldsymbol{x})$ (which will also be useful to determine the force and stresslet on the solid sphere):

$$\begin{aligned}\frac{\partial u_j}{\partial x_i} = &\left[\frac{1}{r} h'(r)\, x_i\, \delta_{jk} + g(r)\, (\delta_{ij}\, x_k + x_j\, \delta_{ik}) + \frac{1}{r} g'(r)\, x_i\, x_j\, x_k\right] E^{\infty}_{kl}\, x_l + \\ &\Big(h(r)\, \delta_{jk} + g(r)\, x_j\, x_k\Big) E^{\infty}_{kl}\, \delta_{li}.\end{aligned} \tag{2.211}$$

Note that the bracketed expression is identical to the 'velocity' dyad of the Stokes flow problem for a solid sphere (2.113); the additional terms found here arise from

the velocity gradient of the undisturbed flow, those enclosed by parenthesis, which are clearly absent in the Stokes flow problem because there is a uniform velocity field far away from the particle.

The Laplacian of $\boldsymbol{u}^h(\boldsymbol{x})$ is obtained by application of the divergence to Equation (2.211); with some patience it is found that

$$\nabla^2 u^h_{jk} = \left[\left(h''(r) + \frac{4}{r}h'(r) + 4g(r)\right)\delta_{jk} + \left(g''(r) + \frac{8}{r}g'(r)\right)x_j\, x_k\right] E^\infty_{kl}\, x_l = 0. \tag{2.212}$$

Analogous elementary properties to those used in Section 2.3.1 were used to arrive to the above equation. Since $\delta_{jk}$ and $x_j\, x_k$ are arbitrary tensors, $\nabla^2\boldsymbol{u}^h(\boldsymbol{x}) = \boldsymbol{0}$ only if the parenthetical expressions vanish identically to zero. Therefore, the problem of requiring $\nabla^2\boldsymbol{u}^h(\boldsymbol{x}) = \boldsymbol{0}$ is reduced to the solution of a set of ordinary differential equations for the functions $h(r)$ and $g(r)$:

$$g''(r) + \frac{8}{r}g'(r) = 0, \tag{2.213}$$

$$h''(r) + \frac{4}{r}h'(r) + 4g(r) = 0, \tag{2.214}$$

where both differential equations are of equidimensional form with general solutions $r^n$ and $r^{-n}$. It is advantageous to determine first the homogeneous solutions to the above set of equations. Substitution of $g(r) = h(r) = r^{-n}$ results in the corresponding algebraic expressions given below:

$$n(n-7)\, r^{-n-2} = 0, \tag{2.215}$$

$$n(n-3)\, r^{-n-2} = 0, \tag{2.216}$$

where it is easy to see that there are solutions for $n = 7$ and $n = 3$, respectively, such that $g(r) = Br^{-7}$ and $h(r) = Cr^{-3} + D$. The constant $D$ ensures that the velocity field reduces to the unperturbed flow far away from the particle. By assuming that the particular solution is also of equidimensional form $h^p(r) = \mathscr{E}\, r^{-n}$, the following

algebraic equation results from the complete differential equation for $h(r)$:

$$n(n-3)\,\mathscr{E}\,r^{-n-2} = -4\,B\,r^{-7}, \tag{2.217}$$

where there is a solution if $n = 5$ and $\mathscr{E} = -2B/5$. Hence, the final expressions for the scalar functions are:

$$f(r) = A\,r^{-5}, \quad g(r) = B\,r^{-7}, \tag{2.218}$$

$$h(r) = -\frac{2}{5}B\,r^{-5} + C\,r^{-3} + D. \tag{2.219}$$

From here on the particular form of the velocity field $\boldsymbol{u}^p(\boldsymbol{x})$ is considered. Note that the form of the pressure gradient expressed by Equation (2.208) confirms that $u^p_{jk} = \mathscr{P}(r)\,x_j\,x_k\,E^\infty_{kl}\,x_l$ is a consistent expression for the particular velocity field. (The reader may recall that this form of the velocity field is analogous to that of the Stokes flow problem.) Substitution of the obtained pressure gradient (2.208) and the Laplacian of $\boldsymbol{u}^p(\boldsymbol{x})$, which is easily deduced from Equation (2.212), into the creeping flow equation (2.199) results in the expression shown below:

$$\eta\left[2f(r)\delta_{jk} + \frac{1}{r}f'(r)x_jx_k\right]E^\infty_{kl}x_l = \eta\left[4\mathscr{P}(r)\delta_{jk} + \left(\mathscr{P}''(r) + \frac{8}{r}\mathscr{P}'(r)\right)x_jx_k\right]E^\infty_{kl}x_l, \tag{2.220}$$

where the solution to the algebraic part of the above equation is

$$\mathscr{P}(r) = \frac{1}{2}f(r) = \frac{1}{2}A\,r^{-5}. \tag{2.221}$$

The reader may verify with ease that $\nabla^2 p(\boldsymbol{x}) = 0$ (2.209) is recovered by the substitution of $\mathscr{P}(r) = f(r)/2$ into the differential part of Equation (2.220). It is interesting that the same proportionality between $\mathscr{P}(r)$ and $f(r)$ has also been found in the problems of Stokes flow about a solid sphere and a fluid drop, which suggests that the dependence of the fluid flow about the particle with the pressure is

principally a geometrical one. This concludes the demonstration that the particular part of the velocity field is intrinsically related to the pressure.

Although the imposition of $\nabla^2 p(\boldsymbol{x}) = 0$ to the pressure field indirectly satisfies the equation of continuity ($\boldsymbol{\nabla} \cdot \boldsymbol{u}(\boldsymbol{x}) = 0$), it is instructive to verify that the complete expression of $\boldsymbol{u}(\boldsymbol{x}) = \Big[h(r)\boldsymbol{\delta} + G(r)\boldsymbol{x}\boldsymbol{x}\Big] \cdot \boldsymbol{E}^{\infty} \cdot \boldsymbol{x}$ agrees with the conservation of mass requirement. Moroever, there are currently four unknown constants for a total of three boundary conditions for the velocity field that have not been used; this indicates that one additional relation is needed in order to determine the flow about the solid sphere. The equation of continuity is obtained by application of the divergence operator to the velocity field:

$$\frac{\partial u_j}{\partial x_j} = \left[\frac{1}{r}h'(r) + rg'(r) + 5g(r) + r\mathscr{P}'(r) + 5\mathscr{P}(r)\right] x_k \, E^{\infty}_{kl} \, x_l = 0, \tag{2.222}$$

where after some elementary operations it is found that terms associated with the constants $B$ and $D$ cancel out with $h'(r)/r + rg'(r) + 5g(r)$, and those proportional to $A$ vanish with $\mathscr{P}'(r) + 5\mathscr{P}(r)$ leaving $-3C\, r^{-4}$ unbalanced. Thus, it follows that $C$ must be equal to zero for $\boldsymbol{\nabla} \cdot \boldsymbol{u}(\boldsymbol{x}) = 0$.

Application of the pertaining boundary conditions reveals that the values of the constants are:

$$A = -5\, a^3, \quad B = \frac{5}{2}\, a^5, \quad D = 1, \tag{2.223}$$

such that the scalar functions now read:

$$f(r) = -5\, a^3\, r^{-5}, \quad g(r) = \frac{5}{2}\, a^5\, r^{-7}, \tag{2.224}$$

$$h(r) = 1 - \left(\frac{a}{r}\right)^5. \tag{2.225}$$

The pressure and velocity fields can now be expressed as:

$$p(\boldsymbol{x}) = \eta\big[ -5\,a^3\,r^{-5}\boldsymbol{x}\big] \cdot \boldsymbol{E}^{\infty} \cdot \boldsymbol{x}, \tag{2.226}$$

$$\boldsymbol{u}(\boldsymbol{x}) = \left[\left(1 - \left(\frac{a}{r}\right)^5\right)\boldsymbol{\delta} + \frac{5}{2}\Big( -a^3\,r^{-5} + a^5\,r^{-7}\Big)\boldsymbol{x}\,\boldsymbol{x}\right] \cdot \boldsymbol{E}^{\infty} \cdot \boldsymbol{x}, \tag{2.227}$$

where it is notable that the bracketed expressions correspond to the 'pressure' vector $\boldsymbol{P}(\boldsymbol{x})$ and 'velocity' dyad $\boldsymbol{V}(\boldsymbol{x})$ for a solid sphere in a general elongational flow. Now that both the pressure and velocity fields have been found, it is possible to determine the net force $\boldsymbol{F}$, torque $\boldsymbol{T}$ and stresslet $\boldsymbol{S}$ on the particle exerted by the elongational flow. The shear-force tensor $\boldsymbol{G}$ and shear-torque tensor $\boldsymbol{H}$, which relate the imposed rate-of-strain $\boldsymbol{E}^{\infty}$ with the respective force and torque on the particle, are determined for completeness.

The net force on the solid sphere imparted by the elongational flow can be shown to be identically zero by integration of the fluid stress at the surface of the particle:

$$\boldsymbol{F} = \oint_{S_p} \boldsymbol{n} \cdot \boldsymbol{\sigma}\ \mathrm{d}S_p, \tag{2.228}$$

where the normal stress at the surface of the particle is found to be (the efforts to arrive to the sought expression are reduced by noting that $h(a) = G(a) = 0$):

$$n_i\sigma_{ij} = \eta\,a^{-1}\left[a\,h'(a)\delta_{jk} + \Big( -f(a) + h'(a)/a + 2a\,G(a)\Big)x_j\,x_k\right] E^{\infty}_{kl}\,x_l, \tag{2.229}$$

where the parenthetical (or position dyad) expression vanishes at the surface of the particle such that the above equation simplifies to $\boldsymbol{n}\cdot\boldsymbol{\sigma} = 5\,\eta\,a^{-1}\boldsymbol{E}^{\infty}\cdot\boldsymbol{x}$. Therefore, the force on the particle may be conveniently expressed as:

$$\boldsymbol{F} = 5\,\eta\,a^{-1}\left[\oint_{S_p} \boldsymbol{x}\ \mathrm{d}S_p\right] \cdot \boldsymbol{E}^{\infty}, \tag{2.230}$$

where the symmetry property of the rate-of-strain tensor has been used. It follows from the surface integral of the position vector $\boldsymbol{x}$ that the force on the particle is identically zero.

The torque on the particle is given by the first moment of the fluid stress at its surface ($r = a$):

$$\begin{aligned} \boldsymbol{T} &= \oint_{S_p} \boldsymbol{x} \times (\boldsymbol{n} \cdot \boldsymbol{\sigma}) \ \mathrm{d}S_p, \\ &= 5\,\eta\, a^{-1} \left[ \oint_{S_p} \boldsymbol{x} \times \boldsymbol{x} \ \mathrm{d}S_p \right] \cdot \boldsymbol{E}^{\infty}, \end{aligned} \tag{2.231}$$

where it is clear from the above that the resultant torque on the particle is zero because of the identity $\boldsymbol{x} \times \boldsymbol{x} = \boldsymbol{0}$. This is the expected result on account of the symmetry of the elongational flow and the spherical geometry of the particle.

The stresslet is given by the second moment of the fluid stress at the surface of the particle:

$$\begin{aligned} \boldsymbol{S} &= \oint_{S_p} \boldsymbol{x}\, (\boldsymbol{n} \cdot \boldsymbol{\sigma}) \ \mathrm{d}S_p, \\ &= 5\,\eta\, a^{-1} \left[ \oint_{S_p} \boldsymbol{x}\, \boldsymbol{x} \ \mathrm{d}S_p \right] \cdot \boldsymbol{E}^{\infty}, \end{aligned} \tag{2.232}$$

where the well-known result for the stresslet on a solid particle in an elongational flow follows by substitution of the integral identity $\left( \oint \boldsymbol{x}\, \boldsymbol{x} \ \mathrm{d}S_p = 4\pi a^4/3 \ \boldsymbol{\delta} \right)$ [13]:

$$\boldsymbol{S} = \frac{20}{3} \pi \eta a^3 \boldsymbol{E}^{\infty}. \tag{2.233}$$

This result for the stresslet is more general than that given in [13] because it is not tied to any particular case of straining flow (e.g. axisymmetric elongational flow). The interesting finding is that the stresslet on the solid sphere is the same regardless of the apparatus used to generate the straining flow (provided that the effect of the boundaries of the device are negligible). It is important to point out that the second moment of the surface tractions actually yields the hydrodynamic dipole, which in

general can be broken down into symmetric and antisymmetric parts; the symmetric part of the hydrodynamic dipole corresponds to the stresslet and the antisymmetric one is the rotlet (a quantity associated with the torque) [31]. Being the straining flow inherently irrotational it follows immediately that the hydrodynamic dipole only consists of its symmetric component—the stresslet.

In the context of hydrodynamic resistances, there is a third-rank tensor $\boldsymbol{G}$ (the shear-force tensor) that relates the hydrodynamic force $\boldsymbol{F}$ on the body with the undisturbed rate-of-strain tensor $\boldsymbol{E}^{\infty}$ [31, 70]:

$$\boldsymbol{F} = \eta\, \boldsymbol{G} : \boldsymbol{E}^{\infty}. \tag{2.234}$$

For the solid sphere it is straightforward to see that the force on the particle can be rewritten in the following manner by means of Equations (2.230) and (2.229):

$$\boldsymbol{F} = \eta \left[ \oint_{S_p} 5\, a^{-1} \boldsymbol{\delta}\, \boldsymbol{x}\ \mathrm{d}S_p \right] : \boldsymbol{E}^{\infty}, \tag{2.235}$$

where from Equation (2.234) it unfolds that the bracketed quantity corresponds to the shear-force tensor $\boldsymbol{G}$. From the integral identity of the position vector $\boldsymbol{x}$ (and the above findings) one can deduce automatically that the shear-force is a third-rank tensor of zeros ($\boldsymbol{G} = \boldsymbol{0}$) for the net force to vanish at the surface of the sphere.

The shear-torque $\boldsymbol{H}$ is a third-rank tensor that relates the torque on the body with the undisturbed rate-of-strain tensor [31, 70]:

$$\boldsymbol{T} = \eta\, \boldsymbol{H} : \boldsymbol{E}^{\infty}, \tag{2.236}$$

where by following an analogous procedure for the derivation of the shear-force it is found that the torque can be expressed in the following form:

$$\boldsymbol{T} = \eta \left[ \oint_{S_p} 5\, a^{-1}\, (\boldsymbol{x} \times \boldsymbol{\delta}\, \boldsymbol{x})\ \mathrm{d}S_p \right] : \boldsymbol{E}^{\infty}, \tag{2.237}$$

where it is evident that the shear-torque is a third-rank tensor of zeros ($\boldsymbol{H} = \boldsymbol{0}$) because of the integral identity of the position vector $\boldsymbol{x}$ and because $\boldsymbol{x} \times \boldsymbol{\delta} = \boldsymbol{0}$ (a second-rank tensor).

For the stresslet $S_{ij}$ one can deduce from the above that there is a fourth-rank identity tensor $\delta_{ik}\delta_{jl}$ that relates the undisturbed rate-of-strain tensor $E^{\infty}_{kl}$ with the stresslet on the solid sphere [31].

From the above results of the force, torque and stresslet on the solid sphere in a rate-of-strain flow, one can propose the singularities that describe the disturbance velocity field $\boldsymbol{u}_D(\boldsymbol{x})$ caused by the impeding effect that the particle inflicts on the flow:

$$\boldsymbol{u}_D(\boldsymbol{x}) = -a^5\, r^{-5}\, \boldsymbol{E}^{\infty} \cdot \boldsymbol{x} + \frac{5}{2}\left(-a^3\, r^{-5} + a^5\, r^{-7}\right)\, \boldsymbol{E}^{\infty} : \boldsymbol{x}\boldsymbol{x}\, \boldsymbol{x}, \tag{2.238}$$

where the second term has been re-expressed with respect to the double-dot product for reasons that will become apparent soon. Note that the so-called singularity solutions of Stokes flow for a solid sphere in a rate-of-strain field can be obtained alternatively via a multipole expansion [31], however, the approach adopted here relies on the existing analogy with the singularities of the Stokes problem (Section 2.3.2) with those associated to a rate-of-strain field. It can be deduced from the above results of zero force and torque on the solid sphere, that higher order singularities than those related to the disturbances caused by the solid sphere in a uniform flow are needed. (The reader may recall from Section 2.3.2 that a point-force and a degenerate quadrupole completely define the disturbances caused by a solid sphere in a uniform velocity field.) Therefore, the disturbance field may be expressed in terms of higher-order derivatives of the Oseen tensor $J_{jk} = r^{-1}\delta_{jk} + r^{-3}x_j x_k$. Since the disturbance velocity field is a vectorial quantity and the rate-of-strain is a second order-tensor it is natural to explore singularities of the form: $E^{\infty}_{ji}\nabla_i J_{jk}$ and $E^{\infty}_{ji}\nabla^2_l\left(\nabla_i J_{jk}\right)$, where $\nabla_i J_{jk}$ and $\nabla^2_l\left(\nabla_i J_{jk}\right)$ are the gradient and Laplacian of the

gradient of the Oseen tensor, respectively. (From the rules of indicial notation for tensors, it is seen that $l$ is a dummy index.) Note that the double-dot product of the rate-of-strain tensor with the Oseen tensor derivatives result in a vectorial quantity, which suggests that at least the dimensionality of the chosen terms is appropriate to describe the disturbance velocity field. Another argument that supports this choice is the analogy with the Stokes flow problem, in the sense that it is the Oseen tensor and its Laplacian that fully describe the disturbance field that consists of first-order spherical harmonics; only that now, it is the gradient of the Oseen tensor and the corresponding Laplacian that are chosen to define the second-order disturbances in a straining field. A generalization to this analogy for the singularities of Stokes flow in a perturbed *nth*-order ambient flow by a solid sphere is available in [31].

It is quite useful to present here expressions for the gradient and Laplacian of the gradient of the Oseen tensor (equivalent expressions can be found in [31]):

$$\nabla_i J_{jk} = r^{-3}\left(\delta_{ij}x_k + x_j\delta_{ik} - x_i\delta_{jk}\right) - 3\,r^{-5}x_i x_j x_k, \tag{2.239}$$

$$\nabla_l^2\left(\nabla_i J_{jk}\right) = -6\,r^{-5}\left(\delta_{jk}x_i + \delta_{ij}x_k + \delta_{ik}x_j\right) + 5\cdot 6\,r^{-7}x_i x_j x_k. \tag{2.240}$$

Note that with the exception of the expression proportional to $r^{-3}$ in the gradient of the Oseen tensor all the other decaying terms above have matching powers of $r^{-n}$ with the disturbance field $\boldsymbol{u}_D(\boldsymbol{x})$ (Equation 2.238). Nonetheless, it turns out that after carrying out the double-dot product with the rate-of-strain tensor $\left(E^{\infty}_{ji}\nabla_i J_{jk}\right)$ the parenthetical expression proportional to $r^{-3}$ vanishes identically due to the symmetry of the rate-of-strain field $\left(E^{\infty}_{ij} = E^{\infty}_{ji}\right)$ such that only the terms that match the decaying terms in $\boldsymbol{u}_D(\boldsymbol{x})$ remain. The expressions that result from the double-dot products are shown below for convenience:

$$E^{\infty}_{ji}\nabla_i J_{jk} = -3\,r^{-5}E^{\infty}_{ji}\,x_i x_j x_k, \tag{2.241}$$

$$E^{\infty}_{ji}\nabla_l^2\left(\nabla_i J_{jk}\right) = -2\cdot 6\,r^{-5}E^{\infty}_{kj}x_j + 5\cdot 6\,r^{-7}E^{\infty}_{ji}\,x_i x_j x_k, \tag{2.242}$$

where the appearing factor of two is, again, a consequence of the symmetry of the rate-of-strain field. After some elementary algebraic operations one can express $\boldsymbol{u}_D(\boldsymbol{x})$ in terms of the above singularities to obtain the sought result:

$$\boldsymbol{u}_D(\boldsymbol{x}) = \frac{20}{3}\pi\eta a^3 \boldsymbol{E}^\infty : \left(1 + \frac{a^2}{10}\nabla^2\right) \frac{\boldsymbol{\nabla J}(\boldsymbol{x})}{8\pi\eta}, \tag{2.243}$$

where it is found that the disturbance field of a solid sphere in a rate-of-strain field consists of the stresslet (Equation 2.233) and degenerate octupole. The appearance of only these singularities confirms the result that the solid sphere is both force and torque–free in a rate-of-strain field. This closes the analysis of the flow of a solid sphere in a general straining flow.

### 2.3.5 The stresslet produced by a fluid drop in a general straining flow

A closed-form expression is derived here for the stresslet of a fluid drop subject to a general straining flow $\boldsymbol{u}^\infty = \boldsymbol{E}^\infty \cdot \boldsymbol{x}$, where $\boldsymbol{E}^\infty$ is the unperturbed rate-of-strain tensor, and $\boldsymbol{x}$ is the position vector with respect to a set of axes centered on the drop. The only assumptions made here regarding $\boldsymbol{E}^\infty$ are that it must be symmetric $\left(E^\infty_{jk} = E^\infty_{kj}\right)$ and traceless $(E^\infty_{kk} = 0)$; the former condition is a direct consequence of the definition of the rate-of-strain tensor [13], and the latter is necessary for the undisturbed flow to satisfy conservation of mass. The flow is analyzed in the limit of zero distortions such that the drop retains its spherical shape; the general conditions to meet this criteria can be found in § 2.2.3. Due to the similarities of the analysis with the problem of Stokes flow about a fluid drop (Section 2.3.3) and the analogous problem of a general straining flow past a solid sphere (Section 2.3.4) the exposition is limited to the problem statement, governing equations and main results to keep the presentation as concise as possible.

The governing equations of fluid motion in the creeping flow limit (no inertia effects) consists of the Stokes equations for each fluid phase ($j = 0, 1$):

$$\boldsymbol{\nabla} p^{(j)}(\boldsymbol{x}) = \eta_j \nabla^2 \boldsymbol{u}^{(j)}(\boldsymbol{x}), \quad \boldsymbol{\nabla} \cdot \boldsymbol{u}^{(j)}(\boldsymbol{x}) = 0, \tag{2.244a}$$

$$u_r^{(j)} = 0, \ [\boldsymbol{n} \cdot \boldsymbol{u}(\boldsymbol{x})] = 0, \ [\boldsymbol{n} \cdot \boldsymbol{\sigma}(\boldsymbol{x})] = 0, \quad \text{at} \quad r = a, \tag{2.244b}$$

$$\boldsymbol{u}^{(0)}(\boldsymbol{x}) = \boldsymbol{E}^{\infty} \cdot \boldsymbol{x}, \quad \text{as} \quad r \to \infty, \tag{2.244c}$$

where $p^{(j)}(\boldsymbol{x})$ and $\boldsymbol{u}^{(j)}(\boldsymbol{x})$ are the velocity and pressure fields of the *jth* fluid phase. The stress tensor is assumed to be of Newtonian character for all the fluid phases: $\boldsymbol{\sigma}^{(j)}(\boldsymbol{x}) = -p^{(j)}(\boldsymbol{x})\,\boldsymbol{\delta} + \eta_j \left( \boldsymbol{\nabla} \boldsymbol{u}^{(j)}(\boldsymbol{x}) + \left( \boldsymbol{\nabla} \boldsymbol{u}^{(j)}(\boldsymbol{x}) \right)^t \right)$, where superscript $t$ here denotes the transpose operator, and $\eta_j$ is the corresponding dynamic viscosity. The usual boundary conditions at the fluid–fluid interface are imposed. There can be no flow normal to the surface of the drop, and there can be no jumps in the velocity and surface tractions from one fluid phase to another. The brackets here denote a jump in the enclosed quantity from the inner ($j = 1$) to the exterior fluid phase (ambient fluid, $j = 0$).

In similarity with the aforementioned problems, a suitable form for the pressure $p^{(j)}(\boldsymbol{x})$ and velocity $\boldsymbol{u}^{(j)}(\boldsymbol{x})$ fields are proposed for each fluid phase:

$$p^{(j)}(\boldsymbol{x}) = \eta_j \boldsymbol{P}^{(j)}(\boldsymbol{x}) \cdot \boldsymbol{E}^{\infty} \cdot \boldsymbol{x}, \tag{2.245}$$

$$\boldsymbol{u}^{(j)}(\boldsymbol{x}) = \boldsymbol{V}^{(j)}(\boldsymbol{x}) \cdot \boldsymbol{E}^{\infty} \cdot \boldsymbol{x}, \tag{2.246}$$

where the 'pressure' vector $\boldsymbol{P}^{(j)}(\boldsymbol{x})$ and 'velocity' dyad $\boldsymbol{V}^{(j)}(\boldsymbol{x})$ have the familiar forms:

$$\boldsymbol{P}^{(j)}(\boldsymbol{x}) = \eta_j f_j(r) \boldsymbol{x}, \tag{2.247}$$

$$\boldsymbol{V}^{(j)}(\boldsymbol{x}) = h_j(r) \boldsymbol{\delta} + g_j(r) \boldsymbol{x}\boldsymbol{x} + \frac{1}{2} f_j(r) \boldsymbol{x}\boldsymbol{x}, \tag{2.248}$$

where $f_j(r), g_j(r)$ and $h_j(r)$ are scalar functions of the radial position $r$ of each fluid phase. Note that the last term of the 'velocity' dyad is coupled to the fluid pressure,

and ensures that the flow everywhere satisfies conservation of mass. The form of the coupling of the 'velocity' dyad in this problem is just a consequence of the spherical geometry of the body, as discussed in whole in § 2.3.1 and § 2.3.3. By following an analogous procedure to that presented in the referenced sections it can be found that the scalar functions associated with the ambient flow are given by:

$$h_0(r) = \left[1 - \frac{\lambda}{1+\lambda}\left(\frac{a}{r}\right)^5\right], \tag{2.249}$$

$$g_0(r) = \frac{5\lambda}{2\,(1+\lambda)}\,a^5 r^{-7}, \quad f_0(r) = -\frac{2+5\lambda}{1+\lambda}\,a^3 r^{-5}, \tag{2.250}$$

and those of the internal flows are:

$$h_1(r) = -\frac{3}{2\,(1+\lambda)}\left[1 - \frac{5}{3}\left(\frac{r}{a}\right)^2\right], \tag{2.251}$$

$$g_1(r) = -\frac{25}{4\,(1+\lambda)}\,a^{-2}, \quad f_1(r) = \frac{21}{2\,(1+\lambda)}\,a^{-2}. \tag{2.252}$$

It follows upon substitution of the scalar functions that the velocity fields of each fluid phase are given by the following expressions:

$$\begin{aligned}\boldsymbol{u}^{(0)}(\boldsymbol{x}) = &\left[1 - \frac{\lambda}{1+\lambda}\left(\frac{a}{r}\right)^5\right]\,\boldsymbol{E}^{\infty}\cdot\boldsymbol{x} \\ &+\left(-\frac{2+5\lambda}{2\,(1+\lambda)}\,a^3 r^{-5} + \frac{5\lambda}{2\,(1+\lambda)}\,a^5 r^{-7}\right)\,\boldsymbol{x}\boldsymbol{x}\cdot\boldsymbol{E}^{\infty}\cdot\boldsymbol{x},\end{aligned} \tag{2.253a}$$

$$\boldsymbol{u}^{(1)}(\boldsymbol{x}) = -\frac{3}{2\,(1+\lambda)}\left[1 - \frac{5}{3}\left(\frac{r}{a}\right)^2\right]\,\boldsymbol{E}^{\infty}\cdot\boldsymbol{x} - \frac{1}{1+\lambda}\,a^{-2}\,\boldsymbol{x}\boldsymbol{x}\cdot\boldsymbol{E}^{\infty}\cdot\boldsymbol{x}, \tag{2.253b}$$

and the pressure fields are simply given by:

$$p^{(0)}(\boldsymbol{x}) = -\,\eta_0\frac{2+5\lambda}{1+\lambda}\,a^3 r^{-5}\,\boldsymbol{x}\cdot\boldsymbol{E}^{\infty}\cdot\boldsymbol{x}, \tag{2.254a}$$

$$p^{(1)}(\boldsymbol{x}) = \eta_1\frac{21}{2\,(1+\lambda)}\,a^{-2}\,\boldsymbol{x}\cdot\boldsymbol{E}^{\infty}\cdot\boldsymbol{x}. \tag{2.254b}$$

Note that the velocity and pressure fields of the ambient flow reduce to those on solid sphere in the limit of $\lambda \to \infty$, as one may intuitively expect. On similar grounds, the velocity and pressure fields for the internal flows decay to zero because

the internal phase behaves as a solid one. The reader is encouraged to verify that the pressure and velocity fields above reduce to those defined in Equation (2.104) for an elongational flow $\boldsymbol{E}^{\infty} = -\dot{\gamma}\left(\boldsymbol{e}_x\boldsymbol{e}_x + \boldsymbol{e}_y\boldsymbol{e}_y - 2\boldsymbol{e}_z\boldsymbol{e}_z\right)$. (It will prove to be useful to express the components of the position vector $\boldsymbol{x}$ with respect to spherical coordinates $(r, \vartheta, \phi)$ to carry out the proof.)

Due to the similarities of this problem with that of a solid sphere in a straining flow, it is conspicuous that the drop is both force and torque–free in a general rate-of-strain field, such that it is not necessary to calculate the surface tractions and their first moment over the outer surface of the drop to demonstrate these claims. For the sake of completeness, nonetheless, the proof is carried out by showing that the disturbance field of the fluid drop in a rate-of-strain field is solely defined by a stresslet and degenerate octupole. (The absence of a point-force and rotlet in the disturbance field is sufficient evidence to convince oneself that the straining flow does not impose forces and couples on the fluid drop.) By following a similar procedure to that conducted for the calculation of the disturbance field of a solid sphere in terms of Stokes flow singularities, the corresponding disturbance field for the fluid drop is found:

$$\boldsymbol{u}_D(\boldsymbol{x}) = \frac{4}{3}\pi\eta_0 a^3 \frac{2+5\lambda}{1+\lambda}\boldsymbol{E}^{\infty} : \left(1 + \frac{a^2\lambda}{2\left(2+5\lambda\right)}\nabla^2\right)\frac{\boldsymbol{\nabla}\boldsymbol{J}(\boldsymbol{x})}{8\pi\eta_0}, \tag{2.255}$$

where it is seen that it consists of the mentioned singularities (stresslet and degenerate octupole) [31]. (Note that there is a typographical mistake for the disturbance field in the cited reference.) In the limit of a drop that exhibits solid-like behavior ($\lambda \to \infty$) the disturbance field for a particle of spherical shape is recovered, as it should. It is interesting that the ambient flow about a bubble ($\lambda \to 0$) is only perturbed by a stresslet, where one can attribute this to the negligible resistance the bubble imparts on the surrounding fluid to flow. Despite the negligible viscosity of the bubble it seems that it cannot fully relax the local rate-of-strain such that

a stresslet field is still observed. Nevertheless, it is noteworthy that the stresslet generated by the bubble is about an order of magnitude less than that of a solid sphere. Note that under realistic conditions the drop (or bubble) deforms in an attempt to even out the difference in the normal stresses at its surface, and therefore, it is expected that the theory overestimates the actual stresslet. Nevertheless, it is of relevance to mention that the theoretical analysis carried out by Schowalter *et al.* [46] on the drop shape by the rate-of-strain field revealed that within the limit of small distortions the stresslet remains unchanged. (The authors made no direct statements regarding the stresslet, however it is quite obvious from their results.) At least for bubbles subject to substantial deformations the stresslet vanishes [54]; supporting the notion that under large deformations the local rate-of-strain can be relaxed considerably.

### 2.3.6 The interior and exterior flows of a fluid drop in a shearing flow

Shear flows develop wherever there is a velocity gradient transversal to the principal direction of the flow. In practice, shear flows are very common and fairly easy to generate. For example, a shear flow can be produced in a fluid bounded by infinitely long walls moving parallel to each other with a relative velocity (sliding parallel plates) [13], by the counter-rotation of two concentric cylinders in a thin gap of fluid (Couette flow) [49], in a cone and plate rheometer [1], and also in between co-rotating eddys of turbulent flows [78] to mention a few typical examples. It is relevant to point out that in a Couettle flow the spacing between the concentric cylinders must be small enough to ensure a linear shear flow; otherwise, the resulting flow is characterized by non-uniform velocity gradients.

In this section closed-form expressions are arrived for the flows that develop within and about a fluid drop subject to a uniform shear flow in the absence of inertia. The first to solve this problem for a non-deformable spherical drop was Taylor [11] with a procedure analogous to the one presented here with the exception

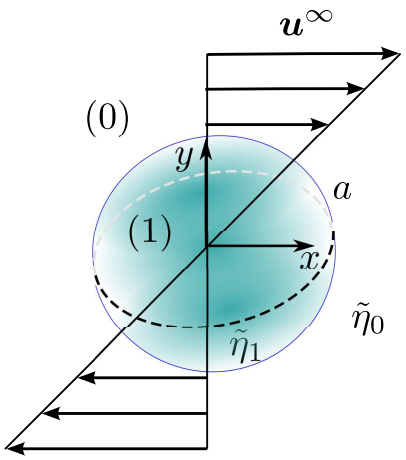


Figure 2–11: A neutrally buoyant fluid sphere of radius $a$ suspended in a viscous fluid that undergoes a uniform shear flow. The index $(j)$ denotes the fluid phase of dynamic viscosity $\tilde{\eta}_j$.

that the flow is analyzed with respect to a spherical coordinate system in this study. The secondary purpose is to provide arguments that indicate that the resultant force and torque on the fluid drop imparted by the applied shear flow are identically zero. For the purposes of showing the latter, it suffices to consider the situation of a non-deformable spherical drop. (It is clear that the symmetry of the imposed flow deforms the drop into a symmetric shape that does not experience force-related distortions [56].) Studies concerned with the calculation of the drop shape in a linear shear flow can be found here [46, 47, 55, 59, 79, 80]. Despite the simplicity of this study, the analysis and results presented here are fundamental for the understanding of some of the problems addressed in the chapters that follow.

Figure 2–11 provides a schematic of a neutrally buoyant drop suspended in a viscous fluid undergoing a uniform shearing motion. The undisturbed far away from the fluid drop for this type of flow is simply given by:

$$\boldsymbol{u}^{\infty} = \boldsymbol{E}^{\infty} \cdot \boldsymbol{x} + \boldsymbol{\Omega}^{\infty} \times \boldsymbol{x} = \dot{\gamma}\, y\, \boldsymbol{e}_x, \tag{2.256}$$

where $\dot{\gamma}$ is the imposed shear rate (or the gradient) of the imposed flow, the second-rank tensor $\boldsymbol{E}^{\infty} = 1/2\,\dot{\gamma}\,(\boldsymbol{e}_x\boldsymbol{e}_y + \boldsymbol{e}_y\boldsymbol{e}_x)$ is the rate-of-strain tensor and the vector

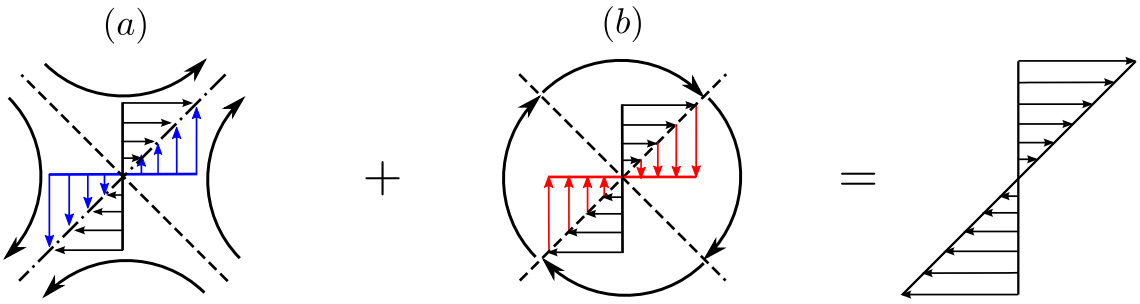


Figure 2–12: Constituents of the uniform shear flow $\boldsymbol{u}^{\infty} = \dot{\gamma} y\, \boldsymbol{e}_x$: $(a)$ Straining flow with its axis of strain (elongation) arranged at a diagonal with the $x$–$y$ axes $1/2\,\dot{\gamma}\,(y\boldsymbol{e}_x + x\boldsymbol{e}_y)$. $(b)$ The solid-body rotation $1/2\,\dot{\gamma}\,(y\boldsymbol{e}_x - x\boldsymbol{e}_y)$ of the fluid with axis of rotation into the page from the perspective of the observer (clockwise rotation).

$\boldsymbol{\Omega}^{\infty} = -1/2\,\dot{\gamma}\,\boldsymbol{e}_z$ is the angular velocity of the undisturbed flow, and the vector $\boldsymbol{x} = (x\,\boldsymbol{e}_x + y\,\boldsymbol{e}_y + z\,\boldsymbol{e}_z)$ defines the position of any point in space with respect to the set of axes centered on the fluid drop. A sketch that shows that the shear flow can be broken down into a straining plus a rotational flow is provided in figure 2–12. Note that the linearity of the limit of zero Reynolds number permits this decomposition of the flow.

The equations that govern the fluid flow of the phases (Stokes equations) with the pertaining boundary conditions are presented in spherical coordinates $(r, \vartheta, \phi)$ to take advantage of the shape of the drop (shown in non-dimensional form):

$$\boldsymbol{\nabla} p^{(j)} = \eta_j \nabla^2 \boldsymbol{u}^{(j)}, \quad \boldsymbol{\nabla} \cdot \boldsymbol{u}^{(j)} = 0, \tag{2.257a}$$

$$u_r^{(j)} = 0, \ [\boldsymbol{n} \cdot \boldsymbol{u}] = 0, \ [\boldsymbol{n} \cdot \boldsymbol{\sigma}] = 0, \quad \text{at} \quad r = 1, \tag{2.257b}$$

$$\boldsymbol{u}^{(0)} = \boldsymbol{u}^{\infty}, \quad \text{as} \quad r \to \infty, \tag{2.257c}$$

where $\boldsymbol{n}$ is the unit normal vector at the surface of the drop (which conventionally points outward from the inner to the ambient fluid), and the brackets denote a jump in the enclosed quantity. Note that the boundary conditions ensure the tangent components of the fluid velocity and stresses to be continuous at the fluid–fluid

interface. (As discussed in Section 2.2.3 the shape of the drop is obtained when the normal component of the stress is continuous; however this calculation lies outside the scope of this work.) The following scales have been used to non-dimensionlize length, fluid velocity and stress: $a$, $\dot{\gamma}a$, and $\tilde{\eta}_0\dot{\gamma}$, respectively. From here on all quantities are presented in non-dimensional form for simplicity.

It is instructive to start by showing that the undisturbed flow $\boldsymbol{u}^\infty$ satisfies the Stokes equations (2.257). Index notation is used here to represent tensors since demonstrations follow more naturally. For convenience the representation of the undisturbed flow in index notation is shown below:

$$u_i^\infty = E_{ij}^\infty x_j + \Omega_j^\infty x_k \epsilon_{jki}, \tag{2.258}$$

where $\epsilon_{jki}$ is the permutation symbol [13]. It is straightforward to see that continuity of mass ($\boldsymbol{\nabla} \cdot \boldsymbol{u}^\infty = 0$) is satisfied by the undisturbed flow, as shown in the next steps:

$$\begin{aligned}
\nabla_i u_i^\infty =& E_{ij}^\infty \frac{\partial x_j}{\partial x_i} + \Omega_j^\infty \frac{\partial x_k}{\partial x_i} \epsilon_{jki}, \\
=& E_{ij}^\infty \delta_{ji} + \Omega_j^\infty \delta_{ki} \epsilon_{jki}, \\
=& E_{ii} + \Omega_j^\infty \epsilon_{jii}, \\
=& 0,
\end{aligned}$$

where it seen that continuity of mass is satisfied because the rate-of-strain tensor is traceless ($E_{ii} = 0$) and because the permutation symbol is zero if an index is repeated ($\epsilon_{jii} = 0$). This result agrees with one's intuition since there are no means for a uniform shear flow (or any other flows) under steady state conditions to change the amount of fluid contained in an arbitrary control volume. In particular to this problem, the rate-of-strain tensor of the undisturbed flow $E_{ij}^\infty$ consists of solely off-diagonal terms such that the constraint $E_{ii} = 0$ is satisfied automatically. Note that the identity property of the gradient of the position vector (i.e. $\partial x_i / \partial x_j = \delta_{ij}$) has been used in the above steps [13].

It can also be shown that the undisturbed flow $\boldsymbol{u}^\infty$ satisfies the creeping flow equation $\boldsymbol{\nabla} p^\infty = \eta_0 \nabla^2 \boldsymbol{u}^\infty$, where $p^\infty$ is the undisturbed pressure field. So far, nothing has been mentioned about the pressure far away from the drop since it is implicit that it is a constant quantity. This can be demonstrated via calculation of the velocity gradient $\boldsymbol{\nabla u}^\infty$, and since it is also required for the calculation of the Laplacian of $\boldsymbol{u}^\infty$ (i.e. $\nabla^2 \boldsymbol{u}^\infty = \boldsymbol{\nabla} \cdot \boldsymbol{\nabla u}^\infty$) it is seen in more detail prior to showing that $\boldsymbol{u}^\infty$ obeys the creeping flow equation. The steps required to determine the velocity gradient of the undisturbed flow are presented below:

$$\begin{aligned}
\nabla_l u_i^\infty =& E_{ij}^\infty \frac{\partial x_j}{\partial x_l} + \Omega_j \frac{\partial x_k}{\partial x_l}, \\
=& E_{ij}^\infty \delta_{jl} + \Omega_j^\infty \delta_{kl} \epsilon_{jki}, \\
=& E_{il}^\infty + \Omega_j^\infty \epsilon_{jli}.
\end{aligned}$$

Note that even though there is a contribution from the rotational field to the velocity gradient $\boldsymbol{\nabla u}^\infty$, it can be easily shown that it does not appear in the rate-of-strain of the flow $\boldsymbol{\Gamma}^\infty = 1/2 \left( \boldsymbol{\nabla u}^\infty + (\boldsymbol{\nabla u}^\infty)^t \right)$:

$$\Gamma_{il}^\infty = \frac{1}{2} \left[ \nabla_i u_l^\infty + \nabla_l u_i^\infty \right], \tag{2.259}$$

$$= \frac{1}{2} \left[ E_{il}^\infty + E_{li}^\infty + \Omega_j \left( \epsilon_{jli} + \epsilon_{jil} \right) \right], \tag{2.260}$$

$$= E_{il}^\infty, \tag{2.261}$$

because of the symmetric and anti-symmetric properties of the applied rate-of-strain ($E_{il}^\infty = E_{li}^\infty$) and the rotational flow ($\epsilon_{jli} = -\epsilon_{jil}$); hence the rate-of-strain of the flow is due to the applied rate of strain. It is straightforward to see from the above analysis that $\nabla^2 u_i^\infty = \nabla_l \left( \nabla_l u_i^\infty \right) = \nabla_l \left( E_{il}^\infty + \Omega_j^\infty \epsilon_{jli} \right) = 0$ because both $E_{il}^\infty$ and $\Omega_j^\infty$ are constant quantities independent of position. This implies that the undisturbed pressure field must be uniform for the creeping flow equation to be satisfied.

Here it is briefly shown that the undisturbed vorticity (a measure of the local spin of the fluid) is just a consequence of the solid-body rotation of the fluid with no contribution from the local rate of strain since this type of flow is irrotational. The vorticity of the undisturbed flow is calculated as follows ($\boldsymbol{w}^{\infty} = \boldsymbol{\nabla} \times \boldsymbol{u}^{\infty}$):

$$\begin{aligned} w_n^{\infty} = \nabla_l u_i^{\infty} \epsilon_{nli} &= E_{ij}^{\infty} \frac{\partial x_j}{\partial x_l} \epsilon_{nli} + \Omega_j^{\infty} \frac{\partial x_k}{\partial x_l} \epsilon_{jki} \epsilon_{nli}, \\ &= E_{ij}^{\infty} \delta_{jl} \epsilon_{nli} + \Omega_j^{\infty} \delta_{kl} \epsilon_{jki} \epsilon_{nli}, \\ &= E_{il}^{\infty} \epsilon_{nli} + \Omega_j^{\infty} \delta_{kl} \epsilon_{jki} \epsilon_{nli}, \end{aligned}$$

where it is evident that $E_{il}^{\infty} \epsilon_{nli} = 0$ because of the combined symmetry of the rate-of-strain tensor $E_{il}^{\infty} = E_{li}^{\infty}$ and the asymmetry of the permutation symbol $\epsilon_{nli} = -\epsilon_{nil}$. The last term, associated with the rotational flow, can be simplifed by means of the well known property of the permutation symbol $\epsilon_{jki}\epsilon_{nli} = (\delta_{jn}\delta_{kl} - \delta_{jl}\delta_{kn})$, as shown below:

$$\begin{aligned} w_n^{\infty} &= \Omega_j^{\infty} \delta_{kl} \left( \delta_{jn} \delta_{kl} - \delta_{jl} \delta_{kn} \right), \\ &= \Omega_j^{\infty} \left( \delta_{jn} \delta_{kk} - \delta_{jn} \right), \\ &= 2\, \Omega_j^{\infty} \delta_{jn}, \\ &= 2\, \Omega_n^{\infty}. \end{aligned}$$

Note that the identity $\delta_{kk} = 3$ has been used to derive at the well-known relation of the vorticity with the angular velocity [13]: $\boldsymbol{w}^{\infty} = 2\, \boldsymbol{\Omega}^{\infty}$.

The solution to the equations of fluid motion in the limit of zero Reynolds number (absence of inertia) is given by Lamb [31], in which the velocity field of the *jth* fluid phase $\boldsymbol{u}^{(j)}$ is expressed as an infinite series of spherical harmonics:

$$\boldsymbol{u}^{(j)} = \sum_{n=-\infty}^{\infty} \left[ \frac{(n+3)\, r^2\, \nabla p_n^{(j)}}{2\eta_j (n+1)(2n+3)} - \frac{n\, \boldsymbol{x}\, p_n^{(j)}}{\eta_j (n+1)(2n+3)} \right] + \sum_{n=-\infty}^{\infty} \left[ \nabla \Phi_n^{(j)} + r \nabla \chi_n^{(j)} \times \boldsymbol{e}_r \right], \tag{2.262}$$

where $p_n^{(j)}$, $\Phi_n^{(j)}$ and $\chi_n^{(j)}$ are *nth* order spherical harmonics associated with the fluid pressure, potential flows, and swirling flows, respectively:

$$p_n^{(j)} = r^n \sum_{m=0}^{n} P_n^{(m)}(\theta) \left( a_{nm}^{(j)} \cos m\phi + \tilde{a}_{nm}^{(j)} \sin m\phi \right), \tag{2.263}$$

$$\Phi_n^{(j)} = r^n \sum_{m=0}^{n} P_n^{(m)}(\theta) \left( b_{nm}^{(j)} \cos m\phi + \tilde{b}_{nm}^{(j)} \sin m\phi \right), \tag{2.264}$$

$$\chi_n^{(j)} = r^n \sum_{m=0}^{n} P_n^{(m)}(\theta) \left( c_{nm}^{(j)} \cos m\phi + \tilde{c}_{nm}^{(j)} \sin m\phi \right), \tag{2.265}$$

where $\theta = \cos\vartheta$, $P_n^{(m)}(\theta)$ is the *nth* order associated Legendre polynomial of mode $m$, and that the coefficients are constants to be determined from the boundary conditions of the Stokes equations (Equation 2.257). The properties of the associated Legendre polynomials and recursive formulas (which are quite useful for the numerical implementation of the Legendre functions in a programming language such as Fortran) are a standard subject of mathematical handbooks [81, 82]. Note that the above spherical harmonics $p_n, \Phi_n, \chi_n$ are associated with flows that develop inside drops and those imposed far away. To describe disturbance flows—such as those that arise by the presence of a solid sphere that is held at a fixed position in space—the following decaying harmonics are needed:

$$p_{-n-1}^{(j)} = r^{-n-1} \sum_{m=0}^{n} P_n^{(m)}(\theta) \left( A_{nm}^{(j)} \cos m\phi + \tilde{A}_{nm}^{(j)} \sin m\phi \right), \tag{2.266}$$

$$\Phi_{-n-1}^{(j)} = r^{-n-1} \sum_{m=0}^{n} P_n^{(m)}(\theta) \left( B_{nm}^{(j)} \cos m\phi + \tilde{B}_{nm}^{(j)} \sin m\phi \right), \tag{2.267}$$

$$\chi_{-n-1}^{(j)} = r^{-n-1} \sum_{m=0}^{n} P_n^{(m)}(\theta) \left( C_{nm}^{(j)} \cos m\phi + \tilde{C}_{nm}^{(j)} \sin m\phi \right). \tag{2.268}$$

Note that both growing and decaying spherical harmonics are functions that satisfy intrinsically the Laplace equation: $\nabla^2 p_n = \nabla^2 \Phi_n = \nabla^2 \chi_n = 0$. (The Laplacian operator in spherical coordinates can be found elsewhere, for instance, it can be found in the Appendix provided by Deen [13]).

As one may suspect, growing harmonics will be used to describe the internal flows of the drop and the undisturbed flow far away, and decaying ones for the disturbance flows that develop in the surrounding fluid due to the hindrance that the presence of the drop imposes on the applied flow $\boldsymbol{u}^{\infty}$. To this end, it is convenient to first express the undisturbed flow with respect to spherical coordinates for the purposes of guessing the order $n$ and mode $m$ of the spherical harmonics that characterize the internal and ambient flows. It is a straightforward procedure to find the velocity components of the undisturbed flow $\boldsymbol{u}^{\infty} = y\,\boldsymbol{e}_x$ (non-dimensional form) by expressing both $y$ and $\boldsymbol{e}_x$ with respect to spherical coordinates (the reader may find useful the Appendix given by Deen [13]):

$$u_r^{\infty} = \frac{1}{2} r \sin^2\vartheta \sin 2\phi, \tag{2.269a}$$

$$u_{\vartheta}^{\infty} = \frac{1}{2} r \left(\sin\vartheta\cos\vartheta\right) \sin 2\phi, \quad u_{\phi}^{\infty} = \frac{1}{2} r \sin\vartheta \cos 2\phi - \frac{1}{2} r \sin\vartheta, \tag{2.269b}$$

where it will become apparent soon that $1/2\, r \sin\vartheta$ corresponds to the solid-body rotation ($\boldsymbol{\Omega}^{\infty} \times \boldsymbol{x}$) of the undisturbed flow, and that the remaining terms derive from the straining motions ($\boldsymbol{E}^{\infty} \cdot \boldsymbol{x}$). It is noteworthy that even though the undisturbed flow is unidirectional with respect to Cartesian coordinates ($u_x^{\infty} = y, u_y^{\infty} = u_z^{\infty} = 0$), three velocity components are needed in a spherical coordinate system; this finding and the dependence of the velocity components on the polar angle $\phi$ elucidates that the flow far away is not axisymmetric but inherently 3D. The order and mode of the spherical harmonics that describe the undisturbed flow can be deduced by recalling that straining flows are irrotational and that there is a uniform pressure field $p^{\infty}$ far away; the latter can be conventionally set to zero (as discussed in Section 2.2.1) without affecting the results, but more importantly, this implies that no spherical harmonics related to the pressure are needed to define the undisturbed flow (i.e. $p_n^{\infty} = 0$). Irrotational flows are characterized by a zero vorticity $\boldsymbol{w}$ and it is evident that the only candidate that fits this description is $\Phi_n^{\infty}$ because potential

flows are irrotational in nature [13]: $\boldsymbol{w}^{\infty} = \boldsymbol{\nabla} \times \boldsymbol{\nabla}\Phi_n^{\infty} = \mathbf{0}$ (this result agrees with the elementary analysis of the undisturbed flow prior to showing Lamb's solution). From these arguments one can deduce that $n = 2$ and $m = 2$ spherical harmonics describe the straining motions of the undisturbed flow:

$$\Phi_2^{\infty} = \frac{1}{12} r^2 P_2^{(2)}(\theta) \sin 2\phi, \tag{2.270}$$

where $P_2^{(2)}(\vartheta) = 3\sin^2\vartheta$ and the prefactor $\left(\tilde{B}_{22}^{\infty} = 1/12\right)$ can be easily found from the calculation of the radial component of Lambs's solution and setting it equal to that of the undisturbed flow. The reader may verify that the velocity components of the undisturbed flow (Equation 2.269) can be recovered (with the exception of the rotational field) from Lamb's solution by substitution of $\Phi_2^{\infty}$ spherical harmonic.

By following an analogous analysis, one can deduce from the rotational component of the flow $u_{\phi}^{\infty} = 1/2\, r \sin\vartheta$ that $m = 0$ and $n = 1$ spherical harmonics meet the sought form:

$$\chi_1^{\infty} = \frac{1}{2}\, r \cos\vartheta, \tag{2.271}$$

which is quite obvious that $m = 0$ because there is no $\phi$–dependence on the rotional component of the flow $u_{\phi}^{\infty}$, and the appearance of $\sin\vartheta$ suggests that $n = 1$. (There are no other spherical harmonics $\chi_n^{\infty}$ that can result in the same expression because of the orthogonality property of the spherical harmonics.) At this point it is useful to take advantage of the linearity property of Stokes flow to analyze separately the straining and rotational motions of the applied flow. Due to the simplicity of a pure rotational field it is considered first, since it turns out that the undisturbed rotational flow satisfies the Stokes equations and boundary conditions for each fluid phase: $\boldsymbol{u}^{(j)} = \boldsymbol{u}^{\infty} = \boldsymbol{\Omega}^{\infty} \times \boldsymbol{x}$. Note that this velocity field is continuous everywhere such that there is no jump in the fluid velocity accross the interface of the drop with the ambient fluid. The last requirement, which stipulates that the fluid stresses must be continuous at the interface is satisfied automatically because the rotational

field does not generate fluid stresses [13], which it is easy to see this from the rate-of-strain tensor (which is the same for all fluid phases): $E_{jk} = (\nabla_j u_k + \nabla_k u_j)/2 = \Omega_l (\epsilon_{jkl} + \epsilon_{kjl})/2 = \Omega_l (\epsilon_{jkl} - \epsilon_{jkl})/2 = 0$. Then, it follows that the flow is stress–free everywhere because of the Newtonian character of the fluids (the index that denotes the fluid phases has been omitted to avoid confusion with the indicial notation for tensors): $\sigma_{jk} = -p\delta_{jk} + 2\eta E_{jk} = 0$, which is derived from the finding that $E_{jk} = 0$ and $p = 0$ everywhere. Formally speaking, the pressure is uniform $p = p^{\infty}$ such that there can no jump in the fluid stress across the fluid–fluid interface for the rotational contribution of the undisturbed flow. Thus, all the fluid phases simply undergo a solid-body rotation with the same angular velocity of the undisturbed rotational velocity regardless of the viscosity of the fluid phases.

In contrast to the rotational component to the flow, there are flow disturbances caused by the presence of the fluid drop because it cannot fully relax the local rate of strain. Therefore, decaying harmonics are needed to define the ambient flow in addition to those that describe the undisturbed flow. Note that the ambient flow must reduce to the unperturbed flow at distances far from the drop, such that it is natural to include them because the ambient flow must satisfy the boundary conditions at the surface of the drop and at infinity. Thus, the velocity field of the ambient fluid is proposed to consist of the following decaying spherical harmonics plus the undisturbed flow:

$$\boldsymbol{u}^{(0)} = \frac{1}{2}\boldsymbol{x}p^{(0)}_{-3} + \boldsymbol{\nabla}\Phi^{(0)}_{-3} + \boldsymbol{u}^{\infty}, \tag{2.272}$$

where the prefactor of $1/2$ is obtained by setting $n = -3$ for the decaying harmonics,

$$p^{(0)}_{-3} = \tilde{A}_0 r^{-3} P^{(2)}_2(\theta) \sin 2\phi, \tag{2.273}$$

and

$$\Phi^{(0)}_{-3} = \tilde{B}_0 r^{-3} P^{(2)}_2(\theta) \sin 2\phi. \tag{2.274}$$

Note that the subscripts on the constants correspond to the fluid index instead of the order and mode of the spherical harmonics to simplify the notations. It follows, in an analogous manner, that the internal flows consist of spherical harmonics that grow with the radial dimension of order $n = 2$ and mode $m = 2$:

$$\boldsymbol{u}^{(1)} = \frac{5}{2 \cdot 3 \cdot 7} r^2 \boldsymbol{\nabla} p_2^{(1)} - \frac{2}{3 \cdot 7} \boldsymbol{x} p_2^{(1)} + \boldsymbol{\nabla} \Phi_2^{(1)}, \tag{2.275}$$

where the prefactors arise by setting the specified order $n$ into Lamb's solution,

$$p_2^{(1)} = \tilde{A}_1 r^2 P_2^{(2)}(\theta) \sin 2\phi, \tag{2.276}$$

and

$$\Phi_2^{(1)} = \tilde{B}_1 r^2 P_2^{(2)}(\theta) \sin 2\phi. \tag{2.277}$$

From this point onward it is just a matter of generating the system of algebraic equations for the unknown coefficients that result from application of the boundary conditions to the velocity fields $\boldsymbol{u}^{(j)}$. The condition of zero flows normal to the surface of the drop $\left(\boldsymbol{e}_r \cdot \boldsymbol{u}^{(j)} = 0\right)$ results in the following pair of algebraic equations (in non-dimensional form):

$$\frac{1}{7}\tilde{A}_1 + 2\tilde{B}_1 = 0, \tag{2.278}$$

$$\frac{3}{2}\tilde{A}_0 - 9\tilde{B}_0 + \frac{1}{2} = 0. \tag{2.279}$$

The requirement of having a zero jump in the velocity tangent to the surface of the drop $(\boldsymbol{\delta} - \boldsymbol{x}\boldsymbol{x}) \cdot \left(\boldsymbol{u}^{(1)} - \boldsymbol{u}^{(0)}\right) = \boldsymbol{0}$ yields an additional algebraic equation:

$$\frac{5}{7}\tilde{A}_1 + 6\tilde{B}_1 = 6\tilde{B}_0 + \frac{1}{2}, \tag{2.280}$$

where both the azimuthal and polar components of the velocity result in equivalent algebraic expressions for the coefficients (linearly dependent). Application of the zero jump in the shear stresses provides the final equation. Once more, the azimuthal and polar components of the shear stress normal to the surface of the drop ($\tau_{r\vartheta}$ and

$\tau_{r\phi}$) give out equivalent expressions such that only $\tau_{r\vartheta}$ is shown here for the *jth* fluid phase at the surface of the drop:

$$\tau_{r\vartheta} = \eta_j \, r \frac{\partial}{\partial r}\left(\frac{u_\vartheta^{(j)}}{r}\right), \tag{2.281}$$

where to arrive at the above expression it has been noted that $\partial u_r^{(j)}/\partial\vartheta = 0$ because of the no-penetration condition at $r = 1$. Evaluation of the zero jump in the shear stresses $(\boldsymbol{\delta} - \boldsymbol{xx}) \cdot \left(\boldsymbol{\tau}^{(1)} - \boldsymbol{\tau}^{(0)}\right) = \mathbf{0}$ at $r = 1$ lends the final equation:

$$\frac{1}{7}\lambda\tilde{A}_1 + 3\tilde{B}_0 = 0, \tag{2.282}$$

where the scaling of the viscosity with that of the ambient results in the following dimensionless parameters: $\lambda = \eta_1 = \tilde{\eta}_1/\tilde{\eta}_0$ and $\eta_1 = 1$. The above system of algebraic equations is linearly independent, and results in the following values for the coefficients of the spherical harmonics of the internal and exterior flows:

$$\tilde{A}_1 = \frac{7}{4}\frac{1}{1+\lambda}, \quad \tilde{B}_1 = -\frac{1}{8}\frac{1}{1+\lambda}, \tag{2.283}$$

$$\tilde{A}_0 = -\frac{1}{6}\left(\frac{2+5\lambda}{1+\lambda}\right), \quad \tilde{B}_0 = -\frac{1}{12}\frac{\lambda}{1+\lambda}. \tag{2.284}$$

Therefore, the velocity components of the ambient fluid are given by the following expressions (in non-dimensional form):

$$u_r^{(0)} = \frac{1}{2}\left[r - \frac{2+5\lambda}{2\,(1+\lambda)}\,r^{-2} + \frac{3\lambda}{2\,(1+\lambda)}\,r^{-4}\right]\sin^2\vartheta\sin 2\phi, \tag{2.285a}$$

$$u_\vartheta^{(0)} = \frac{1}{2}\left[r - \frac{\lambda}{1+\lambda}\,r^{-4}\right](\sin\vartheta\cos\vartheta)\sin 2\phi, \tag{2.285b}$$

$$u_\phi^{(0)} = \frac{1}{2}\left[r - \frac{\lambda}{1+\lambda}\,r^{-4}\right]\sin\vartheta\cos 2\phi - \frac{1}{2}r\sin\vartheta. \tag{2.285c}$$

It is easy to see that the velocity components of the undisturbed flow are recovered as $r \to \infty$. The velocity components of the interior flows are presented below:

$$u_r^{(1)} = \frac{3}{4\,(1+\lambda)}\, r\left(r^2-1\right)\sin^2\vartheta \sin 2\phi, \tag{2.286a}$$

$$u_\vartheta^{(1)} = \left[\frac{5}{4\,(1+\lambda)}\, r^3 - \frac{3}{4\,(1+\lambda)}\, r\right](\sin\vartheta\cos\vartheta)\sin 2\phi, \tag{2.286b}$$

$$u_\phi^{(1)} = \left[\frac{5}{4\,(1+\lambda)}\, r^3 - \frac{3}{4\,(1+\lambda)}\, r\right]\sin\vartheta\cos 2\phi - \frac{1}{2} r \sin\vartheta. \tag{2.286c}$$

The reader is instigated to check that the velocity fields and shear stresses are continuous at the drop surface ($r = 1$), as established by the boundary conditions for the fluid–fluid interface. Another enriching exercise is to verify that the velocity fields of a fluid drop in a general straining flow (Equation 2.253) with the rate-of-strain tensor and rotational field of this problem reduce to the above velocity fields. As one may expect from previous problems, the interior flows in the limit of $\lambda \to \infty$ vanish identically to zero because of the solid-like behavior of the internal phase in this limit.

A sketch of the velocity field both inside and outside the drop is provided in figure 2–13. The observed circulation flow within the drop is just the result of applying a solid-body rotation in the $-z$–direction to the straining velocity field. It is noteworthy that the flow near the outer surface of the drop is characterized by the sweeping motion of the fluid, and that it has a similar profile to that of a rigid sphere under 'freely' suspended conditions.

Given that the velocity fields have been obtained, one may proceed to calculate the resultant force $\boldsymbol{F}$ and torque $\boldsymbol{T}$ on the fluid drop by direct means. However, the inherent symmetry of the velocity fields indicate that the resultant force and torque on the drop are both zero. Note that the solid-body rotation of the fluid phases is stress–free such that there can be no torque from this component of the fluid flow, and clearly, the straining flow cannot produce a net torque about a spherical body.

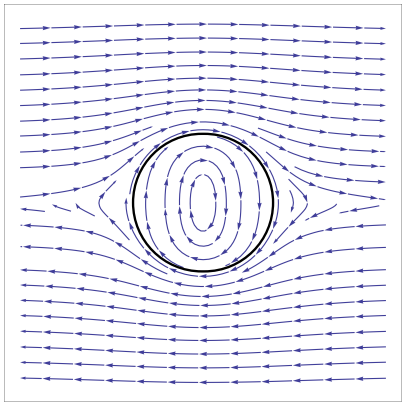

Figure 2–13: The velocity field of a fluid drop subject to a linear shear flow. The shown field corresponds to the velocity field at the $x$–$y$ plane.

Similar arguments support that the resultant force on the fluid drop is identically zero.

It has been shown that the velocity fields of the drop and ambient fluid are characterized by the same mode $m$ of the spherical harmonics of the undisturbed flow, and that the interior and exterior flows retain the symmetric character of the applied flow. This is a direct consequence of the governing equations being linear and the symmetric shape of the immersed body. In fact, one may use Lamb's solution to determine the velocity fields for the axisymmetric problems considered in Section 2.2 to find that only $m = 0$ spherical harmonics are necessary to solve the boundary value problem. Note that for more complex problems the same rule of thumb holds, however, a series of spherical harmonics of growing orders $n$ may be needed, as it will be found in the subsequent chapters of this dissertation.

## 2.4 Effective viscosity of a dilute dispersion of drops in linear flows

The calculation of the effective viscosity of a dilute dispersion in a steady shear flow is a fundamental topic covered in several textbooks [1, 13, 20, 21, 31, 67, 83]. Nonetheless, it is included here to make the chapter self-contained, and to provide the reader an overall picture of the material contained in the chapters that follow. The study of the mechanical properties of a dispersed phase, which may be a fluid or

solid one, in a continuous fluid phase is an active area of research of central importance to industrial, technological and biological applications. Typical examples of such heterogeneous systems are cements, paints, inks, ointments, foods, pharmaceuticals, bio-lubricants and blood [1]. When the characteristic size of the constituents of the dispersed phase is small compared to the length scale of the imposed flow (such as the spacing of walls in a plane Couette flow), the dispersion can be treated as a homogeneous fluid with effective properties [21], and one is usually concerned with changes in the effective viscosity with the applied shear rate $\dot{\gamma}$.

In general, the effective viscosity of a dispersion depends on numerous parameters such as the nature of the continuous fluid phase (e.g. Non-Newtonian properties), the size, shape and spacing of individual particles, flow-induced deformations, electrostatic interactions, thermal fluctuations in the fluid (Brownian motion), the volume fraction occupied by the particles, fluid and particle inertia, hydrodynamic interactions, and the dynamics of the particles in the imposed flow [20, 21, 47, 54, 84–87]. (Here the term 'particles' has been used to denote the dispersed phase in a general way; nonetheless, by no means it is meant that the dispersed phase is limited to a solid one.) Einstein was the first to obtain an expression for the effective viscosity of a dispersion of solid spheres in a steady shear flow under dilute conditions [88]. Then, Jeffery extended Einstein's result to a dispersion of spheroidal particles under the hypothesis that the particles adopt closed-orbits that correspond to the minimum energy of dissipation under the influence of weak inertia effects [89]. It is important to mention that such assumption was needed since at vanishing Reynolds number the theory did not predict any tendency of the spheroids to adopt any preferential orbit; in fact, the particles were found to exhibit an infinite number of closed-orbits that depend solely on the initial orientation of the particle, namely the arrangement of the axis of revolution of the spheroid relative to the direction of the undisturbed flow. The effective viscosity of dumb-bell shaped particles have

been studied in the absence of inertia by Nir & Acrivos [76], and later on by Harper & Chang, who incorporated weak inertia effects to demonstrate (in opposition to Jeffery's hypothesis) that fluid inertia induces an orbit-drift towards the maximum energy of dissipation [90]. The effect of weak Brownian motion on the effective viscosity of a dilute suspension of spheroidal particles in a steady shear flow has been considered by several authors [85, 91, 92]. (Recently, Einarsson *et al.* [93] considered both particle and fluid inertia on the motions of spheroidal particles in a steady shear flow; however, the authors did not reported the effective viscosity of the dispersion.) Taylor extended Einstein's result to a dilute dispersion of drops in a steady shear flow in the limit of non-deformable fluid–fluid interfaces [11]. Subsequently, Schowalter *et al.* [46] determined the leading correction of the drop shape to the effective viscosity to find that shape distortions lead to non-Newtonian behavior of the dispersion in a steady shear flow (i.e. non-zero normal stresses). Analogous calculations were performed for double emulsions (concentric drops dispersed in another fluid) by Stone & Leal [10]. Visco-elastic behavior has also been found in dilute dispersions of drops in oscillating shear flows, also known as small amplitude oscillating shear flows (SAOS) [54, 80]. (The analysis of particle motions in time-dependent flows are outside the scope of this dissertation.) Interestingly, a dispersion of spheroidal particles subject to weak Brownian motions can also exhibit visco-elastic behavior in oscillating shear flows [94]. Beyond the infinite dilution limit ($\phi \to 0$), Batchelor demonstrated a quadratic contribution in the volume fraction $\phi$ to the effective viscosity of a dispersion of solid spheres that interact hydrodynamically via pair-wise interactions [95], and a similar contribution to the effective viscosity in a dispersion of non-interacting solid spheres subject to Brownian motions [96].

Following Batchelor the bulk stress of a dilute dispersion involves an average of the stress over the volume of the system $V$ (the suspended particles plus the continuous fluid phase) such that an analogous constitutive equation for the bulk stress

$\langle \Sigma_{ij} \rangle$ can be written with respect to the bulk rate-of-strain $\langle E_{ij} \rangle$ in an analogous form to that of an ordinary Newtonian fluid [97]:

$$\langle \Sigma_{ij} \rangle = -\mathscr{P}_{eff}\, \delta_{ij} + 2\, \eta_{eff} \langle E_{ij} \rangle, \tag{2.287}$$

where $\mathscr{P}_{eff}$ is the effective pressure, $\eta_{eff}$ is the effective viscosity of the dispersion, and the corresponding volume averages of the bulk stress and rate-of-strain tensors are simply given by:

$$\langle \Sigma_{ij} \rangle = \frac{1}{V} \int_V \sigma_{ij}\, \mathrm{d}V, \quad \langle E_{ij} \rangle = \frac{1}{V} \int_V E_{ij}\, \mathrm{d}V. \tag{2.288}$$

Rewritting the bulk stress into separate contributions of the continuous fluid phase and the particles yields the following expression:

$$\langle \Sigma_{ij} \rangle = \frac{1}{V} \int_{V - \Sigma_n V_n} \left( -p\, \delta_{ij} + 2\eta_0 E_{ij} \right)\, \mathrm{d}V + \sum\nolimits_n \int_{V_n} \sigma_{ij}\, \mathrm{d}V, \tag{2.289}$$

where the stress of a Newtonian fluid has been introduced above for the continuous fluid phase, the sum is over all the particles in the suspension, and $V_n$ is the volume of the *nth* particle. From above, it follows immediately that the effective pressure is simply the isotropic contribution of the stress of the continuous fluid phase:

$$\mathscr{P}_{eff} = \frac{1}{V} \int_{V - \Sigma_n V_n} p\, \mathrm{d}V. \tag{2.290}$$

The volume integral of rate-of-strain field may be further broken down into:

$$\eta_0 \int_{V - \Sigma_n V_n} 2\, E_{ij}\, \mathrm{d}V = \eta_0 \int_V 2\, E_{ij}\, \mathrm{d}V - \eta_0 \sum\nolimits_n \int_{V_n} 2\, E_{ij}\, \mathrm{d}V, \tag{2.291}$$

$$= 2\, \eta_0\, \langle E_{ij} \rangle - \eta_0 \sum\nolimits_n \oint_{S_p} \left( n_i u_j + n_j u_i \right)\, \mathrm{d}S_p, \tag{2.292}$$

where $n_i$ is the unit normal vector at the surface of the particle. (The surface integral above may be derived effortlessly for a spherical particle, in particular since the result applies to other shapes, by expressing the rate-of-strain tensor of a Newtonian fluid

as $2E_{ij} = \nabla_i u_j + \nabla_j u_i$, followed by the differential relation $\nabla_i u_j + \nabla_j u_i = n_i \partial u_j / \partial r + n_j \partial u_i / \partial r$, and integration in spherical coordinates with $\mathrm{d}V = r^2 \sin\vartheta \, \mathrm{d}r \, \mathrm{d}\vartheta \, \mathrm{d}\phi$.)

It is far more convenient to rewrite the integral of the stress over the volume of the particle of Equation (2.288) as a surface integral by the aid of the divergence theorem for tensors and the following relation:

$$\int_{V_n} \sigma_{ij} \, \mathrm{d}V = \int_{V_n} \nabla_k \left( \sigma_{ki} \, x_j \right) \, \mathrm{d}V - \int_{V_n} \left( \nabla_k \sigma_{ki} \right) x_j \, \mathrm{d}V, \tag{2.293}$$

where the latter term vanishes identically if the particles are force–free. Application of the divergence theorem for tensors to the above expression demonstrates that the volume integral reduces to the hydrodynamic dipole of the particle [13, 31]:

$$\int_{V_n} \sigma_{ij} \, \mathrm{d}V = \oint_{S_p} n_k \, \sigma_{ki} \, x_j \, \mathrm{d}S_p. \tag{2.294}$$

By substitution of the above results into the expression for the bulk stress (Equation 2.288) one finds the constitutive equation of the bulk stress with the volume-averaged rate-of-strain field of the dispersion:

$$\langle \Sigma_{ij} \rangle = -\mathscr{P}_{eff} \, \delta_{ij} + 2 \, \eta_0 \, \langle E_{ij} \rangle + \frac{1}{V} \sum_n \oint_{S_p} \left[ n_k \, \sigma_{ki} \, x_j - \eta_0 \left( n_i u_j + n_j u_i \right) \right] \mathrm{d}S_p, \tag{2.295}$$

where the latter term corresponds to the particle contribution to the bulk stress and accounts for the additional viscous dissipation due to the presence of the particles in the dispersion. If the dispersion has a uniform size distribution of non-interacting isotropic particles (valid in the dilute limit) the bulk stress simplifies to:

$$\langle \Sigma_{ij} \rangle = -\mathscr{P}_{eff} \, \delta_{ij} + 2 \, \eta_0 \, \langle E_{ij} \rangle + \frac{N}{V} \oint_{S_p} \left[ n_k \, \sigma_{ki} \, x_j - \eta_0 \left( n_i u_j + n_j u_i \right) \right] \mathrm{d}S_p, \tag{2.296}$$

where $N$ is the total number of particles in the dispersion. The major implication is that knowing the contribution to the stress of a single particle suffices to arrive at a closed-form expression for the constitutive equation for the bulk stress, and hence, the effective viscosity of the dispersion.

If the dispersion consists of non-deformable drops subjected to a steady shear flow of a Newtonian fluid, the particle contribution to the bulk stress just arises from the hydrodynamic dipole of the particle, which is obvious in view of the symmetry of the shear flow. This is the case because there can be no contribution to the bulk stress associated with the integral of the superficial velocities on an isotropic particle in a linear shear flow. The reader may verify this claim for a spherical drop by direct means via substitution of the ambient flow $\boldsymbol{u}^{(0)}(\boldsymbol{x})$ defined in Equation (2.253) into the corresponding expression above, followed by the demonstration that both surface integrals: $\oint_{S_p} \boldsymbol{x}\,\boldsymbol{E}^{\infty}\cdot\boldsymbol{x}\,\mathrm{d}S_p$ and $\oint_{S_p} \boldsymbol{x}\boldsymbol{x}\,\boldsymbol{x}\cdot\boldsymbol{E}^{\infty}\cdot\boldsymbol{x}\,\mathrm{d}S_p$ become exactly zero. In a similar manner, the solid-body rotation of the ambient also does not contribute either, as shown in the steps below:

$$\oint_{S_p} r^{-1}\left(x_l u_i + x_i u_l\right)\,\mathrm{d}S_p = \oint_{S_p} r^{-1}\left(x_l x_k \Omega_j^{\infty}\epsilon_{jki} + x_i x_k \Omega_j^{\infty}\epsilon_{jkl}\right)\,\mathrm{d}S_p, \tag{2.297}$$

$$= \frac{4}{3}\pi a^3\left(\delta_{lk}\Omega_j^{\infty}\epsilon_{jki} + \delta_{ik}\Omega_j^{\infty}\epsilon_{jkl}\right) = 0, \tag{2.298}$$

where the integral identity of the dyad of the position vector has been used to arrive at the sought result, which is quite evident from the properties of the permutation symbol. Henceforth, the constituve equation for the bulk stress of a dilute dispersion of drops is:

$$\langle\Sigma_{ij}\rangle = -\mathscr{P}_{eff}\,\delta_{ij} + 2\,\eta_0\left(1 + \frac{2+5\lambda}{2\,(1+\lambda)}\phi\right)\langle E_{ij}\rangle, \tag{2.299}$$

where the volume fraction is given by

$$\phi = \frac{\frac{4}{3}\pi a^3}{V}. \tag{2.300}$$

To derive the final expression for the bulk stress of the dispersion it has been noted that for a dilute dispersion the volume-averaged rate-of-strain is nearly equal to the undisturbed rate-of-strain $\langle E_{ij}\rangle = E_{ij}^{\infty}$ [13], and that the hydrodynamic dipole reduces to the stresslet of a single drop, as defined in Equation (2.255). An exact

expression for the effective viscosity unfolds by making use of the analogy of the present constitutive equation with that of a Newtonian fluid:

$$\eta_{eff} = \eta_0 \left( 1 + \frac{2 + 5\lambda}{2\,(1 + \lambda)} \phi \right), \tag{2.301}$$

where it is seen that Einstein's result for a dispersion of solid spheres is recovered in the limit $\lambda \to \infty$, as pointed out first by Taylor [11].

# CHAPTER 3
# DYNAMICS OF A JANUS DROP IN A UNIFORM FLOW[1]

## 3.1 Abstract

The motion of a Janus drop under a uniform external flow is considered. First, we analyze the equilibrium shape of a Janus-like drop in a motionless ambient fluid, i.e., the special case of a nearly spherical compound drop with a nearly flat internal interface. This configuration is realizable when the liquids comprising the drop have close interfacial tensions with the ambient fluid, but a small interfacial tension between each other. Then, we consider the flow past a perfect Janus drop composed of two hemispherical domains each occupied by a different fluid. For the sake of simplicity, all the interfaces are assumed nondeformable. The problem is solved both analytically, by means of the Lamb expansion, and numerically. The relation between the flow velocity and the force imposed on the drop, which is a generalization of the classical Hadamard–Rybczynski formula, is found. A torque is also imposed on the drop in the general case. The stable regime of motion of a torque-free drop is found to be axisymmetric, with the less viscous fluid at the upstream face. For this particular configuration, the deformation of the internal interface is also found

[1] This chapter is a reproduction of the article: S. Shklyaev, A. O. Ivantsov, M. Díaz-Maldonado and U. M. Córdova-Figueroa, "Dynamics of a Janus drop in an external flow", *Phys. Fluids*, v. **25**, 082105 (2013). This reprint complies with the copyright terms of the American Institute of Physics. The link to the online article is the following: http://dx.doi.org/10.1063/1.4817541

employing a perturbation technique, whereas the distortion of the drop surface can be safely neglected.

## 3.2 Introduction

The importance and perspectives of Janus particles were predicted by de Gennes in his Nobel lecture [98] more than twenty years ago. Last decade has witnessed a boom in the study of multicompartmental particles and their simplest representative, a Janus particle. Potential applications of these particles range from useful blocks in the design of modern (smart) materials to sensors or self-propelling particles (motors). For this reason many groups are elaborating the experimental methods of Janus particle synthesis, see the surveys in Refs. [99] and [100].

One of such techniques provides the main application of Janus drops[101–103] being very promising because both particle size and compartment can be precisely controlled. This approach includes a microfluidic generation of a Janus drop usually by means of a two-step method: a sequence of two Y-junctions with opposite wettabilities (e.g., hydrophilic and hydrophobic) of the boundaries. One-step production of Janus drops is discussed in Reference [104]; creation of drops containing three liquids is described in Reference [105]. Usually the liquids comprising the Janus drop contain a dispersed monomer, and further polymerization (by means of heating, ultraviolet radiation, etc.) of the monomer produces a Janus particle.

Another important application of Janus drops is creating amphiphilic particles, e.g., by adsorption of nanoparticles (or polymers, surfactant molecules) of different chemical or physical functionalities at the drop surface. Such Janus drops or particles made of these drops can then be collected at the interface [106, 107]. This allows emulsion stabilization and can be used in other applications.

Despite the considerable progress in the synthesis and manipulation of Janus drops, their dynamics is hardly studied, especially theoretically. Janus drop generation in a Y-junction (or a pair of junctions) is a challenging problem from a

computational point of view, because of moving curved interfaces and contact lines, intermolecular interactions of liquids with hydrophilic or hydrophobic solid walls, etc. However, even the simplest problems, such as dynamics of a single Janus drop in a uniform or shear flow, have not been addressed yet, although such data are important to control the behavior of a Janus drop or their ensemble. Moreover, to the best of our knowledge, the corresponding experiments have also been absent so far.

The velocity of a microfluidic flow is rather small and therefore the problem can be solved within the Stokes approximation. A considerable progress is achieved in this field and the main techniques are described in classical books [20, 31]. The general formalism in application to the solid particles implies finding the resistance/mobility tensors (see Reference [72] and references therein). In other words, one has to express the force, torque, and stress tensor applied to a particle via the velocity, angular velocity, and shear rate of the flow in the absence of the particle or vice versa. Such a relation for a stick-slip particle, consisting of two patches, slip and no-slip ones, was calculated by Swan and Khair [77]. Using the boundary integral formulation, the authors derived a Faxén-type formula. In particular, they showed the coupling between a force and rotation and demonstrated that the particle can migrate parallel to the velocity gradient in a one-dimensional shear flow. A similar, though less general, problem – a particle with nonuniform slip at the surface in a uniform flow – was considered independently by Willmott [42].

Even for a single-fluid drop such a formalism fails [108]. For instance, there is no means to couple the torque exerted on a drop with the difference between the angular velocities of the drop and the ambient. Indeed, a rotational motion of a drop, which is described by a velocity field, can hardly be associated with a single angular velocity. Moreover, the torque is created by a nonuniform force, which, in turn, generates a flow inside the drop; therefore, in contrast to a solid particle, the

external influence on a drop cannot be characterized by a single vector quantity (the torque), the whole distribution of the force over the drop is needed. On the other hand, a drop in an external flow has an additional degree of freedom; the interface can deform and the position of the interface should be found along with the flow velocity. Such a coupling, generally speaking, makes the problem nonlinear even within the Stokes approximation. The only exception is the case of a weakly deformable drop (the large surface tension suppresses the interface distortion), where the flow velocity can be found for an unperturbed spherical interface and then the interface distortion is calculated.

The dynamics of a single-fluid drop in a uniform [51, 52] or shear/extensional[55, 56, 108] flow is a classical problem. Recent progress in microfluidics has aroused a great interest in compound drops and their ensembles. Several simple types of compound drops were analyzed in a uniform external flow: (i) a thin-layer patch of one liquid on a nearly spherical drop of a different liquid [109, 110], (ii) a gas-liquid drop with gas phase partially engulfed by a motionless liquid film [111], (iii) concentric [112] or (iv) eccentric [113] spheres (see also the survey on compound drops in Reference [7]). The behavior of a concentric double emulsion drop in an extensional flow was investigated in Reference [10]; combining a perturbation technique and a boundary element method, the authors studied both small and finite distortions of the interfaces. This analysis allows calculating the bulk viscosity of dilute A-type multiple emulsion (a single internal drop for each external one) [10]. However, the analysis of compound drops in external flows lacks in study of such an important object as Janus drops. The present paper aims to generalize Refs. [51] and [52] to a Janus drop, a compound drop which comprises two hemispherical liquid domains.

The paper is organized as follows: We state the problem in Section 3.3 which consists of two subsections. In Section 3.3.1 the existence of a compound drop close to Janus one is discussed in terms of a weak distortion from the combination of

two perfect hemispheres. In Section 3.3.2 the problem of the Stokes flow past a Janus drop is formulated. The axisymmetric problem is analyzed in Section 3.4; the case, when the external flow is parallel to the internal interface, is studied in Section 3.5. We demonstrate that the velocity field (and hence the force and torque imposed on a drop) for arbitrary orientation between the internal interface and the flow can be represented as a superposition of the velocities for these two particular problems. Then, in Section 3.6, we study two different situations: fixed orientation of the drop with respect to the flow (Section 3.6.1) and dynamics of a torque-free drop (Section 3.6.2). Small deflections of the interfaces are found for the latter case in Section 3.6.3. Concluding remarks are presented in Section 3.7.

## 3.3 Problem formulation

### 3.3.1 Shape of equilibrium drop

Prior to analyzing the flow past a Janus drop, let us briefly discuss the conditions under which a compound drop is close to a perfect Janus drop – a combination of two hemispheres. In other words, we are interested in the situation, where (i) the internal interface is almost flat and (ii) the sum of contact angles $\alpha_1 + \alpha_2$ is close to $\pi$, see figure 3–1(a). This analysis is in a close connection with the recent paper, Reference [114] (see also Reference [7]), but we present some additional important information for the particular case of a "half-and-half" drop. It is intuitively clear that the surface tensions have to be related as follows $\tilde{\gamma}_{01} \approx \tilde{\gamma}_{02} \gg \tilde{\gamma}_{12}$, where $\tilde{\gamma}_{ij}$ is the surface tension at the interface between $i$th and $j$th fluids; $i = 0$ corresponds to the ambient. (Henceforth tildes are prescribed to the dimensional characteristics.) It should be emphasized that typically the first inequality, $\tilde{\gamma}_{01} \approx \tilde{\gamma}_{02}$, ensures the second one, $\tilde{\gamma}_{01} \gg \tilde{\gamma}_{12}$.

In dimensionless form the problem is governed by the two ratios of the surface tension,

$$\gamma_{01} = \frac{\tilde{\gamma}_{01}}{\tilde{\gamma}_{12}}, \quad \gamma_{02} = \frac{\tilde{\gamma}_{02}}{\tilde{\gamma}_{12}}. \tag{3.1}$$

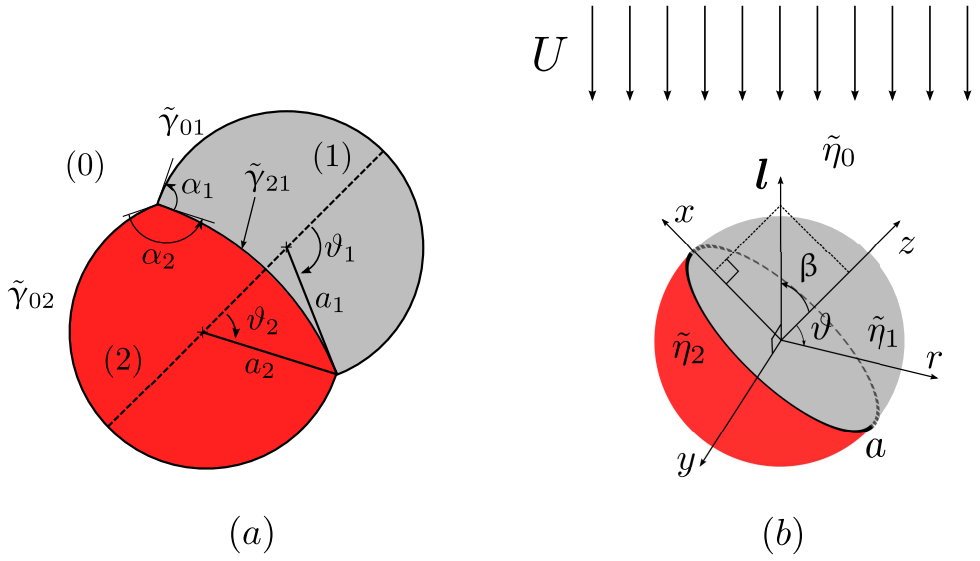


Figure 3–1: Model sketches: (a) Equilibrium Janus-like drop with contact angles $\alpha_{1,2}$; the dashed line is the symmetry axis. The radius $a_0$ and angle $\theta_0$ for the internal interface are introduced in the similar manner as $a_{1,2}$ and $\theta_{1,2}$, respectively; (b) A Janus drop in an external flow $-U\boldsymbol{l}$. The angle β indicates the drop orientation with respect to the flow: $\beta = 0$ corresponds to the internal interface normal to the external flow (axisymmetric problem, Section 3.4), whereas $\beta = \pi/2$ corresponds to the internal interface parallel to the external flow (Section 3.5).

From the computational point of view it is more convenient to deal with the mean interfacial tension at the external surface of the drop $\gamma = (\gamma_{01} + \gamma_{02})/2$ and the difference of the interfacial tensions, $[\gamma] = \gamma_{02} - \gamma_{01}$. Within this subsection we assume $\gamma_{02} \geq \gamma_{01}$ or $[\gamma] \geq 0$, which for the static problem can be achieved by numbering the liquids.

The base state of the compound drop in a motionless liquid is the following: the pressure in each fluid is uniform, whereas the interfaces are spherical segments [7]. For the general case, the shape of the half-and-half compound drop is determined

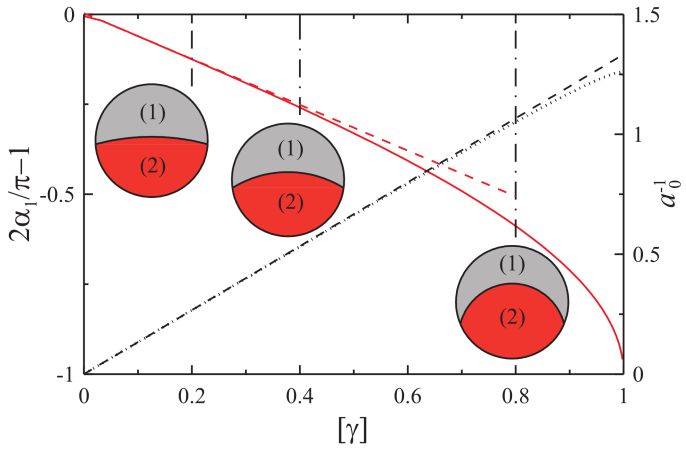


Figure 3–2: Variation of the contact angle $\alpha_1$ (the solid line, left axis) and the curvature of the internal interface $a_0^{-1}$ (the dotted line, right axis) with the difference of the surface tensions $[\gamma]$ for $\gamma = 100$. The dashed lines correspond to the asymptotic formulas, Equation (3.3). Vertical dashed-dotted lines indicate the values of $[\gamma]$ for which the drop shapes are shown.

by the following relations:

$$\frac{\gamma_{01}}{a_1} = \frac{\gamma_{02}}{a_2} - \frac{1}{a_0}, \tag{3.2a}$$

$$\gamma_{01}\cos\vartheta_1 = \gamma_{02}\cos\vartheta_2 - \cos\vartheta_0, \tag{3.2b}$$

$$\gamma_{01}\sin\vartheta_1 = \gamma_{02}\sin\vartheta_2 - \sin\vartheta_0, \tag{3.2c}$$

$$a_0\sin\theta_0 = a_1\sin\theta_1 = a_2\sin\theta_2, \tag{3.2d}$$

$$V_{1,2} \mp V_0 = 2, \tag{3.2e}$$

$$V_{1,2} = a_{1,2}^3\left(2 \mp 2\cos\vartheta_{1,2} \mp \cos\vartheta_{1,2}\sin^2\vartheta_{1,2}\right), \tag{3.2f}$$

$$V_0 = a_0^3\left(2 - 2\cos\vartheta_0 - \cos\vartheta_0\sin^2\vartheta_0\right), \tag{3.2g}$$

representing the balance of pressures, two projections of the tangential forces imposed on the triple line, obvious geometric constraint, and fixed volumes ($2\pi/3$ by the appropriate choice of the lengthscale) of each liquid, respectively. Here $\vartheta_0$ ($a_0$) is the analog of $\vartheta_{1,2}$ ($a_{1,2}$) for the internal interface which is not shown in figure 3–1(a). In fact, one out of these conditions is not independent; e.g., Equation (3.2c) can be derived combining Equations (3.2a) and (3.2d).

For a drop close to Janus one, the above mentioned mean surface tension is large, whereas the difference of surface tensions is small. Expanding the variables which appear in Equation (3.2) with respect to both small $\gamma^{-1}$ and $[\gamma]$, one can readily derive

$$\alpha_{1,2} = \frac{\pi}{2} + \frac{1}{2\gamma} \mp [\gamma], \ a_0^{-1} = \frac{4}{3}[\gamma]. \tag{3.3}$$

These approximate formulas are compared with the numerical results in figure 3–2 for different $[\gamma]$ and $\gamma = 100$. The shapes of the drops are also shown in this figure. It is clear that for $[\gamma] < 0.2$, Equation (3.3) works well, and the drop can be treated as a perfect Janus one with high accuracy.

In fact so large value of $\gamma$ is not needed, even for $\gamma = 5$, the calculations performed are in a good agreement with the analytical solution, Equation (3.3), and only slightly differ from those shown in figure 3–2. It is worth noting that the solid line in figure 3–2 agrees well with the following formula

$$\cos\alpha_1 = [\gamma], \ \alpha_2 \approx \pi - \alpha_1,$$

valid at large $\gamma$ and finite $[\gamma] < 1$. (This relation can be derived by equating the tangential forces exerted on the drop interface at the triple line.) In order to calculate $a_0$ within the same approximation, a transcendent equation should be solved numerically; this solution agrees well with the dotted line in figure 3–2.

Thus, a real compound drop is close to the Janus one in a wide parameter range.

### 3.3.2 Stokes flow

Let us now consider dynamics of a Janus drop in an external uniform flow $-U\boldsymbol{l}$, see figure 3–1(b). For simplicity, it is assumed that each internal fluid occupies a hemispherical domain of radius $a$ and that all interfaces are nondeformable. (This restriction will be relaxed in Section 3.6.3.) Therefore, below we deal with a perfect Janus drop; for Janus-like drop, described by Equation (3.3), the corrections to the flow are proportional to small $[\gamma]$ and $\gamma^{-1}$ and can be calculated by means of a

perturbation technique. These cumbersome calculations lie outside the scope of the current work.

Keeping in mind numerous applications of Janus drops in microfluidics, we analyze the problem in the framework of the Stokes approximation, thus seeking for the creeping flow only. In order to guarantee these conditions, one has to set both the capillary number $Ca_{12} = \tilde{\eta}U/\tilde{\gamma}_{12}$ and the Reynolds number $Re = Ua\tilde{\rho}/\tilde{\eta}$ small [115]. Here $\tilde{\rho}$ and $\tilde{\eta}$ are the typical (for instance, the mean values) density and dynamic viscosity of the system, respectively; the minimum value of the surface tension enters $Ca_{12}$ in order to ensure all the interfaces being nondeformable. We do not present the formal expansion in powers of $Ca_{12}$, just mentioning that the small $O(Ca_{12})$ interface deformations induced by the flow are slaved. These deformations can be found from the balance of normal stresses, see Section 3.6.3, whereas the $O(1)$ flow is calculated for the nondeformable interfaces without taking the normal stresses into account [115].

We introduce spherical coordinates $r, \vartheta, \phi$ [see figure 3–1(b)], which are coupled to the Cartesian coordinates in the usual way. The $x$-axis is chosen in such a manner that the external flow (or vector $\boldsymbol{l}$) is parallel to the $x-z$ plane and $l_x \geq 0$ ($l_x$ vanishes for the axisymmetric problem, see Section 3.4); the $y$-axis is directed so as to make the coordinate system a right-handed one. The boundary value problem governing the drop dynamics reads:

$$\nabla \cdot \boldsymbol{v}^{(j)} = 0, \quad -\nabla p^{(j)} + \eta_j \nabla^2 \boldsymbol{v}^{(j)} = 0, \tag{3.4a}$$

$$v_n^{(j)} = 0, \quad [\boldsymbol{v}_\tau] = [\sigma_{n\tau}] = 0 \text{ at } r = 1, \tag{3.4b}$$

$$v_n^{(1,2)} = 0, \quad [\boldsymbol{v}_\tau] = [\sigma_{n\tau}] = 0 \text{ at } \vartheta = \frac{\pi}{2}, \tag{3.4c}$$

$$\boldsymbol{v}^{(0)} = -\boldsymbol{l} \text{ at } r \gg 1. \tag{3.4d}$$

Here $j$ is each of the numbers $0, 1, 2$; $j = 0$ is again prescribed to the ambient, see figure 3–1(b), whereas in contrast to Section 3.3.1 for the internal fluids the

inequality $\tilde{\eta}_1 \leq \tilde{\eta}_2$ holds true. (Thus, the choice of the first and second fluids in Section 3.3.1 can differ from that in the rest of the paper.) The vectors $\boldsymbol{n}$ and $\boldsymbol{\tau}$ are, respectively, normal and tangential to the corresponding interface. (For the general case $\tau$-component of the velocity is a two-dimensional vector field.) The stress tensor is Newtonian: $\sigma_{lk}^{(j)} = \eta_j \left( \nabla_l v_k^{(j)} + \nabla_k v_l^{(j)} \right) - p^{(j)} \delta_{lk}$. The brackets denote a jump in the corresponding characteristics across the interface; the direction of this jump will be specified, wherever needed. Later on we will not use the brackets in formulas for any other purposes. All the remaining notations are conventional.

The problem is written in the dimensionless form with $U$, $a$, $\tilde{\eta}_0 U/a$ used as the scales for the velocity, length, and pressure, respectively. Therefore, $\eta_0 = 1$ in Equations (3.4), whereas $\eta_{1,2} = \tilde{\eta}_{1,2}/\tilde{\eta}_0$ are the dimensionless parameters of the problem. The third dimensionless parameter defines the unit vector $\boldsymbol{l} = (\sin\beta, 0, \cos\beta)$, $0 \leq \beta \leq \pi$, which indicates the mutual orientation of the drop and the external flow. Two limiting orientations, $\beta = 0$ (or $\beta = \pi$) and $\beta = \pi/2$ are analyzed in Sections 3.4 and 3.5, respectively. Due to linearity of the problem, the solution for any intermediate case can be represented as a combination of these two cases.

The objective is to calculate the flows past and inside the drop, the force $\boldsymbol{F}$ imposed on the drop (in units of $\tilde{\eta}_0 a U$)

$$\boldsymbol{F} = \oint \boldsymbol{\sigma} \cdot \boldsymbol{n} \mathrm{d}S, \tag{3.5}$$

and the torque $\boldsymbol{T}$ (nondimensionalized by means of $\tilde{\eta}_0 a^2 U$)

$$\boldsymbol{T} = \oint \boldsymbol{r} \times (\boldsymbol{\sigma} \cdot \boldsymbol{n}) \mathrm{d}S, \tag{3.6}$$

where the integrations are performed over the drop surface, $r = 1$.

Two practically important situations are possible: (i) the fixed drop, which can neither move nor rotate under external force and torque and (ii) the torque-free drop, which is oriented so that the total torque vanishes. In other words, $\beta$ is kept

fixed for case (i) and $\beta = \beta_{eq}$ has to be calculated for case (ii). It is intuitively clear that for case (ii) $\beta_{eq}$ is either zero or $\pi$ and the former value, $\beta_{eq} = 0$, corresponds to the stable state. Let us imagine an occasional increase in $\beta$ from zero value to the situation sketched in figure 3–1(b). It enhances the area of the more viscous fluid on the left-hand side of the drop, whereas on the right-hand side the area of the less viscous fluid increases. Therefore, the viscous drag on the former part becomes larger and an overall torque inhibits the initial turn. In contrast, for $\beta = \pi$ the resulting torque increases the initial perturbation. A more rigorous analysis of the situation is carried out in Section 3.6.2.

## 3.4 Axisymmetric flow

### 3.4.1 Vector potential formulation

For $\beta = 0$ the problem becomes two-dimensional and therefore the vector potential $\psi$ can be introduced:

$$\boldsymbol{v} = \nabla \times \{\psi(r, \vartheta)\boldsymbol{e}_\phi\} \tag{3.7}$$

or, in components,

$$v_r = \frac{1}{r \sin \vartheta} \partial_\vartheta \left(\sin \vartheta \psi\right), \; v_\vartheta = -\frac{1}{r} \partial_r (r\psi).$$

It is worth noting that $\psi$ is coupled with the conventional Stokes streamfunction [20] $\psi_c$ (associated with the flow streamlines) according to the relation

$$\psi_c = r \sin \vartheta \psi. \tag{3.8}$$

In terms of the vector potential, the boundary value problem, Equation (3.4), is rewritten as follows:

$$\begin{aligned} D^2\psi^{(j)} &= 0, && (3.9a)\\ \psi^{(j)} &= 0,\ [\partial_r\psi] = \left[\eta\partial_r^2\psi\right] = 0 \text{ at } r = 1, && (3.9b)\\ \psi^{(1,2)} &= 0,\ [\partial_\vartheta\psi] = \left[\eta\partial_\vartheta^2\psi\right] = 0 \text{ at } \vartheta = \frac{\pi}{2}, && (3.9c)\\ \psi^{(0)} &= -\frac{r}{2}\sin\vartheta \text{ at } r \gg 1. && (3.9d) \end{aligned}$$

The operator $D$ is introduced by the following relation:

$$Df = \nabla^2 f - \frac{1}{r^2\sin^2\vartheta} f$$

for any $f(r,\vartheta)$.

We represent the vector potentials of the ambient as follows:

$$\psi^{(0)} = \sum_{n=1}^{\infty} \frac{A_n P_n^{(1)}(\theta)}{r^{n+1}}\left(1-r^2\right) + \psi_S,\ \psi_S = \frac{1}{4}\left(3 - \frac{1}{r^2} - 2r\right)\sin\vartheta, \quad (3.10)$$

where $\theta = \cos\vartheta$, $\psi_S$ corresponds to the flow past a solid sphere, and $P_n^{(1)}$ is the associate Legendre polynomial:

$$P_n^{(1)}(\theta) = \sqrt{1-\theta^2}\frac{dP_n(\theta)}{d\theta},$$

i.e., in the notations of Reference [82] we use $P_{n1} = -P_n^1$ as the associate Legendre polynomials.

Inside the drop the vector potentials are given by:

$$\begin{aligned} \psi^{(1,2)} &= \eta_{2,1}\sum_{n=1}^{\infty}\left\{B_n T_n(\theta) \pm C_n r R_n(\theta)\right\} r^{2n+1} + \sum_{n=1}^{\infty} D_n P_{2n}^{(1)}(\theta) r^{2n}\left(1-r^2\right), && (3.11)\\ T_n &= \frac{P_{2n+1}^{(1)}(\theta)}{P_{2n+1}^{(1)}(0)} - \frac{P_{2n-1}^{(1)}(\theta)}{P_{2n-1}^{(1)}(0)},\ R_n = \frac{P_{2n+2}^{(1)}(\theta)}{Q_{2n+2}(0)} - \frac{P_{2n}^{(1)}(\theta)}{Q_{2n}(0)}, && (3.12) \end{aligned}$$

where $Q_n = \theta P_n' - n(n+1)P_n$ and therefore $Q_{2n}(0) = -2n(2n+1)P_{2n}(0)$.

The vector potential given by Equation (3.10) solves the biharmonic equation, Equation (3.9a), ensures both vanishing $\psi^{(0)}$ at $r = 1$ and correct asymptotics far from the drop, whereas $\psi^{(1,2)}$ given by Equation (3.11) satisfy Equation (3.9a) and the boundary conditions at $\vartheta = \pi/2$.

Substituting this ansatz for $\psi^{(j)}$ into the remaining boundary conditions at $r = 1$ and cutting the series at $2N$th spherical harmonics, one arrives at a set of $5N$ linear algebraic equations for $5N$ coefficients: $A_n$ $(1 \leq n \leq 2N)$ and $B_n, C_n, D_n$ $(1 \leq n \leq N)$. This set of equations is solved numerically. In order to guarantee the convergence, $N$ is chosen from 60 to 120 depending on $\eta_1$ and $\eta_2$; more terms should be retained for the case $\eta_2 \gg 1 \gg \eta_1$ (or $\tilde{\eta}_2 \gg \tilde{\eta}_0 \gg \tilde{\eta}_1$). An example of such a system is provided by a toy Janus "drop" which comprises a solid and a gaseous hemispheres. It is worth noting that in most microfluidic applications the viscosities of all three fluids are relatively close. Therefore, the limiting case $\eta_2 \gg 1 \gg \eta_1$ seems to be unimportant from practical point of view. Involving the higher order Legendre polynomials inevitably leads to additional care about round-off errors, hence the number of digits in computations has to be increased. Finally, it should be noted that the series for the stress tensor converges nonuniformly, but no singularities take place for the motionless triple line.

For the axisymmetric case the force given by Equation (3.5) has the only component $F_z = 2\pi(3 - 4A_1)$, which agrees with the classical expression by Payne and Pell [116]. ($F_z$ is directed against the $z$-axis; here and below we omit the sign of the force.) The overall torque, Equation (3.6), vanishes in view of the obvious symmetry arguments.

### 3.4.2 The limiting case $\eta_1 = \eta_2$

First we stress that even in the limiting case of equal internal viscosities $\eta_1 = \eta_2 = \eta$ {here and below $\eta = (\eta_1 + \eta_2)/2$ is the mean viscosity of the drop}, the problem does not reduce to an uniform flow past a drop studied by Hadamard [51]

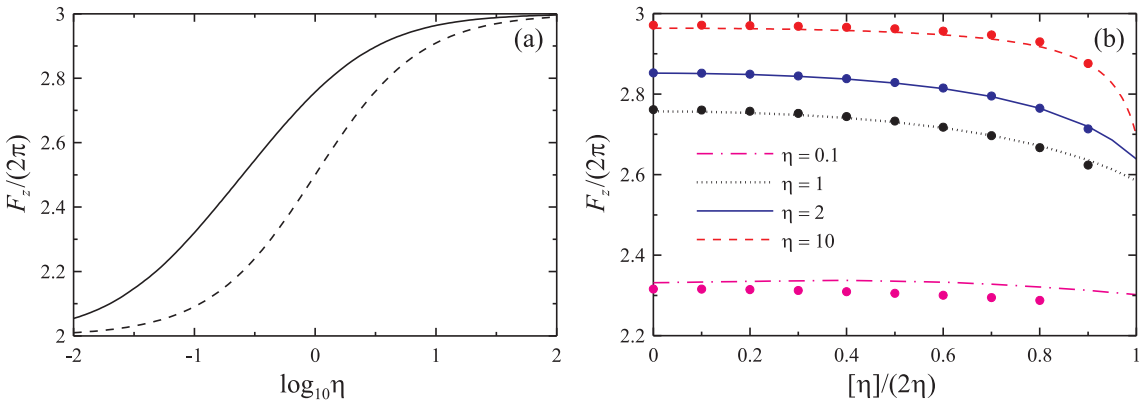


Figure 3–3: The force $F_z/(2\pi)$ (in units $\tilde{\eta}_0 aU$) imposed on the Janus drop. Panel (a): Variation of $F_z/(2\pi)$ with $\eta$ for $\eta_1 = \eta_2 = \eta$. The solid line represents numerical results; the dashed line shows the Hadamard–Rybczynski formula, Equation (3.13). Panel (b): Variation of $F_z/(2\pi)$ with $[\eta]/(2\eta) = (\eta_2 - \eta_1)/(\eta_1 + \eta_2)$ for various mean viscosities of the drop $\eta = (\eta_1 + \eta_2)/2$; results of DNS (ANSYS Fluent) are shown by the dots.

and Rybczynski [52]. Indeed, the nondeformable interface inside the drop prohibits the motion found in the cited papers. Thus, right away, one can expect that a Janus drop is intermediate between a single-fluid drop and a solid particle in terms of hydrodynamic resistances. Mathematically, the problem is simplified in the limiting case $\eta_1 = \eta_2$, because the coefficients $D_n$ and $A_{2n}$ vanish to ensure that the solution is even in $\theta$ or, in other words, to guarantee the symmetry properties $\psi(r, \vartheta) = \psi(r, \pi - \vartheta)$. Particularly, this shows that both velocity components vanish at the internal interface. Calculations of the force acting on the drop are shown in figure 3–3(a), and these are compared against the Hadamard–Rybczynski formula:

$$F_z = 2\pi \frac{2 + 3\eta}{1 + \eta}. \tag{3.13}$$

As can be seen from the figure, for any given $\eta$, the force imposed on the drop lies in between the force on a rigid particle $F_z = 6\pi$, and the force given by Hadamard–Rybczynski formula, Equation (3.13). It is also clear, that the force $F_z$ grows from $4\pi$ (low viscosity drop) to $6\pi$ (high viscosity drop), as $\eta$ ranges from zero to infinity. (In these two limiting cases, the internal interface produces negligible effect.) It

should be mentioned that similar results, the force varying between the Hadamard-Rybczynski formula to the Stokes one, were also found in a number of systems, such as compound drops [110, 112] and drop motion in presence of surfactants [117].

### 3.4.3 Different internal viscosities

For different viscosities $\eta_1$ and $\eta_2$ it is useful to present the results in terms of the mean drop viscosity $\eta$ and the viscosity difference, $[\eta] = \eta_2 - \eta_1$. Keeping in mind that $[\eta] \leq 2\eta$ for any $\eta$, one can conclude that the weighted viscosity difference $[\eta]/(2\eta)$ is more convenient for presentation purposes. It is easy to show that $\eta_{1,2} = \eta\{1 \mp [\eta]/(2\eta)\}$. The results of calculations for nonzero $[\eta]$ are presented in figure 3–3(b). As one can see from this figure, the force slightly depends on the redistribution of this "average" viscosity between the internal fluids. Indeed, at $[\eta] \leq \eta$ the variation of the force does not exceed 1%. Recalling that in most microfluidic applications the viscosity contrast inside the drop is rather small, one can conclude that figure 3–3(a) provides a good approximation of the force imposed on the drop.

With further increase in $[\eta]$ the force becomes smaller. Note, that the case $\eta_2 \gg \eta_1$ ($2\eta \approx [\eta]$) should be thought of as a combination of two liquids with a large difference in the viscosities rather than a liquid-gas pair. In the latter case there is no means to sustain a Janus drop. The force diminution is especially pronounced for the extremal situation $\eta_2 \gg 1 \gg \eta_1$, which, as we stated above, is not practically important.

The flow inside and outside the drop is demonstrated in figure 3–4; keeping in mind the axial symmetry, one concludes that a couple of toroidal vortices appear inside the drop. It should be noticed that the $\vartheta$-component (longitudinal) velocity at the drop surface is nonnegative; thus, both liquids are co-rotating; the vorticities (or the vector potentials) are of the same sign in both hemispheres. Such a system of vortices ensures a correct velocity matching at the drop surface, but it leads to

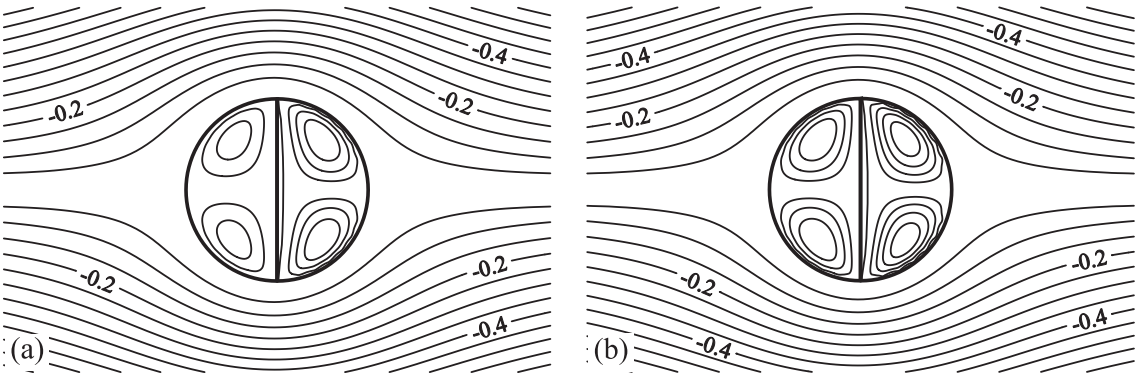


Figure 3–4: The isolines of the velocity potential $\psi$ for axisymmetric flow, $\eta_2 = 1.5$, $\eta_1 = 0.5$ (a) and $\eta_2 = 0.7$, $\eta_1 = 0.3$ (b). The step between the isolines is 0.05 for the external flow and 0.005 inside the drop.

counter-propagating flows at the internal interface, which is obviously impossible. In order to prevent such an effect, an additional vortex appears in a less viscous liquid near the internal interface. Its boundary is plotted by the unclosed streamline adjacent to the internal interface. The intensity of this counterflow is rather small and the streamlines cannot be shown on the scale of figure 3–4. It is evident, that for the limiting case $[\eta] = 0$ the additional vortex is not needed because the longitudinal components of the velocity are zero at the internal interface.

It is readily seen that the intensity of the flow in the drop is much smaller than in the surrounding fluid; the step between the isolines is ten times smaller in the former case. This effect is mainly caused by the above-mentioned additional hindrance to the flow in the drop owing to the internal interface. Another evident result is that the flow is more intensive in the first (less viscous) liquid.

As we have noted above, the convergence of the series, Equations (3.10) and (3.11), for the vector potentials is rather slow. In order to confirm the results independently, we also perform direct numerical simulations (DNS) by means of ANSYS Fluent software. To that end we solved the problem inside a spherical domain $r = 20$ with a space-uniform velocity kept fixed at the external boundary of the domain. Nonuniform tetrahedral mesh comprising 52 000 cells is used with a

refinement near the drop interface. We use Body Force Weighted scheme for pressure spatial discretization and Third-Order MUSCL scheme for the momentum equation. ANSYS Fluent offers the Volume-of-fluid (VOF) method for modeling two or more immiscible fluids by solving a single set of momentum equations and tracking the volume fraction of each fluid over the domain. However, this model is inconvenient for nondeformable interfaces. Therefore, we use the simplified approach, when, similarly to the conventional Level set method, the transient layer is introduced near the interfaces, but the equation for level set function is not solved, which keeps the interfaces fixed. In order to satisfy the boundary conditions, additional source terms are added, which prevent the fluid motion across the interfaces. The Reynolds number $Re_0 = Ua/\tilde{\eta}_0$ in computations is chosen 0.1. The results of DNS are presented in figure 3–3(b) and they are in a good agreement with the analytical approach. The difference of the results becomes more pronounced in the above-mentioned case $\eta_2 \gg 1 \gg \eta_1$ ($[\eta] \approx 2\eta \gg 1$), which is the most complicated from computational point of view but practically unimportant.

It is also clear that no separate analysis is needed for $\beta = \pi$; this limiting case corresponds to the opposite direction of the external flow, which, in view of linearity, only changes the sign of the force keeping its absolute value fixed.

### 3.5 External flow, parallel to the internal interface ($\beta = \pi/2$)

In the case $\beta = \pi/2$ the second (more viscous) fluid is assumed to be situated at $z < 0$, i.e., the flow directed oppositely to the $x$-axis has to produce the torque parallel to the $y$-axis. (The replacement of fluids 1 and 2 only changes the sign of the torque.) For this particular case the calculations are more complicated because of the three-dimensional structure of the velocity fields. To that end we implement the Lamb representation of the velocity, see also Reference [20] and [31]:

$$\boldsymbol{v}^{(j)} = \nabla \times \left(\boldsymbol{r}\chi^{(j)}\right) + \nabla\Phi^{(j)} + \nabla^{-2}\left(\nabla\bar{p}^{(j)}\right) + \boldsymbol{v}_{\infty}^{(j)}, \tag{3.14}$$

where $\nabla^{-2}$ is the inverse of the Laplace operator, $\bar{p}^{(j)} = p^{(j)}/\eta_j$, $\boldsymbol{v}_\infty^{(0)} = -\boldsymbol{l}$ far from the drop. From the computational point of view, it is convenient to choose $\boldsymbol{v}_\infty^{(1,2)} = 0$ at the drop surface, i.e., $\boldsymbol{v}_\infty^{(0)}$ is the Stokes flow past a solid sphere of unit radius. The components of this field are given by:

$$v_{\infty r}^{(0)} = -L(r)\sin\vartheta\cos\phi,\ v_{\infty\vartheta}^{(0)} - M(r)\theta\cos\phi,\ v_\phi^{(0)} = M(r)\sin\phi, \tag{3.15}$$

$$L(r) = 1 - \frac{3}{2r} + \frac{1}{2r^3},\ M(r) = 1 - \frac{3}{4r} - \frac{1}{4r^3}. \tag{3.16}$$

Scalar Lamb's functions $\chi$, $\Phi$, and $p$ solve Laplace's equation. The series for these functions as well as for the velocity fields are given in Appendix B.1.

### 3.5.1 Small viscosity difference

For arbitrary $[\eta]$, calculations are massive but in the limiting case of small $[\eta]/\eta$ (recall, $[\eta] = \eta_2 - \eta_1$) a certain simplification is possible. Indeed, for equal internal viscosities the problem is reduced to that solved by Hadamard [51] and Rybczynski [52]. The corresponding solution reads:

$$v_r^{(1,2)} = V_r^{(1,2)} \equiv \mu(1-r^2)\sin\vartheta\cos\phi, \tag{3.17a}$$

$$v_\vartheta^{(1,2)} = V_\vartheta^{(1,2)} \equiv \mu(1-2r^2)\cos\vartheta\cos\phi, \tag{3.17b}$$

$$v_\phi^{(1,2)} = V_\phi^{(1,2)} \equiv -\mu(1-2r^2)\sin\phi, \tag{3.17c}$$

$$v_r^{(0)} = V_r^{(0)} \equiv -\left(1 + \frac{\alpha}{r} + \frac{\nu}{r^3}\right)\sin\vartheta\cos\phi, \tag{3.17d}$$

$$v_\vartheta^{(0)} = V_\vartheta^{(0)} \equiv -\left(1 + \frac{\alpha}{2r} - \frac{\nu}{2r^3}\right)\cos\vartheta\cos\phi, \tag{3.17e}$$

$$v_\phi^{(0)} = V_\phi^{(0)} \equiv \left(1 + \frac{\alpha}{2r} - \frac{\nu}{2r^3}\right)\sin\phi, \tag{3.17f}$$

$$\mu = \frac{1}{2(1+\eta)},\ \alpha = -\frac{2+3\eta}{2(1+\eta)},\ \nu = \frac{\eta}{2(1+\eta)}.$$

In this case the $x$-component of the force is given by the classical expression, Equation (3.13), and there is no torque applied to the drop.

At small $[\eta]/\eta$ the velocity fields $\boldsymbol{V}^{(j)}$, Equation (3.17), should be supplemented by the $O([\eta]/\eta)$-correction $\boldsymbol{u}^{(j)}$. Such a correction obviously solves the boundary

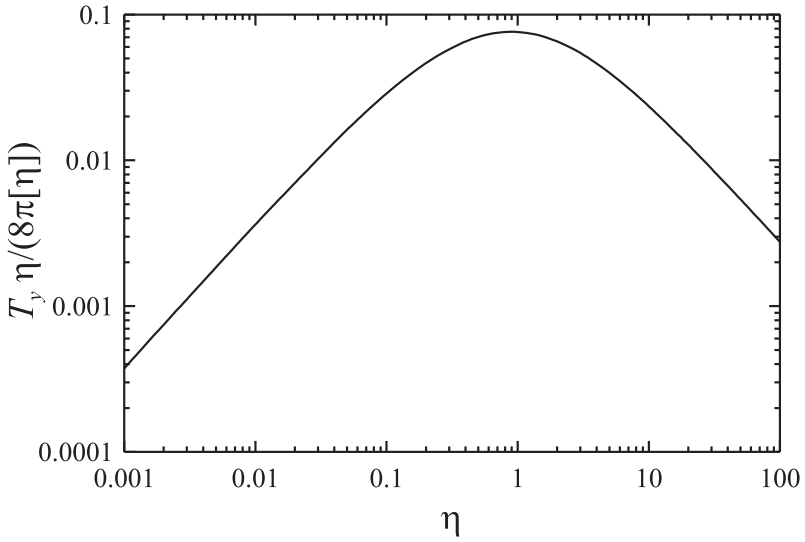


Figure 3–5: Variation of the rescaled torque $T_y\eta/(8\pi[\eta])$ (in units $\tilde{\eta}_0 a^2 U$) acting on the Janus drop for small $[\eta]/(2\eta) = (\eta_2 - \eta_1)/(\eta_1 + \eta_2)$ with the mean viscosity of internal fluids $\eta = (\eta_1 + \eta_2)/2$.

value problem similar to Equations (3.4) with the replacement of the shear stress balance at $r = 1$ by

$$\partial_r \frac{\eta u_\vartheta^{(1,2)} - u_\vartheta^{(0)}}{r} = \pm\eta\partial_r \frac{V_\vartheta}{r},\ \partial_r \frac{\eta u_\phi^{(1,2)} - u_\phi^{(0)}}{r} = \pm\eta\partial_r \frac{V_\phi}{r}, \tag{3.18}$$

where the upper (lower) sign is prescribed to the interface between the ambient and the first (second) fluid. The first correction obeys an additional symmetry condition:

$$\left\{u_r^{(0,1)}, u_\vartheta^{(0,1)}, u_\phi^{(0,1)}\right\}_\vartheta = \left\{-u_r^{(0,2)}, u_\vartheta^{(0,2)}, -u_\phi^{(0,2)}\right\}_{\pi-\vartheta}, \tag{3.19}$$

so that the meridional components of the velocity coincide in both internal fluids, whereas the radial and azimuthal components are opposite. This symmetry property simplifies the analysis to a great extent, although numerical summation is still needed; the details of calculations are presented in Appendix B.2. It ensues from the analysis presented there, that the force does not have $O([\eta]/\eta)$ correction but the torque does. This correction is presented in figure 3–5.

It can be readily seen from the figure that the torque is maximum for a certain value of $\eta$ and it tends to zero in two opposite limits of small and large $\eta$. Again,

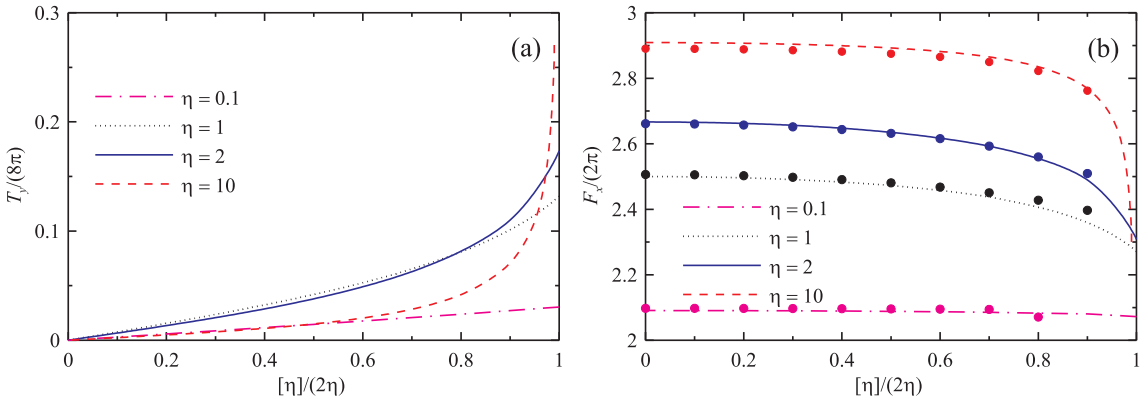


Figure 3–6: Variation of the torque $T_y/(8\pi)$ (in units $\tilde{\eta}_0 a^2 U$) (a) and the force $F_x/(2\pi)$ (in units $\tilde{\eta}_0 a U$) (b) imposed on the Janus drop with $[\eta]/(2\eta) = (\eta_2 - \eta_1)/(\eta_1 + \eta_2)$ for different mean viscosities $\eta$ of the drop. Results of DNS (ANSYS Fluent) are shown as dots.

the former case should be thought of as a water-like drop in an oil rather than a bubble in a liquid, because two gases cannot form an internal interface. The reason for vanishing $T_y$ in this case is clear, the viscous stress is almost zero at the drop surface. The pressure field, which produces a force directed to the drop center, clearly does not create a torque. Mathematically this vanishing stems from the factor $\eta$ in the right-hand side of Equation (3.18). In the latter case, for large $\eta$, the right-hand side of Equation (3.18) remains finite despite the large factor $\eta$ because the velocities of the internal fluids are small, see Equation (3.17). Moreover, $\boldsymbol{u}^{(j)}$ is inversely proportional to $\eta$, even for the ambient, in order to ensure the balance of shear stresses. Therefore, e.g., $\partial_r(u_\vartheta^{(1)}/r)$ is equal to $\partial_r(V_\vartheta^{(1)}/r)$ at $r = 1$, whereas the $O([\eta]/\eta)$ correction to the stress produced by the surrounding fluid can be disregarded. (The correction to the velocity in the ambient can then be found from the velocity continuity at $r = 1$.) In both limiting cases of small and large $\eta$, the asymptotics $\eta$ and $\eta^{-1}$ agree well with the numerical values presented in figure 3–5.

### 3.5.2 Finite viscosity difference

For arbitrary value of $[\eta]/\eta$, the full three-dimensional representation of the velocities given in Appendix B.1 is used. The results of calculations are presented in figure 3–6. At small $[\eta]/\eta$ the torque agrees well with the results shown in figure 3–5. For $\eta = 0.1$, the coincidence is good even for $[\eta]/(2\eta)$ close to unity. With increase in the mean viscosity of the drop the domain of applicability of the results for small $[\eta]/(2\eta)$ shrinks; the nonlinear corrections augment the total torque. As one can expect, the convergence of the series becomes worse with increase in the viscosity contrast; again this effect is especially pronounced for larger $\eta$.

In figure 3–6(b) the force exerted on the Janus drop is depicted. According to the analysis at small $[\eta]$, the correction to Equation (3.13) is quadratic in terms of $[\eta]$. Moreover, at small and moderate mean viscosity of the drop the force is almost independent of the viscosity contrast; for example, at $\eta = 1$, the force variation remains within 10%, whereas the weighted viscosity difference $[\eta]/(2\eta)$ increases from zero to its maximal value, unity.

We also perform the DNS in 3D case, the results are presented in figure 3–6(b); the forces obtained within two approaches agree well; similarly to the axisymmetric case the discrepancy grows as $[\eta]/(2\eta)$ tends to unity, the reader may compare with figure 3–3(b).

## 3.6 Dynamics of the Janus drop

### 3.6.1 The force for the arbitrary β (fixed drop)

Below, on the ground of Sections 3.4 and 3.5 we address the dynamics of a Janus drop, starting with the simplest case, where both the position and orientation of the drop (the angle $\beta$) are fixed by certain external force and torque. Analysis of the more realistic situation, motion of a freely rotating drop under a prescribed external force, is postponed to Section 3.6.2.

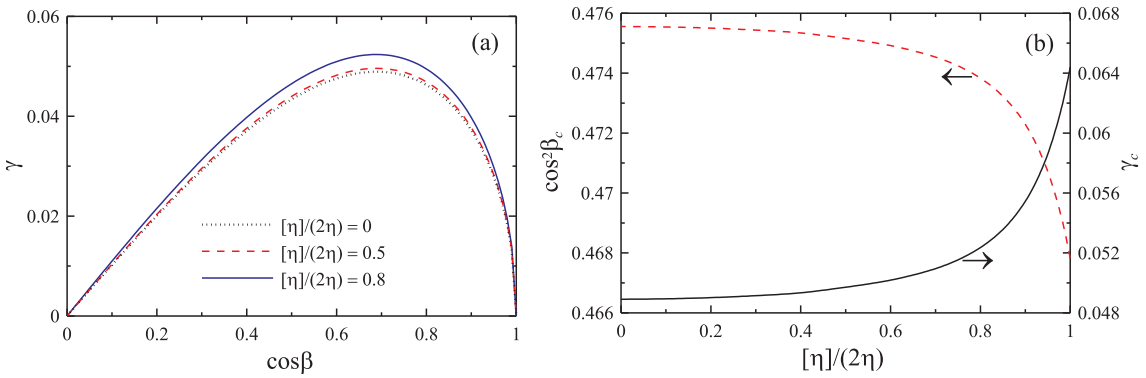


Figure 3–7: Force acting on a fixed Janus drop for $\eta = (\eta_1 + \eta_2)/2 = 1$. (a) Variation of the angle $\delta$ between the external flow and force on the drop with $\cos\beta$ for different $[\eta]/(2\eta)$, see Equation (3.20); (b) Variation of the maximum angle $\delta_c$ in radian (the solid line, right axis) and the value of $\beta_c$ for which $\delta$ reaches its maximum (the dashed line, left axis) with the weighted viscosity difference $[\eta]/(2\eta)$, see Equation (3.21).

It is clearly seen from figures 3–3(b) and 3–6(b), that the analogs of the Hadamard–Rybczynski force for two orientations of the Janus drop depend on the viscosities $\eta_1$ and $\eta_2$ in a qualitatively similar manner. However, they do not coincide exactly, which means that the force applied to a fixed drop is *not parallel* to the flow. (It should be emphasized that for a half-and-half stick-slip sphere,[42, 77] the force is always parallel to the velocity.) The simple calculation shows that the angle $\delta$ between the vector $-\boldsymbol{l}$ and the total force $\boldsymbol{F}$ is given by

$$\cos\delta = \frac{F_x + (F_z - F_x)\cos^2\beta}{\sqrt{F_x^2 + (F_z^2 - F_x^2)\cos^2\beta}}. \tag{3.20}$$

With increase in $\beta$ from zero to $\pi$, this angle reaches its maximum value $\delta_c$ at $\beta = \beta_c$, where

$$\cos\delta_c = \frac{2\sqrt{F_x F_z}}{F_x + F_z}, \quad \cos^2\beta_c = \frac{F_x}{F_x + F_z}. \tag{3.21}$$

An example of calculations are presented in figure 3–7. One can readily see that the angle between the force and the velocity does not exceed 0.065 rad or 3.7 degrees. Another important feature is that the angle is mainly determined by the mean viscosity $\eta$; the variation of $\delta$ with the weighted viscosity difference is almost absent at $[\eta]/(2\eta) < 0.75$.

### 3.6.2 Stable regime for a freely rotating drop

Now we proceed with the more realistic situation of the drop moving by the action of an external force without imposing a torque. In this situation the drop should be torque-free, i.e., it is oriented in such a way that the internal interface is perpendicular to the external flow. One has only to choose between two opposite possibilities, $\beta_{eq} = 0$ and $\beta_{eq} = \pi$. As stated above, simple physical intuition dictates that the former state is stable. In fact, calculations performed in Section 3.5 allows presenting more rigorous arguments. Indeed, let us imagine that the drop with the equilibrium angle $\beta_{eq} = 0$ occasionally gets a small gain in $\beta$. Therefore, in addition to the axisymmetric flow there appears a small 3D component with the velocity proportional to $U \sin\beta$. Since, similarly to the situation shown in figure 3–6(b), $z > 0$ corresponds to the first (less viscous) fluid, the $y$-component of the torque is positive. Thus the viscous torque rotates the drop back trying to decrease the initial distortion. In the opposite case, $\beta_{eq} = \pi$, the first (less viscous) fluid is situated at $z < 0$, i.e., the $y$-component of the torque is negative and it increases the initial perturbation of the angle.

A more subtle situation takes place for the sedimentation of the Janus drop under the action of gravity; an example of Janus drop motion under gravity can be found in Reference [118]. Dealing with the sedimentation, we assume the dimensionless mean drop density $\rho = (\tilde{\rho}_1 + \tilde{\rho}_2)/(2\tilde{\rho}_0)$ larger than unity. If, oppositely to the viscosity difference—$\eta_1 < \eta_2$—the first fluid is more dense, the terminate state remains the same, with the less viscous fluid at the upstream half. At the opposite ratio of the densities, $\tilde{\rho}_1 < \tilde{\rho}_2$, there appears a competition between the viscous and gravitational torques. Since both torques are proportional to $\sin\beta$, nontrivial equilibrium states are impossible and either $\beta_{eq} = 0$ or $\beta_{eq} = \pi$ in the stable state. The former situation occurs, when the viscosity "wins," i.e., $\tilde{\eta}_0 \tilde{U} a^2 T_y > (3/8)[\rho]\tilde{\rho}_0 g a V/2$, where

$\tilde{U} = mg/(\tilde{\eta}_0 a F_z)$ is the velocity of the drop sedimentation, $V$ and $m = (\tilde{\rho}_1 + \tilde{\rho}_2)V/2$ are the volume and mass of the drop, respectively; $[\rho] = (\tilde{\rho}_2 - \tilde{\rho}_1)/\tilde{\rho}_0$.

Thus, $\beta_{eq} = 0$ corresponds to the stable sedimentation under the condition

$$T_y > \frac{3}{16} F_z \frac{[\rho]}{\rho}, \tag{3.22}$$

otherwise, the opposite regime with $\beta_{eq} = \pi$ is stable.

In the opposite case of rising drop ($\rho < 1$), only the sign in the right-hand side of Equation (3.22) should be changed, because in this case the two torques compete for $\tilde{\rho}_1 > \tilde{\rho}_2$.

### 3.6.3 Deformation of the internal interface

In the previous analysis, we have neglected the deformations of the interfaces by assuming the surface tension (or inverse capillary numbers) asymptotically large. In this subsection, small deformations of the interfaces are calculated by means of a perturbation technique. To that end we calculate the pressure field via the Stokes equation with already known $\psi^{(j)}$ (and hence $\boldsymbol{v}^{(j)}$) and take into account the normal stress balance conditions [115].

As demonstrated in Section 3.3.1, two fluids (1 and 2) form a Janus drop suspended in a third fluid (0), when $\tilde{\gamma}_{01} \approx \tilde{\gamma}_{02} \gg \tilde{\gamma}_{12}$. It means that the external surface of the drop remains almost nondeformable, whereas the internal interface can be distorted more easily. Mathematically, the ratio of these deformation is proportional to small $\gamma^{-1} = 2\tilde{\gamma}_{12}/(\tilde{\gamma}_{01} + \tilde{\gamma}_{02})$; therefore, only the deformation of the internal interface is studied below. Recall that for finite $\gamma^{-1}$ the drop is not perfect Janus one even without any flow, see Equation (3.3). The analysis is restricted to the axisymmetric case, which shown to be more relevant from a physical point of view, see Section 3.6.2.

The internal interface is determined by the equation $z = \zeta(r)$, where the function $\zeta(r)$ has to be found from the balance of normal stresses:

$$\begin{aligned} [p - \sigma_{\vartheta\vartheta}] &= -Ca_{12}^{-1}\Delta\zeta, \text{ at } \vartheta = \frac{\pi}{2}; \\ \Delta &= \frac{1}{r}\frac{d}{dr}\left(r\frac{d}{dr}\right), \end{aligned} \tag{3.23}$$

where $[f] = (f_2 - f_1)_{z=0}$. Recall that the capillary number is small, $Ca_{12} = \tilde{\eta}_0 U/\tilde{\gamma}_{12} \ll 1$. The interface deformation $\zeta$ is of order $Ca_{12}$, which justifies the calculation based on the unperturbed interfaces and velocity fields.

Equation (3.23) has to be supplemented by the conditions

$$\zeta = 0 \text{ at } r = 1, \tag{3.24}$$

$$\int_0^1 \zeta r \mathrm{d}r = 0. \tag{3.25}$$

The former condition, Equation (3.24), guarantees that the triple line remains unperturbed because of the strong inequality $\tilde{\gamma}_{12} \ll \tilde{\gamma}_{01} \approx \tilde{\gamma}_{02}$. (In fact, the triple line displacement is proportional to both $Ca_{12}$ and $\gamma^{-1}$, thus vanishing in the order of approximation used here.) The latter condition, Equation (3.25), fixes the volumes of each internal fluid.

The pressure fields corresponding to the vector potentials of internal fluids given by Equation (3.11) have the following forms:

$$\begin{aligned} p^{(1,2)} &= -2\eta_1\eta_2 \sum_{n=1}^{\infty} 2n(4n+1)B_n \frac{P_{2n-1}(\theta)}{P_{2n-1}^{(1)}(0)} r^{2n-1} \\ &\quad -2\eta_{1,2} \sum_{n=1}^{\infty} (2n+1)(4n+3)\left\{D_n \pm \frac{\eta_{2,1}C_n}{Q_{2n}(0)}\right\} P_{2n}(\theta) r^{2n} + p_0^{(1,2)}, \end{aligned} \tag{3.26}$$

whereas the normal viscous stress is given by

$$\sigma_{\vartheta\vartheta}^{(1,2)}\left(\vartheta = \frac{\pi}{2}\right) = -2\eta_{1,2} \sum_{n=1}^{\infty} 2n(2n+1)D_n P_{2n}(0) r^{2n-2}\left\{2n - r^2(2n+2)\right\}. \tag{3.27}$$

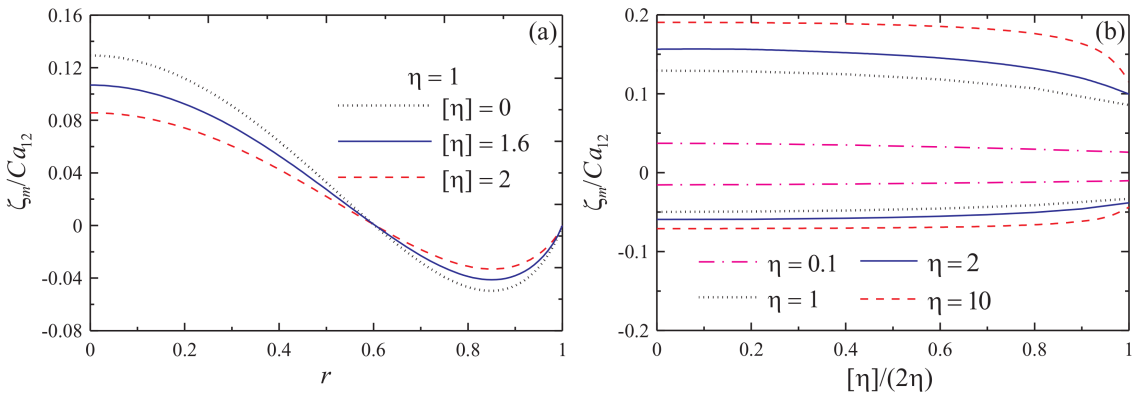


Figure 3–8: Deformation of the internal interface by the flow. (a): Profiles $\zeta(r)$ at $\eta = (\eta_1+\eta_2)/2 = 1$ and $[\eta] = \eta_2 - \eta_1 = 0,\ 1.6,\ 2$ (dotted, solid, and dashed lines, respectively). (b): Variation of maximum and minimum value of $\zeta$ with $[\eta]/(2\eta)$ for different $\eta$.

It is worth noting that the series terms in the pressure field do not contain contributions independent of $r$, whereas $\sigma_{\vartheta\vartheta}$ does contain a constant proportional to $[\eta]$. However, the latter constant just renormalizes the difference $[p_0] = p_0^{(2)} - p_0^{(1)}$ and for brevity it is neglected below. (Recall that the absolute value of the pressure is obviously unimportant for incompressible liquids, only the pressure difference plays a role.)

Solution to Equation (3.23) is given by

$$\zeta = Ca_{12}\left\{\sum_{n=1}^{\infty}\frac{Z_n}{(2n+2)^2} + \frac{[p_0]}{4}r^2 + \zeta_0\right\}, \tag{3.28}$$

$$Z_n = -2\eta_1\eta_2\frac{4n+3}{n}C_n - 2[\eta](2n+1)(2n+3)P_{2n}(0)\left\{(2n+1)D_n + (2n+2)D_{n+1}\right\}.$$

The two constants, $[p_0]$ and $\zeta_0$, which appear in the solution, are determined by Equations (3.24) and (3.25). A simple calculation leads to

$$\zeta = Ca_{12}\sum_{n=1}^{\infty}\frac{Z_n}{(2n+2)^2}\left(2\frac{n+1}{n+2}r^2 - \frac{n}{n+2} - r^{2n+2}\right).$$

The shapes of the interface for $\eta = 1$ are demonstrated in figure 3–8(a); the deformations shown in this figure are typical within the whole range of $\eta_{1,2}$. The maximum deflection (the interface is distorted in the direction of the first liquid) occurs at the

center $r = 0$ and the minimum one (the distortion is in the direction of the second liquid) takes place at a certain $r = r_m$. This structure of the interface deformation can be expected from the Hadamard–Rybczynski flow; indeed, near the drop surface the $\vartheta$-component of the velocity is positive and therefore $\zeta < 0$ near the triple line. In contrast, at the center of the drop, the flow has the opposite direction and $\zeta$ is positive there. Although the internal interface changes the Hadamard–Rybczynski flow in the way discussed in Section 3.4, the interface deformation still follows this flow.

Variation of maximum and minimum values of the interface distortion are shown in figure 3–8(b). With increase in $\eta$ the deformation becomes larger, but this effect is caused by nondimensionalization only. Indeed, a more appropriate way of introducing capillary number, which characterizes the deformation of the internal interface, is the scaling of $\tilde{\gamma}_{12}$ with the internal viscosities, for example, $(\tilde{\eta}_1+\tilde{\eta}_2)U/\tilde{\gamma}_{12} = 2Ca_{12}\eta$. It means that the deformation at fixed $2Ca_{12}\eta$ is larger for smaller $\eta$ and it is more pronounced for a less viscous drop, as one intuitively expects.

Increasing the viscosity contrast $[\eta]$ at fixed $\eta$, one can readily see the decrease in the interface deformation. Indeed, with growth of $[\eta]$, the typical flow velocity in the first liquid $v_1$ grows, whereas $v_2$ decays. In spite of the flow intensification, the pressure difference proportional to $\eta_2 v_2 - \eta_1 v_1$ shrinks, which makes the deformation smaller.

### 3.7 Concluding remarks

The motion of a Janus drop in an external uniform flow is addressed. Starting with the equilibrium configuration, we first find the shape of a nearly Janus drop in the absence of the flow. To that end the limiting case of small $[\gamma] = (\tilde{\gamma}_{02} - \tilde{\gamma}_{01})/\tilde{\gamma}_{12}$ and $\gamma^{-1} = 2\tilde{\gamma}_{12}/(\tilde{\gamma}_{01} + \tilde{\gamma}_{02})$ is analyzed. The former condition means that the difference of the surface tensions at the drop surface is small in comparison with the surface tension at the internal interface $\tilde{\gamma}_{12}$. The latter condition means that

$\tilde{\gamma}_{12}$ is small with respect to the surface tension at the drop surface. Under these conditions both internal fluids occupy almost hemispherical domains.

Then, the Stokes flow past the perfect Janus drop is studied. At a small capillary number, the interfaces are assumed nondeformable due to the flow. Two generic cases, when the internal interface is (i) perpendicular to the external flow ($\beta = 0$, axisymmetric flow) and (ii) parallel to the flow ($\beta = \pi/2$, three-dimensional problem) are analyzed. It is shown that for any other value of $\beta$ the velocity field can be represented as a superposition of the two above-mentioned solutions.

For $\beta = 0$ the vector potential of the velocity is introduced; it is presented by Equations (3.10) and (3.11) with the coefficients determined numerically. It is important that even for the equal internal viscosities, the problem is not reduced to the Hadamard–Rybczynski solution [51, 52]. Indeed, the internal interface, with zero normal velocity there, provides an additional hindrance. Therefore, as shown in figure 3–3(a) the total force imposed on the Janus drop is larger than that for a single-fluid drop but less than for a solid sphere.

A small distortion of the internal interface is also found for this particular configuration. (The deformation of the drop surface is less by the factor $\gamma^{-1}$.) The interface follows the Hadamard–Rybczynski flow, the deflection is directed to the first (less viscous) liquid in the center and to the second (more viscous) liquid near the triple line.

For $\beta \neq 0$, the Lamb expansion of the velocity is used, see Equation (3.14) and Appendix B.1. In this case, there also appears a torque [see figure 3–6(a)], which tries to turn the freely rotating drop in such a way that $\beta = 0$. The stable configuration corresponds to the less viscous fluid situated at the upstream face of the drop.

We also confirm the results of analytical method by direct numerical computations for rather small Reynolds number, ANSYS Fluent is used to that end. This

numerical approach can be applied to relax some of the model restrictions, such as hemispherical domains occupied by the internal fluids. In fact, we do not expect qualitative difference in dynamics of such a realistic Janus drop. However, some important aspects needed for the experiments and/or technologies (such as the stable configuration, intensity of the flow inside the Janus drop, etc.) can be computed.

In contrast to a single-fluid drop, for a Janus one the imposed torque and the angular velocity of drop rotation can be coupled. Indeed, the Janus drop has an additional internal interface, where the normal velocity can be prescribed which corresponds to the drop rotation around the axis belonging to the internal interface. On the other hand, if the torque is normal to the internal interface, the Janus drop is similar to the single-fluid one. Therefore, a Janus particle is an object intermediate between a simple drop and a solid particle, for which the "external forcing" (the velocity, angular velocity, and shear rate of the ambient far from the particle) and the "response" (force, torque, and stress applied to the particle) are coupled via the mobility tensor. From practical point of view, it is important to study a Janus drop behavior under a uniform shear. We expect that dynamics of a Janus drop under this condition has a certain similarity to the stick-slip sphere [42, 44, 77]. The generic feature is that the spherical body with a broken fore-and-aft symmetry behaves in an external flow like a spheroid or other body of revolution; hence dynamics similar to that found in Reference [89] is expected.

We have completely disregarded mixing processes in the analysis, which can be important in view of large contrast in the surface tensions, the surface tension at the internal interface, $\tilde{\gamma}_{12}$, is smaller than the others, $\tilde{\gamma}_{01}$ and $\tilde{\gamma}_{02}$. On the one hand, generally speaking, small surface tension does not necessarily results in mixing; if the liquids have complex and different structures of molecules, the pair of internal fluids still can be immiscible. On the other hand, the flow inside the drop is shown to be of small intensity, especially near the internal interface, where the stagnant

zone develops. Hence, the role of advection in a mixing is negligible, whereas another candidate, the molecular diffusion, is rather small. The typical values of the Schmidt number, the ratio of the characteristic times of mass and momentum diffusion is at least about 100 for most of liquid mixtures. Therefore, having been created, Janus drop has enough time to relax the momentum and, consequently, approach the stable state, before the mixing produces a valuable effect. Thus, the mixing in a forced Janus drop has to be studied only for the stable configuration.

# CHAPTER 4
# THE ANISOTROPIC RESPONSE OF A JANUS DROP TO A SHEARING FLUID[1]

## 4.1 Abstract

The force and couple that result from the shearing motion of a viscous, unbounded fluid on a Janus drop are the subjects of this investigation. A pair of immiscible, viscous fluids comprise the Janus drop and render it with a 'perfect' shape: spherical with a flat, internal interface, in which each constituent fluid is bounded by a hemispherical domain of equal radius. The effect of the arrangement of the internal interface (drop orientation) relative to the unidirectional shear flow is explored within the Stokes regime. Projection of the external flow into a reference frame centered on the drop simplifies the analysis to three cases: (*i*) a shear flow with a velocity gradient parallel to the internal interface, (*ii*) a hyperbolic flow, and (*iii*) two shear flows with a velocity gradient normal to the internal interface. Depending on the viscosity of the internal fluids, the Janus drop behaves as a simple fluid drop or as a solid body with broken fore and aft symmetry. The resultant couple arises from both the straining and swirling motions of the external flow in analogy with bodies of revolution. Owing to the anisotropic resistance of the Janus

[1] Part of this chapter is a reproduction of the published article: M. Díaz-Maldonado and U. M. Córdova-Figueroa, "On the anistropic response of a Janus drop to a viscous shearing fluid", *J. Fluid Mech.*, v. **770**, R2 (2015). The contents of the cited article have been reprinted with permission from Cambridge University Press. A link to the online article is provided here: http://dx.doi.org/10.1017/jfm.2015.148

drop, it is inferred that the drop can migrate lateral to the streamlines of the undisturbed shear flow. The grand resistance matrix is reported for a Janus drop with similar internal viscosities.

## 4.2 Introduction

Compound multiphase drops arise in diverse processes of engineering interest such as direct-contact heat exchangers, melting of ice particles falling in the atmosphere, rapid evaporation of liquids at superheated conditions, explosions of multicomponent fuel drops, and in several other settings [7]. Typically, a pair of fluid phases immersed in a host fluid constitute the compound multiphase drop, where one of the phases may engulf completely or partially its counterpart [8]. A limiting configuration of actual interest for the fabrication of anisotropic particles arises when two drops (of similar interfacial tension) undergo partial engulfment, leading to the formation of a compound drop of nearly spherical shape and almost flat, internal interface [114]. This particular object is usually referred to as a Janus drop — named after the Roman god. The Janus drop is considered to be 'perfect' when the constituent fluid phases are bounded each by a hemispherical domain of equal radii, or equivalently when the drop exhibits a flat, internal interface [119], where the latter is referred to as 'the internal interface' from this point onward for brevity.

This study aims to characterize the hydrodynamic response (forces and couples) of a 'perfect' Janus drop by the shearing motion of a viscous unbounded fluid (which is an ubiquitous flow type), and consider how this response is affected by the drop orientation (a factor absent in single-phase drops). A schematic representation of a Janus drop of arbitrary orientation in a simple shear flow is provided in figure 4–1. The Janus drop plus the suspending fluid constitute a system of three phases; and the dynamic viscosity of the $jth$ fluid phase is denoted by $\tilde{\eta}_j$. The orientation of

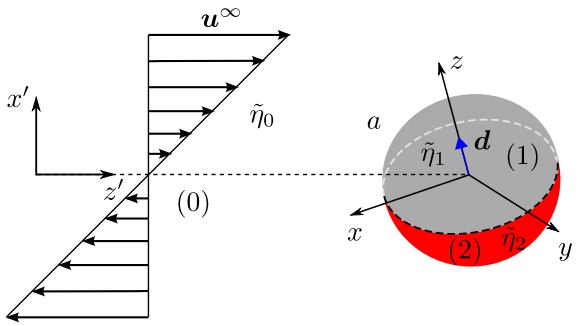


Figure 4–1: A 'perfect' Janus drop subject to a unidirectional shear flow. The vector $\boldsymbol{d}$ is parallel to the axis of symmetry of the Janus drop and points towards the less viscous fluid.

the Janus drop is defined by the unit vector $\boldsymbol{d}$, which is normal to the internal interface. This study reveals that the anisotropic properties of the Janus drop arise from the presence of the internal interface; the viscosity of the constituent fluids is of secondary importance.

Previous theoretical studies have considered the dynamics of compound multiphase drops in streaming axisymmetric flows [112, 113], and in Marangoni-driven flows [120, 121]. Fluid motion is usually analysed in the limit of non-deformable interfaces with the exception of the contributions of Chervenivanova & Zapryanov [122] and Voung & Sadhal [123]. The latter study reveals little dependence of the drag force with shape distortions, which justifies the neglect of interface deformations of prior studies. Stone & Leal [10] studied the deformation and breakup of concentric drops in linear flows. Recently, Shardt *et al.* [124] studied the dynamics of a Janus drop in a simple shear flow, however, within the restriction of a two-dimensional (2D) flow everywhere.

It is intriguing to note that cross-flow migration of compound multiphase drops appears to be a fairly unexplored problem despite important implications in mixing phenomena and viscosity of a suspension. For example, in mixing processes, drops are subject to lateral migration owing to shape distortions associated with hydrodynamic interactions. Lateral migration tends to align, for instance, a pair of drops

initially separated by some finite distance [45]. If in addition the drops are rising due to the action of buoyancy, the trailing drop may catch up to the leading one and ultimately, experience coalescence. A noteworthy effect of cross-flow migration in a colloidal suspension is that the flow properties become inhomogeneous because of the non-uniform spatial-distribution of the dispersed phase [84, 125]. A classic example of this latter phenomenon is observed when an initially uniform dispersion of neutrally buoyant spheres is subject to a bounded Poiseuille flow (pressure-driven flow in a circular duct). In the presence of weak inertia, the disperse phase tends to form a rim about midway the centerline and the walls of the duct [126]. It is noteworthy that a suspension of neutrally buoyant spheres in a simple shear flow experiences 'shear-thicknening' under the influence of weak inertia [127]. (The interested reader may refer to the work of Haddadi & Morris [128] for a recent view of the issue of inertial effects on suspension rheology.) Interestingly, a Janus drop can display cross-flow migration in a streaming flow because of the anisotropic resistance imparted by the internal interface [119]. From the perspective of hydrodynamic resistances, the Janus drop behaves as a body of revolution (e.g. spheroid), such that the drag force is generally not parallel to the flow. The key finding is that cross-flow migration can occur without the influence of interface deformations associated with wall interactions or non-uniform velocity gradients, which are needed to induce the migration of single-phase drops. The reader interested in the subjet of lateral migration of simple drops is referred to the review of Leal [84].

The outline of the article is presented here. The problem statement is formulated in Section 4.3, where for an arbitrary drop orientation the external shear flow is broken down into flows with a velocity gradient normal and parallel to the internal interface. The equations that govern fluid motion are presented in Section 4.4, and solved in the creeping motion limit in Section 4.5. The influence of the viscosity

of the three fluid phases is incorporated into the analysis for completeness. In Section 4.5.1, it is shown that the Janus drop behaves as a single-phase drop under the action of a shear flow with a velocity gradient parallel to the internal interface. The force imposed on the Janus drop by a plane hyperbolic flow are analysed in Section 4.5.2. It is found that the equilibrium orientation of the Janus drop in a hyperbolic flow occurs when the internal interface is aligned with the axis of strain or compression. The Janus drop is expected to respond with a couple that restores this particular arrangement under an external perturbation. In Section 4.5.3 the force and couple imposed by a shear flow with a velocity gradient normal to the internal interface of the Janus drop are studied. It is found that the resultant couple unfolds from both the straining and rotating components of the shear flow in similarity with bodies of revolution. From a practical point of view, knowledge of the behaviour of a Janus drop in a shear flow is a first step in understanding its dynamics in experiments (e.g. Poiseuille flows or microfluidic settings). Along this line of thought, the migration velocity of a Janus drop lateral to a streaming flow is presented in Section 4.5.4. Concluding remarks are given in Section 4.7, where the conditions for the occurrence of the cross-flow migration of a Janus drop in a shear flow are briefly discussed. In the Section 4.6 the grand resistance matrix is reported on account of their potential relevance to experimenters. Since Janus drops typically comprise fluids of similar viscosity in microfluidic settings [129] ($\tilde{\eta}_1 \approx \tilde{\eta}_2$), the results are narrowed down to this limit of practical interest. Interestingly, the coupling tensor, which characterizes the torque on a body in a streaming flow and the force in a rotational flow, is found to be identically zero at the center of hydrodynamic reaction of the Janus drop. Additionally, at the center of hydrodynamic reaction it is found that the shear-force vanishes, and therefore, the dynamics of a 'freely' suspended Janus drop in a shear flow are identical to those of a symmetric

spheroid of revolution [89]. In other words, a 'freely' suspended Janus drop translates with the local streaming velocity of the undisturbed flow and its orientation undergoes a periodic-orbit identical to that of a spheroid. The stresslet produced by a Janus drop with $\tilde{\eta}_1 \approx \tilde{\eta}_2$ in an elongational flow (axisymmetric) reduces to the stresslet produced by a single-phase drop. For transversal straining flows the stresslet is found to be intermediate to that of a single-phase drop and a solid sphere. The stresslet of a Janus drop subject to a shear flow with a velocity gradient parallel to the internal interface is identical to that of a single-phase drop.

## 4.3 Problem statement

Figure 4–1 depicts a neutrally buoyant Janus drop immersed in a viscous shearing fluid, which is denoted by '0'. The Janus drop comprises two internal fluids denoted by '1' and '2'. The dynamic viscosity of each fluid phase ($j = 0, 1, 2$) is defined by $\tilde{\eta}_j$; conventionally, it is assumed that $\tilde{\eta}_1 \leq \tilde{\eta}_2$. The principal objective of this investigation is to calculate the force and couple on a Janus drop centerd in a simple shear flow with zero mean velocity:

$$\boldsymbol{u}^{\infty} = \frac{1}{2} G \left( \boldsymbol{E}^{\infty} \cdot \boldsymbol{x'} + \boldsymbol{e}'_z \times \boldsymbol{x'} \right) = G\, x' \boldsymbol{e}'_z, \tag{4.1}$$

where $G$ is a constant shear rate, $\boldsymbol{E}^{\infty}$ is the rate-of-strain tensor of the undisturbed flow, and $\boldsymbol{x'} = (x', y', z')$ is a set of space-fixed Cartesian coordinates, with corresponding unit vectors $(\boldsymbol{e}'_x, \boldsymbol{e}'_y, \boldsymbol{e}'_z)$, that ensure a unidirectional flow. The drop orientation effect is considered by projecting $\boldsymbol{u}^{\infty}$ into a reference frame centerd and affixed to the Janus drop $\boldsymbol{x} = (x, y, z)$ via the transformation $\boldsymbol{x'} = \mathsf{A}\, \boldsymbol{x}$, where the transformation matrix $\mathsf{A}$ parametrizes the drop orientation from a coincident arrangement of both sets of axes:

$$\mathsf{A} = \begin{pmatrix} \cos\alpha & 0 & -\sin\alpha \\ -\sin\alpha \sin\beta & \cos\beta & -\cos\alpha \sin\beta \\ \sin\alpha \cos\beta & \sin\beta & \cos\alpha \cos\beta \end{pmatrix}, \tag{4.2}$$

where $\alpha$ and $\beta$ are the corresponding Euler angles that define the drop orientation.

Projection of $\boldsymbol{u}^{\infty}$ into $\boldsymbol{x}$ results in a superposition of flows, which are categorized with respect to the arrangement of the velocity gradient relative to the internal interface. Flows with a velocity gradient normal and parallel to the internal interface are denoted by $\boldsymbol{v}$ and $\boldsymbol{w}$, respectively. Note that the use of the transformation matrix formulation shows the relevance of the drop orientation with regard to its resistance to the external flow, however, the appearance of the Euler angles in the resulting flows hinders somewhat their presentation. In order to circumvent this, the transformation is carried out equivalently in terms of fundamental operations (expressions are written in non-dimensional form):

$$\boldsymbol{v}_{\perp} = \boldsymbol{\delta} \cdot \boldsymbol{u}^{\infty} = \; x\boldsymbol{e}_z, \tag{4.3a}$$

$$\boldsymbol{v}_{\parallel} = -\frac{1}{2}\boldsymbol{E}^{\infty} \cdot \boldsymbol{x} + \frac{1}{2}\boldsymbol{e}_z \times \boldsymbol{x} = -z\boldsymbol{e}_x, \tag{4.3b}$$

$$\boldsymbol{v}^{xz} = -\boldsymbol{P} \cdot \boldsymbol{u}^{\infty} \cdot \boldsymbol{P} = \; x\boldsymbol{e}_x - z\boldsymbol{e}_z, \tag{4.3c}$$

$$\boldsymbol{w} = \boldsymbol{u}^{\infty} \times \boldsymbol{e}_x = \; x\boldsymbol{e}_y, \tag{4.3d}$$

where $\boldsymbol{\delta}$ is the identity tensor, the unit dyad $\boldsymbol{P} = -\boldsymbol{e}_k\boldsymbol{e}_l$, and the subscripts $\perp$ and $\parallel$ emphasize that the principal direction of the shear flow is normal and parallel to the internal interface, respectively. Note that $\boldsymbol{v}_{\parallel}$ simply results from a reflection of the straining part of the flow, that $\boldsymbol{v}^{xz}$ is a permutation of $\boldsymbol{u}^{\infty}$ into a hyperbolic flow, and that $\boldsymbol{w}$ is obtained via arrangement of the whole velocity field into a plane parallel to the internal interface. An illustration of the relation between the flows orthogonal to the internal interface is provided in figure 4–2 for further clarification. Arrangement of the straining axis of $\boldsymbol{v}^{xz}$ at a diagonal with the internal interface plus a rotational field yields either $\boldsymbol{v}_{\parallel}$ or $\boldsymbol{v}_{\perp}$ depending on the direction of the arrangement, as depicted in figure 4–2*a* and 4–2*b*, respectively.

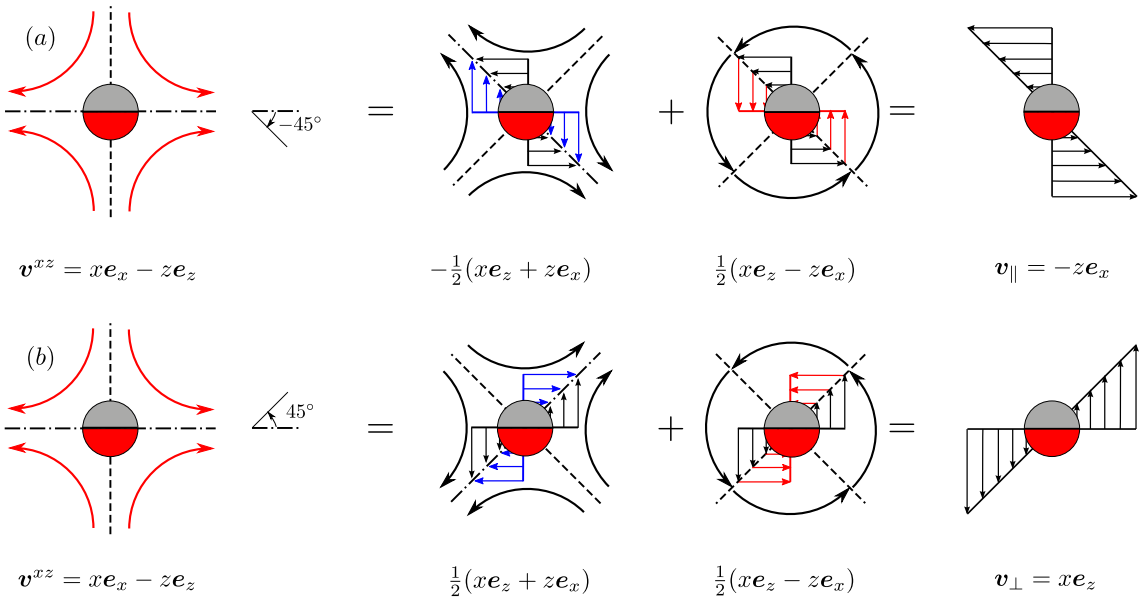


Figure 4–2: Transformation of $\boldsymbol{v}^{xz}$ into $\boldsymbol{v}_{\parallel}$ and $\boldsymbol{v}_{\perp}$. $(a)$ Alignment of the straining axis (dot-dashed line) of $\boldsymbol{v}^{xz}$ at a $-45°$ angle from its horizontal arrangement, plus a rotational field yields $\boldsymbol{v}_{\parallel}$. $(b)$ Alignment of the straining axis at a $45°$ angle from its horizontal position, plus a rotational field results in $\boldsymbol{v}_{\perp}$.

## 4.4 Governing equations

As a first step in exploring the behaviour of a Janus drop in a simple shear flow, fluid motion is analysed in the absence of inertia and in the limit of non-deformable interfaces. In terms of dimensionless groups, fluid motion is characterized by both a negligible Reynolds number, $Re = a^2 G/\nu_0 \ll 1$, and capillary number, $Ca = a\,\eta_0\,G/\gamma \ll 1$, where $a$ is the radius of the Janus drop, $\nu_0$ and $\eta_0$ are the kinematic and dynamic viscosity of the ambient, respectively, and $\gamma$ is the interfacial tension of the internal fluids (the limiting interfacial tension in practice, for instance see the work of Torza & Mason [8]).

The governing equations are written in non-dimensionalized form by adopting the following scales for length, fluid velocity and pressure: $a$, $aG$ and $\tilde{\eta}_0 G$, respectively. Under the aforementioned assumptions, fluid flow is described by the Stokes

equations, which are conveniently presented in spherical coordinates $(r, \vartheta, \phi)$:

$$\nabla \cdot \boldsymbol{u}^{(j)} = 0, \quad -\nabla p^{(j)} + \eta_j \nabla^2 \boldsymbol{u}^{(j)} = 0, \tag{4.4a}$$

$$\boldsymbol{n} \cdot \boldsymbol{u}^{(j)} = 0, \; [\boldsymbol{u}] = [\boldsymbol{n}\cdot\boldsymbol{\sigma}] = \boldsymbol{0}, \text{ at } r = 1, \tag{4.4b}$$

$$\boldsymbol{n} \cdot \boldsymbol{u}^{(1,2)} = 0, \; [\boldsymbol{u}] = [\boldsymbol{n}\cdot\boldsymbol{\sigma}] = \boldsymbol{0}, \text{ at } \vartheta = \pi/2, \tag{4.4c}$$

$$\boldsymbol{u}^{(0)} = \boldsymbol{u}^{\infty} \text{ as } r \to \infty, \tag{4.4d}$$

where $\boldsymbol{n}$ is the unit normal vector at interfaces, which is directed outward at every point on the outer surface and, analogously, at the internal interface it points from fluid '2' to fluid '1'. The fields $\boldsymbol{u}^{(j)}$ and $p^{(j)}$ denote the respective velocity and pressure of the *jth* fluid phase of viscosity $\eta_j = \tilde{\eta}_j/\tilde{\eta}_0$. All fluids are incompressible and Newtonian, $\sigma_{lk}^{(j)} = -p^{(j)}\,\delta_{lk} + \eta_j \left(\nabla_l\, u_k^{(j)} + \nabla_k\, u_l^{(j)}\right)$, where $\delta_{lk}$ is the Kronecker delta. At interfaces $u_n = 0$ because fluids are immiscible. The brackets specify a jump of the fluid velocity and stresses at interfaces. At $r = 1$ this jump is directed from the internal to the ambient fluid and at $\vartheta = \pi/2$ it is directed from fluid '2' to fluid '1'. Far away from the drop, the flow reduces to the undisturbed velocity $\boldsymbol{u}^{\infty}$ (any of the flows presented in Section 4.3).

Continuity of the normal stress at interfaces only enters at the leading order of the expansion in the $Ca \ll 1$ limit. One may venture on determining the small shape distortions via a perturbation technique, however it is expected that it will only bring a correction of $O(Ca)$ to the fluid forces. Note that under the considered conditions — unbounded and linear flow — deflection of interfaces are expected to be point-symmetric, as for single-phase drops (the reader may refer to the survey of Rallison [56]), and therefore, have zero influence whatsoever on the behaviour of multiphase drops. For example, the results of Stone & Leal [10] indicate that a concentric multiphase drop undergoes point-symmetric deformations in an unbounded, linear flow. In fact, that finding is not limited to concentric drops since Shklyaev *et al.* [119] also found point-symmetric distortions on a Janus drop in a uniform

external flow. For the purposes of exploring the dynamics and behaviour of a Janus drop in a shear flow, there is little gain — on account of the aforementioned arguments — in determining the small deflections to the internal interface. Nevertheless, accounting for shape distortions is certainly rewarding in studies concerned with the conditions for drop breakup, coalescence, and rheology of a suspension [9, 47, 48, 53–56, 59, 79, 80, 130–136].

The force $\boldsymbol{F}$ on the drop is obtained by integrating the stresses at its surface ($r = 1$):

$$\boldsymbol{F} = \oint \boldsymbol{n} \cdot \boldsymbol{\sigma} \, \mathrm{d}S, \tag{4.5}$$

where $S$ is the area of the outer surface, and the couple (or torque) $\boldsymbol{T}$ is calculated by:

$$\boldsymbol{T} = \oint \boldsymbol{x} \times (\boldsymbol{\sigma} \cdot \boldsymbol{n}) \, \mathrm{d}S. \tag{4.6}$$

The following scales render non-dimensional $\boldsymbol{F}$ and $\boldsymbol{T}$: $a^2\tilde{\eta}_0 G/2$ and $a^3\tilde{\eta}_0 G/2$, respectively, which guarantee that $\boldsymbol{T}$ reduces to that of a solid sphere when $\eta_1 = \eta_2 \gg 1$. Variation of $\boldsymbol{F}$ and $\boldsymbol{T}$ with the viscosity of the fluids is presented in terms of the drop mean viscosity $\eta = (\eta_2 + \eta_1)/2$ and viscosity contrast $\Delta\eta/2\eta = (\eta_2 - \eta_1) \,/\, (\eta_2 + \eta_1)$.

The viscosity contrast quantifies the deviation of the Janus drop from one with equal viscosity ($\eta_1 = \eta_2$). The limit of $\Delta\eta/2\eta \ll 1$ may be of particular interest to experimenters because of the similar viscosities of the constituent fluids in practice [8, 129], nonetheless, solutions are sought in the full range $(0, 1)$ for completeness. (Outside that domain there are no physical solutions.) In the limit of $\Delta\eta/2\eta \to 1$ and $\eta \gg 1$ the Janus drop is composed by a fluid of negligible and another of very high viscosity, however, this limit may not be of much relevance in practice.

## 4.5 Solution

Shear flow past a body is, inherently, a three-dimensional (3D) problem. For example, the disturbances caused by a fixed solid-sphere result in a three-dimensional flow. For a Janus drop subject to a simple shear flow the motion of the fluid phases

can be described via Lamb's generalized solution [31] (in non-dimensionalized form):

$$\boldsymbol{u}^{(j)} = \sum_{n=-\infty}^{\infty} \left[ \frac{(n+3)\, r^2\, \nabla \bar{p}_n^{(j)}}{2(n+1)(2n+3)} - \frac{n\, \boldsymbol{x}\, \bar{p}_n^{(j)}}{(n+1)(2n+3)} \right] + \sum_{n=-\infty}^{\infty} \left[ \nabla \Phi_n^{(j)} + r \nabla \chi_n^{(j)} \times \boldsymbol{e}_r \right], \tag{4.7}$$

where the spherical harmonics that describe the pressure field have been scaled with the viscosity of the corresponding fluid phase $\bar{p}_n^{(j)} = p_n^{(j)}/\eta_j$, $\Phi_n^{(j)}$ defines potential flows, and $\chi_n^{(j)}$ characterizes swirling flows in each fluid phase. The the following spherical harmonics characterize the flow of the suspending fluid:

$$\bar{p}_n^{(0)} = \frac{2(-2n+1)}{(n+1)} E_n P_n^{(1)}(\theta) r^{-n-1} \cos\phi, \tag{4.8a}$$

$$\Phi_n^{(0)} = -\frac{E_n}{(n+1)} P_n^{(1)}(\theta) r^{-n-1} \cos\phi, \tag{4.8b}$$

$$\chi_n^{(0)} = -H_n P_n^{(1)}(\theta) r^{-n-1} \sin\phi, \tag{4.8c}$$

with corresponding series coefficients $E_n, H_n$, and $P_n^{(1)}(\theta)$ is the first associated Legendre polynomial of order $n$ with $\theta = \cos\vartheta$. Analogously the internal flows are described by:

$$\bar{p}_n^{(1,2)} = -\left\{ \frac{2(4n+1)}{(2n-1)} B_n^{(1,2)} \frac{P_{2n-1}^{(1)}(\theta)}{P_{2n-1}^{(1)}(0)} + \eta_{2,1} \frac{2(2n+1)(4n+3)}{(2n+3)} D_n \frac{P_{2n}^{(1)}(\theta)}{Q_{2n}(0)} r \right\} r^{2n-1} \cos\phi, \tag{4.9a}$$

$$\Phi_n^{(1,2)} = -\left\{ \frac{B_n^{(1,2)}}{(2n+1)} \frac{P_{2n+1}^{(1)}(\theta)}{P_{2n+1}^{(1)}(0)} + \eta_{2,1} D_n \frac{P_{2n+2}^{(1)}(\theta)}{Q_{2n+2}(0)} r \right\} r^{2n+1} \cos\phi + \left\{ F_n P_{2n-1}^{(1)} - \eta_{2,1}\, G_n \frac{P_{2n}^{(1)}(\theta)}{Q_{2n}(0)} r \right\} r^{2n-1} \cos\phi, \tag{4.9b}$$

$$\chi_n^{(1,2)} = \left\{ A_n^{(1,2)} P_{2n}^{(1)} r^{2n} - \eta_{2,1} G_n \frac{P_{2n-1}^{(1)}(\theta)}{P'_{2n-1}(0)} r^{2n-1} \right\} \sin\phi, \tag{4.9c}$$

with series coefficients $B_n^{(1,2)}, A_n^{(1,2)}, D_n, F_n, G_n$, and $Q_{2n}(0) = -2n(2n+1)P_{2n}(0)$. The tangent no-slip condition at the internal interface imposes the following constraint:

$$B_n^{(2)} - B_n^{(1)} = \frac{2n(2n-1)(2n+1)}{2(4n+1)} Q_{2n}(0)\,(A_n^{(2)} - A_n^{(1)}). \tag{4.10}$$

Although the obtained solution is exact, the series coefficients require numerical determination. Truncation of the expansion up to order $N$ and matching of the velocity fields at the surface of the drop ($r = 1$) results in a $(10N \times 10N)$ system of linear equations for the unknown coefficients, which is solved with the linear algebra package (lapack). The truncation order is increased systematically until convergence is achieved.

### 4.5.1 Shear flow with a velocity gradient parallel to the internal interface

It is straightforward to show that $\boldsymbol{w} = x\boldsymbol{e}_y$ results in $\boldsymbol{F} = \boldsymbol{T} = \boldsymbol{0}$, which is realized by noting that the Janus drop behaves as a single-phase drop. The particular, yet instructive, situation of a Janus drop with $\eta_1 = \eta_2$ reveals that the flows of a single-phase drop [11] satisfy the boundary value problem, and consequently, the forces and couples are identically zero. It is simple to see from the interior flows of a single-phase drop given in Equation (2.286) that there are no flows normal to the $x$–$y$ plane ($u_\vartheta^{(j)} = 0$ at $\vartheta = \pi/2$) on account of the innate symmetry of the shear flow; hence, the no-penetration condition is satisfied automatically for a Janus drop when the internal interface lies along the $x$–$y$ plane as in this scenario. Evidently, the fluid stresses are continuous across the internal interface since the interior flows satisfy the Stokes equations over the volume of the sphere such that the boundary value problem is fully described by the velocity fields of a single-phase drop. Note that the situation is not so different for a Janus drop with different internal viscosities. As in the former case, the internal interface creates a system of velocity gradients that preserves the symmetric character of the flow, which guarantees that $\boldsymbol{F} = \boldsymbol{T} = \boldsymbol{0}$. It is expected that this result holds for a Janus drop with volume ratios of the internal

fluids other than 1:1 despite the fact that the internal flows will differ from that of a single-phase drop.

The symmetry arguments for a Janus drop formed by a pair of hemispherical domains still hold. Continuity of the velocity at interfaces requires all fluids to undergo a solid body rotation: $u^{(j)}_{r,\vartheta} = u^{\infty}_{r,\vartheta} = 0$; $u^{(j)}_{\phi} = u^{\infty}_{\phi} = 1/2\ r\sin\vartheta$. (It is evident that the velocity fields satisfy the boundary value problem for a Janus drop with an arbitrary volume ratio.) This pure rotational motion generates zero fluid stresses everywhere, and hence the force and couple on the drop are identically zero ($\boldsymbol{F} = \boldsymbol{T} = \boldsymbol{0}$). Obtaining the velocity fields that arise from the straining component of the shear flow is a formidable problem (aside from the obvious situation of a Janus drop with internal volume ratios of 1:1). Nonetheless, it is plausible to expect that the spherical harmonics that solve the fluid flow problem retain the symmetric character of the undisturbed flow (i.e. $\boldsymbol{F} = \boldsymbol{T} = \boldsymbol{0}$), and the unnecessary spherical harmonics — those associated with a force and a couple — vanish to zero. This simple result is a feature of Lamb's general solution for a spherical body (the reader is referred to Chapter 4 of Kim & Karrila [31]). The principal observation is that all fluids simply undergo a solid-body rotation and the straining field cannot impose a net force or torque in this particular arrangement.

### 4.5.2 Plane hyperbolic flow with a velocity gradient normal to the internal interface

The force and couple imposed by the hyperbolic flow, $\boldsymbol{v}^{xz} = x\boldsymbol{e}_x - z\boldsymbol{e}_z$, on the Janus drop are considered. An illustration of the flow about the Janus drop is shown in figure 4–2*a*.

Results show that $\boldsymbol{F} = \boldsymbol{T} = \boldsymbol{0}$ for a Janus drop with $\eta_1 = \eta_2$. Once again, an analogous behavior of the flow fields of a Janus drop with those of a single-phase drop exists, such that the boundary value problem is satisfied identically. Although the velocity fields of the single-phase drop given in Equation (2.104) correspond to the

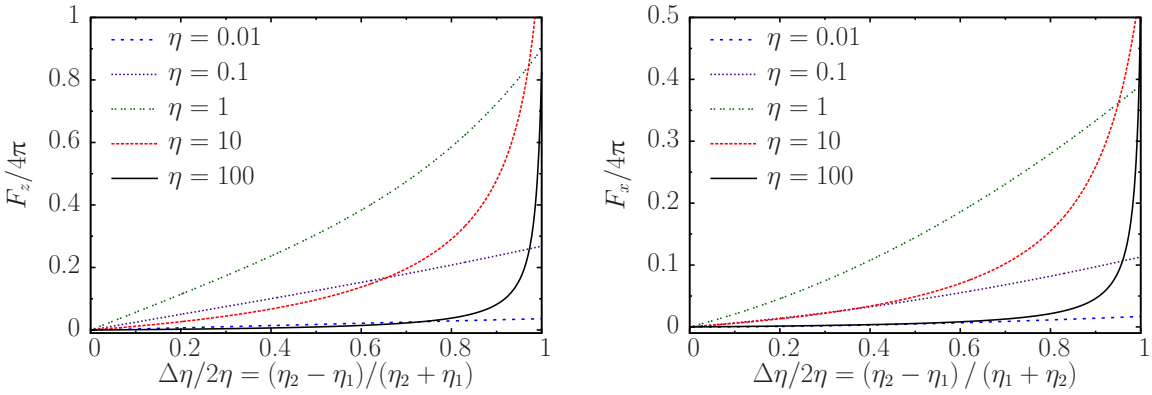


Figure 4–3: Variation of the force $F_z$ (in units of $a^2\tilde{\eta}_0 G$) with the viscosity contrast at constant values of $\eta$ when the Janus drop is subject to $\boldsymbol{v}^{xz}$ ($a$). The force $F_x$ (in units of $a^2\tilde{\eta}_0 G$) on the Janus drop under the action of $\boldsymbol{v}_{\parallel}$ with increasing viscosity contrast at constant values of $\eta$ ($b$).

scenario of a pure elongational flow, the same symmetry arguments that support that there are no flows normal to the internal interface hold because a pure elongational flow simply consists of a superposition of the $2D$ straining flow considered here plus another one acting in the $y$–$z$ plane. Note that even for a Janus drop of different internal viscosities $F_x = 0$ and $\boldsymbol{T} = \boldsymbol{0}$ due to the symmetry of the flow. And thus, the underlying observation is that in this flow-to-drop arrangement there are no means of the flow to induce drop rotation, and that the natural tendency of the Janus drop is to have its axis of symmetry aligned with any of the principal axes of the flow. Results indicate that the axisymmetric part of the flow imposes a force $F_z$ that grows monotonically with $\Delta\eta/2\eta$, as shown by figure 4–3$a$. Initially, the force is of $O(\Delta\eta/2\eta)$, which is best shown by the plot with $\eta = 1$, where deviation from linearity is less than 10% up to $\Delta\eta/2\eta = 0.55$. At greater values of $\Delta\eta/2\eta$ the force grows quadratically because of a higher order system of velocity gradients. In the dual limit of $\Delta\eta/2\eta \to 1$ and $\eta \gg 1$ the numerical results indicate that the force $F_z$ scales as $\eta_2/\eta_1 \gg 1$. An interpretation of this result follows from the observation that the force on the drop solely arises from the deviatoric stresses of the most viscous fluid. (Evidently, from the perspective of the ambient fluid

the hemispherical domain of the less viscous fluid acts as a perfect 'slip' surface of zero resistance to fluid flow.) It is reasonable to expect that the velocity of the most viscous fluid decays as $\eta_2^{-1}$, and hence, the length scale $L/a$ over the velocity gradient changes must be of $O(\eta_1/\eta_2) \ll 1$ in order to account for the divergence of the net force. Consequently, the force must satisfy the scaling: $F_z/a^2\tilde{\eta}_0 G \sim a/L$. It is interesting to note that the force required to maintain fixed a 'slip–stick' sphere (under analogous conditions) scales with the 'slipping' length $\lambda/a \gg 1$ (which is readily inferred from the results of Ramachandran & Khair [44]). By regarding the Janus drop as a model for a 'slip–stick' sphere — which is likely to be valid exclusively in this extreme case — the length $L/a$ can be interpreted as an inverse 'slipping' length. Although the scaling of the force with $a/L$ are arrived from an analysis that considers the most viscous fluid, continuity of the surface tractions at the outer surface of the drop dictates that the velocity of the ambient much change over the same length-scale $L/a$ since $u^{(0)} \sim 1$.

The non-monotonic dependence of the force $F_z$ with the mean viscosity $\eta$ is clearly depicted by the plots. For finite values of $\Delta\eta/2\eta$ the force $F_z$ decays with decreasing $\eta$ (on account of the small viscous stresses) and with increasing $\eta$ (a solid-like limiting behaviour). It is interesting to note that the net force reported here is the manifestation of the center of hydrodynamic reaction $\boldsymbol{x}^{cr}$ being displaced from the flow stagnation point. In fact, it is found that the Janus drop experiences a zero net force when $\boldsymbol{x}^{cr}$ coincides with the flow stagnation-point of a general straining flow. Positioning the flow stagnation point at $\boldsymbol{x}^{cr}$ results in a streaming plus a straining flow with respect to the set of coordinates $\boldsymbol{x}$ centered on the Janus drop. Summation of the forces of both contributions results in a zero net force. The main result is that the shear-force tensor vanishes at the center of hydrodynamic reaction $\boldsymbol{x}^{cr}$; a formal prove of this result is provided in Section 4.6.

### 4.5.3 Shear flows with a velocity gradient normal to the internal interface

The forces and couples exerted by the shear flows, $\boldsymbol{v}_{\parallel} = -z\boldsymbol{e}_x$ and $\boldsymbol{v}_{\perp} = x\boldsymbol{e}_z$, are considered here. Figure 4–2 shows how the shear flows are broken down into straining and rotating constituents.

In view of the innate symmetry of the shear flows, it is evident that $\boldsymbol{F} = \boldsymbol{0}$ when $\eta_1 = \eta_2$. Particularly for $\boldsymbol{v}_{\perp}$ the force is always zero ($\boldsymbol{F} = \boldsymbol{0}$) regardless of $\Delta\eta/2\eta$; there can be no net force in the $z$ direction, and also because the $x$ component of the straining and rotating fields of $\boldsymbol{v}_{\perp}$ are equal in magnitude but opposite in direction, as shown in figure 4–2$b$. Figure 4–3$b$ depicts the effect of $\Delta\eta/2\eta$ on the force $F_x$ when the Janus drop is subject to $\boldsymbol{v}_{\parallel}$, and it is notable that the effect is analogous to that found in a hyperbolic flow (figure 4–3$a$). It is important to point out that the appearance of a force is just the manifestation of $\boldsymbol{x}^{cr}$ being displaced from the centerline of the shear flow (in the coincident situation $\boldsymbol{F} = \boldsymbol{0}$ because of the zero coupling and shear-force tensors).

Figure 4–4 shows variation of the resultant couple $T_y$ (in units of $a^3\tilde{\eta}_0 G$) with the mean viscosity ($\eta = \eta_1 = \eta_2$). The solid-line depicts $T_y$ owing to $\boldsymbol{v}_{\perp}$, and the dashed-line shows its counterpart $\boldsymbol{v}_{\parallel}$. It is readily seen that the couple in $\boldsymbol{v}_{\perp}$ is of greater magnitude than $\boldsymbol{v}_{\parallel}$ except in the extreme cases $\eta \ll 1$ (negligible viscous stresses) and $\eta \gg 1$ (solid-like limit), where the Janus drop behaves as an isotropic body and the direction of the shear flow becomes irrelevant. It is obvious that the pressure does not contributes to the resultant couple because it is the isotropic component of the fluid stress. Only the viscous contribution of the stress results in a couple on the drop, and this one vanishes identically as the mean drop viscosity approaches zero ($\eta \ll 1$). (The outer surface of the Janus drop can be regarded as a perfect 'slip' surface in this extreme case.) Note that even though the couple vanishes in this limit, the internal flows of the Janus drop differ from those of a

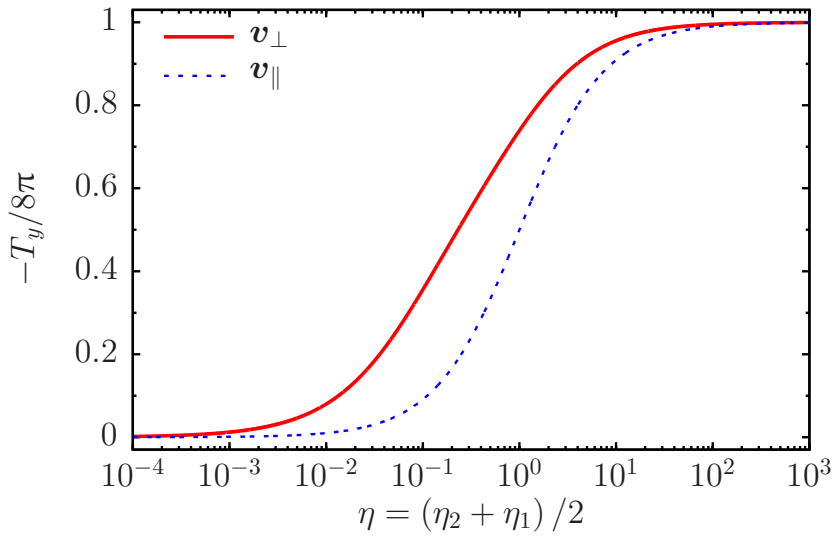


Figure 4–4: The couple $T_y$ (in units of $a^3\tilde{\eta}_0 G$) on a Janus drop with $\eta_1 = \eta_2$.

single-phase drop. A qualitative picture of the velocity fields inside and outside the Janus drop are shown in Figure 4–5. Note that the exterior flows exhibit no appreciable differences when compared to those about a single-phase drop shown in figure 2–13; the influence of the internal interface is evident by comparing againts the circulation flows of a single-phase drop. One may infer that the couple exerted by $\boldsymbol{v}_\perp$ is greater than its counterpart $\boldsymbol{v}_\parallel$ because the internal interface prohibits, to a greater extent, the circulation flows of a single-phase drop (figure 4–5*b*). Note that the differences of the couples shown in figure 4–4 indicates that the resultant couple on the drop unfolds from both the straining and rotating components of the flow. (Otherwise, $\boldsymbol{v}_\parallel$ and $\boldsymbol{v}_\perp$ would generate the same curve.) Perhaps, it is more relevant to point out that even a Janus drop with $\eta_1 = \eta_2$ displays anisotropic properties, solely because of the presence of the internal interface.

The influence of $\Delta\eta/2\eta$ on $T_y$ in $\boldsymbol{v}_\parallel$ and $\boldsymbol{v}_\perp$ is seen in figure 4–6 for selected values of the mean viscosity. It is noteworthy that the dependence of $T_y$ with $\Delta\eta/2\eta$ is analogous to the dependence of the force in a streaming flow [119], in the sense that the qualitative features are retained. (For small $\Delta\eta/2\eta$ the couple is $O(1)$,

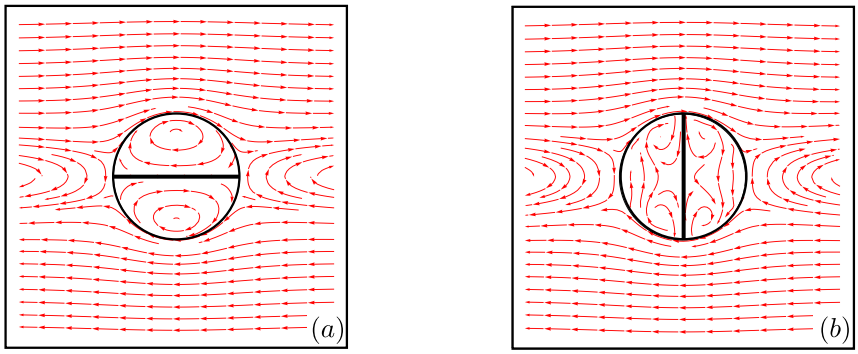


Figure 4–5: The velocity fields of a Janus drop subject to $\boldsymbol{v}_{\parallel}$ $(a)$ and $\boldsymbol{v}_{\perp}$ $(b)$.

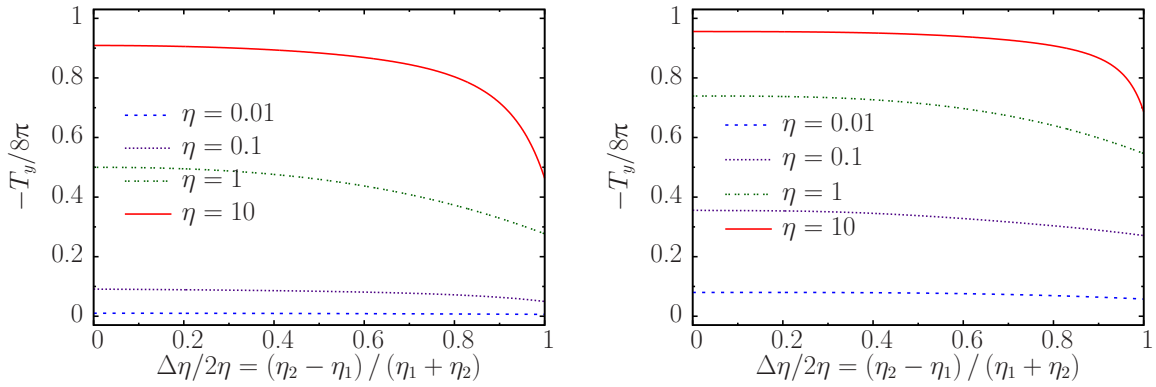


Figure 4–6: Variation of the couple $T_y$ (in units of $a^3\tilde{\eta}_0 G$) with the viscosity contrast at constant values of the mean viscosity for $\boldsymbol{v}_{\parallel}$ $(a)$ and $\boldsymbol{v}_{\perp}$ $(b)$.

constant, and equal to the $\eta_1 = \eta_2$ case.) Further increase of $\Delta\eta/2\eta$ induces a decay of $T_y$ at a quadratic rate of the order of $(\Delta\eta/2\eta)^2$. This marked decrease of $T_y$ is in agreement with the observation that the less viscous fluid sets up the magnitude of the couple.

### 4.5.4 Cross-streaming velocity of a Janus drop in a uniform flow

A closed-form expression for the cross-stream velocity of a Janus drop is obtainable when the drop moves with a relative velocity $(u_z - u_{z,\infty})$ along the streamlines of a uniform flow. The external force required to sustain drop motion must pass through the center of reaction $\boldsymbol{x}^{cr}$ to prevent rotation. The sought result is obtained by finding the migration velocity $u_{x,m}$ that cancels out the forces lateral to the undisturbed flow (this is analogous to the settling of anisotropic bodies presented

by Happel & Brenner [20]). It is found that $u_{x,m}$ depends on the angle $\alpha$ from the scalar product $\boldsymbol{d}\cdot\boldsymbol{u}^{\infty}$, the resistance functions to translation, $X^A$ and $Y^A$ (tabulated in the Section 4.6), and the drop relative velocity:

$$u_{x,m} = \frac{\left(X^A - Y^A\right)\cos\alpha\sin\alpha}{X^A - \left(X^A - Y^A\right)\cos^2\alpha}\left(u_z - u_{z,\infty}\right). \tag{4.11}$$

Note that $u_{x,m}$ does not depend on the drop size due to its spherical shape, and that lateral migration does not occur when the axis of symmetry of the Janus drop is aligned or normal to the streamlines of the undisturbed flow. This behaviour is akin of a symmetric spheroid of revolution (the reader is referred to Chapter 4 of Happel & Brenner [20].) The drop orientation $\alpha^*$ that maximizes the migration velocity is readily found in terms of the resistance functions to translation: $\alpha^* = \cos^{-1}\left(X^A/(X^A + Y^A)\right)$, where $\alpha^*$ is found to be approximately equal to 45° because $X^A$ and $Y^A$ are close in magnitude. Therefore, the maximum migration velocity occurs when the internal interface is nearly at a diagonal with the direction of the uniform flow. Equation (4.11) may be used to estimate the instantaneous cross-streaming velocity of a Janus drop in a linear shear flow provided that $\Delta\eta/2\eta$ is small. It is important to note that the Janus drop will also be subject to rotation on account of the net hydrodynamic torque on the drop such that the cross-streaming velocity will fluctuate in time. A thorough analysis of the cross-streaming velocity of a Janus drop in a linear shear flow is performed in the next chapter.

## 4.6 Grand resistance matrix of a Janus drop

In this section the grand resistance matrix for a Janus drop is reported at the hydrodynamic center of reaction $\boldsymbol{x}^{cr}$. The determination proceeds by assuming that the form of the resistance tensors for symmetric bodies of revolution apply to a Janus drop based on its spherical shape. In general, the values of the resistance tensors that comprise the grand resistance matrix change from one location to another on the body; however, some values of the resistance tensors can be zero at the hydrodynamic

center of reaction $\boldsymbol{x}^{cr}$. This simplification is exploited here to reduce the number of quantities to report at the expense of carrying out fundamental analyses on the resistance tensors. The grand resistance matrix relates the force $\boldsymbol{F}$, torque $\boldsymbol{T}$ and stresslet $\boldsymbol{S}$ on the Janus drop in a general ambient flow (the followed notation is that of Kim & Karrila [31]):

$$\begin{pmatrix} \boldsymbol{F} \\ \boldsymbol{T} \\ \boldsymbol{S} \end{pmatrix} = \tilde{\eta}_0 \begin{pmatrix} \boldsymbol{A} & \tilde{\boldsymbol{B}} & \tilde{\boldsymbol{G}} \\ \boldsymbol{B} & \boldsymbol{C} & \tilde{\boldsymbol{H}} \\ \boldsymbol{G} & \boldsymbol{H} & \boldsymbol{M} \end{pmatrix} \begin{pmatrix} \boldsymbol{U}^{\infty} - \boldsymbol{u} \\ \boldsymbol{\Omega}^{\infty} - \boldsymbol{\omega} \\ \boldsymbol{E}^{\infty} \end{pmatrix}, \tag{4.12}$$

where $(\boldsymbol{U}^{\infty} - \boldsymbol{u})$ and $(\boldsymbol{\Omega}^{\infty} - \boldsymbol{\omega})$ are the solid-body motions of translation and rotation, respectively, of the ambient flow in a reference frame where the Janus drop is stationary, $\boldsymbol{A}$ is the translation tensor (second-rank), $\boldsymbol{B}$ is the coupling tensor (second-rank), $\boldsymbol{C}$ is the rotation tensor (second-rank), $\boldsymbol{G}$ is the shear-force tensor (third-rank), $\boldsymbol{H}$ is the shear-torque tensor (third-rank), and $\boldsymbol{M}$ is a fourth-rank tensor that relates the stresslet to the undisturbed rate-of-strain tensor $\boldsymbol{E}^{\infty}$. Here the tilde on top of a tensor quantity denotes its transpose. On account of the symmetry of the Janus drop, the resistance tensors can be expressed with respect to the unit vector $\boldsymbol{d}$ that defines the drop orientation due to the inherent analogy with solid bodies of revolution (tensors and vectors are shown here in indicial notation for convenience [18]):

$$A_{ij} = X^A\, d_i d_j + Y^A\, (\delta_{ij} - d_i d_j)\,, \tag{4.13a}$$

$$B_{ij} = Y^B \epsilon_{ijk} d_k, \tag{4.13b}$$

$$C_{ij} = X^C\, d_i d_j + Y^C\, (\delta_{ij} - d_i d_j)\,, \tag{4.13c}$$

$$G_{ijk} = X^G \left( d_i d_j - \frac{1}{3}\delta_{ij} \right) d_k + Y^G\, (d_i \delta_{jk} + d_j \delta_{ik} - 2 d_i d_j d_k)\,, \tag{4.13d}$$

$$H_{ijk} = \tilde{H}_{kij} = Y^H\, (\epsilon_{ikl} d_j + \epsilon_{jkl} d_i)\, d_l, \tag{4.13e}$$

$$M_{ijkl} = X^M d^{(0)}_{ijkl} + Y^M d^{(1)}_{ijkl} + Z^M d^{(2)}_{ijkl}, \tag{4.13f}$$

where $X$, $Y$ and $Z$ are scalar functions for the specified tensor quantity, the superscript $n$ of $d_{ijkl}^{(n)}$ is not to be confused with the fluid phase index $j$; these are tensor quantities related to the five elemental basis tensors that generate the universal rate-of-strain tensor given here:

$$\boldsymbol{E}^{\infty} = \begin{pmatrix} \frac{1}{2}\left(E_{xx} - E_{yy} - E_{zz}\right) & E_{xy} & E_{xz} \\ E_{yx} & \frac{1}{2}\left(-E_{xx} + E_{yy} - E_{zz}\right) & E_{yz} \\ E_{zx} & E_{zy} & E_{zz} \end{pmatrix}. \tag{4.14}$$

Note that the rate-of-strain tensor above is symmetric and traceless (the sum of the diagonal elements is zero). The rate-of-strain tensor $\boldsymbol{E}^{\infty}$ can be broken down into its elemental components in the following manner:

$$E_{ij}^{\infty} = d_{ijkl}^{(0)} E_{lk}^{\infty} + d_{ijkl}^{(1)} E_{lk}^{\infty} + d_{ijkl}^{(2)} E_{lk}^{\infty}, \tag{4.15}$$

where

$$d_{ijkl}^{(0)} = \frac{3}{2}\left(d_i d_j - \frac{1}{3}\delta_{ij}\right)\left(d_k d_l - \frac{1}{3}\delta_{kl}\right), \tag{4.16a}$$

$$d_{ijkl}^{(1)} = \frac{1}{2}\left(d_i\delta_{jl}d_k + d_j\delta_{il}d_k + d_j\delta_{jk}d_l + d_j\delta_{ik}d_l - 4d_i d_j d_k d_l\right), \tag{4.16b}$$

$$\begin{aligned} d_{ijkl}^{(2)} = \frac{1}{2}\big(&\delta_{ik}\delta_{jl} + \delta_{jk}\delta_{il} - \delta_{ij}\delta_{kl} + d_i d_j\delta_{kl} + \delta_{ij}d_k d_l - d_i\delta_{jl}d_k - d_j\delta_{il}d_k \\ &- d_i\delta_{jk}d_l - d_j\delta_{ik}d_l + d_i d_j d_k d_l\big). \end{aligned} \tag{4.16c}$$

By adopting the convenient choice for the orientation vector $\boldsymbol{d} = \boldsymbol{e}_z$, followed by some routinary operations, one can determine the sought relationships with respect to the basis tensors:

$$\boldsymbol{d}^{(0)} : \boldsymbol{E}^{\infty} = \frac{E_{zz}}{2}\boldsymbol{E}^{(1)}, \quad \boldsymbol{d}^{(1)} : \boldsymbol{E}^{\infty} = E_{xz}\boldsymbol{E}^{(4)} + E_{yz}\boldsymbol{E}^{(5)}, \tag{4.17a}$$

$$\boldsymbol{d}^{(2)} : \boldsymbol{E}^{\infty} = \frac{1}{2}\left(E_{xx} - E_{yy}\right) + E_{xy}\boldsymbol{E}^{(3)}, \tag{4.17b}$$

where the basis tensors are shown below:

$$\boldsymbol{E}^{(1)} = \begin{pmatrix} -1 & 0 & 0 \\ 0 & -1 & 0 \\ 0 & 0 & 2 \end{pmatrix}, \quad \boldsymbol{E}^{(2)} = \begin{pmatrix} 1 & 0 & 0 \\ 0 & -1 & 0 \\ 0 & 0 & 0 \end{pmatrix}, \tag{4.18a}$$

$$\boldsymbol{E}^{(3)} = \begin{pmatrix} 0 & 1 & 0 \\ 1 & 0 & 0 \\ 0 & 0 & 0 \end{pmatrix}, \quad \boldsymbol{E}^{(4)} = \begin{pmatrix} 0 & 0 & 1 \\ 0 & 0 & 0 \\ 1 & 0 & 0 \end{pmatrix}, \tag{4.18b}$$

$$\boldsymbol{E}^{(5)} = \begin{pmatrix} 0 & 0 & 0 \\ 0 & 0 & 1 \\ 0 & 1 & 0 \end{pmatrix}. \tag{4.18c}$$

Due to the symmetry of the Janus drop all hydrodynamic information is contained in the scalar functions $X$, $Y$ and $Z$; $X$ is a function that describes flows of axisymmetric character, and the remaining two functions correspond to flows transversal to the drop orientation (axis of symmetry) $\boldsymbol{d}$. For example, the drag force $F$ on a Janus drop in a uniform flow parallel to the drop axis of symmetry $(U^\infty - u)\,\boldsymbol{d}$ is proportional to the scalar function $X^A$: $F = \tilde{\eta}_0\, X^A\,(U^\infty - u)$. On the other hand, if the uniform flow is normal to the drop orientation the drag force is given in terms of the other scalar function: $F = \tilde{\eta}_0\, Y^A\,(U^\infty - u)$. Evidently, for an arbitrary flow direction the drag force depends on both $X^A$ and $Y^A$; the dominating function (if any) will depend on the direction of the flow relative to the drop orientation $\boldsymbol{d}$. For a solid sphere the scalar functions are identical to each other: $X^A = Y^A = 6\pi a$, as it should, because the particle has an isotropic hydrodynamic resistance to a uniform flow. As one may suspect, the determination of the scalar functions $X^A$ and $Y^A$ can be realized by choosing advantageous directions of the flow such that a unique scalar function contributes to the drag force. For straining flows, it is convenient to

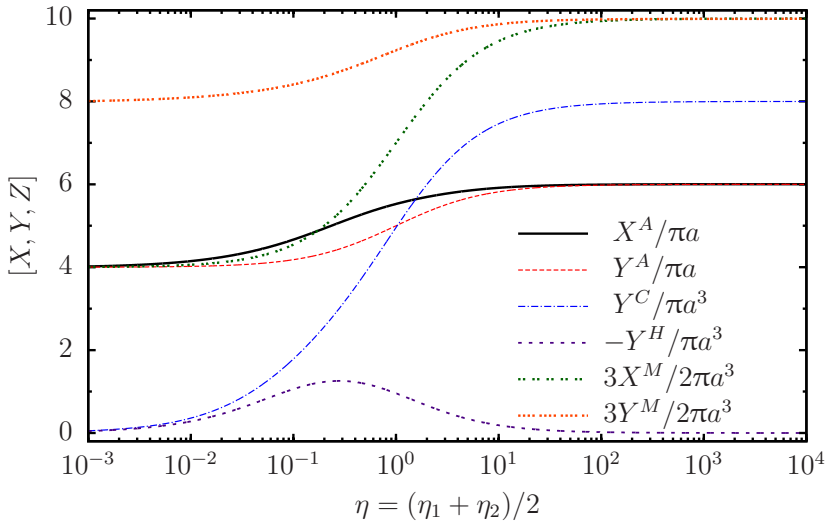


Figure 4–7: Dependence of the resistance functions with the mean drop viscosity $\eta$ for the case of equal internal viscosities. The resistance function $Z^M$ has been omitted because it is identical to $X^M$.

assume that the undisturbed flow consists of one of the basis rate-of-strain tensors $\boldsymbol{E}^{(n)}$ above to determine the corresponding scalar functions.

Without additional introductory remarks, the non-vanishing resistance functions for a Janus drop with equal internal viscosities ($\eta_1 = \eta_2$) are shown in figure 4–7. It is evident that the hydrodynamic center of reaction is located at the geometrical center of the Janus drop ($\boldsymbol{x}^{cr} = \boldsymbol{0}$) and that the shear-force tensor is zero $\left(X^G = Y^G = 0\right)$ because of the combined effect of the drop spherical shape and equal internal viscosities. (These results are expected to apply even when for a curved internal interface.) The resistances functions due to translation $X^A$ and $Y^A$ exhibit the appropriate limits for a low viscosity drop ($\eta \ll 1$) and a solid sphere ($\eta \gg 1$). The relation $X^A \geq Y^A$ holds for any value of the mean drop viscosity $\eta$ because of the additional resistance imposed by the internal interface to the external uniform flow in the axisymmetric case, in agreement with the results presented in Chapter 3. An exact expression has been found for $Y^A/2\pi a = (2 + 3\eta)\,/\,(1 + \eta)$ because in this case the resistance of the Janus drop to the external uniform flow is equal to that of

a single-phase drop. The circulation flows of Hadamard–Rybczynski [51, 52] satisfy the pertaining boundary conditions for the Stokes equations for a Janus drop with equal internal viscosities.

The resistance function due to rotation $Y^C$ varies from zero (no resistance) to that of a solid sphere ($8\pi a^3$) in the corresponding limits. It is important to point out that the zero resistance to rotation found in the limit of a low viscosity Janus drop ($\eta \ll 1$) does not means that the Janus drop exhibits the behavior of a simple fluid drop. A simple fluid drop cannot resist the rotational motion of the surrounding fluid regardless of the drop viscosity $\eta$. This is the case because a simple drop can only undergo a solid-body rotation with the ambient fluid as dictated by the no-slip tangent condition at the surface of the drop. (This goes in contrast to a solid body, which can rotate relative to the ambient by means of an external torque.) Hence, the resistance to rotation for a single-phase drop is an undefined quantity because there are no means of specifying a relative angular velocity for the single-phase drop without violating continuity of either the tangential velocity or stress. For a Janus drop the situation is rather different. One can easily envision a Janus drop rotating relative to an ambient flow because of the rate of change of the orientation of the internal interface in time. From a mathematical point of view, the presence of the internal interface provides the necessary degrees of freedom for the Janus drop to satisfy continuity of both the tangential velocity and stress at the outer surface of the drop. Following the mentioned arguments, the resistance to rotation about the axis of symmetry of the Janus drop $X^C$ is undefined in this special case because the drop exhibits the behavior of a single-phase drop (Section 4.5.1).

The resistance function associated with the shear-torque $Y^H$ is seen to vanish at low values of mean viscosity and in the solid sphere limit. The former situation is evident because the viscous stresses are accountable for the shear-torque and in this case these are negligible. In the latter case the rate-of-strain field does not produce a

shear-torque because in this limit the Janus drop essentially behaves as an isotropic rigid-body; a formal demonstration of this result for a solid sphere is performed in Section 2.3.4. The negative sign of $Y^H$ implies that the resistance of the Janus drop to a rate-of-strain field is analogous to that of an oblate spheroid, which corroborate the results given in Section 4.5.3 that show that the net torque in a shear flow is greater when the direction of the flow is parallel to the axis of symmetry of the Janus drop. (One may reproduce the plots presented in that section by appropriate combinations of the torques due to rotation and straining motion of the ambient fluid.)

The theoretical results demonstrate that the stresslet of a Janus drop with equal internal viscosities ($\eta_1 = \eta_2$) in a pure elongational flow is identical to that of a single-phase drop: $X^M = 2\pi/3a^3\,(4 + 10\eta)\,/(1 + \eta)$; it turns out that the interior and exterior flows of a single-phase drop satisfy the Stokes equations with corresponding boundary conditions for a Janus drop in this special limit. This finding has been corroborated against the numerically obtained results. (It is a straightforward task to show that the the velocity fields of a single-phase drop derived in Section 2.2.4 satisfy the boundary value problem for a Janus drop with equal internal viscosities.) In the context of the physics at fluid–fluid interfaces, the internal interface has no influence on the flows that develop inside the Janus drop because of the inherent symmetry of the imposed elongational flow. It follows that the absence of the flow-disturbances caused by the presence of the internal interface ensures that the exterior flows match those of a single-phase drop. It is noteworthy that the resistance function $Y^M$ is of greater magnitude than $X^M$ for most values of the mean drop viscosity, presumably due to the flow disturbances caused by the internal interface to the internal circulation flows. This is supported by the results in the limit of a Janus drop with a low mean viscosity ($\eta \ll 1$); otherwise no differences would be observed between the two resistance functions in this limit. On

the other hand, there are no differences in stresslet at the extreme scenario of a Janus drop with high mean viscosity ($\eta \gg 1$), where it is seen that both resistance functions saturate to that of a solid sphere $20\pi/3a^3$, which agrees with the expected result because the flow disturbances caused by the no-penetrability of the internal interface are negligible $O(\eta^{-1})$ to those that arise by the solid-like behavior of the internal fluid phases. Lastly, the stresslet function of a Janus drop in a rate-of-strain field of the form given by the basis $\boldsymbol{E}^{(3)}$ is identical to that of a single-phase drop: $Z^M = X^M = 2\pi/3a^3\,(4+10\eta)\,/(1+\eta)$, which is obvious in view of the arrangement of the principal axes of the rate-of-strain field. The principal axes of strain and compression act along the flat, internal interface such that the flows that develop both inside and outside the Janus drop match those of a single-phase drop. (Precisely, the principal axes of the rate-of-strain field act in the $x$–$y$ plane with respect to the set of coordinates centered on the Janus drop; if necessary, refer to figure 4–1 for further clarification). As in the case of a pure elongational flow, the presence of the internal interface does not perturb the natural circulation of the internal fluids, and therefore, the velocity fields of a Janus drop match those of a single-phase drop in this rate-of-strain field $\boldsymbol{E}^{(3)}$. It is relevant to point out that differences in the resistance functions ($X^M$ and $Y^M$) has important implication on the rheological properties of a dilute dispersion of Janus drops in linear shear flow. It will be demonstrated in the subsequent chapter that this leads to a difference in the normal components of the bulk stress, as opposed to Newtonian fluids that exhibit no differences in the normal components of the fluid stress in a linear shear flow. This completes the discussion of the resistance functions for a Janus drop of equal internal viscosities. From this point onward, the effect of the viscosity contrast on the resistance tensors is considered.

Following Happel and Brenner [20], the hydrodynamic center of reaction correspond to the position that the coupling tensor is symmetric. By making use of the

transformation law for the coupling tensor, followed by some elementary operations it is straightforward to show that the hydrodynamic center of reaction $\boldsymbol{x}^{cr}$ is located along the axis of symmetry of the Janus drop $\boldsymbol{d}$; it will be shown later that this has important implications on the dynamical behavior of a Janus drop in a general ambient flow.

The transformation law of the coupling tensor for a body of any shape is the following (in indicial notation) [20, 31]:

$$B_{ij} = B^O_{ij} - x^{cr}_k \epsilon_{kli} A_{lj}, \tag{4.19}$$

where $\boldsymbol{B}$ is the coupling tensor at the center of reaction, and $\boldsymbol{B}^O$ is the coupling tensor at any other point of reference; the translation tensor $\boldsymbol{A}$ stays constant regardless of the location in the body, in the same manner the translational velocity is unchanged from one point to another. For the coupling tensor to be symmetric at the center of reaction, the antisymmetric parts of the right hand side of the above equation must vanish identically. The above tensors are broken down here into symmetric and antisymmetric parts, respectively, for completeness of the presentation:

$$B_{ij} = \frac{1}{2}\left(B_{ij} + B_{ji}\right) + \frac{1}{2}\left(B_{ij} - B_{ji}\right), \tag{4.20}$$

$$x^{cr}_k \epsilon_{kli} A_{lj} = \frac{1}{2}\left(x^{cr}_k \epsilon_{kli} A_{lj} - x^{cr}_k \epsilon_{klj} A_{li}\right) + \frac{1}{2}\left(x^{cr}_k \epsilon_{kli} A_{lj} + x^{cr}_k \epsilon_{klj} A_{li}\right). \tag{4.21}$$

The requirement that $B_{ij} = B_{ji}$ implies that the antisymmetric components of $\boldsymbol{B}^O$ and $\boldsymbol{x}^{cr} \times \boldsymbol{A}$ must vanish identically:

$$\left(B^O_{ij} - B^O_{ji}\right) - \left(x^{cr}_k \epsilon_{kli} A_{lj} + x^{cr}_k \epsilon_{klj} A_{li}\right) = 0. \tag{4.22}$$

By rewriting the above resistance tensors in terms of $\boldsymbol{d}$, followed by the multiplication of the inverse of the translation tensor $\left(A^{-1}_{ni} = \left(X^A\right)^{-1} d_n d_i + \left(Y^A\right)^{-1}\left(\delta_{ni} - d_n d_i\right)\right)$ on both sides of the above equation, and some elementary operations one can demonstrate that the center of reaction is located along the axis of symmetry of the Janus

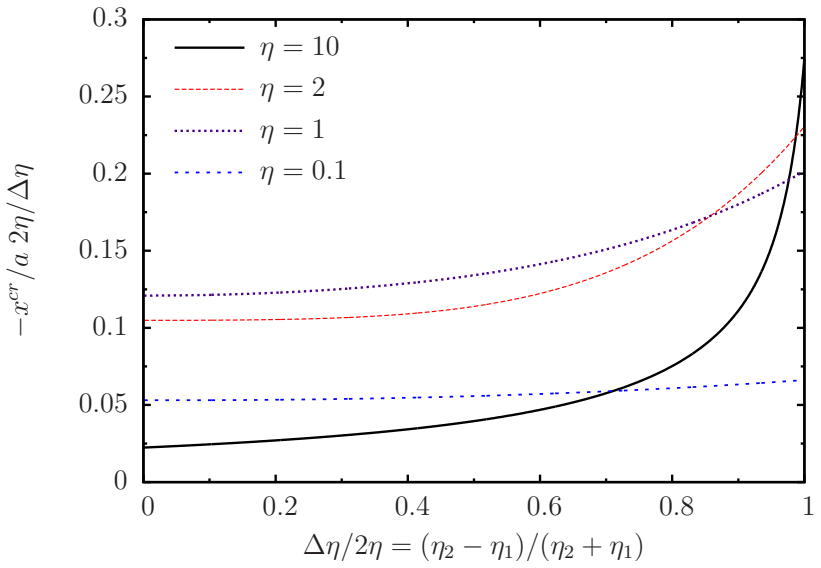


Figure 4–8: Variation of the hydrodynamic center of reaction $\boldsymbol{x}^{cr} = x^{cr}\boldsymbol{d}$ with the viscosity contrast $\Delta\eta/2\eta$ at constant values of the mean drop viscosity $\eta$.

drop: $x_k^{cr} = -\left(Y_O^B/Y^A\right) d_k$, where $Y_O^B$ is taken to be the coupling tensor at the center of the Janus drop, and its value can be readily determined from the results of Chapter 3. (To arrive at this result it is convenient to assume that $\boldsymbol{d} = \boldsymbol{e}_z$ without incurring in a loss of generality.) Figure 4–8 shows the location of the center of reaction $\boldsymbol{x}^{cr}$ with increasing values of the viscosity contrast $\Delta\eta/2\eta$ while maintaining constant the mean drop viscosity $\eta$. In order to improve visualization of the plots, $\boldsymbol{x}^{cr}$ has been scaled with $\Delta\eta/2\eta$; nonetheless, for zero viscosity contrast ($\eta_1 = \eta_2$) the center of reaction is located at the geometrical center of the Janus drop. The quadratic dependence of $\boldsymbol{x}^{cr}$ for small values of viscosity contrast ($\Delta\eta/2\eta \ll 1$) indicates that the center of reaction grows linearly with $\Delta\eta/2\eta$ (which may be the case for most Janus drops in experimental conditions since the internal viscosities are not too different in general [8, 114, 129]). The negative sign implies that the center of reaction is displaced towards the most viscous fluid that comprises the Janus drop, which is analogous to what one would expect for a solid of revolution that consists of an aggregate of spheres of unequal radii. For the aggregate of spheres, the center of

reaction approaches the larger sphere as the relative size of the pair increases [76]. In the case of a Janus 'slip–stick' sphere the hydrodynamic center of reaction coincides with the geometrical center of the particle and the coupling tensor is also zero [44].

It immediately follows from the finding that $\boldsymbol{x}^{cr} = -Y_O^B/Y^A\,\boldsymbol{d}$ that the coupling tensor vanishes identically at the hydrodynamic center of reaction ($\boldsymbol{B} = \boldsymbol{0}$), as shown below:

$$
\begin{aligned}
B_{ij} &= B_{ij}^O - x_k^{cr}\epsilon_{kli}A_{lj}, \\
&= Y_O^B\epsilon_{ijk}d_k - \left[x_k^{cr}\epsilon_{kli}\left(X^A d_l d_j + Y^A\left(\delta_{lj} - d_l d_j\right)\right]\right), \\
&= Y_O^B\epsilon_{ijk}d_k - \left[-\frac{Y_O^B}{Y^A}\,d_k\epsilon_{kli}\left(X^A d_l d_j + Y^A\left(\delta_{lj} - d_l d_j\right)\right)\right], \\
&= Y_O^B\epsilon_{ijk}d_k - \left(-Y_O^B d_k\epsilon_{kli}\delta_{lj}\right), \\
&= Y_O^B\left(\epsilon_{ijk} + \epsilon_{kji}\right)d_k, \\
&= Y_O^B\left(\epsilon_{ijk}d_k - \epsilon_{ijk}\right)d_k = 0,
\end{aligned}
$$

where it has been noted that terms that involve $d_k d_l \epsilon_{kli} = 0$ to arrive at the final result. Note that this finding holds regardless of the viscosity contrast $\Delta\eta/2\eta$ of the Janus drop because the analysis has been carried out without any reference to this quantity. A zero coupling tensor means there is no coupling of the force (torque) with the angular motions (translational motions) at the center of reaction $\boldsymbol{x}^{cr}$. The relevant implication of having a zero coupling tensor is that the hydrodynamic center of reaction and the 'free' center of rotation coincide with each other [31], and therefore, the study of the dynamics of a Janus drop can be carried out without the aid of the mobility tensors. (The grand mobility matrix is useful to determine the translational, rotational velocities, and the rate-of-strain field of the particle by knowing the applied force, torque, and stresslet; this is the exact opposite information to that conveyed by the grand resistance matrix.)

It is appropriate to show now that the shear-force tensor vanishes at the hydrodynamic center of reaction since the relevant information to achieve this has been presented. The objective is to demonstrate that $X^G = Y^G = 0$ when the flow stagnation point of the straining flow $\boldsymbol{u}^\infty = \boldsymbol{E}^\infty \cdot \boldsymbol{x}$ coincides with $\boldsymbol{x}^{cr}$. This simply means that translation of the stagnation point of the undisturbed flow to $\boldsymbol{x}^{cr}$ results in two elemental contributions:

$$\boldsymbol{u}^\infty = \boldsymbol{E}^\infty \cdot \boldsymbol{x} + \boldsymbol{U}^\infty, \tag{4.23}$$

where $\boldsymbol{U}^\infty = \boldsymbol{E}^\infty \cdot \boldsymbol{x}^{cr}$; the undisturbed flow now consists of the original rate-of-strain field plus and a uniform flow component due to the translation of the stagnation point. The net force $\boldsymbol{F}$ on the Janus drop is simply the sum of the two contributions:

$$F_i = \tilde{\eta}_0 G^O_{ijk} E^\infty_{kj} + \tilde{\eta}_0 A_{ij} E^\infty_{jk} x^{cr}_k, \tag{4.24}$$

where $G^O_{ijk}$ is the shear-force tensor at the center of the Janus drop. By following an analogous procedure to that used to show that the coupling tensor vanishes at $\boldsymbol{x}^{cr}$, one can find the following expression for the overall force in this special situation. The net force transversal to the axis of symmetry of the Janus drop is considered first for reasons that will become apparent soon:

$$F_i = \tilde{\eta}_0 \left[ Y^G_O \left( E^\infty_{ik} d_k - 2 d_i d_j d_k E^\infty_{kj} \right) - Y^B_O \left( E^\infty_{ik} d_k - d_i d_j d_k E^\infty_{kj} \right) \right], \tag{4.25}$$

where for the rate-of-strain field $\boldsymbol{E}^\infty = G/2\,(\boldsymbol{e}_1\boldsymbol{e}_3 + \boldsymbol{e}_3\boldsymbol{e}_1)$, it is easy to see that $d_i d_j d_k E^\infty_{kj} = G\,(d_1 d_3)\,d_i = 0$ because $d_1 = d_2 = 0, d_3 = 1$, and therefore, the net force on the Janus drop reduces to $F_i = \tilde{\eta}_0 \left( Y^G_O - Y^B_O \right) E^\infty_{ik} d_k$. To proceed further it is useful to recall that the net force on a Janus drop subject to the shear flow $\boldsymbol{v}_\perp$ is zero; from this finding the link between $Y^G_O$ and $Y^B_O$ can be established:

$$\boldsymbol{F}^O = \tilde{\eta}_0 Y^G_O E^\infty_{ik} d_k + Y^B_O \epsilon_{ijk} d_k = \frac{1}{2} G \tilde{\eta}_0 \left( Y^G_O - Y^B_O \right) \boldsymbol{e}_1, \tag{4.26}$$

where $\boldsymbol{F}^{O}$ is the force found at the center of the Janus drop for the shear flow $\boldsymbol{v}_{\perp}$ problem; the following equivalencies have been used to derive the final expression above $E^{\infty}_{ik}d_k = G/2$ and $\epsilon_{ijk}d_k\Omega^{\infty}_j = -G/2$. It is obvious that for the force on the Janus drop to vanish in the shear flow $Y^G_O = Y^B_O$. Otherwise, this would result in a contradiction to the evident symmetry arguments: that there can be no net force on a spherical Janus drop when the principal direction of the shear flow is normal to the internal interface regardless of the values of the viscosity contrast $\Delta\eta/2\eta$. This analysis demonstrates that there can be no forces transversal to the axis of symmetry of the Janus drop when the flow stagnation-point of a straining flow coincides with $\boldsymbol{x}^{cr}$. The equality $Y^G_O = Y^B_O$ implies that $Y^G = 0$, which is the resistance function that corresponds to the shear-force tensor at the hydrodynamic center of reaction. This result is in opposition to other bodies of revolution with broken fore and aft symmetry [75, 76], in which the shear-force tensor does not vanish at the hydrodynamic center of reaction. It is important to point out that even though the resistance tensors reported for the aggregate of spheres system have the analogous form to those presented here, the resistance tensors for that system exclusively adopt those forms at the hydrodynamic center of reaction. On the other hand, a symmetric body of revolution retains the same forms for the resistance tensors from point to point.

Here it is shown that the component of the net shear-force parallel to the axis of symmetry of the Janus drop also vanishes at $\boldsymbol{x}^{cr}$. The net force component of this force is given by:

$$F_i = \tilde{\eta}_0 X^G_O \left( d_i d_j d_k E^{\infty}_{kj} - \frac{1}{3} E^{\infty}_{ik} d_k \right) - \tilde{\eta}_0 Y^B_O \frac{X^A}{Y^A} d_i d_j d_k E^{\infty}_{jk}, \tag{4.27}$$

where the quantities $d_i d_j d_k E^{\infty}_{kj} = -G$ and $E^{\infty}_{ik} d_k = -G$ in a rate-of-strain field $\boldsymbol{E}^{\infty} = G\left(\boldsymbol{e}_1\boldsymbol{e}_1 - \boldsymbol{e}_3\boldsymbol{e}_3\right)$. Substitution of these values into the above equation and requiring the Janus drop to be force–free (i.e. $X^G = 0$) reveals the following constraint for

the resistance functions: $X_O^G = 3Y_O^B/2\left(X^A/Y^A\right)$. This relation has been verified by comparison of the values returned by the formula against those obtained numerically from Lamb's solution with reasonable agreement, provided that the precise location of the hydrodynamic center of reaction is in general a taxing calculation (comparison not shown in this dissertation). This concludes the demonstration that the shear-force vanishes identically at the hydrodynamic center of reaction. The underlying implication is that a 'freely' suspended Janus drop in a linear shear flow does not undergo the so-called "drift" velocity that bodies of revolution with broken fore and aft symmetry exhibit (e.g. the spherical cap and dumb-bell shaped solids). Perhaps, it is even more relevant to point out that this theoretical result is in qualitative agreement with the experimental observations of Torza & Mason [8], which reveal no indication of a Janus drop to undergo a "drift" velocity in a linear shear flow despite the deviations in the drop shape with respect to this simplified model. Although there is no strictly one-to-one correspondence with a Janus 'slip–stick' sphere, it is important to point out that the shear-force tensor also vanishes at the hydrodynamic center of reaction [44]. Note that 'slip–stick' sphere also categorizes as a body of revolution with geometrical symmetry that can exhibit hydrodynamic properties of solids that lack fore and aft symmetry; Therefore, it is natural to compare the behavior of a Janus drop against the 'slip–stick' sphere in a general ambient flow.

Another implication of a zero shear-force tensor $\left(X^G = Y^G = 0\right)$ is that the torque imposed by a rate-of-strain field remains constant regardless of the point chosen to calculate the first moment of the surface tractions. This follows by considering the translation of the shear-torque from one reference location to another:

$$\boldsymbol{T}(\boldsymbol{x}^{cr}) - \boldsymbol{T}(\boldsymbol{x}^{O}) = \left(\boldsymbol{x}^{O} - \boldsymbol{x}^{cr}\right) \times \oint_{S_p} \boldsymbol{n} \cdot \boldsymbol{\sigma} \, \mathrm{d}S_p, \tag{4.28}$$

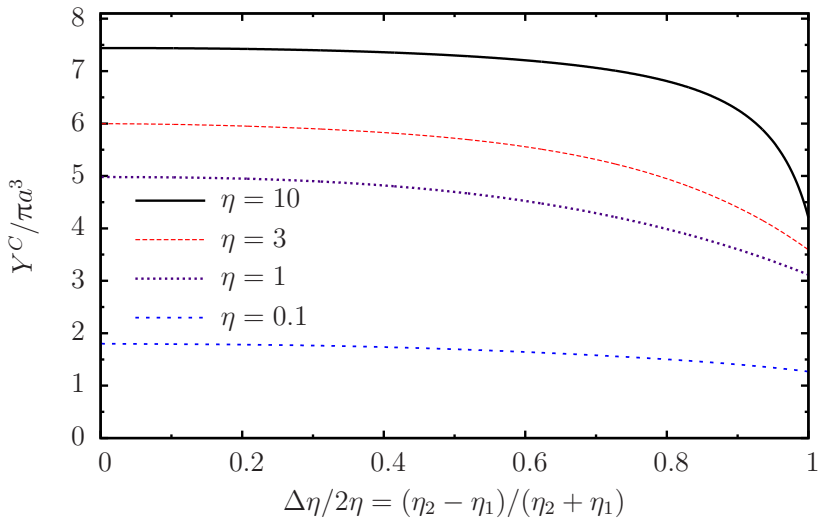


Figure 4–9: Dependence of the resistance to rotation transversal to the axis of symmetry of the Janus drop with the viscosity contrast $\Delta\eta/2\eta$ at constant values of the drop mean viscosity $\eta$.

where the surface integral of the stresses vanish identically because of the zero shear-force tensor to obtain $\boldsymbol{T}(\boldsymbol{x}^{cr}) = \boldsymbol{T}(\boldsymbol{x}^{O})$. Therefore, there is no need for a transformation law for the shear-torque in this case because the torque at $\boldsymbol{x}^{cr}$ is identical to the torque imparted by the rate-of-strain field at the geometrical center of the Janus drop. In fact, one can arrive at an analogous result for the stresslet, as above, to find that the stresslet remains constant regardless of the calculation reference (i.e. $\boldsymbol{S}(\boldsymbol{x}^{cr}) = \boldsymbol{S}(\boldsymbol{x}^{O})$). The only quantity that requires a transformation law is the rotation tensor in this problem (Happel & Brenner [20] provides the transformation law for this quantity): $\boldsymbol{C} = \boldsymbol{C}^{O} - \boldsymbol{x}^{cr} \times \boldsymbol{A} \times \boldsymbol{x}^{cr}$. This finalizes the analysis of the resistance tensors of the Janus drop. The reminder of this section is dedicated to the presentation of the effects of the viscosity contrast $\Delta\eta/2\eta$ on the resistance tensors.

The decreasing effect of the viscosity contrast on the rotation tensor is presented in figure 4–9. (The rotation tensor is reported with respect to the hydrodynamic center of resistance via the corresponding transformation law.) The plots partly

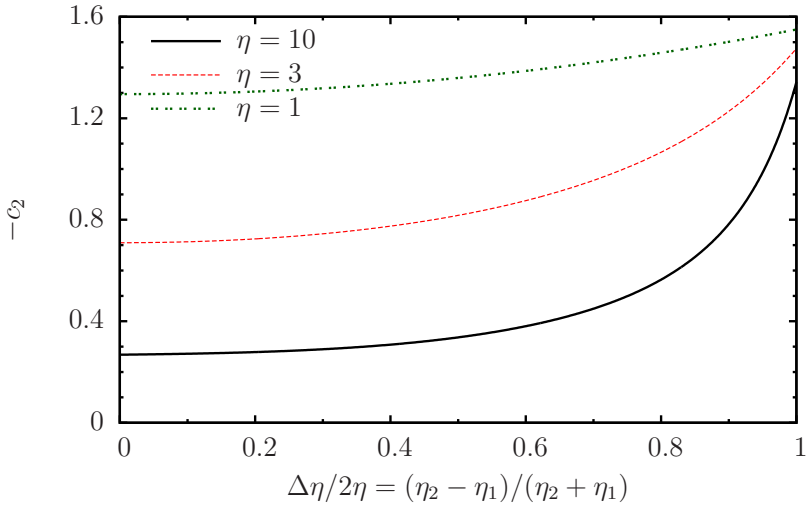


Figure 4–10: The dependence of the shear-torque resistance with the viscosity contrast and the mean drop viscosity $\eta$.

explain the decrease of the torque with increasing $\Delta\eta/2\eta$ found in a linear shear flow presented in Section 4.5.3. The observed trends are consistent with simple intuition; the overall resistance to rotation decreases as the difference in the internal viscosities grows. The possible explanation to this result is that there is a reduction of the surface tractions accountable to the generation of a couple on the Janus drop; note that the upper bound of the couple magnitude is determined by the less viscous hemisphere. The influence of the mean drop viscosity $\eta$ is to increase the rotation tensor until the solid sphere plateau is reached $\left(Y^C = 8\pi a^3\right)$.

Figure 4–10 illustrates the variation of the shear-torque with increasing viscosity contrast $\Delta\eta/2\eta$ at constant values of the mean drop viscosity. Again, the minus sign of the shear-torque indicates that the Janus drop offers a resistance to a linear shear flow analogous to that of an oblate spheroid of revolution. (The torque is greater when the principal direction of the shear flow is parallel to the axis of symmetry $\boldsymbol{d}$.) In contrast to other quantities considered so far, the shear-torque is seen to increase with the viscosity contrast. At first it may seem as a contradictory

result because the overall torque on a Janus drop in a linear shear flow decreases with the viscosity contrast $\Delta\eta/2\eta$; however, the main contributor to the observed torque in a linear shear flow is the solid-body motion of the ambient flow. The straining motion of the surrounding fluid produces a torque but at a lesser extent because the rate-of-strain is intrinsically an irrotational field. The phenomenon held accountable for the generation of a torque in a rate-of-strain field is expected to be quite different from its rotational counterpart. Presumably the shear-torque is a consequence of the velocity gradients that develop from the obstruction imposed by the no-penetrability property of the internal interface. Another interpretation that supports this argument is that disturbances associated by the presence of the internal interface give rise to a stresslet when the Janus drop rotates in a quiescent fluid. It is worth pointing out that the solid-body rotation of symmetric spheroidal particles also produce a stresslet under 'freely' suspended conditions in a linear ambient flow [31]. On the other hand, the solid-body rotation of an isotropic particle under 'freely' suspended conditions does not produce a stresslet in a linear ambient flow on account of the zero shear-torque tensor $\left(Y^H = 0\right)$.

The dependence of the stresslet resistance functions of axisymmetric $X^M$ and transversal $Y^M$ rate-of-strain fields with $\Delta\eta/2\eta$ are illustrated in figure 4–11. Note that the basis tensor $\boldsymbol{E}^{(1)}$ corresponds to an axisymmetric rate-of-strain field, and the basis tensors $\boldsymbol{E}^{(4)}$ and $\boldsymbol{E}^{(5)}$ define a rate-of-strain field transversal to the axis of symmetry $\boldsymbol{d}$ of the Janus drop. For the latter case the axis of strain is at a diagonal with respect to the internal interface of the Janus drop. In this case, it is clear that the circulation flows are completely different to those that develop in a single-phase drop on account of the no-penetrability property of the internal interface. In the limit of small viscosity contrast $(\Delta\eta/2\eta)$ the stresslet remains nearly constant to that found in a Janus drop with equal internal viscosities with a leading term of the order of $(\Delta\eta/2\eta)^2$; this explains the quadratic curvature of

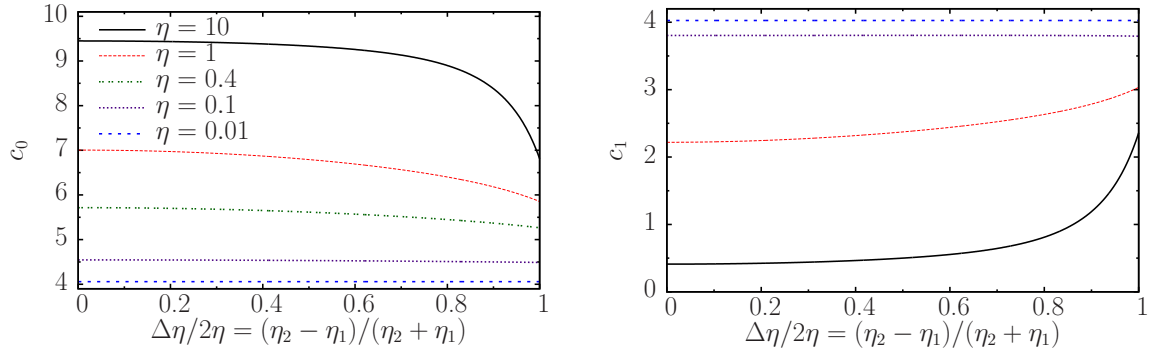


Figure 4–11: Variation of the stresslet resistance functions with the viscosity contrast $\Delta\eta/2\eta$ for selected values of the mean drop viscosity $\eta$. The resistance function $X^M$ is related to (axisymmetric) elongational flows, and $Y^M$ is associated to straining flow with principal axes at a diagonal with the axis of symmetry $\boldsymbol{d}$ of the Janus drop.

the stresslet functions as the viscosity contrast is increased. The reason why there is no linear dependence of the stresslet with the viscosity contrast is because the disturbance field $\boldsymbol{u}_D(\boldsymbol{x})$ in the small viscosity contrast limit ($\Delta\eta/2\eta \ll 1$) consists of a series of odd spherical harmonics; since the stresslet is a symmetric quantity the contribution of this disturbance field to the stresslet is zero. The observed reduction of the stresslet at greater values of $\Delta\eta/2\eta$ is attributable to the further loss of symmetry of the disturbance flows produced by the difference in the internal viscosities. Note that continuity of the fluid stresses at the internal interface dictates that the velocity gradients on the less viscous fluid must be greater than its more viscous counterpart $\boldsymbol{\nabla u}^{(1)} > \boldsymbol{\nabla u}^{(2)}$ such that there is an 'imbalance' in the overall stress at the outer surface of the Janus drop leading to the observed reduction in the stresslet since, once more, this is a symmetric quantity. This effect is, of course, less pronounce as the mean drop viscosity is decreased since this parameter imposes a restriction to how great the difference in the internal viscosities can be.

Table 4–1 provides numerical values of the resistance functions in the limit of a Janus drop of $\Delta\eta/2\eta \ll 1$, in view of the possibility to compare against experimental measurements of these quantities.

Table 4–1: Variation of the non-zero scalar resistance functions with the mean viscosity of the Janus drop (note that $Z^M = X^M$).

| $\eta$ | $X^A/2\pi a$ | $Y^A/2\pi a$ | $Y^C/\pi a^2$ | $-Y^H/\pi a^3$ | $3X^M/2\pi a^3$ | $3Y^M/2\pi a^3$ |
|---|---|---|---|---|---|---|
| 0 | 2.000 | 2.000 | 0.000 | 0.000 | 4.000 | 8.000 |
| 0.01 | 2.068 | 2.010 | 0.359 | 0.280 | 4.059 | 8.085 |
| 0.1 | 2.339 | 2.091 | 1.786 | 1.059 | 4.545 | 8.419 |
| 1.0 | 2.758 | 2.500 | 4.957 | 0.957 | 7.000 | 9.225 |
| 2.0 | 2.852 | 2.667 | 5.997 | 0.663 | 8.000 | 9.493 |
| 3.0 | 2.893 | 2.750 | 6.504 | 0.504 | 8.500 | 9.623 |
| 4.0 | 2.917 | 2.800 | 6.806 | 0.406 | 8.800 | 9.697 |
| 5.0 | 2.931 | 2.833 | 7.006 | 0.340 | 9.000 | 9.750 |
| 10.0 | 2.963 | 2.909 | 7.460 | 0.187 | 9.455 | 9.865 |
| 100.0 | 2.996 | 2.990 | 7.941 | 0.021 | 9.941 | 9.985 |
| $\infty$ | 3.000 | 3.000 | 8.000 | 0.000 | 10.000 | 10.000 |

## 4.7 Conclusions

The response (forces and couples) of a Janus drop to the shearing motion of the suspending fluid is investigated in the limit of small Reynolds number and capillary number (non-deformable interfaces). It is found that for an arbitrary drop orientation the shear flow can be broken down into flows with a velocity gradient parallel and normal to the internal interface, which greatly reduces the analysis to four elemental problems. Although an exact solution is found via Lamb's generalized solution, numerical evaluation of the series coefficients is needed to calculate the forces and couples.

Only when the velocity gradient of the shear flow is parallel to the internal interface the Janus drop behaves as a single-phase drop. For transversal shear flows the no-penetration condition at the internal interface prohibits the circulation flows of a single-phase drop, and therefore novel phenomena is found. The resultant couple on the Janus drop arises from both the straining and rotating motions of the external flow, in analogy with a spheroid of revolution. In this case the Janus drop exhibits an anisotropic resistance to the shear flow because of the variation of the the couple with the drop orientation.

The resistance matrix formulation reveals that the coupling tensor is identically zero at the center of hydrodynamic reaction $\boldsymbol{x}^{cr}$, and that the net force in a general straining flow is zero when the flow stagnation point coincides with $\boldsymbol{x}^{cr}$. One may deduce from the results of this investigation that a 'freely' suspended Janus drop in a shear flow undergoes a rigid body motion with a variable rotating speed while moving along the streamlines of the undisturbed flow.

It is interesting to note that Janus drops can exhibit cross-flow migration in a shear flow by means of an external force (e.g. gravity) in the streamwise direction that moves the drops with a speed that differs to the undisturbed velocity. Depending on the magnitude of the applied force and shearing rate, the Janus drop may exhibit a net migration or a periodic cross-streaming velocity in time. Net migration is expected to occur at small shearing rates with the migration velocity given by Equation (4.11). In the latter case the imposed force is not large enough to induce the net migration of the Janus drop in a shear flow such that its position transversal to the streamlines of the undisturbed flow is periodic in time. (This is further investigated in the next chapter.) The key observation is that cross-flow migration of a Janus drop can occur without the influence of walls and non-uniform velocity gradients, which are required to produce the cross-flow migration of a simple fluid drop. This final observation has relevant implications on the effective viscosity of a dispersion of Janus drops flowing in microfluidic settings by Poiseuille (pressure-driven) flows. If the drops are buoyant, the action of gravity forces parallel to the axis of the tube will tend to induce the lateral migration of the drops away from the centerline of the flow; this is plausible because this region is characterized by lower shear rates (gradients) than those near the wall. This, in turn, promotes the non-uniform distribution of drops lateral to the walls of the tube, in which most of them are expected to be concentrated midway between the tube axis and the wall.

Implying that the effective viscosity of the dispersion also depends on the spatial distribution of the Janus drops.

# CHAPTER 5
# DYNAMICS AND RHEOLOGY OF JANUS DROPS IN A STEADY SHEAR FLOW

## 5.1 Abstract

The behavior and rheological properties of a dispersion of Janus drops (or Janus emulsion) under a steady shear flow are explored in the infinite dilution limit. To achieve analytical progress, the Janus drops are assumed to consist of a pair of fluids bounded to hemispherical domains of equal radii. At 'freely' suspended conditions the Janus drops undergo periodic orbits in a shear flow that are intermediate to that of a solid sphere and a disk that depend on the viscosities of the internal fluids. Non-Newtonian behavior is found for this system on account of the anisotropic hydrodynamics of the Janus drops. The viscosity of the Janus emulsion that corresponds to the minimum energy of dissipation is analogous to that derived by Taylor (1932) Proc. R. Soc. A 138, 41–48 for a dispersion of simple drops. It is also found that an external force can induce the Janus drops to adopt a preferential orientation in a shear flow. Interestingly, a neutrally buoyant Janus drop with a displaced center of gravity can migrate lateral to the undisturbed shear flow; it is inferred that this phenomenon can lead to spatial-dependent rheology in pressure-driven flows.

## 5.2 Introduction

An understanding of the rheological properties of heterogeneous systems (e.g. colloids, emulsions, gels, foams) is of central relevance to emerging technologies, industrial and engineering applications. A classic example is the implementation of high performance damping mechanisms for racing cars by taking advantage of the rapid

increase of the viscous properties of magneto-rheological fluids upon application of a magnetic field [137]. It is also well-known that a myriad of consumer products, which are typically made up by colloidal dispersions and emulsions [1], have been generated as a result of the numerous experimental and theoretical studies that have elucidated their rich rheological properties.

For compound multiphase drops it is surprising that rheological studies appear to be lacking from both experimental and theoretical grounds despite their diverse number of applications. The high selectivity to mass transport of compound multiphase drops make them attractive for the micro-encapsulation of cells [2], drug-delivery and food processing applications [3], purification of water resources [4], micro-reactors [5], and single-cell analysis [6] to mention a few examples. Compound multiphase drops have also found important applications in the fabrication of particles with precisely engineered features [138], materials processing [120, 139, 140], self-propulsion at the microscopic scale [141], have served as a useful model to study the dynamics and rheological properties of blood cells [142, 143], among several other applications of engineering interest [7]. From both fundamental and technological viewpoints, it is of crucial interest to evaluate the impact on the rheological properties of the host fluid by the presence of the compound multiphase drops, since it is the rheology of the complex fluid that ultimately determines if it is suitable for its intended application.

Besides the theoretical studies conducted by Davis & Brenner [9] and Stone & Leal [10] that have considered the rheology of double emulsions—also known as globules or encapsulated drops—in linear flows, it seems that the rheological properties of compound multiphase drops with partial engulfment have not been addressed previously; possibly because of the added complexity of the drop shape to the calculation of the flow. Thus, the principal purpose of this study is to close the gap towards the determination of the rheology of partly engulfed multiphase drops in a

steady shear flow via the analysis of a simpler, yet representative member of this class—the Janus drop. The term Janus, which takes after the mythological god of two faces present in ancient Roman literature, highlights that the drop consists of two parts of equal geometry but of different properties.

Microfluidic techniques are quite popular for the fabrication of Janus drops because of the precise control one can attain over the size of the drops such that it is a feasible task to produce a dispersion of Janus drops (also known as a Janus emulsion) with a nearly uniform size distribution [103, 114, 144, 145]. Recently, Zarzar *et al.* [146] generated Janus drops with a diverse number of interesting features such as magnetic, light and pH-sensitive properties with the aid of reconfigurable emulsification techniques and microfluidics. The collection of these recent accomplishments open venues of opportunities to the use of Janus drops in multidiciplinary research and to the development of emulsions with adaptive rheological properties. Therefore, the study of the rheology of Janus drops is not limited to the description of the rheological properties of compound multiphase drops; there is also an inherent motivation to do so because of the promising applications of Janus drops. The creation of Janus drops with specialized properties is a rapidly growing field, and therefore it is of interest to attain an understanding on how these attributes can affect the rheology of Janus drops. This study aims to shed some light on how the geometry and fluid properties of Janus drops determine their behavior and rheology in a steady shear flow.

In general, it is insightful to have some knowledge of the flow at the microscopic level (individual particles or network structure) of complex fluids (colloidal dispersions, gels, emulsions, etc) to interpret the observed rheological behavior at the macroscopic scale. For compound multiphase drops, there has been considerable progress on the analytical treatment of axisymmetric flows in the limit of low-Reynolds-number flows [7, 113, 120–123, 142, 147]. Numerical studies have

principally addressed the problem of simulating large changes in shape and breakup of compound multiphase drops subject to external flows in confinement and open domains [148–152]. Typically changes in drop shape are considered as deviations from the initial equilibrium configuration in the absence of fluid motion. The theory to determine the drop shape at such static conditions was first introduced by Torza & Mason [8] that is founded on the minimization of the interfacial energy of the compound multiphase drop. The analysis of the formation of compound multiphase drops in microfluidic settings can be found in [153].

Particularly for Janus drops, Shardt *et al.* [124] performed numerical simulations to study the dynamics of 2D Janus drops in a linear shear flow. Analytical progress on the determination of the hydrodynamics of Janus drops in an ambient flow has been achieved recently in a series of articles. In the first part of the series [119], the dynamics of a Janus drop in a uniform flow was analyzed as a function of the drop orientation and viscosity, where it is found that the Janus drop displays an anisotropic hydrodynamic resistance to the flow similar to that of a solid-spheroid of revolution. The second part [154] addresses the problem of a Janus drop subject to an ambient fluid that undergoes a linear shear flow. In that study the description of the hydrodynamics of the Janus drop is completed via the calculation of the grand resistance matrix developed by Brenner [68]. Thus, these two studies provide the essential information to analyze, from a theoretical point of view, the rheological properties (zero-shear viscosity and differences in the normal stresses) of a Janus emulsion in the special limit the drops do not "see" each other. In other words, the macroscopic behavior of the Janus emulsion is determined by the dynamics of the individual drops—in spirit this is analogous to the behavior of an ideal gas.

In this investigation the rheology of Janus drops are probed under a steady shear flow and at infinite dilution conditions. The analysis is realized within the limit of no deflections to fluid–fluid interfaces because it is aniticipated that such effects will

only bring small departures (of the order of the capillary number) from Newtonian behavior, as in the case of single-phase drops [46]. For this system, nonetheless, the anisotropic hydrodynamics of the Janus drops are found to produce significant non-Newtonian effects via differences in the normal stresses. Additionally, since the typical length scales of Janus drops in experiments are well above the sub-micron scale, stochastic effects associated to Brownian motion are entirely neglected in this study. The article is organized as follows. A model description is presented in Section 5.3. The preferential orientation of a Janus drop 'trapped' in a linear shear flow is studied in Section 5.3. The dynamics of a 'freely' suspended Janus drop is considered in Section 5.4, in which it is found that the Janus drop exhibits Jeffery-like orbits intermediate to that of a solid-sphere and a disk. The analysis of the cross-flow migration of a Janus drop in a linear shear flow is carried out in Section 5.5. From the results of this phenomenon it is inferred that a dispersion of multiphase drops in a Poiseuille flow (pressure-driven flow) can exhibit a non-uniform spatial distribution, and thus, spatially-dependent rheology. The article concludes in Section 5.6 with the calculation of the zero-shear viscosity of a dilute Janus emulsion subject to a linear shear flow. Interestingly, it is found that the zero-shear viscosity that corresponds to the minimum energy of viscous dissipation has an analogous form to that derived by Taylor [11] for a dispersion single-phase drops, but with the difference that the drop viscosity is equal to the mean viscosity of the pair of fluids that comprise the Janus drop. In contrast to the rheology of double emulsions [10], non-Newtonian behavior is found in the non-deformable limit on account of the anisotropic hydrodynamics of the Janus drops.

## 5.3 Model description

The simple model presented here for Janus drops is expected to be useful to attain some understanding on the dynamics and rheology of multiphase drops subjected to simple shear flows. A generalized schematic that depicts the principal

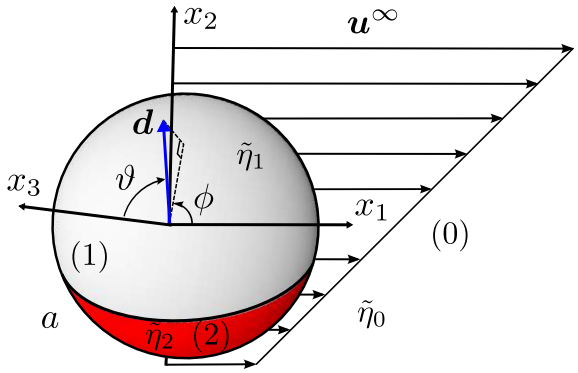


Figure 5–1: Unidirectional shear flow $\tilde{u}_1^\infty$ ($\tilde{u}_2^\infty = \tilde{u}_3^\infty = 0$) past a 'perfect' Janus drop of radius $a$. The fluids that constitute the Janus drop are confined to equally sized hemispheres. The symbol $(j)$ denotes the corresponding fluid phase of dynamic viscosity $\tilde{\eta}_j$ ($j = 0, 1, 2$). The unit vector $\boldsymbol{d}$ denotes the direction of the axis of symmetry of the Janus drop, and it is defined with respect to a set of right-handed Cartesian axes fixed in space $(x_1, x_2, x_3)$. The components of this vector are related to the azimuthal $\vartheta$ and polar $\phi$ angles of a spherical coordinate system in the traditional manner.

features shared in common by the problems considered in this study is provided in figure 5–1. The sketch shows a 'perfect' Janus drop of radius $a$ immersed in a viscous ambient fluid '0' that executes a simple shear flow of non-zero mean velocity (uniform shear plus a streaming flow). The undisturbed velocity $\tilde{\boldsymbol{u}}^\infty$ is expressed in dimensional quantities and presented in index notation:

$$\tilde{u}_1^\infty = G\tilde{x}_2 + U^\infty, \tag{5.1}$$

where $G$ is the applied shear rate, $U^\infty$ is the mean velocity of the undisturbed flow, and $\tilde{\boldsymbol{x}}$ is the position vector. The notation to use a tilde on top of field variables (i.e. position, velocity, stress, etc) and fluid properties (density and viscosity) is followed throughout this document to distinguish between their dimensional and non-dimensional form. The orientation of the Janus drop is given by the unit vector $\boldsymbol{d}$ (defined with respect to the space-fixed axes) that is conventionally assumed to point towards the less viscous internal fluid ($\tilde{\eta}_1 \leq \tilde{\eta}_2$); this axis of symmetry is conveniently used to characterize the drop orientation relative to the direction of the undisturbed flow.

The following assumptions pertain to this work: (*i*) The pair of fluids '1' and '2' that comprise the Janus drop are bounded to equal hemispherical domains such that a flat interface separates them. (*ii*) All fluids phases ($j = 0, 1, 2$) are immiscible, incompressible, and Newtonian (shear independent viscosity). (*iii*) The fluid–fluid interfaces are considered non-deformable and clean of surfactant agents. (*iv*) Fluid motion occurs without the influence of inertia effects. It suffices to point out that for the Janus drop to approach the 'perfect' shape (spherical with a flat internal interface), the interfacial tension of the each internal fluid with the ambient has to be much larger than the interfacial tension with its counterpart (i.e. $\tilde{\gamma}_{10}, \tilde{\gamma}_{20} \gg \tilde{\gamma}_{12}$). The conditions to have nearly 'perfect' Janus drops have been reported in great detail by others [114, 119, 129] and therefore, it is not necessary to reproduce that information here. A complete theory for the determination of the shape and configuration of compound multiphase drops in the absence of fluid flows is provided by Torza & Mason [8]. For the remaining kinematical assumptions to hold valid, one only requires the capillary, $Ca = \tilde{\eta}_0 aG/\tilde{\gamma}_{12}$, and Reynolds number, $Re = \tilde{\rho}_0 a^2 G/\tilde{\eta}_0$, to be small, $\tilde{\eta}_0$ is the dynamic viscosity and $\tilde{\rho}_0$ is the density of the ambient fluid, and $\tilde{\gamma}_{12}$ is the interfacial tension of the internal fluids. This can be realized effortlessly in practice by application of a sufficiently small shear rate. Particularly, Torza & Mason [8] carried out experimental observations of the dynamics of a Janus-like compound drop in a shear flow at reasonably small shear rates (around $0.1\, s^{-1}$) to produce a low-Reynolds-number flow ($Re \sim 10^{-6}$) constrained to a small capillary number in the order of magnitude of $10^{-1}$.

The characteristic scales for length, fluid velocity and stresses are taken to be: $a$, $Ga$, $\tilde{\eta}_0 G$, respectively. The viscosity of the internal fluids is non-dimensionalized by the ambient viscosity $\eta_{1,2} = \tilde{\eta}_{1,2}/\tilde{\eta}_0$. Parameterization of the viscous properties of the Janus drop is conveniently realized via the mean drop viscosity $\eta = (\eta_1 + \eta_2)/2$

and viscosity contrast $\Delta\eta/2\eta = (\eta_2 - \eta_1) / (\eta_2 + \eta_1)$. It is clear that when the viscosity contrast is zero the Janus drop comprises fluids of equal viscosities ($\eta_1 = \eta_2 = \eta$) such that the viscous properties are solely determined by the single parameter $\eta$. For non-zero $\Delta\eta/2\eta$ some interesting features of the Janus drop are found. One of such traits is considered in the next section, in which the conditions a Janus drop can adopt a preferential orientation in a simple shear flow are explored. An important application of this behavior is proposed in Section 5.6 to investigate the rheological properties of a dispersion of Janus drops. Since the dynamics of the Janus drops must be known to study the rheology of this system, the analysis is incorporated in this work for completeness (Section 5.4). In this section the steady orientation of a Janus drop (deterministic behavior) in a simple shear flow is investigated. For the Janus drop to adopt a preferential orientation a hydrodynamic coupling must exist; to this end, an external force $\boldsymbol{F}^e$ must act at any location other than the hydrodynamic center of reaction $\boldsymbol{x}_{cr}$. For calculation purposes, it is assumed that the force passes through the geometrical center of the Janus drop. In general, this ensures that the center of reaction does not coincide with the geometrical center when the Janus drop is made up by fluids of different viscosities. It is also assumed that the force maintains the geometrical center of the Janus drop at a coincident arrangement to the centerline of the shear flow. The source of the external force is left unspecified since it is immaterial for the purposes of carrying out the analysis; however, this may be achieved in practice by means of gravity or optical traps. (There is a fair number of studies that have relied on optical trapping to maintain drops fixed in space in the presence of external flows; the interested reader is referred to Summers *et al.* [155] and the references therein.) Note that the sole purpose of $\boldsymbol{F}^e$ is to fix the location of the Janus drop in space; it only has an indirect influence over the preferential orientation adopted by the Janus drop in a simple shear flow. Depending on the shear to mean velocity $Ga/U^\infty$, the mean drop viscosity $\eta$ and

contrast $\Delta\eta/2\eta$, the Janus drop can exhibit a preferential orientation in a simple shear flow due to its lack of fore and aft symmetry (which is purely hydrodynamic in nature because the drop conforms to a spherical shape). The relevant point here is that the Janus drop experiences a torque from both the shearing and streaming motions of the ambient fluid that can balance each other at an appropriate shear to mean velocity ratio $Ga/U^{\infty}$. Note that even in the limit of small values of viscosity contrast ($\Delta\eta/2\eta \ll 1$), there is a shear to mean velocity ratio $Ga/U^{\infty}$ that can be found such that the net torque on the Janus drop vanishes at some orientation $\boldsymbol{d}$. In practice one would observe that the Janus drop rotates until the drop adopts a preferential orientation, which is nothing more than a consequence of the balance of the torques. Nevertheless, it is important to note that $\boldsymbol{d}$ must initially lie in the plane of the shear gradient of the undisturbed flow $x_1$–$x_2$ plane (or equivalently $\vartheta = \pi/2$) for this to occur; otherwise, there are additional torques along the $x_1$ and $x_2$–axes that cannot be balanced by the streaming velocity for evident reasons such that a preferential orientation cannot occur. A simple approach to overcome this arrangement issue is to fabricate a neutrally buoyant Janus drop with an eccentric center of gravity; the Janus drop will tend to position $\boldsymbol{d}$ in the plane of shear if gravity is also in the plane of shear. (However, one would need to account for the gravitational torque on the final orientation of the Janus drop.) An advantage of this setup is that the drop orientation can be characterized exclusively by the polar angle $\phi$.

The analysis presented here entirely neglects the dynamics of rotation of the Janus drop prior to reaching its steady orientation, since it is obvious that the preferential orientation is independent of such initial conditions, as in the case of spheroidal particles in an extensional flow, which consistently become aligned with one of the principal axes regardless of the initial positioning [84]. This allows for a simple analysis to the problem by seeking an orientation $\boldsymbol{d}$ that is torque–free. The

procedure to determine the torque and force on the Janus drop follows the classic direct approach of integrating the fluid stress at the outer surface of the drop. The constitutive equation of a Newtonian fluid is used to calculate the stress from the velocity field of the ambient fluid, which is coupled to the motion of the internal fluid phases of the Janus drop via the so-called Stokes equations. Variation of the undisturbed flow with the drop orientation $\boldsymbol{d}$ is taken into account by projecting the laboratory frame-based flow into a set of axes affixed to the Janus drop via a transformation matrix. Without further preliminary remarks, the Stokes equations are presented (in non-dimensional form) for each fluid phase with respect to a spherical coordinate system $(r, \vartheta, \phi)$ that takes advantage of the geometry of the Janus drop:

$$\boldsymbol{\nabla} \cdot \boldsymbol{u}^{(j)} = 0, \quad -\boldsymbol{\nabla} p^{(j)} + \eta_j \nabla^2 \boldsymbol{u}^{(j)} = 0, \tag{5.2a}$$

$$\boldsymbol{n} \cdot \boldsymbol{u}^{(j)} = 0, \ [\boldsymbol{u}] = [\boldsymbol{n} \cdot \boldsymbol{\sigma}] = \boldsymbol{0}, \ \text{at } r = 1, \tag{5.2b}$$

$$\boldsymbol{n} \cdot \boldsymbol{u}^{(1,2)} = 0, \ [\boldsymbol{u}] = [\boldsymbol{n} \cdot \boldsymbol{\sigma}] = \boldsymbol{0}, \ \text{at } \vartheta = \pi/2, \tag{5.2c}$$

$$\boldsymbol{u}^{(0)} = \boldsymbol{u}_\infty \text{ as } r \to \infty, \tag{5.2d}$$

where $\boldsymbol{n}$ is the unit normal vector at fluid–fluid interfaces, where at the outer drop surface it is directed outward, and at the internal interface it points from fluid '2' to fluid '1'. The quantities $\boldsymbol{u}^{(j)}$ and $p^{(j)}$ designate the respective velocity and pressure fields of the *jth* fluid phase. The stress tensor is that of a Newtonian fluid (in index notation): $\sigma_{lk}^{(j)} = -p^{(j)}\,\delta_{lk} + \eta_j \left( \nabla_l\, u_k^{(j)} + \nabla_k\, u_l^{(j)} \right)$, where $\delta_{lk}$ is the identity tensor. At interfaces the normal component of the fluid velocity is zero ($u_n = 0$) because of the immiscibility of the fluids (no mixing of the fluid phases). The brackets designate a jump of the enclosed quantity at interfaces. At the outer surface ($r = 1$) the jump is directed from the internal to the ambient fluid, and at the internal interface ($\vartheta = \pi/2$) it is directed from the inner fluid '2' to fluid '1'. At distances far from the Janus drop ($r \to \infty$) the flow reduces to the undisturbed velocity $\boldsymbol{u}_\infty$ projected to the set of axes of local to the Janus drop.

Integration of the surface tractions at the outer drop surface ($r = 1$) yields the hydrodynamic force $\boldsymbol{F}$ on the Janus drop:

$$\boldsymbol{F} = \oint_{S_d} \boldsymbol{n} \cdot \boldsymbol{\sigma} \, \mathrm{d}S_d, \tag{5.3}$$

where $S_d$ is the area of the outer drop surface. The torque $\boldsymbol{T}$ is given by the first moment of the surface tractions:

$$\boldsymbol{T} = \oint_{S_d} \boldsymbol{x} \times (\boldsymbol{n} \cdot \boldsymbol{\sigma}) \, \mathrm{d}S_d. \tag{5.4}$$

Prior to the presentation of results, it is instructive to consider the preferential orientation of the Janus drop in the absence of the shearing motion of the ambient fluid. In such a situation the imposed flow reduces to a uniform flow along the direction of the $x_1$–axis: $\tilde{\boldsymbol{u}}^{\infty} = U^{\infty} \boldsymbol{e}_1$. It is important to recall that there is an external force $\boldsymbol{F^e}$ that prevents the Janus drop from undergoing translational motion, and that there are no restrictions on its rotation. For the purposes of providing physical arguments it is sufficient to bring to the discussion the main findings of the behavior of the Janus drop with different internal viscosities in a uniform streaming flow; the technicalities of this problem has been reported by Shklyaev *et al.* [119]. Now consider the symmetry axis of the Janus drop $\boldsymbol{d}$ to lie in the $x_1$–$x_2$ plane at an arbitrary direction with respect to the undisturbed flow given by the polar angle $\phi$. From the perspective of an observer the Janus drop rotates (due to the coupling of $U^{\infty}$ with the torque) until $\boldsymbol{d}$ becomes aligned with the $x_1$–axis. This turns out to be a configuration where the flow is axisymmetric everywhere, and consequently, torque–free regardless of the internal viscosities of the Janus drop. Note that this is true for any body of revolution with broken fore and aft symmetry; classic examples are the spherical cap [75] and the aggregate of unequally sized spheres [76]. Therefore, it is expected that the axis of symmetry of the Janus drop will be nearly

aligned with the $x_1$–axis in the limiting case of small shear to mean velocity ratio ($Ga/U^\infty \ll 1$). It is important to point out that these arguments only apply to a Janus drop of unequal internal viscosities; in the ideal situation of $\eta_1 = \eta_2$, the Janus drop behaves as a symmetric spheroid of revolution with no tendency to rotate in a streaming flow $\boldsymbol{U}^\infty$ such that there is no preferential orientation; the Janus drop will retain its initial arrangement with respect to the streaming flow. It follows from this observation that there must be a hydrodynamic coupling of the torque $\boldsymbol{T}$ with the streaming velocity $\boldsymbol{U}^\infty$ for the Janus drop to adopt a steady orientation in a simple shear flow.

Figure 5–2*a* shows the preferential orientation of a Janus drop of mean viscosity $\eta = 1$ via the polar angle $\phi$ with increasing $Ga/U^\infty$ while keeping constant the viscosity contrast $\Delta\eta/2\eta$. For small ratios of the shear to mean velocity ($Ga/U^\infty \ll 1$) the preferential orientation $\phi$ grows linearly with $Ga/U^\infty$, in agreement with the above arguments for vanishing shearing rates. It is seen that the Janus drop tends to align its axis of symmetry in the direction of the velocity gradient of the undisturbed flow ($x_2$–axis) for all values of the viscosity contrast $\Delta\eta/2\eta$ as $Ga/U^\infty$ is increased. In this arrangement the torque imparted by the streaming flow (which opposes that of the shear) reaches a maximum value. This becomes apparent by noting that the uniform flow can be broken down into transversal and axisymmetric components about $\boldsymbol{d}$, and that only the transversal component opposes the torque exerted by the shearing motion of the ambient fluid. Beyond this point, further increase of $Ga/U^\infty$ results in a situation where the torque exerted by the shear is greater than that of the uniform flow, such that a preferential orientation cannot occur; the Janus drop simply rotates indefinitely with a periodic speed.

The dependence of the preferential orientation of the Janus drop with $Ga/U^\infty$ and the mean drop viscosity $\eta$ at a fixed viscosity contrast $\Delta\eta/2\eta = 0.4$ is presented in figure 5–2*b*. It is readily seen that there is a non-monotonic dependence of the

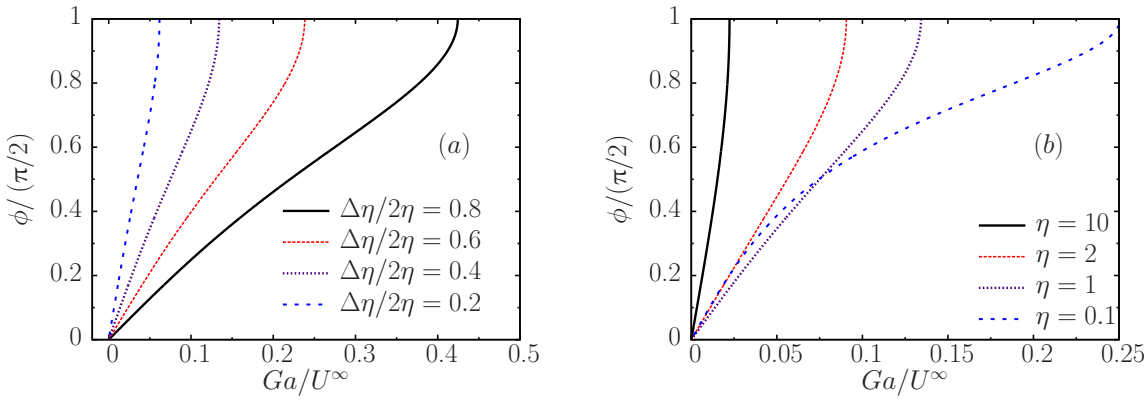


Figure 5–2: (Colors online) Influence of the shear to mean velocity ratio $Ga/U^\infty$ on the preferential orientation of a Janus drop of $(a)$ constant mean viscosity $\eta = 1$ with selected values of $\Delta\eta/2\eta$, and $(b)$ constant $\Delta\eta/2\eta = 0.4$ with selected values of $\eta$.

preferential orientation with the mean drop viscosity. Interestingly, a Janus drop of relatively low mean viscosity ($\eta = 0.1$) reaches a transversal arrangement of $\boldsymbol{d}$ relative to the direction of the undisturbed flow ($\phi = \pi/2$) at higher shearing rates $Ga/U^\infty$ in comparison with more viscous drops. An explanation to this behavior is that the shear flow becomes less effective on generating a torque than the streaming flow in the low viscosity limit. For Janus drops of greater viscosity the torque exerted by the shearing motion of the ambient is substantial in comparison to that imparted by the streaming counterpart, and therefore, the shear to mean velocity $Ga/U^\infty$ required to arrange the Janus drop into a particular orientation is less.

It is important to point out that without some trapping mechanism it may prove to be difficult to maintain fixed the position of the Janus drop in space. Note that in general the net hydrodynamic force on the Janus drop is not necessarily parallel to the flow because of the anisotropic resistance of the drop [119]. Nonetheless, if the axis of symmetry of the Janus drop $\boldsymbol{d}$ is aligned with the $x_2$–axis the net hydrodynamic force on the Janus drop acts parallel to the direction of the flow ($x_1$–axis), and therefore, a simple body force (such as gravity) may be used to balance the hydrodynamic forces on the Janus drop. The results that follow correspond to this particular situation.

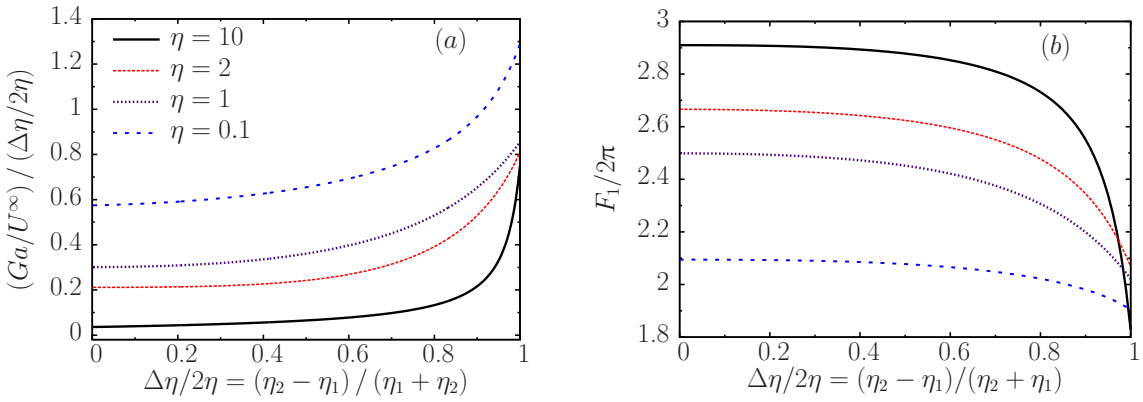


Figure 5–3: (Colors online) The effect of increasing viscosity contrast $\Delta\eta/2\eta$ at fixed values of the mean drop viscosity $\eta$ on ($a$) the shear to mean velocity $Ga/U^\infty$ and ($b$) the net hydrodynamic force $F_1$ (in units of $\tilde{\eta}_0 a U^\infty$).

Figure 5–3$a$ illustrates the dependence of $Ga/U^\infty$ on $\Delta\eta/2\eta$ for constant values of the mean drop viscosity $\eta$. In order to improve the presentation of results $Ga/U^\infty$ is scaled with $\Delta\eta/2\eta$. Note that the flat curvature for small $\Delta\eta/2\eta$ suggests a linear dependence of the shear to mean velocity $Ga/U^\infty$ with the viscosity contrast. The apparent monotonic dependence of $Ga/U^\infty$ with the mean drop viscosity is a consequence of the shear-torque decreasing more rapidly with $\eta$ than the torque imposed by the uniform flow.

The influence of $\Delta\eta/2\eta$ on the net hydrodynamic force $F_1$ (in units of $\tilde{\eta}_0 a U^\infty$) is shown in figure 5–3$b$ for selected values of the mean drop viscosity $\eta$. It is seen that the net force is nearly independent of the viscosity contrast in the limit of small viscosity contrast ($\Delta\eta/2\eta \ll 1$); in fact, the force on the Janus drop is equal to that on a single-phase drop $\tilde{F}_1 = 2\pi\,(2+3\eta)\,/(1+\eta)\,\tilde{\eta}_0 a U^\infty$. This can be understood from a unification of the results found in [119] and [154]; basically, the force imparted by the shearing motion of the ambient is $O(\Delta\eta/2\eta)$; whereas, the force contribution by the streaming motion of the ambient flow predominates because it is $O(1)$. A marked decrease on the force is not seen until both $\Delta\eta/2\eta \to 1$ and $\eta \gg 1$; however, its application may be limited to exceptional situations in practice, as in [145] because one of the internal phases is significantly more viscous than

its counterpart. Note that in general the viscosities of the internal fluid phases are quite similar (for instance see [129, 146]); therefore, it is anticipated that most of the behavior of Janus drops in experiments can be understood from the theory at small viscosity contrast ($\Delta\eta/2\eta \ll 1$). The predicted reduction of the net hydrodynamic force arises because the shear-force acts opposite to the direction of the imposed shear flow.

### 5.4 Dynamics of a 'freely' suspended Janus drop in a linear shear flow

The dynamics (position and orientation in space-time) of a 'freely' suspended Janus drop in a linear shear flow of a Newtonian fluid is investigated with respect to the fixed reference frame $(x_1, x_2, x_3)$. The main steps to arrive at the equations that govern the dynamics of the Janus drop are presented here since these will prove to be useful when studying the cross-streaming velocity of the Janus drop in the next section. On account of the linearity property of Stokes flow, the dynamics of a Janus drop in a general ambient flow are determined by an exact balance of the net hydrodynamic force and torque on a stationary Janus drop in the imposed flow with those on a Janus drop undergoing solid-body motions in a quiescent fluid. It is important to point out that the torque and rotational motion of the Janus drop vary from one reference point to another, as for any other body of revolution; nevertheless, it is obvious that the dynamical behavior must be independent of the reference point taken. For convenience, the free center of rotation $\boldsymbol{x}_{cr}$ is chosen to carry out the present analysis since it turns out that drop translation and rotation are decoupled due to the zero coupling tensor at that location [154]. (Implying that the hydrodynamic center of reaction and free center of rotation are identical). Therefore, it follows that the dynamics of the Janus drop in a linear shear flow is analogous to that of a symmetric spheroid of revolution with an apparent aspect ratio $r_h$ that depends on the internal viscosities of the Janus drop. In similarity with a symmetric spheroid of revolution, the Janus drop translates with the velocity of the undisturbed flow

at the center of free rotation. The equation that describes the rotational dynamics of the Janus drop can be readily derived from the resultant torque $\boldsymbol{T}$ on the Janus drop (presented in non-dimensional form and in index notation):

$$T_k = \left[X^C d_k d_l + Y^C \left(\delta_{kl} - d_k d_l\right)\right] \left(\Omega_l^\infty - \omega_l\right) \\ -Y^H \epsilon_{kln}\, d_n d_m E_{ml}^\infty = 0, \tag{5.5}$$

where $\Omega_l^\infty$ is the rotational velocity of the ambient fluid, $\omega_l$ is the rotational velocity of the Janus drop, $E_{ml}^\infty$ is the undisturbed rate-of-strain tensor, $\epsilon_{kln}$ is the permutation tensor, $X^C$ is the resistance of the Janus drop to undergo rotation about its axis of symmetry, $Y^C$ is the resistance of the Janus drop to rotation transversal to its axis of symmetry, and $Y^H$ defines the shear-torque imposed by the rate-of-strain field. Notably, $X^C$ is inherently zero in contrast to other bodies of revolution because the Janus drop behaves as a single-phase drop in this case [154]. The values of the resistance functions can be found in the cited article. The transcendental equation for the orientation dynamics of the Janus drop can be derived by operating the cross product on both sides of the above equation with the unit vector $d_j$, followed by the use of the well-known identity $\epsilon_{kln}\epsilon_{kji} = (\delta_{lj}\delta_{ni} - \delta_{li}\delta_{nj})$ [13] to arrive at the sought expression, which is identical to that of a spheroidal particle [31]:

$$\dot{d}_i = \omega_l d_j \epsilon_{lji} = \Omega_l^\infty d_j \epsilon_{lji} + B\Big[E_{im}^\infty d_m - E_{jm}^\infty d_m d_j\, d_i\Big], \tag{5.6}$$

where here the dot symbol on top of a variable denotes its differentiation with respect to time, and $B = Y^H/Y^C$ is commonly referred to as the Bretherton constant of the equivalent spheroid [156]. It is important to point out that this result is in accordance with the experimental observations of Torza & Mason [8] of a freely rotating Janus-like compound drop in a linear shear flow. The time evolution of the axis of symmetry $\boldsymbol{d}$ of the partly engulfed drop closely follows the rotation dynamics of a 'freely' suspended spheroid of revolution in a linear shear flow. Another aspect

of their observations relevant to this work is that the compound drop behaves as a symmetric spheroid of revolution despite being comprised by fluids of different viscosities, which supports the theory that dictates that the Janus drop rotates at the free center of rotation $\boldsymbol{x}_{cr}$ in a decoupled manner. A final remark that deserves attention is that interfacial deflections only brought small quantitative changes to the dynamics of the compound drop; this establishes experimental confirmation that the essence of the dynamics of compound drops can be understood without consideration of interfacial deflections at low capillary numbers.

Following Kim & Karrila [31], one can express the components of $\boldsymbol{d}$ with respect to the azimuthal $\vartheta$ and polar $\phi$ angles (which are related to the set of space-fixed axes $(x_1, x_2, x_3)$ in the traditional manner); then, after some elementary operations one obtains the following system of differential equations that characterize the orientation vector $\boldsymbol{d}$ in space-time (shown in non-dimensional form):

$$\dot{\vartheta} = \frac{1}{4}\left(\frac{r_h^2 - 1}{r_h^2 + 1}\right)\sin 2\vartheta \sin 2\phi, \tag{5.7}$$

$$\dot{\phi} = -\frac{1}{r_h^2 + 1}\left(r_h^2 \sin^2\phi + \cos^2\phi\right). \tag{5.8}$$

For convenience the Bretherton constant has been expressed with respect to the apparent hydrodynamic aspect ratio $r_h$ via the archetypal relation $B = (r_h^2 - 1)\,/\,(r_h^2 + 1)$. The solution to the system of differential equations was first presented by Jeffery [89] for a spheroidal particle with its axis of revolution initially placed in the $x_1$–$x_3$ plane ($\phi(t = 0) = 0$):

$$\tan\vartheta = \frac{C}{\left(r_h^2 \sin^2\phi + \cos^2\phi\right)^{\frac{1}{2}}}, \tag{5.9}$$

$$\tan\phi = r_h^{-1} \tan\left(\frac{Gt}{r_h + r_h^{-1}}\right), \tag{5.10}$$

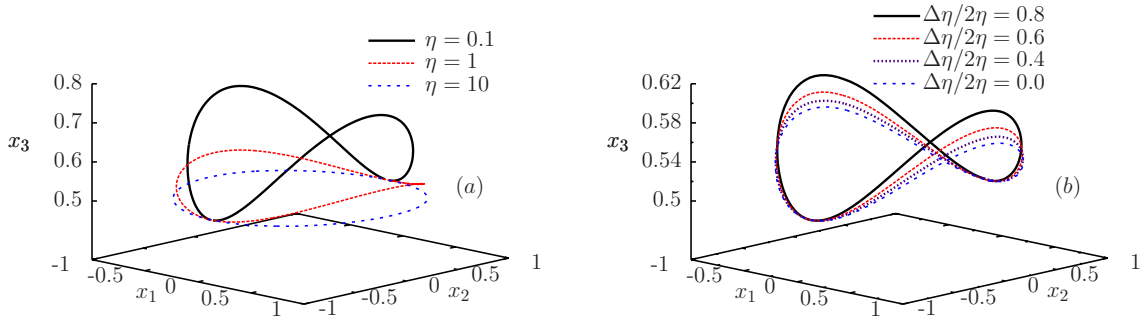


Figure 5–4: (Colors online) $(a)$ Dependence of period orbits with the mean drop viscosity of a Janus drop with equal internal viscosities $\eta_1 = \eta_2$. $(b)$ The effect of the viscosity contrast $\Delta\eta/2\eta$ on the periodic orbits for a constant mean drop viscosity $\eta = 1$.

which describes closed orbits in space-time of period $\tilde{\tau} = 2\pi G^{-1}\left(r_h + r_h^{-1}\right)$. The constant $C$ is known as the orbital constant [31] that parametrizes the initial orientation of the axis of revolution in the azimuthal axis of the spherical coordinate system. When $C = 0$ the Janus drop traces an equatorial orbit in an imaginary unit sphere, and as $C \to \infty$ the Janus drop orientation approaches a degenerate orbit with $\boldsymbol{d}$ aligned with the vorticity axis of the undisturbed shear flow ($x_3$–axis). The periodic orbits of a Janus drop of equal internal viscosities ($\eta_1 = \eta_2 = \eta$) are shown in figure 5–4$a$ for an initial drop orientation with respect to the Euler angles $\vartheta\,(t = 0) = \pi/3$, and $\phi\,(t = 0) = \pi/2$. As one may anticipate, the Janus drop undergoes changes in orientation in a linear shear flow of an effective spheroidal (or top) particle [89, 157]. It is readily seen that as the mean drop viscosity $\eta$ increases, the periodic orbits of the Janus drop approach those of a solid sphere (in which the axis of revolution $\boldsymbol{d}$ describes a cone about the $x_3$–axis). In this limit the torque imposed by the straining flow vanishes to zero such that the drop orientation is determined by the angular motion of the ambient fluid (i.e. $\dot{\boldsymbol{d}} = \boldsymbol{\Omega}^{\infty} \times \boldsymbol{d}$ and $r_h = 1$ as $\eta \to \infty$). The influence of the viscosity contrast on the periodic orbits of a Janus drop with a constant mean viscosity of $\eta = 1$ is presented in figure 5–4$b$. (The same initial

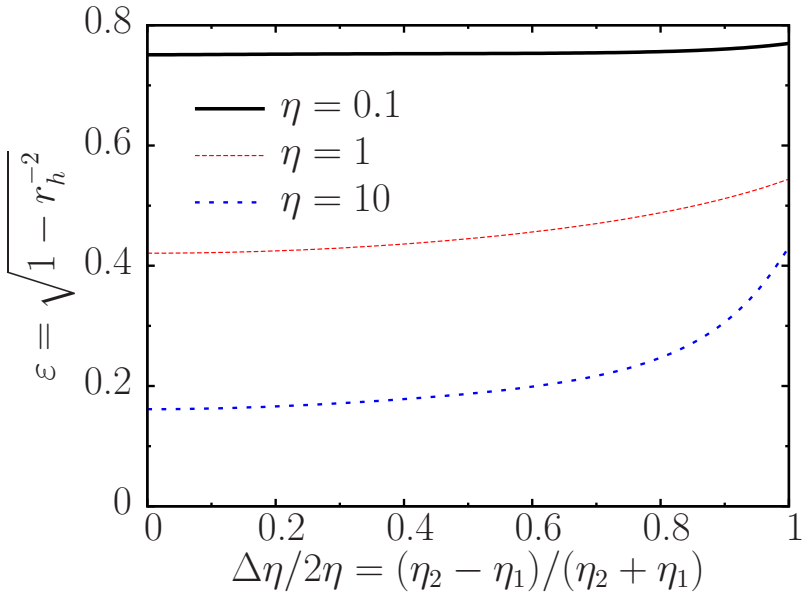


Figure 5–5: (Colors online) Apparent eccentricity factor as a function of the viscosity contrast $\Delta\eta/2\eta$ for constant values of the mean drop viscosity $\eta$.

conditions are used to generate the curves.) The observed shift (or increase in eccentricity) of the periodic orbits as $\boldsymbol{d}$ swepts out of the plane of shear ($x_1$–$x_2$ plane) with increasing values of $\Delta\eta/2\eta$ arises because of the reduction of the torque due to the rotational motion of the ambient fluid in comparison to its straining counterpart. This shift represents a change in the dynamical behavior of the Janus drop from a nearly isotropic body (sphere-like) to a slender oblate spheroid (disk-like); particularly, $r_h = 0.75$ for $\Delta\eta/2\eta = 0.8$. Note that the degree of the shift depends greatly on the viscous properties of the Janus drop, such that it is expected to be less pronounced for more viscous Janus drops of relatively similar internal viscosities. The changes in the dynamical behavior of the Janus drop are best characterized by the eccentricity factor $\varepsilon = \sqrt{1 - r_h^{-2}}$, which is zero for a sphere ($\varepsilon = 0$) and tends to unity ($\varepsilon \to 1$) for a disk-like spheroid. A plot of the eccentricity factor for a Janus drop with constant values of the mean viscosity $\eta$ and increasing viscosity contrast is presented in figure 5–5. From the figure, it follows that the dynamical behavior of a Janus drop lies between the extremes of a solid sphere and a disk.

## 5.5 Cross-streaming velocity of a Janus drop in a shear flow

The objective of this section is to study the cross-streaming velocity of a Janus drop in a shear flow induced by the action of an external force $\boldsymbol{F}_e$ parallel to the streamlines of the undisturbed flow. In principle, it is the anisotropic resistance of the Janus drop to the streaming flow $(\boldsymbol{U}^\infty - \boldsymbol{v})$ that furnishes the cross-streaming phenomena, where $\boldsymbol{v}$ denotes here the translational velocity of the Janus drop. A closely related situation is that of a spheroidal particle that sediments in a quiescent, viscous Newtonian fluid [20]. The analysis presented here follows an analogous treatment to that used in Section 5.4, in which the translational and rotational motions of the Janus drop are derived from overall force and torque balances. It is assumed that the external force acts in such a manner that does not impose a torque on the Janus drop that permits Equation (5.6) to describe the rotational dynamics. The time evolution of the position $\boldsymbol{x}$ of the Janus drop with respect to space-fixed coordinates reads:

$$\dot{x}_k = \boldsymbol{v}_k = u_k^\infty + \left[ \left(X^A\right)^{-1} d_k d_l + \left(Y^A\right)^{-1} \left(\delta_{kl} - d_k d_l\right) \right] F_l^e, \tag{5.11}$$

where $X^A$ and $Y^A$ are the scalar functions that describe the resistance of the Janus drop to streaming flows parallel and perpendicular to the axis of revolution $\boldsymbol{d}$, respectively [154]. Although not shown explicitly, the undisturbed velocity is evaluated at the center of free rotation $\boldsymbol{x}_{cr}$. Note that the external force $\boldsymbol{F}^e$ exclusively acts in the positive direction of the $x_1$–axis, and that the velocity components $v_{2,3}$ correspond to the cross-streaming velocity of the Janus drop. (Naturally, $v_1$ is the velocity of the Janus drop along the streamlines of the undisturbed flow.) Perhaps it is even more relevant to note that the cross-streaming velocity is intrinsically coupled to both the orientation and position of the Janus drop because there is a consequential streaming velocity that arises from the displacement of the drop from the centerline of the shear flow ($x_1$–axis). As a result, the complexity of this problem limits the

analytical progress, which leaves one to rely on a numerical technique in order to provide a solution to the problem. The results presented in this section are obtained by solving the system of differential equations with a fourth-order Runge-Kutta method. Other methods of comparable accuracy were used to validate the results; this is not shown here for the sake of brevity.

By bearing in mind that the results may be of some use to practitioners, the cross-streaming velocity is reported when the axis of revolution of the Janus drop lies in the plane of shear of the undisturbed flow ($x_1$–$x_2$ plane). The justification for choosing this particular configuration is that this corresponds to one of the simplest experimental setups that can be devised to investigate the cross-streaming velocity of the Janus drop for two principal reasons: ($i$) the axis of revolution $\boldsymbol{d}$ stays in the plane of shear such that its angular motion can be measured with more ease (as for any other symmetric spheroid of revolution), and ($ii$) there is only one component of the cross-streaming velocity ($v_3 = 0$). Without incurring in a loss of generality, in this case study the mean velocity of the shear flow is set to zero ($U^\infty = 0$) such that the ambient flow corresponds to a pure shearing flow. It is assumed that at initial conditions ($t = 0$) the free center of rotation of the Janus drop is located at the origin of the set of space-fixed axes ($x_1 = 0, x_2 = 0, x_3 = 0$) with $\boldsymbol{d}$ aligned with the $x_2$–axis (i.e. a vertical alignment with $\vartheta = \pi/2, \phi = \pi/2$). For calculation purposes only, the external force is defined to be equivalent to the drag force on a solid sphere of radius $a$ subject to a uniform flow of velocity $Ga$: $\tilde{F}_1^e = 6\pi\tilde{\eta}_0 G a^2$. The qualitative behavior of the cross-streaming velocity is unchanged with the chosen magnitude of the force nonetheless.

The orientation of the axis of revolution $\boldsymbol{d}$ is plotted alongside the ratio of the cross-streaming velocity to the external force ($v_2/F_1^e$) in figure 5–6$a$ as a function of the dimensionless time for a Janus drop with equal internal viscosities $\eta_1 = \eta_2 = \eta = 1$. The plots show that the cross-streaming velocity is periodic in

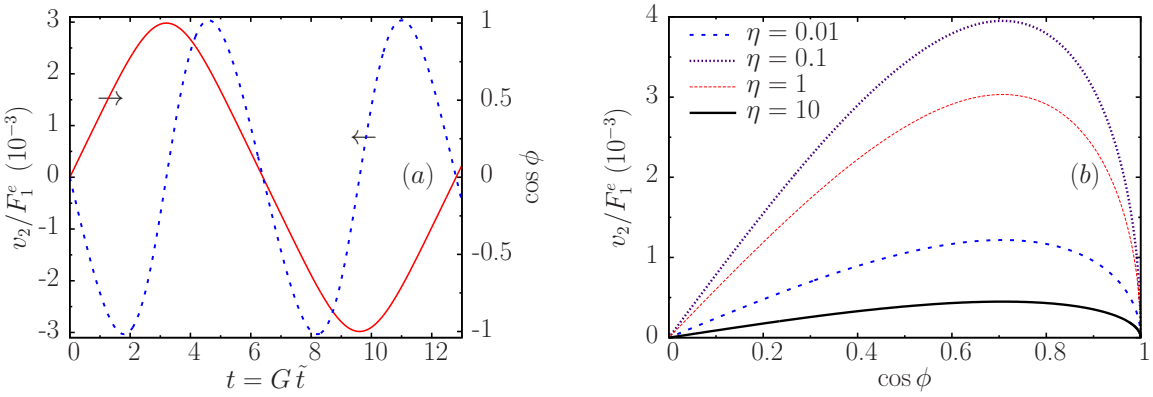


Figure 5–6: (Colors online) (*a*) The solid-line (red) depicts the dynamics of orientation and the dashed-line (blue) shows the non-dimensional ratio of the cross-streaming velocity with the external force. (*b*) Cross-streaming velocity as a function of the arrangement of the axis of revolution of the Janus drop for constant values of $\eta$.

time and that it reaches peak values when the axis of revolution is at a diagonal with respect to the principal direction of the undisturbed shear flow ($\cos\phi = \pm\sqrt{2}/2$), and that it vanishes when it is aligned with any of the principal axes $x_1$ and $x_2$ due to the evident symmetry arguments. Note that at low shear rates, the limit of a Janus drop undergoing cross-flow migration in a streaming flow is recovered. For larger shearing rates, on the other hand, the cross-streaming velocity is quite small. This effect has interesting implications on a dispersion of Janus drops subjected to pressure-driven flows, in which it is inferred from the results of this study that the dispersion exhibits a non-uniform spatial distribution with a higher concentration of Janus drops near the duct boundary. In turn, this effect can lead to rheological properties that depend on the spatial distribution of the Janus drops. It is fitting to point out that spatially-dependent rheological properties of dispersions has been identified to be a problem of central importance of materials processing applications in industry [130].

The non-monotonic dependence of the cross-streaming velocity $v_2$ with the mean drop viscosity is evidently shown in figure 5–6*b*, where $v_2$ decays to zero as $\eta \to \infty$, as it should, since this corresponds to the limit of a solid sphere that has an isotropic

resistance to the external flow. One interesting feature of the results is that the cross-streaming velocity consistently reaches peak values, regardless of the mean drop viscosity $\eta$, when the axis of revolution is at a diagonal with the direction of the undisturbed flow. The effect of the viscosity contrast $\Delta\eta/2\eta$ on the cross-streaming velocity has been found to be quite small under the range of viscous properties that Janus drop have in practice, and for this reason these results have been omitted.

## 5.6 Constitutive equation of a dilute Janus emulsion in a steady shear flow

It is anticipated that the results of this section can be useful to practitioners interested in comparing the theory presented here to rheological measurements of a dispersion of Janus drops in another fluid—also known as Janus emulsions. In order to make analytical progress, calculations are performed at infinite dilution conditions such that there are no interactions among the dispersed particles. Here, the term 'particles' has a general scope that encompasses both fluid and solid bodies. Additionally, due to the various experimental studies [8, 114, 129, 144, 146] that have fabricated Janus drops with radii beyond the micron-size ($\gtrsim 10\,\mu m$), the stochastic effects associated to thermal fluctuations of the suspending fluid (Brownian motion) are entirely neglected in this study. (It is well known that particles above one micron in size are unaffected by Brownian motion [21].) As one may expect, only at sub-micron length scales have Janus drops been observed to be subject to Brownian motion [145]. Therefore, for the purposes of gaining leading and relevant information of the rheology of Janus emulsions, it is appropriate to consider the problem under the simplest scenario of a dilute dispersion of Janus drops subject to a steady shear flow of a Newtonian fluid in the total absence of both inertia effects and Brownian motion.

For a dispersion of bodies of revolution, as in this case, the orientation distribution of the particles in suspension intrinsically determines the rheological properties observed at the macroscopic scale. This is the case because it is the disturbance-flow caused by the particles that lead to an apparent increase in the viscosity of the host fluid. As one may suspect, for certain orientations the particles produce greater disturbances to the flow than others such that it follows, from this simple argument, that the effective rheological properties of the dispersion must depend on the orientation distribution of the particles. The effect of the orientation distribution on the rheology of dispersions comprising bodies of revolution has been the subject of active research right after the publication of Jeffery [89]. For dispersions of sub-micron particles it is the relative importance of Brownian motion to the applied flow that determines the rheology of the dispersion, regardless of the the initial orientation distribution of the particles [92, 94]. On the other hand, in the complete absence of Brownian motion, particle-particle interactions and inertia effects, as in the present study, the orientation distribution is solely determined by the initial orientation of the particles via the so-called Jeffery-orbits. This is in fact, a consequence of the inability of the shear flow to set bodies of revolution into a preferential orientation at zero Reynolds number, as first noted by Jeffery in his study of the dynamics of spheroids of revolution [89]. One can take advantage of this instrinsic behavior of the flow to study the rheology under conditions in which the initial orientation distribution can be controlled. The most straightforward situation to realize this in practice is to have a dispersion with a uniform orientation distribution. Thus, it is in our interest to shed some light on the rheology of a dispersion of Janus drops with a uniform orientation distribution at infinite dilution.

In principle, there are simple strategies that can be used to obtain a dispersion of Janus drops with a uniform orientation distribution; two are proposed here motivated by the findings of Section 5.3 and by application of the latest achievements

on the synthesis of Janus drops with designed properties [146]. The application of a shear flow parallel to the direction of Earth's gravitational field to a dispersion of neutrally buoyant Janus drops with an eccentric gravitational center is a simple method to obtain a dispersion of uniformly aligned Janus drops. To fabricate a neutrally buoyant drop with a center of gravity displaced from the geometrical center the internal fluids must be of differing densities but with a mean density $\tilde{\rho}$ that matches the density of the ambient fluid (i.e. $\tilde{\rho} = (\tilde{\rho}_1 + \tilde{\rho}_2)/2 = \tilde{\rho}_0$ and $\tilde{\rho}_1 \neq \tilde{\rho}_2$). The applied shear rate can be increased systematically until the gravitational torque balances that exerted by the shear flow such that the Janus drops adopt a uniform orientation distribution. The Janus drops will tend to align $\boldsymbol{d}$ with the velocity-gradient of the undisturbed shear flow as the shear rate is increased. (At higher shear rates there is no preferential orientation because the gravitational torque cannot balance that done by the shear flow, in analogy to the problem considered in Section 5.3.) The second method is to apply a magnetic field to a dispersion of magneto-responsive Janus drops; the preparation of such magnetic Janus drops has been reported in [146]. This latter method also offers the possibility of studying the rheological properties at fixed orientations for large magnetic fields; however, the corresponding analysis lies outside the scope of this study. From this point onward the constitutive equation for a dilute Janus emulsion is derived analytically under the mentioned conditions.

Following Batchelor [97], the calculation of the bulk stress $\langle \Sigma_{ij} \rangle$ of a dispersion of 'freely' suspended particles in a linear shear flow involves a volume average of the contributions to the stress of the continuous fluid phase and the dispersed particles. The constitutive equation for the bulk stress of the dispersion of particles in a fluid is defined in an analogous form to that of an ordinary Newtonian fluid but with an additional contribution that arises from the presence of the particles (shown in

non-dimensional form):

$$\langle \Sigma_{ij} \rangle = -\langle p \rangle \, \delta_{ij} + 2 \, \eta_0 \, \langle E_{ij} \rangle + \langle S^p_{ij} \rangle, \tag{5.12}$$

where the angle brackets $\langle \ \rangle$ denotes a volume average of the enclosed quantity, and $\langle S^p_{ij} \rangle$ represents the particle contribution to the bulk stress and it is implicit that it involves a sum over all the particles in the dispersion. For a single particle, $S^p_{ij}$ is the hydrodynamic dipole plus an additional contribution that arises from the distribution of the rate-of-strain field at the surface of the particle [31]:

$$S^p_{ij} = \oint_{S_p} n_k \, \sigma_{ki} \, x_j \ \mathrm{d}S_p - \eta_0 \oint_{S_p} (n_i u_j + n_j u_i) \ \mathrm{d}S_p, \tag{5.13}$$

where $n_i$ is the unit normal vector directed outward at each point over the surface of the particle, and $S_p$ is the outer surface of the particle. For force and torque–free particles in suspension the hydrodynamic dipole reduces to the stresslet: a symmetric tensor that captures the shape and long-range disturbances caused by the particle [13, 31]. Note that the latter surface integral above vanishes identically for a solid particle because the fluid velocity at the surface of the particle solely consists of solid-body motions as dictated by the no-slip tangent condition. Although the superficial velocity of a fluid drop in a linear shear flow develops from the local rate-of-strain in addition to solid-body motions, the surface integral also vanishes on account of the symmetry of the rate-of-strain field. For Janus drops of identical internal viscosities ($\eta_1 = \eta_2$) the surface integral vanishes as well, based on the same symmetry arguments used for a single-phase drop. This finding holds well, even so, for Janus drops of different viscosities provided that $\eta$ adopts finite to moderate values, which is generally the case in practical situations. Therefore, the effect of the superficial distribution of the rate-of-strain field can be safely neglected. For a single Janus drop, the stresslet at an arbitrary drop orientation is given by the

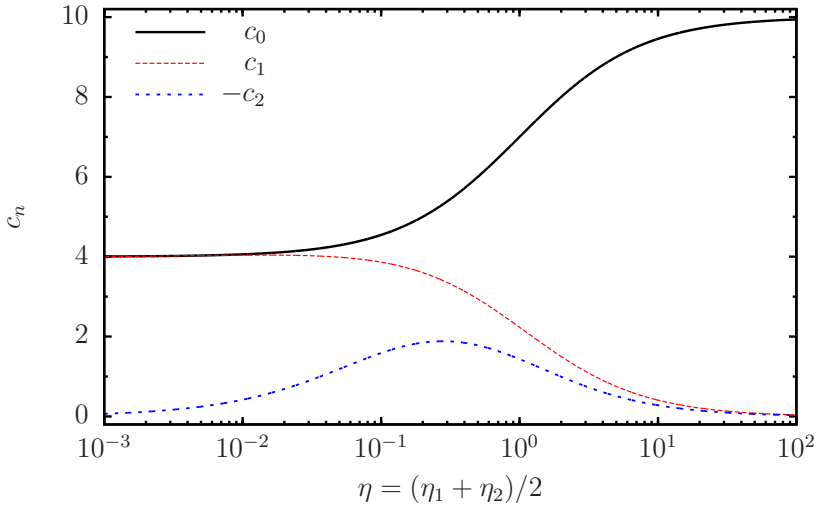


Figure 5–7: (Colors online) Variation of the stresslet functions $c_n$ $(n = 0, 1, 2)$ with the mean drop viscosity $\eta$ for a Janus drop with equal internal viscosities.

following expression:

$$\frac{\tilde{S}^p_{ij}}{\frac{2}{3}\pi\tilde{\eta}_0 G a^3} = c_0 E^\infty_{ij} + c_1\left[\left(d_i E^\infty_{jk} + d_j E^\infty_{ik}\right) d_k - 2 d_i d_j d_k d_l E^\infty_{lk}\right] \tag{5.14}$$
$$+ c_2\left(\epsilon_{ikl} d_j + \epsilon_{jkl} d_i\right) d_l\left(\Omega^\infty_k - \omega_k\right),$$

where the above equation guarantees the stresslet to be a symmetric and traceless tensor, as it should be. The first term at the right-hand side of the equation corresponds to the stresslet of a simple fluid drop in a linear shear flow determined by Taylor [11]: $\tilde{S}^p_{ij} = 2\pi/3\, c_0 \tilde{\eta}_0 a^3 \tilde{E}^\infty_{ij} = 2\pi/3\, \tilde{\eta}_0 a^3 \left(4 + 10\eta\right) / \left(1 + \eta\right) \tilde{E}^\infty_{ij}$. However, in the context of this problem the drop has an equivalent viscosity $\eta = \left(\eta_1 + \eta_2\right)/2$. The additional terms are periodic contributions to the stresslet that depend on the orientation of the Janus drop $\boldsymbol{d}$ relative to the direction of the undisturbed shear flow. Plots of $c_0$, $c_1$ and $c_2$ for a Janus drop that satisfies $\eta_1 = \eta_2 = \eta$ are provided in figure 5–7. It is notable that the stresslet functions $c_{1,2} = 0$ as $\eta \to \infty$ such that the periodicity of the stresslet vanishes identically. Therefore, one can expect right away that the viscosity of a dispersion of hard spheres is recovered in this limit, in

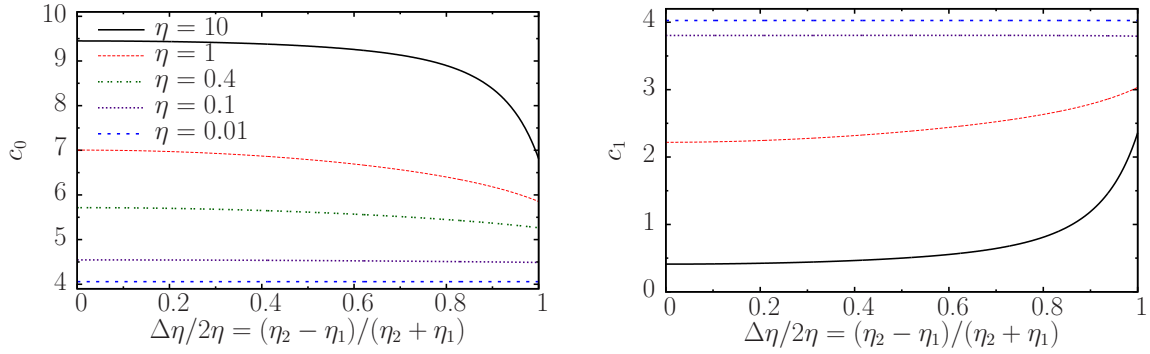


Figure 5–8: (Colors online) Variation of the stresslet functions with the viscosity contrast $\Delta\eta/2\eta$ for selected values of the mean drop viscosity.

analogy with dispersions of single-phase drops [11, 158]. Note that the applicability of Equation (5.14) is expected to hold beyond the limit of equal internal viscosities on account of the weak dependence of the stresslet functions with the viscosity contrast $\Delta\eta/2\eta$ in the range $\eta \lesssim 10$. Figure 5–8 presents plots (that support this claim) of the stresslet functions against $\Delta\eta/2\eta$ while keeping constant the mean drop viscosity $\eta$. In the low mean drop viscosity limit the stresslet functions retain nearly constant values regardless of the increase in $\Delta\eta/2\eta$. An analogous plot for $c_2$ is shown in figure 5–9 that depicts comparable features. In general, the magnitude of this parameter with respect to its counterparts is smaller.

For a dispersion of Janus drops with identical orientations it is obvious that $\langle S^p_{ij}\rangle = n_d\, S^p_{ij}$, where $n_d$ is the number density of the drops. Thus, the constitutive equation for a dilute Janus emulsion becomes:

$$\langle \Sigma_{ij}\rangle = -\langle p\rangle\,\delta_{ij} + 2\,\eta_0\left(1 + \frac{1+\frac{5}{2}\eta}{1+\eta}\Phi\right)E^\infty_{ij} + \frac{1}{2}\eta_0 c_1\Phi\big[\left(d_i E^\infty_{jk} + d_j E^\infty_{ik}\right)d_k \quad (5.15)$$
$$- 2d_i d_j d_k d_l E^\infty_{lk}\big] + \frac{1}{2}\eta_0 c_2\Phi\left(\epsilon_{ikl}d_j + \epsilon_{jkl}d_i\right)d_l\left(\Omega^\infty_k - \omega_k\right),$$

where $\Phi$ is the volume fraction occupied by the Janus drops. The orientation-independent contribution to the bulk stress (second term) is the zero-shear viscosity of a dilute dispersion of single-phase drops [11] with an equivalent viscosity

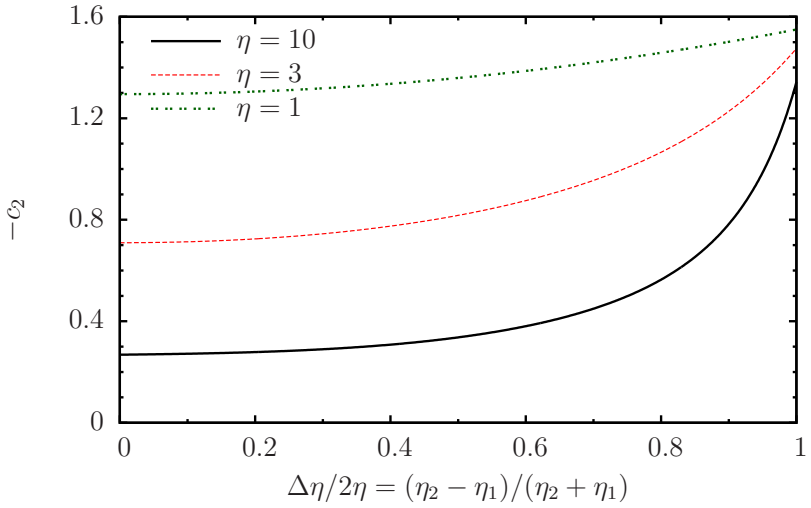


Figure 5–9: (Colors online) The dependence of the stresslet associated to drop rotation with the viscosity contrast and mean drop viscosity.

$\eta = (\eta_1 + \eta_2)/2$. It is interesting to note that this term corresponds to the minimum rate of viscous dissipation for a dilute Janus emulsion. (The choice of denoting the viscosity of the Janus emulsion as the zero-shear viscosity is that it is foreseen that the emulsion will exhibit shear-thinning at higher shearing rates due to the deformation of the drops.) Figure 5–10 presents the variation of the reduced zero-shear viscosity $\eta_r = \left(\langle\tilde{\Sigma}_{12}\rangle - G\tilde{\eta}_0\right)/G\tilde{\eta}_0\Phi$ of the dispersion with the drop viscosity $\eta$ and orientation when $\boldsymbol{d}$ is in the plane of shear. From this figure it is evident that the zero-shear viscosity of a Janus emulsion is intermediate to that of a dispersion of low viscosity drops and hard spheres at infinite dilution conditions. The dependence of the orientation of the Janus drops on the zero-shear viscosity becomes unimportant as $\eta \to \infty$, in agreement with the expectations. The somewhat surprising result is that there is a stronger dependence of the zero-shear viscosity on the drop orientation $\boldsymbol{d}$ for Janus drops of low viscosity ($\eta \ll 1$). In contrast to a single-phase drop, a Janus drop that rotates produces a disturbance-field that originates from the hindrance of the internal interface to the flow that is present even in the low

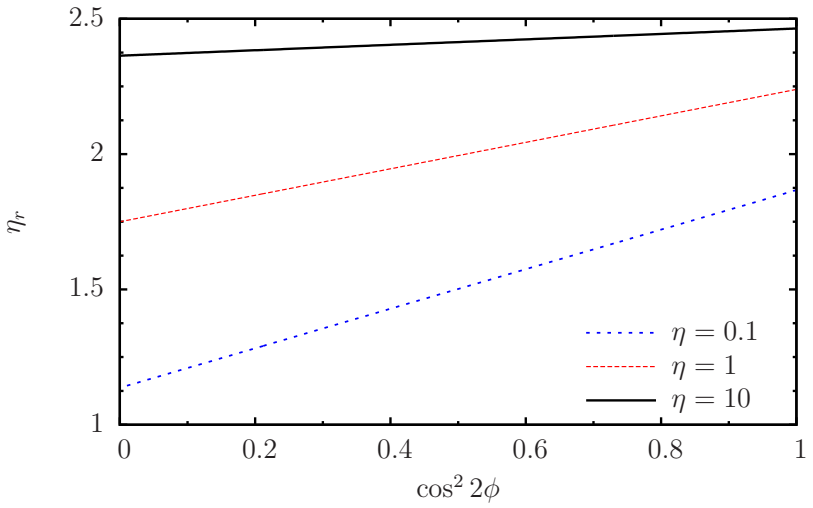


Figure 5–10: The reduced zero-shear viscosity $\eta_r$ of a dilute Janus emulsion as a function of the drop mean viscosity and orientation. The minimum values of $\eta_r$ (at $\cos^2 2\phi = 0$) correspond to Taylor's result for single-phase drops. The axis of symmetry of the dispersed Janus drops $\boldsymbol{d}$ lie in the plane of shear.

viscosity limit.

It is pertinent to compare the obtained zero-shear viscosity against that of double emulsions, a dispersion of concentric drops, in attempt to obtain a broader picture of the rheology of compound multiphase drops. On account of the concentric configuration of double emulsions the zero-shear viscosity is, in general, more sensitive to the separation of the interfaces than the viscous properties of the constituent fluids [10]. For example, the viscosity of a dispersion of hard spheres is recovered for small interfacial separations of the concentric drops with a lesser dependence on the viscosity of the internal fluids (for moderate values). Only when the inner drop size is negligible compared to the outer one, Taylor's viscosity is recovered, as pointed out by Stone & Leal [10]. Therefore the consolidation of these results with the present ones indicate that the lower and upper bounds to the viscosity of a dispersion of compound multiphase drops, in general, correspond to those of single-phase drops and hard spheres, respectively.

The remarkable difference of the rheological properties of Janus emulsions to double emulsions is the appearance of non-Newtonian effects associated to the anisotropic hydrodynamics of Janus drops. Whereas, double emulsions exhibit Newtonian behavior (isotropic bulk stress) in the limit of zero interfacial distortions [10]. The difference in the normal stresses $N_1 = \langle\Sigma_{11}\rangle - \langle\Sigma_{22}\rangle$ and $N_2 = \langle\Sigma_{22}\rangle - \langle\Sigma_{33}\rangle$ of a dilute Janus emulsion in a linear shear flow are readily determined from the bulk stress:

$$N_1 = \eta_0 c_1 \Phi \left(d_2^2 - d_1^2\right) d_1 d_2 E_{12}^{\infty}, \tag{5.16}$$

$$N_2 = \eta_0 c_1 \Phi \left[\frac{1}{2} + \left(d_3^2 - d_2^2\right)\right] d_1 d_2 E_{12}^{\infty}. \tag{5.17}$$

As one may expect, from the intrinsic analogy of spheroids of revolution, there is no direct contribution to the difference in normal stresses from the rotational motions of the Janus drops; the influence of rotation to the normal stresses is as an indirect contribution via changes in orientation $\boldsymbol{d}$. The difference in the first normal stresses $N_1$ vanishes identically when the axis of symmetry of the Janus drop is either parallel to the direction of the undisturbed flow or velocity-gradient (i.e. $d_{1,2} = 1$), and when the axis of symmetry is parallel to any of the principal axes of the rate-of-strain field ($d_1 = \pm d_2$). This is quite the expected result for any spheroidal particle on account of the rotational symmetry about its axis of symmetry. In fact, dilute dispersions of other related bodies of revolution of spherical shape but with anisotropic hydrodynamic properties (e.g. 'slip–stick' spheres) also exhibit the analogous behavior of $N_1$ in a linear shear flow [44]. For other arrangements of $\boldsymbol{d}$, the Janus drop experiences an uneven distribution of the normal stresses over its outer surface. The transition of $N_1$ from compression to tensile normal stresses is consistent to that of an oblate spheroidal particle, in agreement with the expectations for a body that exhibits hydrodynamic properties analogous to that of an oblate spheroid (Section 5.4). The second difference in the normal stresses $N_2$ vanishes wherever $\boldsymbol{d}$ is aligned with any

of the principal axes of the undisturbed flow (velocity and velocity-gradient) or rate-of-strain field (extension and compression axes). It is notable that when $d_3 = 1$ the dispersion behaves as an emulsion with Newtonian properties ($N_{1,2} = 0$) because in this case the Janus drop behaves as a single-phase drop.

It is relevant to point out that differences in the normal stresses can also arise in dispersions of single-phase drops; however, within the limit of small deflections these are of the order of the capillary number $Ca \ll 1$ [46]. From this result, it ensues that the effects of the deflection of the interfaces may not be easily differentiated in experimental settings from those tied to the anisotropic properties of the Janus drops as the capillary number is increased. The obtained results indicate that the anisotropic properties of the Janus drop provide the leading term for the differences in the normal stresses, which establishes a reasonable justification for the neglect interface distortions in this study. It is also important to point out that Torza & Mason [8] did not observed qualitative changes on the dynamical behavior of a near Janus drops with increasing shear rate despite the notable deformation to the interfaces. The analysis of shape distortions is expected to be more meaningful when there are hydrodynamic interactions with other drops or walls and in time-dependent shear flows, as it has been for simple fluid drops [47, 54, 159].

## 5.7 Conclusions

The dynamics and rheology of Janus drops in a linear shear flow of a Newtonian fluid is studied in the limit of low-Reynolds-number flows. Under 'freely' suspended conditions the Janus drops undergo Jeffery-like orbits analogous to that of an oblate spheroidal particle with an effective aspect ratio determined by the viscosities of the three fluid phases. Surprisingly, low viscous Janus drops formed by distinct fluids tend to exhibit disk-like Jeffery orbits, and as one may anticipate, high viscous drops behave as solid spheres (isotropic).

When a Janus drop is 'trapped' at a fixed location by the action of an external

force it can exhibit a preferential orientation depending on the viscous properties of the fluids, velocity, and velocity-gradient of the undisturbed flow. This property may be particularly useful to estimate the local velocity to velocity-gradient in an unknown ambient flow, and to obtain a dispersion of Janus drops with a uniform orientation distribution. The latter is of practical importance to the study of the changes in the rheology of Janus emulsions with respect to the orientation of the drops.

This investigation shows that an external force parallel to the streamlines of the undisturbed shear flow can induce a cross-streaming velocity on the Janus drop. This has interesting implications in a dispersion of Janus drops subject to a pressure-driven flow. When the dispersion is forced to flow in a tube by a pressure head (confined Poiseuille flow), the drops are expected to migrate away from the center to the walls of the tube by means of an external force (e.g. gravity) parallel to the axis of the tube. Near the center of the tube the shear-to-force ratio is small such that the drops undergo cross-flow migration until a zone of higher shear is reached, in which the drops rotation is fast enough to prevent further migration. It is likely that the hydrodynamic interactions with the wall will also affect the location of drops relative to the axis of the tube in this case. This establishes a pure hydrodynamic approach to the separation of multiphase emulsions with potential applications in environmental remediation processes. Additionally, the tendency of Janus drops to approach the boundaries of a tube in a pressure-driven flow can have medical applications. For example, Janus drops can be made selective for the capture of hazardous lipids that accumulate near the walls of blood vessels as a method to reduce cholesterol levels, which is one of the related factors that lead to cardiovascular diseases in the United States [160].

The rheological behavior of Janus drops has been found to share properties with dispersions of single-phase drops and spheroidal particles. Interestingly, the

expression of the zero-shear viscosity is analogous to that derived by Taylor [11] for a dispersion of single-phase drops, but with a drop viscosity equivalent to the mean of the viscosities of the pair of fluids that comprise the Janus drop, $\eta = (\eta_1 + \eta_2)/2$. This corresponds to the minimum rate of viscous dissipation for this system, which occurs when the axis of symmetry of the Janus drop is either parallel to the vorticity axis or any of the principal axes of the rate-of-strain field. The effect of the viscosity contrast of the internal fluids is in general small such that it can be safely neglected in most experimental settings that have been reported in the scientific literature. In comparison to a double emulsion (concentric drops), a dispersion of Janus drops displays non-Newtonian behavior that derives from the anisotropic properties imparted by the internal fluid–fluid interface. Although this study has only considered the rheological properties under 'freely' suspended conditions, it is not difficult to apply the results to conditions in which the orientation of the Janus drops is controlled by external means (e.g. magnetic field). Additionally, there would be an anti-symmetric contribution to the bulk stress intrinsically related to the applied torque; the fundamental relation can be found in the well-known book of Kim & Karrila [31], such that in principle, one can still determine the zero-shear viscosity by accounting for the contribution of the torque to the bulk stress of the dispersion. Nevertheless, it would be interesting to compare the theory presented here to rheological measurements from experiments to advance the understanding of the rich dynamics of multiphase emulsions.

The results of this investigation can also be useful to estimate and understand the dynamics and rheology of other partly engulfed multiphase drops. This expectation is partially supported by the experimental observations carried out by Torza & Mason [8], where it is demonstrated that the dynamics of such drops is similar to that of a spheroid of revolution. It follows from the findings of this study that the zero-shear viscosity of a dispersion of partly engulfed compound drops may be

comparable to Taylor's result under certain circumstances. If the fluids that constitute the partly engulfed drop occupy similar volumes, as for the particular case of a Janus drop, it is likely that Taylor's expression can be used to predict the zero-shear viscosity. For other volume ratios the extrema of a single-phase drop and a solid sphere are expected with a lesser influence of the internal viscosities for short separations of the fluid–fluid interfaces.

# CHAPTER 6
# CONCLUSIONS AND FUTURE DIRECTIONS

The hydrodynamic properties, dynamics and rheology of Janus drops subject to linear ambient flows in the total absence of inertia and interfacial deformations is analyzed in this dissertation. By bearing in mind that the typical length scales of Janus drops in experiments are in the range $10 - 500\,\mu m$, it is considered a reasonable assumption to neglect at first the effects of inertia and interfacial distortions. Particularly, shape distortions are expected to only bring small quantitative deviations to the results considered in this dissertation; thus the essence of the dynamics and rheology of multiphase drops at low-Reynolds-number flows is well captured by the findings of this investigation. The conditions in which inertia and interfacial distortions are of fundamental relevance are discussed later in this chapter for completeness. Nonetheless, under these assumptions important information is derived regarding the general properties and dynamics of multiphase compound drops in a linear flow, which is one of the most common and simpler types of flow to generate in practice.

In Chapter 3 the hydrodynamic behavior of a Janus drop subject to a uniform ambient flow has been considered under conditions where the drop remains stationary in the laboratory reference frame. Interestingly, it is found that the drop exhibits an anisotropic (orientation-dependent) resistance to the imposed flow is in general independent of the viscosities of the fluids that comprise the drop; except in the extreme cases of a Janus drop of very low (negligible viscosity drop) and high mean viscosity (solid sphere limit) in which the behavior is evidently isotropic. This

is best understood by considering the results of the drag force on the Janus drop, which arise due to the stresses imparted by the surrounding fluid. The drag force is found to be of greater magnitude when the undisturbed flow is parallel to the drop axis of symmetry $\boldsymbol{d}$ in comparison to a flow in the transversal direction. This is the first finding that demonstrates that a partially engulfed multiphase drop can exhibit anisotropic hydrodynamic properties. The reason for this observation is that the internal interface that bounds the pair of fluids that comprise the multiphase drop imposes an additional resistance to the flow on account of the no-penetrability property of the interface. The role of the internal interface on the drag force on a multiphase drop was previously considered for double emulsions (a large drop encapsulating a smaller one), in which it is shown that the drag force falls between that of a single-phase drop for a vanishingly small encapsulated drop, and a solid sphere when there is a small separation between the interfaces of the inner and outer drops. Due to the spherical symmetry of the double emulsion, the drag force is always parallel to the direction of the undisturbed flow. On the other hand, the presence of the internal interface of the Janus drop displaces the direction of the drag force relative to the direction of the flow; this behavior is akin of a spheroid of revolution. Particularly, a Janus drop exhibits a hydrodynamic resistance to the uniform flow analogous to that of an oblate spheroidal particle on account of the resistance imparted by its internal interface.

Interestingly, in Chapter 4 the analogy of the Janus drop with an oblate spheroidal particle is observed, again, in a linear shear flow, where the torque on the drop is of greater magnitude when the direction of the shear flow is parallel to the axis of symmetry $\boldsymbol{d}$. Note that for a spheroidal particle, the ability of the shear flow to impose a torque is greater when the flow is parallel to $\boldsymbol{d}$ because in this case the spheroid obstructs the external flow to a greater extent. (For a prolate spheroidal particle the situation is clearly opposite because the fluid flows along the long axis.)

From the hydrodynamic characterization studies realized in Chapters 3 and 4, it follows that the dynamical behavior of a Janus drop is also analogous to an oblate spheroid of revolution under 'freely' suspended conditions in linear shear flow. Chapter 5 joins the results obtained in the mentioned chapters to analyze the behavior of a Janus drop in a general shear flow: a combination of uniform, extensional, and rotational flows. It is found that the Janus drop translates with the velocity of the undisturbed flow at the free center of reaction and undergoes rotation with a variable speed that depends on the local rate-of-strain field. Interestingly, the dynamical behavior of a Janus drop lies in between a slender oblate spheroid (disk-like) for a low viscosity drop and a solid sphere for drop with a high viscosity, where the latter extreme is the expected behavior for a spherical shaped body. In contrast to other solids of revolution, the results of this investigation reveal no tendency of the Janus drop to undergo a "drift" velocity due to the local rate-of-strain field as for dumb-bell shaped bodies and the spherical cap.

The shear viscosity of a force and torque–free dispersion Janus drops in a linear shear flow is found to be given by an expression analogous to that derived by Taylor for a dispersion of single-phase drops but with a drop viscosity equal to the mean viscosity of the Janus drop. Interestingly, it turns out that the difference in viscosities results in a negligible contribution to the shear viscosity. This is partly due to the fact that the stresslet is a symmetric quantity and the viscosity contrast produces an anti-symmetric contribution to the disturbance velocity field; evidently, due to to this trivial argument the stresslet remains constant for small values of the viscosity contrast. Hence the negligible contribution of the viscosity contrast because the stresslet is the sole contributor to the bulk mechanical properties in the infinite dilution limit and 'freely' suspended conditions. Deviation from Newtonian behavior is discovered for this system and it is presumed to be associated to the relative orientation of the drop with respect to the undisturbed velocity field, as

for other solids of revolution. Nevertheless, this needs to be analyzed further under more general conditions such as inertia and interparticle interactions; it is outside of the scope of this dissertation to include those effects into the analysis. However, the contribution is a first step towards the understanding of the mechanical properties of compound multiphase drops. The results of this investigation will be useful when analyzing the macroscopic properties of compound multiphase drops in the limit of vanishing inertia effects, Brownian motion, interparticle interactions, and other influential effects. For the first time it has been shown that non-Newtonian behavior can arise in a system consisting of non-deformable drops, which is quite an interesting result in view of the Newtonian properties of the fluids phases in the system. From this point onward, a number of problems of relevance to the field are proposed based on the findings of this dissertation.

There are a number of pure hydrodynamic and multi-disciplinary problems of relevance that can be proposed based on the findings of this dissertation. Beyond the limits of zero Reynolds-number-flows and interfacial distortions considered in this dissertation there is a plethora of problems that merit attention. The total absence of inertia and interfacial distortions is considered in the hydrodynamic field as standard conditions to analyze the dynamics and mechanical properties of dispersed fluid phases. The principal justification of the neglect of interfacial distortions at zero Reynolds number is that the deflection of the interfaces in unbounded linear flows (as considered in this work) are point-symmetric such that these are expected to only bring small quantitative departures relative to the undeformed case. It is interesting to mention that even weak inertia effects can generate new dynamics into the picture, as it has been found for solid particles and single-phase drops; such that it is worth a while to incorporate the effects of inertia in subsequent studies in order to gain a broader view of the dynamics and rheology of disperse multiphase systems. Note that this problem is not only of interest to industrial applications but also for

the development of new technologies at the colloidal scale, in which weak inertia effects are expected to become prominent as the field evolves further. One of the most interesting findings is that weak inertia can induce cross-flow migration even for solid spheres (which are isotropic in virtue) [126]. Inertia effects can cause an inhomogeneous spatial-distribution of the particles in the dispersion that, in turn, is reflected on the mechanical properties of the bulk. A solid starting point to make analytical progress is to implement strategies that track the kinematical evolution of interfaces in an analogous fashion to those used by Taylor & Acrivos [53], and Frankel & Acrivos [53]. Leal [84] also proposes useful strategies to account for weak inertia effects. Note that those strategies are limited to small departures in shape; to account for greater changes in shape one needs to rely on numerical methods, such as the boundary element method [58] and the immersed boundary method [152] to mention a few among the various methods developed so far.

An important aspect to investigate is if weak inertia effects can lead to deterministic behavior of a Janus drop under 'freely' suspended conditions in a linear shear flow at low Reynolds number. This is a subject of broad implications and of interest to colloidal physicists; the interested reader is referred to the review of Leal [84]. Note that in the total absence of inertia there are infinitely many possible Jeffery-like orbits that the drop orientation can follow based solely on its initial orientation in space. That is, there is no tendency of the Janus drop to consistently reach the same orbit regardless of its initial orientation in the total absence of inertia—this type of motion is categorized as indeterministic behavior. A classic example of deterministic behavior is that of a prolate spheroid in a pure extensional flow; for any initial orientation the spheroid tends to align its axis of symmetry with the axis of extension of the undisturbed flow. The question of interest here is if inertia effects, even if small, can lead to deterministic behavior such that the Janus drop adopts a preferential orbit regardless of its initial orientation in space. This

behavior has important implications on the rheological properties of a dispersion of multiphase systems because there is a certain level of dissipation of energy associated to the preferential orbit. For example, dumb-bell shaped bodies under certain circumstances have a tendency to adopt an orbit that corresponds to the maximum energy of dissipation [90]. For disperse multiphase drops the analysis is expected to be more involved due to changes in the drop shape induced by inertia effects. In this case, one can anticipate that departures from the dynamical behavior exhibited by a body of revolution (e.g. spheroid) arises due to the so-called inertial "drift" and because of the lack of fore and aft symmetry of the flow around the drop that tends to deform it into an asymmetrical shape.

Another problem of interest is the study of the stability of a dispersion of compound multiphase drops. One of the important factors to consider is the ability of the dispersed phase to resist coalescence [48, 135]. For example, coalescence occurs when a pair of homologous fluid drops suspended in another fluid join to form a larger drop, or when a drop becomes 'absorbed' by its bulk homologous fluid phase. In the latter case the drop is suspended in another fluid that is in direct contact with the bulk homologous phase of the drop via a fluid–fluid interface. As the drop rises by buoyancy, it deforms and may ultimately rupture the interface between the ambient fluid and the bulk homologous phase above to undergo coalescence. For a Janus emulsion it would be interesting to study how the anisotropic properties of the drop can affect coalescence. It is possible that under certain conditions the Janus drop can approach the bulk fluid phase above with the non-homologous phase, and this can potentially reduce the probability of coalescence to occur. Such a situation is possible if the bulk fluid phase above is more viscous than the other internal fluid phase of the Janus drop, and if the viscosity of the internal fluid phases control the orientation of the drop as it rises by buoyancy. Since the Janus drop approaches the fluid–fluid interface with the less viscous fluid phase it is possible that it is more

difficult for the drop to break the interface, which may result in an increase in the stability of the emulsion. (Note that this study is a direct implication of the dynamical behavior of Janus drops in a uniform flow presented in Section 3.3.2.) There are several parameters to consider, such as the viscosities of the three fluid phases, the interfacial tensions, but most importantly the history of the flow from a distance far away from the fluid–fluid interface above the Janus drop.

The problem of coalescence of a pair of Janus drops rising in a quiescent fluid is perhaps more interesting and possibly of greater complexity due to the influence of hydrodynamic interactions between the drops. One important parameter to consider is the off-center distance between the drops since under certain circumstances the hydrodynamic interactions may deform the drops in such a manner that the drops eventually become aligned with each other; thus, increasing the chances of coalescence to occur, as in the case of a pair of single-phase drops [45]. It may be worth a while to explore the interplay of viscous to buoyant effects on the orientation of the Janus drops since it is likely to affect the dynamics of the drops; that is, whether the Janus drops become aligned or migrate away from each other.

A pure hydrodynamic problem with several implications to coalescence phenomena, particle dynamics and rheology is the problem of hydrodynamic interactions of a pair of Janus drops in a general ambient flow. The principal factors to consider are the interparticle distance between the geometrical centers and the relative orientations of the drops. In order to reduce the number of scenarios to consider, one has to identify fundamental problems as realized in Chapter 3 to take advantage of the linearity property of Stokes flow to derive results for any arbitrary particle-positions and orientations under constant flow conditions. Then, the problem can be generalized to any direction of the ambient flow. It is instructive to start with a uniform ambient flow, and then extend the analysis to simple-shear flows (Chapter 5). In this problem it is crucial to account for deflection of the fluid–fluid interfaces on

account of the non-uniform velocity-gradients that arise from the hydrodynamic interactions. It is anticipated that the drops will exhibit richer dynamics with some features that fall intermediate between a solid and a single-phase drop. The use of bispherical coordinates may prove to be useful in the study of this problem. The results of this study are expected to provide new insights on the dynamics of Janus drops in a general ambient flow beyond the infinite dilution limit considered in this dissertation. Ultimately, the effective viscosity for a Janus emulsion can be extended to the order of $\phi^2$ (volume fraction) in similarity to the methodology followed by Batchelor [95]. However, one needs to take into account as well shape distortions absent in the cited study because it concerns rigid particles.

An important problem related to the above is that of hydrodynamic interactions of a Janus drop with a solid boundary, such as a plane wall or another particle of different size. Hydrodynamic interactions are of particular relevance to microfluidic applications in which confinement effects are prominent on account of the small gap between the drop surface and the walls. The problem of a Janus drop moving between parallel plates or in a tube is quite challenging and may not have analytical solution. The interested reader may refer to the classic book of Happel & Brenner [20] for further reference on problems of this type that have been solved. Nevertheless, it is more fruitful to consider the problem of a Janus drop interacting with a single plane wall to shed some light on how it affects drop dynamics. The use of bispherical coordinates and the method of reflections to account for short and long-range hydrodynamic interactions, respectively, are feasible candidates to carry out the corresponding analyses [20, 31]. Note, however, that bispherical coordinates tend to have poor convergence to the solution of the flow for very short distances between the particle and the wall. In such cases, one should rely on the lubrication approximation [13]. A problem of relevance is that of a Janus drop translating parallel to the wall. It would be interesting to investigate if the Janus drop

adopts a steady orientation as it translates parallel to the wall, in analogy with a spheroidal particle [161], or if it migrates away from the wall due to the shape distortions induced by the hydrodynamic interactions, as in the case of a single-phase drop [159]. It is probable that multiphase drops will exhibit migration lateral to the wall but it is not so obvious under what conditions, if possible, the drop can adopt a steady orientation. The results of such a study are of fundamental importance in several fields of current interest such as targeted-delivery, lab-on-a-chip and related microfluidic applications [162], dynamics of swimmers and active particles near surfaces [163–166], and can also be useful to attain a greater understanding of the spreading dynamics of cancer cells [143].

There is a rapidly growing interest in achieving autonomous motion of particles in a viscous fluid at colloidal length scales to perform complicated tasks such as targeted-delivery, reparation of damaged tissue, neutralization of pathogens and cancerous tissue, etc [167]. In the scientific literature, these active particles are commonly denoted as *nanomotors*. Some of the major challenges currently faced in the field is the efficient design of nanomotors that can overcome the reversibility property of Stokes flow that makes futile reciprocal-based propulsion methods commonly encountered in everyday experience, such as the propellers used in boats and airplanes. To some extent, autonomous motion has been achieved by artificial devices that mimic the swimming of microorganisms [14, 168, 169], which have been able to realize, slowly but steadily with the passing of time, efficient propulsion in an inertialess world. Another of the major challenges is the ability to produce directed (unbiased) motion at the colloidal scale. For nanomotors of about 1 $\mu m$ in size the thermal fluctuations of the surrounding fluid (Brownian motion) incur in a randomization of the direction of motion. To overcome this issue, the nanomotor has been embedded with a magneto-responsive material to attain motion control in a non-invasive manner (which is particularly important in biological applications) [170];

however, its implementation in applications that require a high degree of control to navigate through may be limited (e.g. microfluidic networks and lab-on-a-chip). Another strategy to overcome the stochastic effects of Brownian motion is to use particles with an asymmetric distribution of mass such that there is a gravitational torque on the particle that opposes that imparted by Brownian motion. This is analogous to the tumbling behavior of a Janus drop under the action of gravity considered in Chapter 3. An advantage of using a Janus drop for achieving self-propulsion is that the drop can be readily synthesized to be neutrally buoyant in the ambient fluid even when the densities of the fluid phases are different. In principle, this is simpler to realize in practice than establishing a density gradient in a solid particle. Note that the use of a gravitational torque to resist Brownian motion implies that the particle rises in the fluid against the gravitational field. Since this may not always be the desired direction of motion, other strategies are needed. Nevertheless, the inherent hydrodynamic behavior of the Janus drop makes it an ideal nanomotor that can resist the effects of rotary Brownian motion without the aid of a gravitational field. (As shown in Chapter 3, in which a Janus drop with different internal viscosities experiences a torque that tends to align the axis of symmetry of the drop with the direction of motion, or equivalently, with the direction of the undisturbed streaming flow.) It is then of interest to investigate the conditions in which a Janus drop that moves autonomously can resist the orientational fluctuations imparted by the surrounding fluid. The conditions to achieve self-propulsion on a Janus drop has been considered recently by Shklyaev [141], in which self-induced gradients in interfacial tension have been shown to be sufficient to induce autonomous motion. It is left to evaluate how efficient is the Janus drop in overcoming the stochastic fluctuations of the surrounding fluid to maintain its direction of motion unchanged, and how fluid-advection can affect the velocity of self-propulsion. Córdova-Figueroa and Brady [171, 172] have established a systematical method to realize this kind of

analysis for the so-called osmotic motor suspended in a dispersion of hard spheres, and the implementation to the problem of interest follows from fundamental principles of conservation of species and heat transfer.

# APPENDICES

# APPENDIX A

## A.1 Spherical cap subject to a uniform pressure field

The objective of this section is to show that the net net force imparted by a uniform pressure field on a spherical cap, which belongs to a class of bodies that lack fore and aft symmetry, is zero. Figure A–1 shows a spherical cap of radius $a$ completely submerged in a fluid with a uniform pressure distribution $p_\infty$. By performing a force balance on the control volume (depicted by the dashed-line) that encloses the spherical cap, one finds that the sum of the normal stresses at the surfaces $S_0$ and $S_1$ must be equal to zero (there are no body forces on the spherical cap):

$$\oint_{S_0} \boldsymbol{n} \cdot \boldsymbol{\sigma} \, \mathrm{d}S + \oint_{S_1} \boldsymbol{n} \cdot \boldsymbol{\sigma} \, \mathrm{d}S = \boldsymbol{0}, \tag{A.1}$$

where $\boldsymbol{n}$ is the corresponding unit normal vector at each surface, the fluid stress solely arises by the uniform pressure field $\boldsymbol{\sigma} = -p_\infty \boldsymbol{\delta}$ (quiescent fluid), and $\boldsymbol{\delta}$ is the identity tensor.

From evident symmetry arguments the forces transversal to the $z$-axis on $S_1$ are identically zero $F_x = F_y = 0$; thus, only the $z$-component of the force needs to be calculated on $S_1$, as shown below:

$$F_z = \boldsymbol{e}_z \cdot \left[ \oint_{S_1} \boldsymbol{n} \cdot \boldsymbol{\sigma} \, \mathrm{d}S \right], \tag{A.2}$$

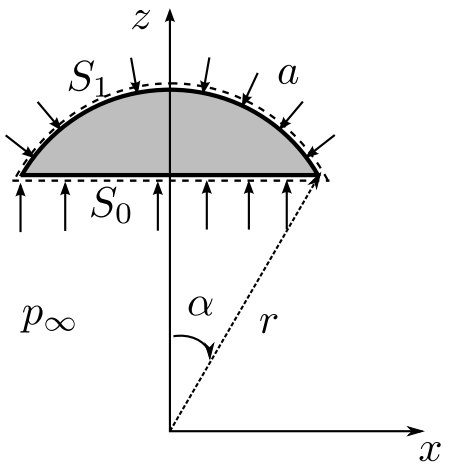


Figure A–1: Spherical cap subject to a uniform pressure field. The surfaces $S_0$ and $S_1$ denote the planar and curved surfaces of the spherical cap, respectively.

where $\boldsymbol{n} = \boldsymbol{e}_r$ on $S_1$, and therefore, the fluid stresses normal to $S_1$ are readily calculated by the following elementary steps:

$$\oint_{S_1} \boldsymbol{n} \cdot \boldsymbol{\sigma} \, \mathrm{d}S = \oint_{S_1} \boldsymbol{e}_r \cdot (-p_\infty \, \boldsymbol{e}_r \boldsymbol{e}_r) \, \mathrm{d}S = \oint_{S_1} -p_\infty \, \boldsymbol{e}_r \, \mathrm{d}S. \tag{A.3}$$

Consider that $\boldsymbol{e}_z$ is a constant unit vector such that it can be readily introduced into the above surface integral to determine the $z$-component of the force on $S_1$:

$$F_z = \oint_{S_1} \boldsymbol{e}_z \cdot (-p_\infty \boldsymbol{e}_r) \, \mathrm{d}S = \oint_{S_1} -p_\infty \cos\vartheta \, \mathrm{d}S, \tag{A.4}$$

where the scalar product has been carried out ($\boldsymbol{e}_z \cdot \boldsymbol{e}_r = \cos\vartheta$) in the latter step. By noting that $\mathrm{d}S = a^2 \sin\vartheta \, \mathrm{d}\vartheta \, \mathrm{d}\phi$ on $S_1$, the surface integral now becomes:

$$F_z = \int_0^{2\pi} \int_0^{\alpha} (-p_\infty \, \cos\vartheta) \, a^2 \, \sin\vartheta \, \mathrm{d}\vartheta \, \mathrm{d}\phi, \tag{A.5}$$

$$= -2\pi a^2 p_\infty \int_0^{\alpha} \sin\vartheta \cos\vartheta \, \mathrm{d}\vartheta, \tag{A.6}$$

$$= -\pi (a \sin\alpha)^2 p_\infty. \tag{A.7}$$

It is easy to see that the factor $\pi(a\sin\alpha)^2$ corresponds to the area of the circular region $S_0$, and that the $z$-component of the force on $S_0$ is equal in magnitude but

opposite in direction to that of $S_1$. Thus it is shown that the net force imparted by a uniform pressure field about a body that lacks fore and aft symmetry is zero.

The result may be generalized to a body of arbitrary shape by choosing a convenient control volume (for example a box) that encloses both the body and part of the fluid that surrounds it. A force balance on the control volume yields the following relation between the forces at the outer $S_2$ and inner surfaces $S_1$ (the outer surface is exposed to the surrounding fluid and the inner surface is adjacent to the surface of the body):

$$\oint_{S_1} \boldsymbol{n} \cdot \boldsymbol{\sigma} \, \mathrm{d}S + \oint_{S_2} \boldsymbol{n} \cdot \boldsymbol{\sigma} \, \mathrm{d}S = \mathbf{0}. \tag{A.8}$$

As in the problem of the spherical cap, the sum of the normal stresses at the outer surface of the control volume $S_2$ result in a zero net force, and therefore, the sum of the stresses at the surface of the body $S_1$ must also be zero, as a consequence the above relation.

In connection with the problem of Stokes flow past a solid body, from the present results one can conclude that the magnitude of the pressure far away does not affect the net drag force.

## A.2 Stokes flow past a solid sphere - transformation of the boundary value problem

It is convenient to start by transforming the undisturbed flow far away from the solid sphere in terms of the stream function $\psi(r, \vartheta)$. From the $u_{r,\infty}$ and $u_{\vartheta,\infty}$ components it is found that

$$\frac{\partial \psi}{\partial \vartheta} = -u_\infty \, r^2 \sin\vartheta \cos\vartheta, \quad \frac{\partial \psi}{\partial r} = -u_\infty \, r \sin\vartheta, \quad \text{as} \quad r \to \infty, \tag{A.9}$$

respectively. By carrying out the integrations with respect to the corresponding dimension one finds that:

$$\psi(r \to \infty, \vartheta) = -\frac{1}{2} u_\infty \, r^2 \sin^2 \vartheta + A(r), \tag{A.10}$$

$$\psi(r \to \infty, \vartheta) = -\frac{1}{2} u_\infty \, r^2 \sin^2 \vartheta + B(\vartheta). \tag{A.11}$$

Note that both expressions are consistent if the constants of integration are equal to some constant value ($A(r) = B(\vartheta) = 0$) that may conveniently be set equal to zero. Therefore, the far field condition expressed with respect to the stream function now reads:

$$\psi(r, \vartheta) = -\frac{1}{2} u_\infty \, r^2 \sin^2 \vartheta, \quad \text{as} \quad r \to \infty. \tag{A.12}$$

Before transforming the remaining boundary conditions, it is useful to propose that the appropriate form of the stream function in this problem is:

$$\psi(r, \vartheta) = f(r) \sin^2 \vartheta. \tag{A.13}$$

Transformation of the no-penetration condition ($u_r = 0$) dictates that:

$$\frac{\partial \psi}{\partial \vartheta} = 0, \quad \text{at} \quad r = a. \tag{A.14}$$

Imposing this condition on the general form of the stream function results in the following expression:

$$\frac{\partial \psi}{\partial \vartheta} = f(r) \left( 2 \sin \vartheta \cos \vartheta \right). \tag{A.15}$$

For the above expression to be zero, the stream function must satisfy:

$$\psi(r = a, \vartheta) = 0, \tag{A.16}$$

because $2 \sin \vartheta \cos \vartheta$ is an 'arbitrary' function of $\vartheta$. (Note that the condition must be met at every angle, which in general has an arbitrary value).

Transformation of the no-slip condition $u_\vartheta = 0$ at the surface of the sphere yields directly the following expression for the stream function:

$$\frac{\partial \psi}{\partial r}(r = a, \vartheta) = 0. \tag{A.17}$$

This concludes transformation of the boundary conditions for the problem of Stokes flow past a stationary solid-sphere.

# APPENDIX B

## B.1 Representation of three-dimensional velocity fields for $\beta = \pi/2$

For $\beta = \pi/2$, we represent the harmonic functions $\chi$, $p$, and $\Phi$ in the surrounding fluid as follows:

$$\chi^{(0)} = \sum_{n=1}^{\infty} H_n r^{-n-1} P_n^{(1)}(\theta) \sin\phi, \tag{B.1a}$$

$$\bar{p}^{(0)} = \sum_{n=1}^{\infty} \frac{2(2n-1)}{n+1} E_n r^{-n-1} P_n^{(1)}(\theta) \cos\phi, \tag{B.1b}$$

$$\Phi^{(0)} = \sum_{n=1}^{\infty} \frac{E_n}{n+1} r^{-n-1} P_n^{(1)}(\theta) \cos\phi. \tag{B.1c}$$

This leads to the following expression for the velocity of this fluid:

$$v_r^{(0)} = \sum_{n=1}^{\infty} E_n P_n^{(1)}(\theta)(r^2-1) r^{-n-2} \cos\phi - L(r) \sin\vartheta \cos\phi, \tag{B.2a}$$

$$v_\vartheta^{(0)} = \sum_{n=1}^{\infty} \left\{ \frac{E_n Q_n(\theta)}{n+1} \left( \frac{n-2}{n} r^2 - 1 \right) + H_n P_n'(\theta) r \right\} r^{-n-2} \cos\phi \tag{B.2b}$$

$$-M(r)\theta\cos\phi,$$

$$v_\phi^{(0)} = \sum_{n=1}^{\infty} \left\{ \frac{E_n P_n'(\theta)}{n+1} \left( \frac{n-2}{n} r^2 - 1 \right) + H_n Q_n(\theta) r \right\} r^{-n-2} \sin\phi \tag{B.2c}$$

$$+M(r)\sin\phi.$$

Inside the drop the Lamb functions are the following

$$\chi^{(1,2)} = \left\{\sum_{n=1}^{\infty} A_n^{(1,2)} r^{2n} P_{2n}^{(1)}(\theta) + \eta_{2,1} \sum_{n=0}^{\infty} G_n r^{2n+1} \frac{P_{2n+1}^{(1)}(\theta)}{P'_{2n+1}(0)}\right\} \sin\phi, \tag{B.3a}$$

$$\begin{aligned}\bar{p}^{(1,2)} &= \sum_{n=0}^{\infty} B_n^{(1,2)} \frac{2(4n+5)}{2n+1} r^{2n+1} \frac{P_{2n+1}^{(1)}(\theta)}{P_{2n+1}^{(1)}(0)} \cos\phi \\ &\quad + \eta_{2,1} \sum_{n=1}^{\infty} D_n \frac{2(2n+1)(4n+3)}{2n+3} r^{2n} \frac{P_{2n}^{(1)}(\theta)}{Q_{2n}(0)} \cos\phi,\end{aligned} \tag{B.3b}$$

$$\begin{aligned}\Phi^{(1,2)} &= -\left\{\sum_{n=0}^{\infty} \frac{B_n^{(1,2)}}{2n+3} r^{2n+3} \frac{P_{2n+3}^{(1)}(\theta)}{P_{2n+3}^{(1)}(0)} + \eta_{2,1} \sum_{n=1}^{\infty} D_n r^{2n+2} \frac{P_{2n+2}^{(1)}(\theta)}{Q_{2n+2}(0)}\right\} \cos\phi \\ &\quad + \left\{\sum_{n=0}^{\infty} F_n r^{2n+1} P_{2n}^{(1)} + \eta_{2,1} \sum_{n=0}^{\infty} G_n r^{2n+2} \frac{P_{2n+2}^{(1)}}{Q_{2n+2}(0)}\right\} \cos\phi.\end{aligned} \tag{B.3c}$$

Therefore the velocity fields can be written as

$$\begin{aligned}v_r^{(1,2)} &= \sum_{n=0}^{\infty} \left( B_n^{(1,2)} \left\{ \frac{P_{2n+1}^{(1)}(\theta)}{P_{2n+1}^{(1)}(0)} - \frac{P_{2n+3}^{(1)}(\theta)}{P_{2n+3}^{(1)}(0)} \right\} r^2 + (2n+1) F_n P_{2n+1}^{(1)}(\theta) \right. \\ &\quad \left. + \eta_{2,1}(2n+2) G_n \frac{P_{2n+2}^{(1)}(\theta)}{Q_{2n+2}(0)} r \right) r^{2n} \cos\phi \\ &\quad + \eta_{2,1} \sum_{n=1}^{\infty} D_n \left\{ \frac{2n(2n+1)}{2n+3} \frac{P_{2n}^{(1)}(\theta)}{Q_{2n}(0)} - (2n+2) \frac{P_{2n+2}^{(1)}(\theta)}{Q_{2n+2}(0)} \right\} r^{2n+1} \cos\phi,\end{aligned} \tag{B.4a}$$

$$\begin{aligned}v_\vartheta^{(1,2)} &= -\sum_{n=0}^{\infty} \left( B_n^{(1,2)} \left\{ \frac{n+2}{(2n+1)(n+1)} \frac{Q_{2n+1}(\theta)}{P_{2n+1}^{(1)}(0)} - \frac{1}{2n+3} \frac{Q_{2n+3}(\theta)}{P_{2n+3}^{(1)}(0)} \right\} r^2 + F_n Q_{2n+1}(\theta) \right. \\ &\quad \left. - \eta_{2,1} G_n \left\{ \frac{P'_{2n+1}(\theta)}{P'_{2n+1}(0)} - \frac{Q_{2n+2}(\theta)}{Q_{2n+2}(0)} \right\} r \right) r^{2n} \cos\phi \\ &\quad + \sum_{n=1}^{\infty} \left( A_n^{(1,2)} P'_{2n}(\theta) - \eta_{2,1} D_n \left\{ \frac{Q_{2n}(\theta)}{Q_{2n}(0)} - \frac{Q_{2n+2}(\theta)}{Q_{2n+2}(0)} \right\} r \right) r^{2n} \cos\phi,\end{aligned} \tag{B.4b}$$

$$\begin{aligned}v_\phi^{(1,2)} &= -\sum_{n=0}^{\infty} \left( B_n^{(1,2)} \left\{ \frac{n+2}{(2n+1)(n+1)} \frac{P'_{2n+1}(\theta)}{P_{2n+1}^{(1)}(0)} - \frac{1}{2n+3} \frac{P'_{2n+3}(\theta)}{P_{2n+3}^{(1)}(0)} \right\} r^2 + F_n P'_{2n+1}(\theta) \right. \\ &\quad \left. - \eta_{2,1} G_n \left\{ \frac{Q_{2n+1}(\theta)}{P'_{2n+1}(0)} - \frac{P'_{2n+2}(\theta)}{Q_{2n+2}(0)} \right\} r \right) r^{2n} \sin\phi \\ &\quad + \sum_{n=1}^{\infty} \left( A_n^{(1,2)} Q_{2n}(\theta) - \eta_{2,1} D_n \left\{ \frac{P'_{2n}(\theta)}{Q_{2n}(0)} - \frac{P'_{2n+2}(\theta)}{Q_{2n+2}(0)} \right\} r \right) r^{2n} \sin\phi,\end{aligned} \tag{B.4c}$$

Here again $Q_n = \theta P'_n - n(n+1)P_n$.

These representations of velocity fields automatically satisfy the Stokes equation and boundary conditions at the internal interface, if

$$[B_n] = \frac{(n+1)(2n+1)^2(2n+3)^2}{4n+5} P_{2n}(0)[A_{n+1}],$$

where, again, $[f] = f_2 - f_1$. In addition, $v_r^{(0)}$ vanishes at $r = 1$.

Substituting this ansatz into remaining boundary conditions at $r = 1$ and projecting these conditions on $P_n^{(1)}$, one obtains the set of linear equations for the coefficients $A_n^{(1,2)}$, $B_n^{(1,2)}$, $D_n$, $E_n$, $F_n$, $G_n$, and $H_n$. This set of equations is solved numerically.

It should be emphasized that the convergence of the series is rather slow because of the presence of jump in the viscosities at $\vartheta = \pi/2$. In order to improve the convergence and to suppress the oscillations of the coefficients for large $n$, these harmonics have to be considered separately. Such an analysis results in the following asymptotics valid at large $n$:

$$A_n^{(1,2)} \sim (-1)^n n^{-7/2},\ [A_n^{(1)}] \sim (-1)^n n^{-13/2},\ B_n^{(1,2)} \sim n^{-2}, \quad \text{(B.5a)}$$

$$[B_n^{(1)}] \sim n^{-3},\ D_n \sim n^{-2},\ F_n \sim (-1)^n n^{-9/2},\ G_n \sim n^{-3}, \quad \text{(B.5b)}$$

$$(E_{2n}, E_{2n+1}) \sim (-1)^n n^{-5/2},\ (H_{2n}, H_{2n+1}) \sim (-1)^n n^{-5/2}, \quad \text{(B.5c)}$$

where according to notations accepted in the paper $[A_n] = A_n^{(2)} - A_n^{(1)}$ and $[B_n] = B_n^{(2)} - B_n^{(1)}$. These asymptotics must be taken into account when the series are cut; for instance, one can set $H_{2N+1} \approx -H_{2N-1}$ instead of simple vanishing $H_{2n+1}$ at $n \geq N$. This procedure improves the convergence to a great extent.

The total force exerted on the drop (in the same units, $\tilde{\eta}_0 a U$) can be expressed as follows:

$$F_x = 2\pi(3 - E_1),\ F_z = 0, \quad \text{(B.6)}$$

whereas for the $y$-component of the torque one obtains

$$T_y = -8\pi H_1. \tag{B.7}$$

### B.2 Simplification of the velocity fields for $\beta = \pi/2$ at small $[\eta]/\eta$

Let us briefly discuss the simplification of the general solutions given in Appendix B.1 at small $[\eta]/\eta$. At the zeroth order with respect to this ratio the solution is given by Eq. (3.17), which corresponds to $F_0 = -E_1 = \mp B_0^{(1,2)} = \mu,\ F_1 = 2\mu/9$ in Equations (B.2) and (B.4), whereas the rest of coefficients vanishes.

The solution $\boldsymbol{u}^{(j)}$ at the first order is provided by the same formulas, Equations (B.2) and (B.4), with the symmetry properties following from Eq. (3.19):

$$F_n = E_{2n+1} = H_{2n} = 0,\ A_n^{(1)} = -A_n^{(2)} = A_n,\ B_n^{(1)} = -B_n^{(2)} = B_n.$$

In particular, from $E_1 = 0$ and Eq. (B.6) one can conclude that the first correction to the velocity field $\boldsymbol{u}^{(j)}$ does not provide a correction to the force imposed onto the drop.

As one can see, the representation of the velocity corrections $\boldsymbol{u}^{(j)}$ contains half of the coefficients appearing in the general case. Indeed, one can satisfy the boundary conditions at $r = 1$ only for $\vartheta \le \pi/2$, the boundary conditions for $\vartheta > \pi/2$ are met automatically due to the symmetry condition, Eq. (3.19).

Again, at large $n$ the problem has to be analyzed separately in order to improve the convergence of the series. This provides

$$A_n \sim n^{-13/2}, B_n \sim n^{-3}, D_n \sim n^{-2},\ G_n \sim n^{-3},\ E_{2n} \sim (-1)^n n^{-5/2},\ H_{2n+1} \sim (-1)^n n^{-7/2},$$

which is closely related to Eq. (B.5).

REFERENCE LIST


[1] R. G. Larson. *The Structure and Rheology of Complex Fluids*. Oxford University Press, 1999.

[2] H. Shintaku, T. Kuwabara, S. Kawano, T. Suzuki, I. Kanno, and H. Kotera. Micro cell encapsulation and its hydrogel-beads production using microfluidic device. *Microsys. Tech.*, 13:951–958, 2007.

[3] R. Vehring. Pharmaceutical particle engineering via spray drying. *Pharm. Res.*, 25:999–1022, 2008.

[4] N. N. Li. Separation of hydrocarbons by liquid membrane permeation. *Ind. Engng. Chem. Proc. Des. Dev.*, 10:215–221, 1971.

[5] M. R. Bringer, C. J. Gerdts, H. Song, J. D. Tice, and R. F. Ismagilov. Microfluidic systems for chemical kinetics that rely on chaotic mixing in droplets. *Phil. Trans. Roy. Soc. Lon. A: Math., Phys. Engng. Sci.*, 362(1818):1087–1104, 2004.

[6] H. N. Joensson and H. AnderssonSvahn. Droplet microfluidics–a tool for single-cell analysis. *Ang. Chem. Int. Ed.*, 51:12176–12192, 2012.

[7] R. E. Johnson and S. S. Sadhal. Fluid mechanics of compound multiphase drops and bubbles. *Ann. Rev. Fluid Mech.*, 17:289–320, 1985.

[8] S. Torza and S. G. Mason. Three-phase interactions in shear and electrical fields. *J. Coll. Int. Sci.*, 33:67–83, 1970.

[9] A. M. J. Davis and H. Brenner. Emulsions containing a third solid internal phase. *J. Engng. Mech. Div. ASCE*, 107:609–621, 1981.

[10] H. A. Stone and L. G. Leal. Breakup of concentric double emulsion droplets in linear flows. *J. Fluid Mech.*, 211:123–156, 1990.

[11] G. I. Taylor. The viscosity of a fluid containing small drops of another fluid. *Proc. R. Soc. A*, 138:41–48, 1932.

[12] H. D. Young, R. A. Freedman, and A. L. Ford. *Sears and Zemansky's University Physics*. Addison-Wesley, 2008.

[13] W. M. Deen. *Analysis of Transport Phenomena*. Oxford University Press, 1998.

[14] E. M. Purcell. Life at low Reynolds number. *Amer. J. Phys.*, 45:3–11, 1977.

[15] R. B. Bird, W. E. Stewart, and E. N. Lightfoot. *Transport Phenomena*. Wiley, 2007.

[16] L. G. Leal. *Advanced Transport Phenomena*. Cambridge University Press, 2007.

[17] L. D. Landau and E. M. Lifshitz. *Fluid Mechanics, Second Edition: Volume 6 (Course of Theoretical Physics)*. Butterworth-Heinemann, 1987.

[18] R. Aris. *Vectors, Tensors and the Basic Equations of Fluid Mechanics*. Dover Publications, 1990.

[19] H. Lamb and R. Caflisch. *Hydrodynamics*. Cambridge University Press, 1993.

[20] J. Happel and H. Brenner. *Low Reynolds Number Hydrodynamics: With special applications to particulate media*. Prentice-Hall, 1965.

[21] W. B. Russel, D. A. Saville, and W. R. Schowalter. *Colloidal Dispersions*. Cambridge University Press, 1989.

[22] M. Stimson and G. B. Jeffery. The motion of two spheres in a viscous fluid. *Proc. Roy. Soc. London. Series A*, 111:110–116, 1926.

[23] J. Happel and B. J. Bryne. (viscous flow in multiparticle systems) motion of a sphere in a cylindrical tube. *Ind. Engng. Chem.*, 46:1181–1186, 1954.

[24] S. Wakiya. Viscous flows past a spheroid. *J. Phys. Soc. Japan*, 12:1130–1141, 1957.

[25] A. T. Chwang and T. Y.-T. Wu. Hydromechanics of low-Reynolds-number flow. Part 1. Rotation of axisymmetric prolate bodies. *J. Fluid Mech.*, 63:607–622, 1974.

[26] A. T. Chwang and T. Y.-T. Wu. Hydromechanics of low-Reynolds-number flow. part 2. Singularity method for Stokes flows. *J. Fluid Mech.*, 67:787–815, 1975.

[27] A. T. Chwang. Hydromechanics of low-Reynolds-number flow. Part 3. Motion of a spheroidal particle in quadratic flows. *J. Fluid Mech.*, 72:17–34, 1975.

[28] A. T. Chwang and T. Y.-T. Wu. Hydromechanics of low-Reynolds-number flow. Part 4. Translation of spheroids. *J. Fluid Mech.*, 75:677–689, 1976.

[29] R. E. Johnson and T. Y.-T. Wu. Hydromechanics of low-Reynolds-number flow. Part 5. Motion of a slender torus. *J. Fluid Mech.*, 95:263–277, 1979.

[30] L. H. Huang and A. T. Chwang. Hydromechanics of low-Reynolds-number flow. Part 6. Rotation of oblate bodies. *J. Engng. Math.*, 20:307–322, 1986.

[31] S. Kim and S. J. Karrila. *Microhydrodynamics Principles and Selected Applications*. Dover, 2005.

[32] S. Goldstein. *Modern Developments in Fluid Dynamics*. Oxford, 1938.

[33] E. Lauga, M. Brenner, and H. Stone. Microfluidics: The no-slip boundary condition. In C. Tropea, A. L. Yarin, and J. F. Foss, editors, *Springer Handbook of Experimental Fluid Mechanics*, pages 1219–1240. Springer Berlin Heidelberg, 2007.

[34] E. Lauga and T. M. Squires. Brownian motion near a partial–slip boundary: A local probe of the no–slip condition. *Phys. Fluids*, 17:–, 2005.

[35] V. S. J. Craig, C. Neto, and D. R. M. Williams. Shear-dependent boundary slip in an aqueous Newtonian liquid. *Phys. Rev. Lett.*, 87:054504, 2001.

[36] D. C. Tretheway and C. D. Meinhart. Apparent fluid slip at hydrophobic microchannel walls. *Phys. Fluids*, 14:L9–L12, 2002.

[37] H. Hervet and L. Léger. Flow with slip at the wall: from simple to complex fluids. *C. R. Phys.*, 4:241 – 249, 2003.

[38] C. Neto, V. S. J. Craig, and D. R. M. Williams. Evidence of shear-dependent boundary slip in Newtonian liquids. *Eur. Phys. J. E – Soft Matter*, 12:71–S74, 2003.

[39] C. Cheikh and G. Koper. Stick–slip transition at the nanometer scale. *Phys. Rev. Lett.*, 91:156102, 2003.

[40] C. L. M. H. Navier. Mémoire sur le lois du mouvement des fluides. *Mémoires de l'Academie Royale des Sciences de l'Instituit de France*, IV:389–440, 1823.

[41] A. B. Basset. *A Treatise on Hydrodynamics*. Dover, 1961.

[42] G. Willmott. Dynamics of a sphere with inhomogeneous slip boundary conditions in Stokes flow. *Phys. Rev. E*, 77:055302, 2008.

[43] H. Luo and C. Pozrikidis. Effect of surface slip on Stokes flow past a spherical particle in infinite fluid and near a plane wall. *J. Engng. Math.*, 62:1–21, 2008.

[44] A. Ramachandran and A. S. Khair. The dynamics and rheology of a dilute suspension of hydrodynamically Janus spheres in a linear flow. *J. Fluid Mech.*, 633:233–269, 2009.

[45] M. Manga and H. A. Stone. Buoyancy-driven interactions between two deformable viscous drops. *J. Fluid Mech.*, 256:647–683, 1993.

[46] W. R. Schowalter, C. E. Chaffey, and H. Brenner. Rheological behavior of a dilute emulsion. *J. Coll. Int. Sci.*, 26:152 – 160, 1968.

[47] D. Barthès-Biesel and A. Acrivos. Deformation and burst of a liquid droplet freely suspended in a linear shear field. *J. Fluid Mech.*, 61:1–22, 1973.

[48] A. S. Geller, S. H. Lee, and L. G. Leal. The creeping motion of a spherical particle normal to a deformable interface. *J. Fluid Mech.*, 169:27–69, 1986.

[49] A. Karnis and S. G. Mason. Particle motions in sheared suspensions: Xxiii. Wall migration of fluid drops. *J. Coll. Int. Sci.*, 24(2):164 – 169, 1967.

[50] K. D. Barton and R. S. Subramanian. The migration of liquid drops in a vertical temperature gradient. *J. Coll. Int. Sci.*, 133:211 – 222, 1989.

[51] J. S. Hadamard. Mouvement permanent lent d'une sphere liquide et visqueuse dans un liquide visqueux. *Compt. Rend. Acad. Sci.*, 152:1735–1738, 1911.

[52] W. Rybczynski. Über die fortschreitende bewegung einer flüssigen kugel in einem zähen medium. *Bull. Acad. Sci. Cracovie (Ser. A)*, pages 40–46, 1911.

[53] T. D. Taylor and A. Acrivos. On the deformation and drag of a falling viscous drop at low Reynolds number. *J. Fluid Mech.*, 18:466–476, 1964.

[54] N. A. Frankel and A. Acrivos. The constitutive equation for a dilute emulsion. *J. Fluid Mech.*, 44:65–78, 1970.

[55] A. Acrivos. The breakup of small drops and bubbles in shear flows*. *Ann. N.Y. Acad. Sci.*, 404:1–11, 1983.

[56] J. M. Rallison. The deformation of small viscous drops and bubbles in shear flows. *Ann. Rev. Fluid Mech.*, 16:45–66, 1984.

[57] J. D. Buckmaster. Pointed bubbles in slow viscous flow. *Journal of Fluid Mechanics*, 55:385–400, 10 1972.

[58] G. K. Youngren and A. Acrivos. On the shape of a gas bubble in a viscous extensional flow. *J. Fluid Mech.*, 76:433–442, 1976.

[59] G. I. Taylor. The formation of emulsions in definable fields of flow. *Proc. R. Soc. A*, 146:501–523, 1934.

[60] J. F. Harper. The motion of bubbles and drops through liquids. *Adv. Appl. Mech.*, 12:59 – 129, 1972.

[61] M. D. Leven and J. Newman. The effect of surfactant on the terminal and interfacial velocities of a bubble or drop. *AIChE J.*, 22:695–701, 1976.

[62] L. E. Rodd, J. J. Cooper-White, D. V. Boger, and G. H. McKinley. Role of the elasticity number in the entry flow of dilute polymer solutions in micro-fabricated contraction geometries. *J. Non-Newtonian Fluid Mech.*, 143:170 –

191, 2007.

[63] S. J. Haward and G. H. McKinley. Instabilities in stagnation point flows of polymer solutions. *Phys. Fluids*, 25:–, 2013.

[64] M. Brust, C. Schaefer, R. Doerr, L. Pan, M. Garcia, P. E. Arratia, and C. Wagner. Rheology of human blood plasma: Viscoelastic versus Newtonian behavior. *Phys. Rev. Lett.*, 110:078305, 2013.

[65] P. A. May and J. S. Moore. Polymer mechanochemistry: techniques to generate molecular force via elongational flows. *Chem. Soc. Rev.*, pages 7497–7506, 2013.

[66] S. J. Haward, V. Sharma, and J. A. Odell. Extensional opto-rheometry with biofluids and ultra-dilute polymer solutions. *Soft Matter*, 7:9908–9921, 2011.

[67] É. Guazzelli and J. F. Morris. *A Physical Introduction to Suspension Dynamics*. Cambridge University Press, 2011.

[68] H. Brenner. The Stokes resistance of an arbitrary particle. *Chem. Engng. Sci.*, 18:1–25, 1963.

[69] H. Brenner. The Stokes resistance of an arbitrary particle—ii: An extension. *Chem. Engng. Sci.*, 19(9):599 – 629, 1964.

[70] H. Brenner. The Stokes resistance of an arbitrary particle—iii: Shear fields. *Chem. Engng. Sci.*, 19(9):631 – 651, 1964.

[71] H. Brenner. The Stokes resistance of an arbitrary particle—iv arbitrary fields of flow. *Chem. Engng. Sci.*, 19(10):703 – 727, 1964.

[72] H. Brenner. The Stokes resistance of an arbitrary particle—Part V.: Symbolic operator representation of intrinsic resistance. *Chem. Engng. Sci.*, 21:97–109, 1966.

[73] H. Brenner. The Stokes resistance of a slightly deformed sphere. *Chem. Engng. Sci.*, 19(8):519 – 539, 1964.

[74] D. R. Foss and J. F. Brady. Structure, diffusion and rheology of Brownian suspensions by Stokesian dynamics simulation. *J. Fluid Mech.*, 407:167–200, 2000.

[75] J. M. Dorrepaal. The Stokes resistance of a spherical cap to translational and rotational motions in a linear shear flow. *J. Fluid Mech.*, 84:265–279, 1978.

[76] A. Nir and A. Acrivos. On the creeping motion of two arbitrary-sized touching spheres in a linear shear field. *J. Fluid Mech.*, 59:209–223, 1973.

[77] J. W. Swan and A. S. Khair. On the hydrodynamics of 'slip–stick' spheres. *J. Fluid Mech.*, 606:115–132, 2008.

[78] A. E. Komrakova, O. Shardt, D. E., and J. J. Derksen. Lattice boltzmann simulations of drop deformation and breakup in shear flow. *Int. J. Mult. Flow*, 59:24–43, 2014.

[79] C. E. Chaffey and H. Brenner. A second-order theory for shear deformation of drops. *J. Coll. Int. Science*, 24:258–269, 1967.

[80] R. G. Cox. The deformation of a drop in a general time-dependent fluid flow. *J. Fluid Mech.*, 37:601–623, 1969.

[81] M. R. Spiegel and J. Liu. *Mathematical Handbook of Formulas and Tables*. McGraw-Hill, 1999.

[82] M. Abramowitz and I. Stegun. *Handbook of Mathematical Functions*. Dover, 1972.

[83] F. A. Morrison. *Understanding Rheology*. Oxford University Press, 2001.

[84] L. G. Leal. Particle motions in a viscous fluid. *Ann. Rev. Fluid Mech.*, 12:435–476, 1980.

[85] E. J. Hinch and L. G. Leal. The effect of Brownian motion on the rheological properties of a suspension of non-spherical particles. *J. Fluid Mech.*, 52:683–712, 1972.

[86] L. Durlofsky, J. F. Brady, and G. Bossis. Dynamic simulation of hydrodynamically interacting particles. *J. Fluid Mech.*, 180:21–49, 1987.

[87] G. Bossis and J. F. Brady. The rheology of Brownian suspensions. *J. Chem. Phys.*, 91:1866–1874, 1989.

[88] A. Einstein. *Investigations on the theory of Brownian movement*. Dover, 1956. (Translation of Einstein's original publications in *Annalen der Physik* between the years of 1905 and 1911.).

[89] G. B. Jeffery. The motion of ellipsoidal particles immersed in a viscous fluid. *Proc. R. Soc. Lond., Ser. A*, 102:161–179, 1922.

[90] E. Y. Harper and I.-D. Chang. Maximum dissipation resulting from lift in a slow viscous shear flow. *J. Fluid Mech.*, 33:209–225, 1968.

[91] H. A. Scheraga. NonNewtonian viscosity of solutions of ellipsoidal particles. *J. Chem. Phys.*, 23:1526–1532, 1955.

[92] H. Brenner. Rheology of a dilute suspension of axisymmetric Brownian particles. *Int. J. Mult. Flow*, 1:195–341, 1974.

[93] J. Einarsson, F. Candelier, F. Lundell, J. R. Angilella, and B. Mehlig. Rotation of a spheroid in a simple shear at small Reynolds number. *Phys. Fluids*, 27:–, 2015.

[94] E. J. Hinch and L. G. Leal. Time-dependent shear flows of a suspension of particles with weak Brownian rotations. *J. Fluid Mech.*, 57:753–767, 1973.

[95] G. K. Batchelor and J. T. Green. The determination of the bulk stress in a suspension of spherical particles to order $c^2$. *J. Fluid Mech.*, 56:401–427, 1972.

[96] G. K. Batchelor. The effect of Brownian motion on the bulk stress in a suspension of spherical particles. *J. Fluid Mech.*, 83:97–117, 1977.

[97] G. K. Batchelor. The stress system in a suspension of force–free particles. *J. Fluid Mech.*, 41:545–570, 1970.

[98] P. G. de Gennes. Soft matter. *Rev. Mod. Phys.*, 64:645–648, 1992.

[99] F. Wurm and A. F. M. Kilbinger. Polymeric Janus particles. *Angew. Chem. Int. Ed.*, 48:8412–8421, 2009.

[100] J. Yoon, K. J. Lee, and J. Lahann. Multifunctional polymer particles with distinct compartments. *J. Mater. Chem.*, 21:8502–8510, 2011.

[101] Z. Nie, W. Li, M. Seo, S. Xu, and E. Kumacheva. Janus and ternary particles generated by microfluidic synthesis: design, synthesis, and self-assembly. *J. Am. Chem. Soc.*, 128:9408–9412, 2006.

[102] C.-H. Chen, R. K. Shah, A. R. Abate, and D. A. Weitz. Janus particles templated from double emulsion droplets generated using microfluidics. *Langmuir*, 25:4320–4323, 2009.

[103] D. Dendukuri and P. S. Doyle. The synthesis and assembly of polymeric microparticles using microfluidics. *Adv. Mater.*, 21:4071–4086, 2009.

[104] H. Hasinovic, S. E. Friberg, and G. Rong. A one-step process to a Janus emulsion. *Journal of Colloid and Interface Science*, 354:424 – 426, 2011.

[105] K.-H. Roh, D. C. Martin, and J. Lahann. Triphasic nanocolloids. *J. Am. Chem. Soc.*, 128:6796–6797, 2006.

[106] E. Bormashenko, Y. Bormashenko, R. Pogreb, and O. Gendelman. Janus droplets: Liquid marbles coated with dielectric/semiconductor particles. *Langmuir*, 27:7–10, 2011.

[107] N. Virgilio and B. D. Favis. Self-assembly of Janus composite droplets at the interface in quaternary immiscible polymer blends. *Macromolecules*, 44:5850–5856, 2011.

[108] Y. Matunobu. Motion of a drop suspended in a viscous flow with arbitrary velocity profile. *J. Phys. Soc. Jpn.*, 29:508–513, 1970.

[109] S. S. Sadhal and R. E. Johnson. Stokes flow past bubbles and drops partially coated with thin films. Part 1. Stagnant cap of surfactant film – exact solution. *J. Fluid Mech.*, 126:237–250, 1983.

[110] R. E. Johnson and S. S. Sadhal. Stokes flow past bubbles and drops partially coated with thin films. Part 2. Thin films with internal circulation – a perturbation solution. *J. Fluid Mech.*, 132:295–318, 1983.

[111] Y. H. Mori. Configurations of gas-liquid two-phase bubbles in immiscible liquid media. *Int. J. Multiphase Flow*, 4:383–396, 1978.

[112] E. Rushton and G. A. Davies. Settling of encapsulated droplets at low Reynolds numbers. *Int. J. Multiphase Flow*, 9:337–342, 1983.

[113] S. S. Sadhal and H. N. Oguz. Stokes flow past compound multiphase drops: the case of completely engulfed drops/bubbles. *J. Fluid Mech.*, 160:511–529, 1985.

[114] J. Guzowski, P. M. Korczyk, S. Jakiela, and P. Garstecki. The structure and stability of multiple micro-droplets. *Soft Matter*, 8:7269–7278, 2012.

[115] L. G. Leal. *Advanaced Transport Phenomena*. Cambridge University Press, 2007.

[116] L. E. Payne and W. H. Pell. The Stokes flow problem for a class of axially symmetric bodies. *J. Fluid Mech.*, 7:529–549, 1960.

[117] V. G. Levich. *Physicochemical Hydrodynamics*. Prentice-Hall, 1962.

[118] H. Hasinovic and S. E. Friberg. Destabilization mechanisms in a triple emulsion with Janus drops. *J. Coll. Int. Sci.*, 361(2):581–586, 2011.

[119] S. Shklyaev, A. O. Ivantsov, M. Díaz-Maldonado, and U. M. Córdova-Figueroa. Dynamics of a Janus drop in an external flow. *Phys. Fluids*, 25:082105, 2013.

[120] D. S. Morton, R. S. Subramanian, and R. Balasubramaniam. The migration of a compound drop due to thermocapillarity. *Phys. Fluids A*, 2:2119–2133, 1990.

[121] L. Rosenfeld, O. M. Lavrenteva, and A. Nir. On the thermocapillary motion of partially engulfed compound drops. *J. Fluid Mech.*, 626:263–289, 2009.

[122] E. Chervenivanova and Z. Zapryanov. On the deformation of compound multiphase drops at low Reynolds numbers. *PhysicoChem. Hydrodyn.*, 11:243–259, 1989.

[123] S. T. Vuong and S. S. Sadhal. Growth and translation of a liquid-vapour compound drop in a second liquid. Part 1. Fluid mechanics. *J. Fluid Mech.*, 209:617–637, 1989.

[124] O. Shardt, J. J. Derksen, and S. K. Mitra. Simulations of Janus droplets at equilibrium and in shear. *Phys. Fluids*, 26:012104, 2014.

[125] J. J. Stickel and R. L. Powell. Fluid mechanics and rheology of dense suspensions. *Ann. Rev. Fluid Mech.*, 37:129–149, 2005.

[126] G. Segré and A. Silberberg. Behaviour of macroscopic rigid spheres in Poiseuille flow Preart 1. determination of local concentration by statistical analysis of particle passages through crossed light beams. *J. Fluid Mech.*, 14:115–135, 1962.

[127] C.-J. Lin, J. H. Peery, and W. R. Schowalter. Simple shear flow round a rigid sphere: inertial effects and suspension rheology. *J. Fluid Mech.*, 44:1–17, 1970.

[128] H. Haddadi and J. F. Morris. Microstructure and rheology of finite inertia neutrally buoyant suspensions. *J. Fluid Mech.*, 749:431–459, 2014.

[129] T. Nisisako, T. Torii, T. Takahashi, and Y. Takizawa. Synthesis of monodisperse bicolored Janus particles with electrical anisotropy using a microfluidic co-flow system. *Adv. Mater.*, 18:1152–1156, 2006.

[130] P. C.-H. Chan and L. G. Leal. The motion of a deformable drop in a second-order fluid. *J. Fluid Mech.*, 92:131–170, 1979.

[131] L. G. Leal and S. H. Lee. Particle motion near a deformable fluid interface. *Adv. Coll. Int. Sci.*, 17:61–81, 1982.

[132] B. K. Chi and L. G. Leal. A theoretical study of the motion of a viscous drop toward a fluid interface at low Reynolds number. *J. Fluid Mech.*, 201:123–146,

1989.

[133] S.-M. Yang and L. G. Leal. Motions of a fluid drop near a deformable interface. *Int. J. Multiphase Flow*, 16:597–616, 1990.

[134] M. Manga and H. A. Stone. Low Reynolds number motion of bubbles, drops and rigid spheres through fluid–fluid interfaces. *J. Fluid Mech.*, 287:279–298, 1995.

[135] H. Yang, C. C. Park, Y. T. Hu, and L. G. Leal. The coalescence of two equal-sized drops in a two-dimensional linear flow. *Phys. Fluids*, 13:1087–1106, 2001.

[136] L. G. Leal. Flow induced coalescence of drops in a viscous fluid. *Phys. Fluids*, 16:1833–1851, 2004.

[137] A. G. Olabi and A. Grunwald. Design and application of magneto-rheological fluid. *Mater. Design*, 28:2658–2664, 2007.

[138] J.-T. Wang, J. Wang, and J.-J. Han. Fabrication of advanced particles and particle-based materials assisted by droplet-based microfluidics. *Small*, 7:1728–1754, 2011.

[139] Y. H. Lee, C. A. Kim, W. H. Jang, H. J. Choi, and M. S. Jhon. Synthesis and electrorheological characteristics of microencapsulated polyaniline particles with melamine–formaldehyde resins. *Polymer*, 42(19):8277–8283, 2001.

[140] R. Tian, Y. D. Zheng, X. Liang, Z. M. Zhou, X. L. Fu, and W. T. Lv. The preparation of microcapsules used for self-healing composites. *Advanced Materials Research*, 233–235:2319–2322, 2011.

[141] S. Shklyaev. Janus droplet as a catalytic micromotor. *EPL (Europhys. Letters)*, 110:54002, 2015.

[142] H.-C. Kan, H. S. Udaykumar, W. Shyy, and R. Tran-Son-Tay. Hydrodynamics of a compound drop with application to leukocyte modeling. *Phys. Fluids*, 10:760–774, 1998.

[143] M. H. Hoskins, R. F. Kunz, J. E. Bistline, and C. Dong. Coupled flow–structure–biochemistry simulations of dynamic systems of blood cells using an adaptive surface tracking method. *J. Fluids and Struct.*, 25:936–953, 2009.

[144] C.-H. Choi, S. Hwang, J.-M. Jeong, S.-M. Kang, J. Kim, and C.-S. Lee. Microfluidic synthesis of anisotropic particles from Janus drop by in situ photopolymerization. *Biomed. Engng. Letters*, 2:95–99, 2012.

[145] J. Jeong, A. Gross, W.-S. Wei, F. Tu, D. Lee, P. J. Collings, and A. G. Yodh. Liquid crystal Janus emulsion droplets: preparation, tumbling, and swimming. *Soft Matter*, 11:6747–6754, 2015.

[146] L. D. Zarzar, V. Sresht, E. M. Sletten, J. A. Kalow, D. Blankschtein, and T. M. Swager. Dynamically reconfigurable complex emulsions via tunable interfacial tensions. *Nature*, 518:520–524, 2015.

[147] D. Tsemakh, O. M. Lavrenteva, and A. Nir. On the locomotion of a drop, induced by the internal secretion of surfactant. *Int. J. Multiphase Flow*, 30:1337–1367, 2004.

[148] I. B. Bazhlekov, P. J. Shopov, and Z. D. Zapryanov. Unsteady motion of a type-A compound multiphase drop at moderate reynolds numbers. *J. Coll. Int. Sci.*, 169:1–12, 1995.

[149] K. A. Smith, J. M. Ottino, and M. Olvera de la Cruz. Encapsulated drop breakup in shear flow. *Phys. Rev. Lett.*, 93:204501, 2004.

[150] C. Zhou, P. Yue, and J. J. Feng. Deformation of a compound drop through a contraction in a pressure-driven pipe flow. *Int. J. Mult. Flow*, 34:102–109, 2008.

[151] X. Qu and Y. Wang. Dynamics of concentric and eccentric compound droplets suspended in extensional flows. *Phys. Fluids*, 24:123302, 2012.

[152] H. Hua, J. Shin, and J. Kim. Dynamics of a compound droplet in shear flow. *Int. J. Heat Fluid Flow*, 50:63–71, 2014.

[153] C. Zhou, P. Yue, and J. J. Feng. Formation of simple and compound drops in microfluidic devices. *Phys. Fluids*, 18:092105, 2006.

[154] M. Díaz-Maldonado and U. M. Córdova-Figueroa. On the anisotropic response of a Janus drop in a shearing viscous fluid. *J. Fluid Mech.*, 770:–, 5 2015.

[155] M. D. Summers, J. P. Reid, and D. McGloin. Optical guiding of aerosol droplets. *Opt. Express*, 14:6373–6380, 2006.

[156] F. P. Bretherton. The motion of rigid particles in a shear flow at low Reynolds number. *J. Fluid Mech.*, 14:284–304, 1962.

[157] P. G. Saffman. On the motion of small spheroidal particles in a viscous liquid. *J. Fluid Mech.*, 1:540–553, 1956.

[158] S. R. Derkach. Rheology of emulsions. *Adv. Coll. Int. Sci.*, 151:1–23, 2009.

[159] Magnaudet J., S. Takagi, and D. Legendre. Drag, deformation and lateral migration of a buoyant drop moving near a wall. *J. Fluid Mech.*, 476:115–157, 2003.

[160] A. H. Lichtenstein, L. J. Appel, M. Brands, M. Carnethon, S. Daniels, H. A. Franch, B. Franklin, P. Kris-Etherton, W. S. Harris, B. Howard, N. Karanja, M. Lefevre, L. Rudel, F. Sacks, L. Van Horn, M. Winston, and J. Wylie-Rosett. Diet and lifestyle recommendations revision 2006: A scientific statement from the American heart association nutrition committee. *Circulation*, 114:82–96, 2006.

[161] S. Wakiya. Effect of a submerged object on a slow viscous flow (report V). Spheroid at an arbitrary angle of attack. *Res. Rep. Fac. Engng Niigata Univ. (Japan)*, 8:17–30, 1959.

[162] S.J. Ebbens. Active colloids: Progress and challenges towards realising autonomous applications. *Curr. Opin. Coll. Int. Sci.*, pages –, 2015.

[163] Y. Or, S. Zhang, and R. M. Murray. Dynamics and stability of low-Reynolds-number swimming near a wall. *SIAM J. App. Dyn. Sys.*, 10:1013–1041, 2011.

[164] G.-J. Li and A. M. Ardekani. Hydrodynamic interaction of microswimmers near a wall. *Phys. Rev. E*, 90:013010, 2014.

[165] S. Chilukuri, C. H. Collins, and P. T. Underhill. Impact of external flow on the dynamics of swimming microorganisms near surfaces. *J. Phys.: Cond. Matter*, 26:115101, 2014.

[166] A. Mozaffari, N. Sharifi-Mood, J. Koplik, and C. Maldarelli. Self-Diffusiophoretic Colloidal Propulsion Near a Solid Boundary. *ArXiv*, 1505:07172, 2015.

[167] Joseph Wang. Cargo-towing synthetic nanomachines: Towards active transport in microchip devices. *Lab Chip*, 12:1944–1950, 2012.

[168] A. Ajdari and H. A. Stone. A note on swimming using internally generated traveling waves. *Phys. Fluids*, 11:1275–1277, 1999.

[169] J. Elgeti, R. G. Winkler, and G. Gompper. Physics of microswimmers–single particle motion and collective behavior: a review. *Rep. Prog. Phys.*, 78:056601, 2015.

[170] R. S. M. Rikken, R. J. M. Nolte, J. C. Maan, J. C. M. van Hest, D. A. Wilson, and P. C. M. Christianen. Manipulation of micro- and nanostructure motion with magnetic fields. *Soft Matter*, 10:1295–1308, 2014.

[171] U. M. Córdova-Figueroa and J. F. Brady. Osmotic propulsion: The osmotic motor. *Phys. Rev. Lett.*, 100:158303, 2008.

[172] U. M. Córdova-Figueroa and J. F. Brady. *Directed motion of colloidal particles via chemical reactions: osmotic propulsion*. PhD thesis, Cal. Ins. Tech., 2008.